STRUCTURAL EVOLUTION OF WESTERN DHARWAR CRATON, SOUTHERN INDIA: INSIGHTS INTO THE ROLE OF FAILED RIFTS IN CRUSTAL GROWTH PROCESSES

Thesis submitted to

GRADUATE SCHOOL OF SCIENCE AND TECHNOLOGY, NIIGATA UNIVERSITY, NIIGATA, JAPAN

For the Degree of Doctor of Philosophy

In

SCIENCE

By

LAKSHMANAN SREEHARI

F17N502G

(Supervisor: **Prof. TSUYOSHI TOYOSHIMA**)

This page is intentionally left blank

To E.V. Kalyani

To the entire working-class community of the world, including my father and mother.

ABSTRACT (English)

Detailed understanding of the Archean crustal evolution will give vital clues about evolutionary mechanism of the early Earth. Only limited volume of Archean cratons are exposed in the Earth crust. Dharwar Craton (DC), southern India, is one among them. DC is the association of two cratonic blocks; Western Dharwar Craton and Eastern Dharwar Craton, separated by Gadag Mandya Shear Zone (GMSZ). Associations of 3.6–3.0 Ga Basement Gneiss, volcano-sedimentary basins (3.4–2.5) and granitic plutons (2.6–2.5 Ga) marks the lithological association in DC. Volcano-sedimentary basins are classified into Sargur Group (~3.4–3.2 Ga) and Dharwar Supergroup (~3.0–2.5 Ga). Understanding the evolutionary process of Dharwar Supergroup and its associated lithologies will give insight into the crustal growth process of WDC.

Detailed structural mapping in Chitradurga Schist Belt (CSB) and Kibbanahalli Schist Belt (KSB) of WDC was carried out. CSB has preserved Sargur Group, Basement Gneiss, Bababudan Group, Chitradurga Group and Hiriyur Group of rocks. Only Bababudan Group of rocks was dominant in KSB. Unconformable relation between Basement Gneiss-Sargur Group and Bababudan Group is defined by rift debrites type >1m size quartzite clast conglomerate or oligomict conglomerate of fluvial/shallow marine origin. A polymictic conglomerate separates Bababudan and Chitradurga Groups; similarly, Chitradurga and Hiriyur Groups are also separated by a polymictic conglomerate. A new zone, Akkanahalli Zone, in the eastern margin of the CSB is proposed which is belonging to Sargur Group. Zircon grains in the metatuff sample from this zone provide an age of 3313±6 Ma.

Six stages of deformation events are recognized in the study area. D_0 and D_1 events are related to sedimentation and peak metamorphism respectively. General trend and megascopic structures in the mapped area have resulted from D_2 event. The D_2 stage structure is distinctly characterized by a fold-and-thrust belt consisting of an NNW–SSE trending fold zone sandwiched between a pair of NNW–SSE trending thrust faults dipping east. Deformation during the D_3 stage resulted in regional-scale sinistral shear zones, such as N–S striking Gadag-Mandya Shear Zone, and

narrow N–S and NW trending sinistral ‘echelon’ shear zones. D_3 sinistral shearing and D_4 dextral shearing are preserved only as local scale deformation event in KSB but as regional scale event in CSB. Based on detailed field survey and structural analysis, it is proposed that CSB and KSB developed in an immature or failed rift setting where shallow marine sequence and shelf deposits are predominant. Debrites were first deposited at the foot of steep slopes of the rifts. Followed by sediments and volcanic rocks that were unconformably deposited horizontally above Basement Gneiss and later got deformed pointing to the temporal evolution of a fold-and-thrust belt from a narrow intracratonic basin. The structural relation, field association and tectonic processes in schist belts of WDC are evidently different from Cenozoic accretionary complex, for example, in Hokkaido, Japan. This emphasis the fact that evolutionary process in WDC is not directly connected to subduction related accretionary processes.

Trace element geochemical analysis of the mafic to intermediate rocks from the study area shows three Types of patterns. Type 1 has Nb-Ta negative anomaly, Type 2 has patterns similar to E-MORB and Type 3 has Zr-Hf positive anomaly. LREE depleted trend is present in Type 1, whereas relatively flat LREE patterns are observed for Type 2 and 3. HREE pattern in some of the samples are flat with one exception. The geochemical variations are related to the degree of crustal contamination experienced during their eruption in connection with the intracratonic extension.

Post-3.0 Ga crustal growth throughout the Western Dharwar Craton can be summarized as three separate events of inversion tectonics. These stages are consisting of three generations of intracratonic failed rift events and three stages of crustal shortening and associated uplifting events (convergence). First rifting event is associated with evolution of Bababudan Group (~2.7–2.6 Ga). Second stage rifting is connected Chitradurga Group’s evolution (~2.6–2.58 Ga) and final or third event rifting is related to Hiriyur Group formation (2.58–2.54 Ga). WDC has strongly been shortened and many fold-thrust belts have been formed, by the third stage of crustal shortening and uplifting event. Mafic to intermediate volcanisms during failed rift events and post-rifting granitic intrusions triggered by the intracratonic

rifting contributed significantly on crustal growth processes in WDC. Mafic to intermediate magmatism and sedimentary supply associated with intracratonic rifting played a crucial role in thermo-chemical balancing of Archean mantle beneath DC. Failed rifting events played a pivotal part in the initiation of crustal growth process in Archean to Phanerozoic tectonic settings. Evidences for failed rifting events are well preserved from the Archean to Phanerozoic.

ABSTRACT (Japanese)

初期地球の進化メカニズムを理解するには，太古代後期の地殻進化を明らかにすることが必要不可欠である。そのための重要な研究対象の１つがインド南部の Dharwar（ダールワール）クラトン（以下，DC）である。DC は，Gadag Mandya（ギャダッグマンディア）剪断帯で区切られた西 Dharwar クラトン（以下，WDC）と東 Dharwar クラトン（以下，EDC）からなり，3.6–3.0 Ga の基盤片麻岩・3.4–2.5 Ga の変堆積岩帯・2.6–2.5 Ga の花崗岩質プルトンから構成される。変堆積岩帯を構成する地層は，3.4–3.2 Ga の Sargur（サルグール）層群と 3.0–2.5 Ga の Dharwar 超層群に分けられる。Dharwar 超層群とそれに関連した地層・岩石の進化プロセスを理解することで，WDC の地殻成長プロセスを理解することができる。

本研究では，WDC の Chitradurga 片岩帯（CSB）と Kibbanahalli 片岩帯（KSB）を主な研究対象とし，詳細な地質図・構造図の作製と構造解析を行った。 CSB は，Sargur 層群，基盤片麻岩，Bababudan（ババブーダン）層群，Chitradurga（チトラドゥルガ）層群，Hiriyur（ヒリユール）層群からなる。KSB は，Bababudan 層群のみから構成される。基盤の片麻岩- Sargur 層群と Bababudan 層群間の不整合は，直径 1m 以上の珪岩礫からなるリフト性のデブライトタイプ礫岩によって，または河成/浅海成起源の oligomict 礫岩によって規定される。Bababudan 層群とその上位の Chitradurga 層群，さらに Chitradurga 層群とその上位の Hiriyur 層群 はそれぞれ Polymictic 礫岩によって境される。CSB の東端には，Sargur 層群からなる Akkanahalli 帯が新たに定義される。この帯の変凝灰岩サンプルのジルコンから，3313±6 Ma の年代が得られた。

本調査地域において 6 ステージの変形イベントが識別された。D0 および D1 イベントは，それぞれ，地層の堆積期および変成作用のピーク期に対応する。調査地域の一般走向（トレンド）と大構造は主に D2 イベントによって形作られた。D2 ステージの構造は NNW-SSE トレンドの褶曲・衝上断層帯によって特徴付けられる。この D2 褶曲・衝上断層帯は２つの NNW-SSE 走向東傾斜の衝上断層の間に挟まれた NNW-SSE トレンドの褶曲帯から構成

される。D3 ステージの変形作用は，N–S 走向の Gadag-Mandya 剪断帯や N–S または NW–SE 走向で雁行配列する狭長な左横ずれ剪断帯を形成させた。D3 左横ずれ剪断変形と D4 右横ずれ剪断変形は，KSB では局所的な変形イベントとして生じたが，CSB では広域的なイベントとして生じている。

詳細な野外調査と構造解析に基づき，CSB と KSB は，主に浅海成シーケンスや陸棚堆積物を堆積させるような未成熟リフトあるいは failed rift として発達したことが明らかとなった。最初，リフトの急斜面の麓にデブライトが堆積するとともに，堆積物と火山岩がリフトを埋積し，さらに基盤の片麻岩の上にオーバーラップして水平に不整合に堆積した。その後，クラトン内の狭長なリフト帯から褶曲・衝上断層帯（片岩帯）へと変貌した。WDC の片岩帯の岩石構成・地質構造・それらの造構過程は，日本の，例えば北海道の新生代付加体のそれらとは明らかに異なっている。これは，WDC の進化過程が沈み込みなどの付加過程に直接関連していないことを強く示唆している。

本調査地域の苦鉄質～中間質岩の微量元素パターンは 3 つのタイプに分けられる。タイプ 1 は Nb-Ta 負の異常を示し，タイプ 2 は E-MORB に似たパターンを持ち，タイプ 3 は Zr-Hf 正の異常を示す。タイプ 1 は LREE が減少するトレンドを示すのに対し，タイプ 2 および 3 は比較的フラットな LREE パターンを示す。一部のサンプルにおける HREE パターンは，一つの例外を除いて，フラットである。これらマグマの地球化学的多様性は，クラトンの伸長テクトニクスに関わる噴火の際に起こった，マグマの地殻汚染の程度の違いを反映していると考えられる。

3.0 Ga 以降の WDC における地殻の成長は，クラトン内の３回の failed rift イベント（伸張テクトニクス）と３回の短縮・隆起テクトニクス（ポストリフトイベント）が繰り返す中で起こったと結論できる。すなわち，３回の反転テクトニクスによる結果である。最初のリフトイベントは，Bababudan 層群（～2.7–2.6 Ga）を堆積させ，太古代後期の地殻成長開始の引き金になったと考えられる。二番目のリフトイベントは Chitradurga 層

群（約 2.6〜2.58 Ga）を堆積させ，最後のリフトイベントは Hiriyur 層群（2.58〜2.54 Ga）を堆積させた。シンリフトの伸張テクトニクス時には苦鉄質〜中間質の火山活動が起こり，ポストリフトの短縮・隆起テクトニクス時には花崗岩の広域的貫入が起こって，それぞれ地殻を成長させた。苦鉄質〜中間質のマグマ活動とクラトン内リフト形成に関連する堆積物供給は，DC の下の始生代マントルの熱化学的バランスに重要な役割を果たしたと考えられる。３回目の短縮・隆起テクトニクスにおける地殻短縮は極めて大きく，WDC 内に褶曲・衝上断層帯を発達させた。以上のように，太古代後期の WDC における大陸地殻成長プロセス・メカニズムにおいて，同様に太古代から顕生代における大陸地殻成長初期において，failed rift イベントが極めて重要な役割を果たしたことが明らかとなった。

Table of Contents

List of Tables

List of figures

ACKNOWLEDGEMENTS

It has been my pleasure to be supervised by Prof. Tsuyoshi Toyoshima; it is impossible to thank him enough here for the time and effort he invested in this project. His hard work for bringing the financial support both for this project and scholarship are also deeply acknowledged. Sincere thanks to my co-supervisor Prof. M Satish–Kumar for all the encouragement, financial support and proper advice. Help and lessons from my co-supervisor Dr. Hayato Ueda especially during zircon analysis are also deeply acknowledged. I find all of them exceptional researchers and inspirational human beings and hope I will meet your expectations in my scientific career.

Thanks to Prof. Sajeev Krishnan, IISc, Bangalore, for being an unofficial guide and mentor throughout my journey. You influenced and changed the direction of my life and for which I will be forever grateful.

All the staff in the Department of Geology, Niigata University are sincerely thanked. Takazawa-Sensei is thanked for his important discussions and suggestions. Toshiro-Sensei's support especially during the fieldwork in Shimoga and during geochemical analyses is specially acknowledged. Kurihara-Sensei is thanked for important discussions during the fieldwork in India. Kenta-Sensei is also thanked for his suggestions. Staffs in International Office and Graduate School of Science and Technology are also sincerely acknowledged.

I thank Dr. Silpa for her unconditional support starting from the very first day I arrived in Japan. I sincerely appreciate the efforts of Katori-San, who helped me during my initial days in Japan. I thank the sincere support from fellow graduate students in Geology department, especially Nabeshyun, Keisuke and Yamada. I would like to express my appreciation to former and present members of structural seminar and special thanks to Ayu and Kanno for timely help and support. Sincere gratitude to Kiran, Sam, Dr. Sayantani, Dr. Anupam and all my football mates in Niigata.

All my family members are thanked for their exceptional support and you all are my biggest inspirations. Special mention to my sister Sreelakshmi

who was always there to attend my nonsensical phone calls, you are amazing!

Dr. Vinod Samuel and Vinod P.G. are two people who always backed me up and talked to me, really appreciate their genuine support.

Durga, Kavya, and Veni three exceptional girls in my friend list are sincerely thanked for their unconditional love and inspiration, the world needs more people like you. Special thanks to Durga for the assistance in writing the thesis.

Friends in IISc Bangalore are deeply appreciated for overwhelming assistance during fieldwork. Justin, Dr. Raj Kumar, Jaseem, Athira, Thanooja, Nidhiya, Appu, Claude, Kiso, Prakash and Thamam all helped during fieldwork, sample sending and necessary arrangements. Thanks for carrying all those samples and driving the car, without that my fieldwork would have been incomplete.

Comrades in CUSAT, Payannur College and Vellora are thanked for endless love, care and support in my life. I enjoyed best part of my life with you. Teachers in Payannur College especially Prof. K.C. Muraleedharan, Dr. Padmanabhan Kavumabai and Sona Rajeevan are thanked for having faith in me. My teachers and friends in TMHSS Vellora are also appreciated for their amazing support and motivation.

Funding agencies in all those projects, which I involved, are thanked. Japan Government and MEXT are acknowledged for providing me scholarship and an opportunity to study in Niigata University.

Finally, sincere gratitude and support to the whole world and medical staffs who are fighting against the pandemic. Hope everything will be normal soon. Thesis writing during the pandemic was not an easy task. Everything went smooth only because of the wonderful people I am surrounded with. I thank all of them once again.

PREFACE

This thesis project started in 2016, when I was a research student in Niigata University. In 2017 I joined Graduate School and from there onwards I got three years to complete this project. The basic idea was to understand the crustal growth mechanism in Archean rocks giving emphasis on structural geology. The fundamental necessity for this kind of a project is proper geological map and extensive fieldwork. Mutual relation between IISc, Bangalore and Niigata University played a crucial role in the completion of the elaborative fieldwork and hence this project. JSPS-DST funding also had a vital role in shaping this work. The first goal of the thesis project was to develop a proper geological map in the southern part of Dharwar Craton giving emphasis to contact relation between strata. The basic field observation and extensive literature review gave the idea of failed rifts and fold-and-thrust belt. The fact that I was staying near a failed rift basin in Niigata also eased my thought process. Failed rifts are 'infant rifts', which 'died' before reaching their maturity level i.e. an ocean. Evidences for episodic failed rift events and a later fold-and-thrust formation are well preserved in my geological map and structural interpretations (Chapter 2). Extension of stable basement and associated narrow basin with mafic volcanic rocks is mapped and presented in Chapter 3. Geochemical characteristics of these rocks are also having signatures of an intracratonic rift setting (Chapter 3). Chapter 2 and Chapter 3 are leading the discussion to the role of failed rifts in crustal growth of Archean Cratons and their role in crust-mantle interaction. Role of failed rifts in temporal evolution of volcano-sedimentary basins in Dharwar Craton is summarized in Chapter 4. Differences in the structure and stratigraphy of failed rifts and accretionary complexes mentioned in the same chapter. Final chapter also addresses the role played by failed rifts in the overall crustal evolution. Tables mentioned in all chapters are provided after the references and in appendix some important route maps that I prepared are also presented.

My final words of advice to you are educate, agitate and organize. Have faith in yourself…

For ours is a battle not for wealth or for power. It is battle for freedom. It is the battle for the reclamation of human personality.

Dr. B.R. Ambedkar

Chapter 1

1 INTRODUCTION

1.1 A general introduction to recent progress in Archaean tectonics

The evolution of the Earth since its formation *ca*. 4.5 Ga has been very dynamic and complex. We learn about the geological transformation of the Earth into its present state by studying the Archaean terranes and from the processes that operates today. The Archaean eon thus is an important segment in the evolutionary history of the Earth. Although about 60% of Earth's crust was emplaced during this time (Rudnick, 1995; Taylor and McLennan, 1995), the Archaean crust expanses only 7–11 million km^2 (Bleeker, 2002, **Fig. 1.1**) of the total exposed crust, which is only 5–7.5% of the total volume of the crust generated. According to Dhuime at al., (2018) 60–80% volume of the crust present now had been produced by 3.0 Ga.

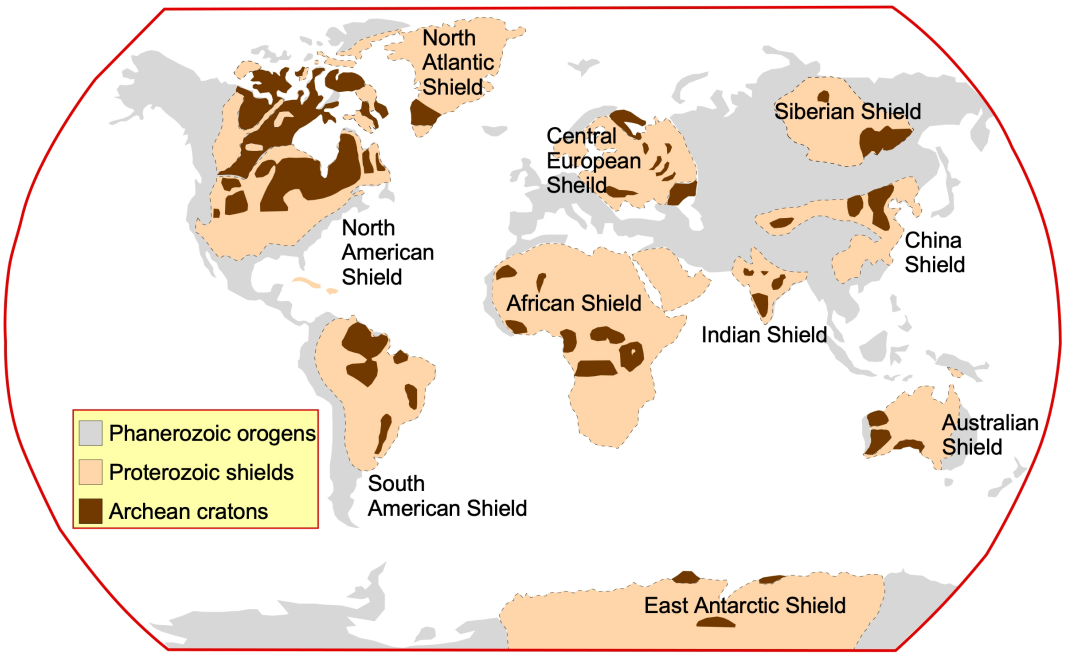

Figure 1.1 *Distribution of Archean Cratons around the globe (Modified after Furnes et al., 2014).*

Experimental and geochemical results show that the Archaean continental crustal growth was induced by the partial melting of tholieitic basalt (Martin, 1999). This view is geologically supported by the dominant presence of tonalite-trondhjemite-granodiorite (TTG) basement in Archaean granite-greenstone and gneissic terrains (Condie, 1981). There are several

models proposed along the past many decades to explain the formation of TTG's and their related tectonic settings. Some researchers suggest that TTGs were formed due to early Earth subduction processes and connected partial melting of hydrated basaltic oceanic slab/crust (e.g., Barker and Arth, 1976; Martin, 1986,1999). This view is highly related to the compositional affinity towards Cenozoic subduction related adakites. However, Smithies (2000) pointed out that the silica and magnesium content in global TTGs is not in agreement with the modern day adakites. Adakite suites are mainly the product of slab-melt mantle interaction represented by its high-Mg low-Si composition and most of the TTGs worldwide does not preserve such evidences. Smithies (2000) pointed out that most of the TTG suites hence do not provide evidences for modern style subduction processes and possibly has resulted from the melting of hydrous basaltic material at the base of a thickened crust. Johnson et al. (2017) demonstrated that the TTGs could form at the base of a thick plateau like basaltic crust through partial melting along a high geothermal gradient considering the TTGs associated with Coucal basalts in the East Pilbara, Western Australia as an example. Corollary of this finding suggests that subduction related process is not required for the growth of Archean proto-continents. These TTG's are overlaid by bimodal volcanic and sedimentary rocks collectively known as 'greenstone belts' (Anhaeusser, 2014). There are two schools of thought regarding the formation of greenstone belts: one is based on the a) 'modern style' plate tectonics and the other relies on gravitational forces related b) 'sagduction'.

a) The continental extension related bimodal volcanism model is proposed by Bruke et al., 1985 to explain the genesis of greenstone belts deposited above the stable continents. Continental extension related volcanic and tectonic processes are documented from different cratons around the globe based on detailed geological mapping, stratigraphic studies, geochemistry and geochronology of the bimodal volcanic rocks. Some examples include Kaapavaal Craton (Bruke et al., 1985, Humbert et al., 2020), Rae Province (Hartlaub et al., 2004), Superior Province

(Sappin et al., 2018) Humbert et al., 2020). In line with the previous studies, it is clear that, understanding of the tectonic history of the 'greenstone belt' allows us to clarify the 'turning point' of the evolutionary process in the early Earth.

b) The Pilbara Craton in Australia is explained using sagduction models (Van Kranendonk, 2002). According to Van Kranendonk et al., 2004, Collins and Van Kranenedonk, 1998, the granitoid domes and associated synclines of volcanic and sedimentary rocks in the East Pilbara Craton are a product of partial convective overturns. Similar gravity associated overturned sequences are reported from Superior Province (Lin et al., 2013), NW Scotland (Johnson et al., 2016), southern Slave Province (Ketchum et al., 2004) and Dharwar Craton (Chardon et al., 1996, 2000).

Understanding the genetic history of Archaean greenstone belts can answer important questions about the early stage crustal growth on the Earth. Advancements in the geological and geochemical studies of the greenstone terrains have made significant implications in mineral exploration and economic geology.

Regardless of the process of formation and its subsequent evolution, the Archaean crust is remarkably different from the geologically more complex post-Archaean continental crust (Brown et al., 2020) and Archaean tectonic movements are significantly different from the Phanerozoic or recent tectonic activities observed. The crust formed during the Hadean to Archaean period is inferred to be thinner than the post-Archaean crust and it is studied that the rate of crustal generation and recycling has been the same even before 3.0 Ga (Korenaga, 2018). Brown et al., 2020 suggests that Late Archaean period, post 3.0 Ga marks the onset of modern style plate tectonics on the Earth. The Archaean-Proterozoic transition between 3.0 and 2.5 Ga is regarded as the time when substantial changes occurred on the Earth in terms of crustal processes (Nicoli et al., 2016). Several researchers consider that this time in the Earth's history marks the onset of plate tectonics (e.g. Belousova et al., 2010; Dhuime et al., 2017). The detritus supply to the convergent zones increased tremendously during this time,

thus resulting in the reworking of existing landmass (Valley et al., 2005; Nicoli et al., 2016). Previous studies show that, crucial geological and geochemical changes on the Earth occurred between 3.0 and 2.0 Ga (Condie, 2018) and these changes can be directly attributed to the initiation of plate tectonics (Dhuime et al., 2012, Dhuime et al., 2017).

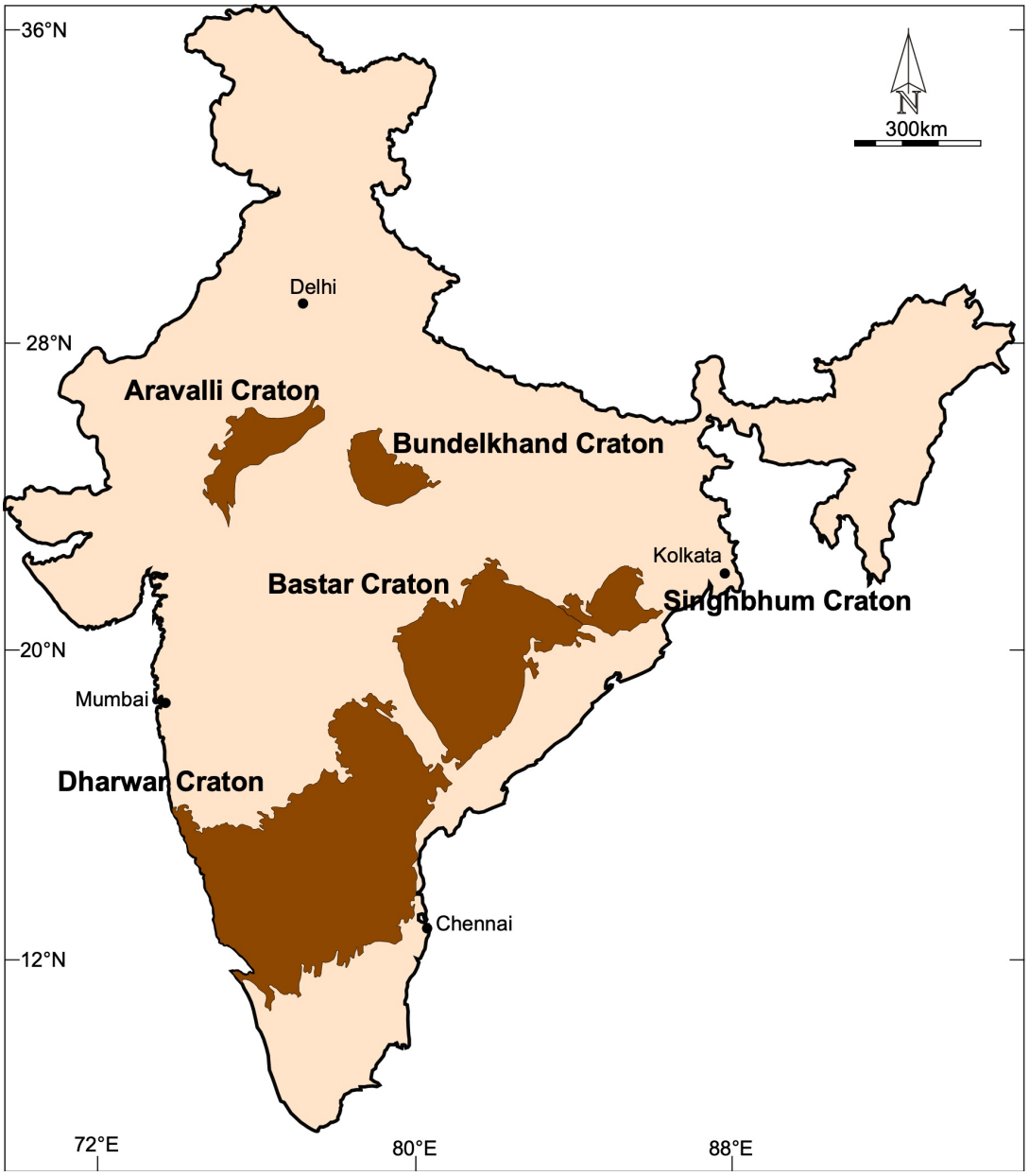

Figure 1.2 *Distribution of Archean Cratons in India*

Advancement in modelling techniques have produced better conceptual models that help us understand the tectonic settings and processes during Archaean (Dhuime et al., 2017, Korenaga et al., 2018). Field-based geological studies are necessary to test and evaluate these proposed models.

The Indian subcontinent is one of the most geologically fascinating continental fragments, with rocks ranging in age from Early Archaean (in Cratons) to recent sediments. There are five major Archaean cratons, Dharwar, Bastar, Singhbhum (southern block) Bundelkhand and Aravalli (Northern Block) cratons (Ramakrishnan and Vaidyanadhan, 2010) (**Fig. 1.2**). The Dharwar craton in southern India is a well exposed Archaean craton overlaid by Meso–Neoarchaean, unmetamorphosed or slightly metamorphosed granite-greenstone belts. In this thesis, I present a field-oriented study of Dharwar craton to evaluate the tectonic models proposed to explain Archaean tectonics.

1.2 A review of Dharwar Craton (DC)

Dharwar Craton (DC) in southern India (**Fig. 1.3a**) is bounded by Eastern Ghats and Arabian Sea to the east and the west respectively. The northern boundary is marked by the Deccan basalts, and the Southern Granulite Terrain (SGT) marks its southern limits (**Fig. 1.3b**).

DC has been studied extensively since late 19th century. Neptunian and Huttonian schools of thought were applied to understand DC geology in the earlier studies (Ramakrishnan and Vaidyanadhan, 2000). R. Bruce Foote and W.F Smeeth put forward two opposing but fundamental classification systems of rocks in D.C. R. Bruce Foote classified the rocks into gneisses and unconformably overlying auriferous schistose rocks (Foote, 1915), while W.F Smeeth called the gneisses, 'Peninsular Gneisses' and proposed an intrusive relationship of them with schistose rocks. Clarification for this debate and the nature of basement gneisses in Western Dharwar Craton was established by S. Iyengar (1920), Pichamuthu (1947, 1967), Rama Rao (1940, 1962), and B. Chadwick. R. Srinivasan, S.M. Naqvi and K. Saha published articles in 1930's that suggested intrusive nature of 'Peninsular Gneiss'. Swami Natha and Ramakrisnan (1981) and D. C. Chadwick et al. (1996,1997) proposed the popular stratigraphic classification of DC. Advancement in geological studies contributed significantly in understanding of DC geology in the 21st century. Recently, number of reviews on Dharwar geology summarized all these advancements (Jayananda et al., 2018, 2019,

2020; Krapez et al., 2020; Manikyamba and Ganguly, 2020; Ram Mohan et al, 2020, Raju and Mazumder, 2020).

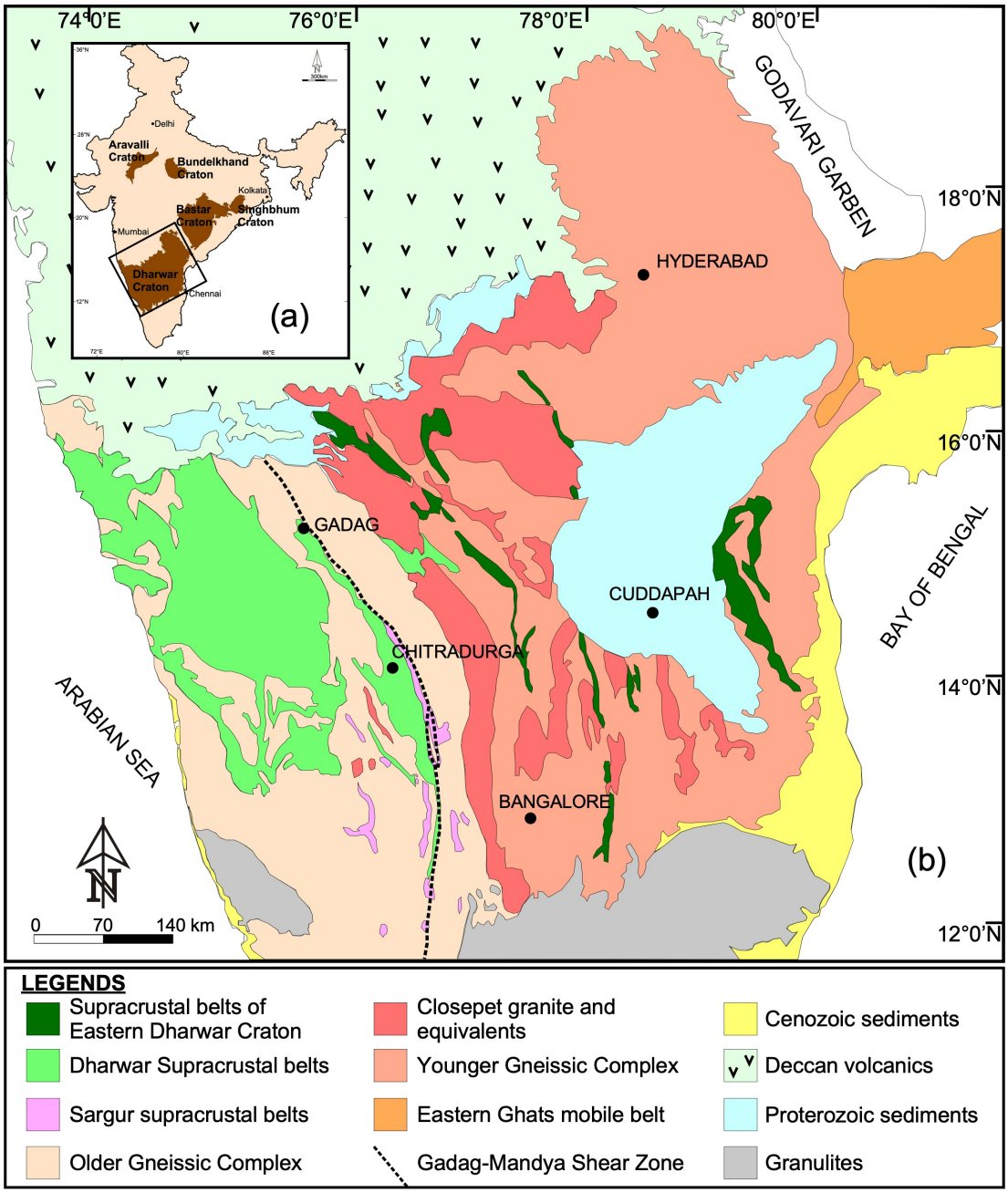

Figure 1.3 *(a) Distribution of Archean Cratons in India (b) Regional-scale sketch map of Dharwar Craton.*

The Dharwar Craton is divided into Western Dharwar Craton (WDC) and Eastern Dharwar Craton (EDC) based on the age, metamorphism, lithology and geophysical studies (**Fig. 1.3b**) (Swami Natha and Ramakrisnan, 1981; Chardon et al., 2007; Jayananda et al., 2013; Vijay Rao et al., 2015). Recent literatures have introduced another segment—Central Dharwar Craton (CDC,

Peucat et al., 2013; Jayananda et al., 2013, 2018, 2020). In this thesis, I will follow the classical two-division style of DC as structural and field evidence for a lithological boundary between CDC and EDC is not distinctly identified yet. On the other hand, WDC and EDC are separated by well-defined mylonitic shear zone called Chitradurga Shear Zone (CSZ, Chadwick et al., 2000) or Gadag Mandya Shear Zone (GMSZ, Sreehari and Toyoshima, 2020). I follow the later nomenclature since it is the conventional style followed for a strike-slip shear zone i.e. mentioning the starting and the ending locations of the shear zone.

Major lithology of the DC can be summarized into three rock types— i) older Basement Gneiss, ii) two generations of volcanosedimentary sequences; namely Sargur group (>3.0 Ga) and Dharwar Supergroup (<3.0 Ga), and iii) 2.7–2.5 Ga calc-alkaline – High-K granitoids (Jayanada et al., 2013; Jayanada et al., 2018, 2020; Krapez et al., 2020; Raju and Mazumder; 2020; Ram Mohan et al., 2020). The summary of age distribution in WDC and EDC are shown in **Figure 1.4.**

Basement Gneiss with inherited zircon ages up to 3607±16 Ma is reported (Guitreau et al., 2017) from WDC. This is the oldest reported agefrom DC. Jayananda et al. (2018) reviewed temporal change in the evolution of granitoid rocks in DC. Authors mentioned chemical and evolutionary histories of TTGs, Sanuktoids and intrusive granites that formed within the time span of 3.60–2.50 Ga. Five major epodes of magmatism are documented by Jayananda et al. (2008) at 3.45–3.30 Ga, 3.23–3.15 Ga, 3.00–2.96 Ga, 2.70–2.60 Ga and 2.56–2.50 Ga. Major populations of last two stages granitoids (2.70–2.60 Ga and 2.56–2.50 Ga) are concentrated in EDC (**Fig. 1.4**).

Sargur Group, the oldest volcano sedimentary sequence in DC is characterised by the presence of ultramafic rocks and it is represented by narrow, linear and dismembered schist belts. Major Sargur Group of rocks is identified in schist belts such as Holenarsipur, Nuggihalli, J.C.Pura, Sargur, Banasandra, K.R. Pet, Ghattihosahalli, Nagamangala and Javanahalli (Ramakrishnan and Vaidyanathan, 2008). Komatiite, serpentinite, dunite, and chromite are the major ultramafic–mafic rocks reported from Sargur Group

(Hokada et al., 2013; Jayananda et al., 2008). Sm-Nd age obtained for Sargur Group komatiite is 3352±110 Ma (Jayananda et al., 2008), while Sm-Nd age for Banasandra belt komatiite is 3137±190 (Maya et al/. 2016) and that of Nuggihalli komatiite is 3125±120 Ma (Mukherjee et al., 2012). Zircon U-Pb age of felsic tuff from Holenarsipur Belt is 3298±7 Ma (Peucat et al., 1995) and from the eastern part of Chitradurga Schist Belt is dated to be 3318±13 Ma (Sreehari and Toyoshima, 2020). Recent literature reported Sm-Nd age of intrusive ultramafic rock from Nuggihalli and Holenarsipur of

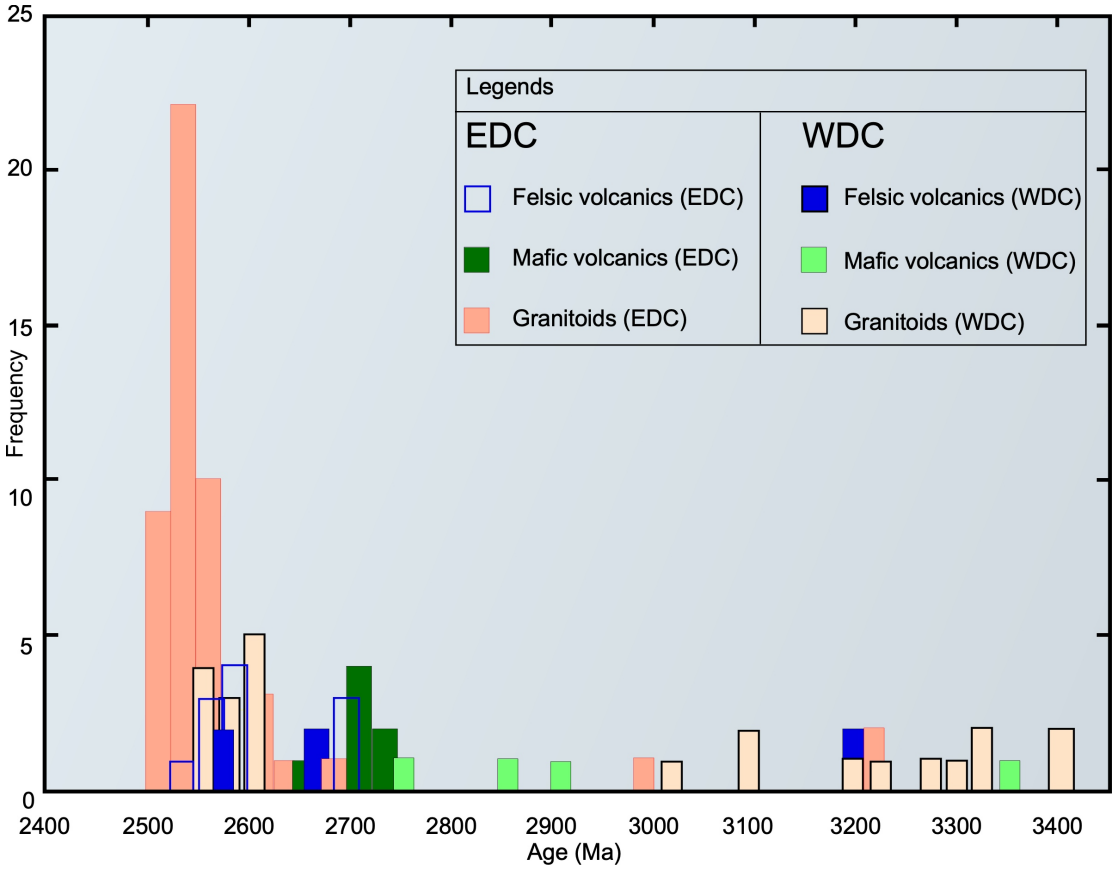

Figure 1.4 *Distribution of volcanic ages in Dharwar Craton (Modified after Ram Mohan et al., 2020)*

Sargur Group as 2934±88 Ma (Patra et al., 2020). Based on this Patra et al. (2020) argued that Sargur Group is an older ultramafic equivalent of Dharwar Supergroup. During my fieldwork, I observed that Sargur Group shows an intrusive relationship with Basement Gneiss and moreover there is a regional scale unconformity separating Sargur Group and Dharwar Supergroup as mentioned in many of the previous literature (Chadwick et al., 1985, Hokada et al., 2013, Krapez et al., 2020 and references there in).

Dharwar Supergroup is divided into Bababudan Group and Chitradurga Group (Radhakrishna and Naqvi, 1986). Detailed discussion about the classification of Dharwar Supergroup and its lithological association is presented in *Chapter 2*.

1.3 Previous tectonic models proposed for the formation of DC

1.3.1 Non-uniformitarian style tectonic evolution

Series of literatures interpreted the schist belts in DC to have been formed by gravity driven tectonic movements without any crustal shortening in regional scale. This process is called 'sagduction' tectonics or vertical tectonics as it involves passive sinking of the cover rock into the basement. This hypothesis is applied to different schist belts of the DC such as Bababudan Schist Belt (Chardon et al., 1998), Chitradurga Schist Belt (Chardon et al., 2008), Kibbanahalli 'Arm' (Chardon et al., 1996) and Kolar Schist belt (Chardon et al., 2002). Vertical tectonic models were used to explain the growth of 'dome and basin' structures in entire DC (Choukroune et al., 1997). Above mentioned studies argue that no crustal thickening took place in the Archaean terranes including DC, instead, crustal growth was facilitated by diapirism (**Fig. 1.5a**). The same authors have driven the further development on the subject by introducing the 'lateral constrictional flow' (LCF) induced crustal growth models in DC (Chardon et al., 2008, 2011). 'Lateral constrictional flow' insist on three-dimensional flow of hot orogeny that combines orogen-normal shortening, lateral constrictional stretching and transtension. In summary, non-uniformitarian concepts explained DC and other Archaean cratons evolved in a non-tectonic style and hence differ with Phanerozoic tectonics and crustal evolution.

1.3.2 Transpression model

A sinistral transpression model was put forward by series of works by Chadwick and co-workers. This model interpreted WDC as a foreland to an accretionary arc in the east i.e. EDC (Chadwick et al., 2000, 2007). According to their model, batholiths represent accretionary arcs and schist belts in EDC are intra-arc

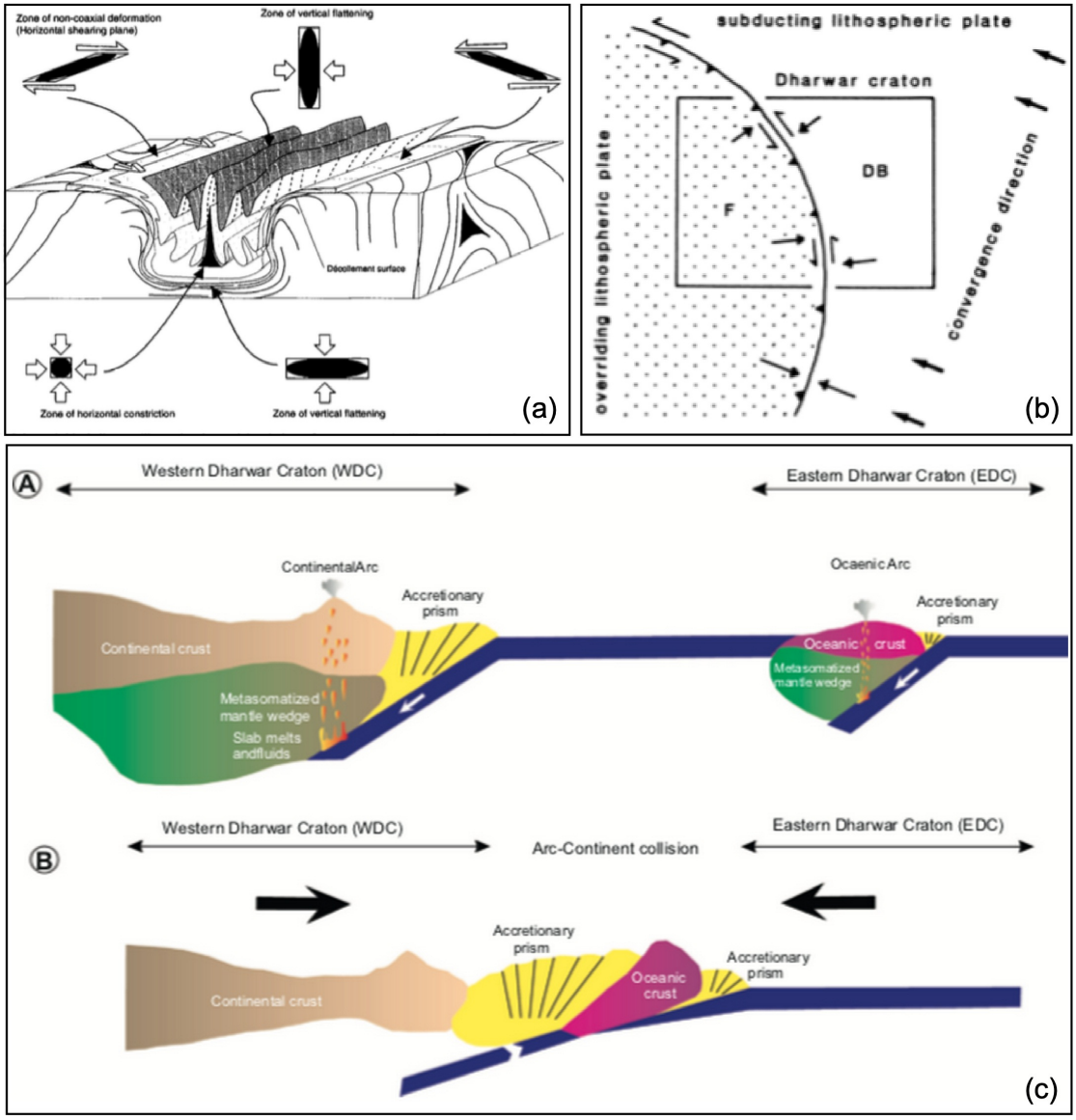

Figure 1.5 *Previous tectonic models for Dharwar Craton (a) Sagduction model (Chardon et al., 1996). (b) Transpression model by Chadwick et al., 2000 (c) Subduction related accretionary complex and associated arc magmatism (Manikyambaet al., 2014)*

basins (Chadwick et al., 2000). These plutonic belts originated in sinistral strike-slip regime and contemporaneous layer-parallel shortening also occurred in schist belts as in a transpression setting (**Fig. 1.5b**, Chadwick et al., 2003).

1.3.3 Accretionary Complex

Schist Belts in DC is mentioned as accretionary complex associated with subduction in many literatures. Basalts in the WDC are interpreted either as arc related or arc rifting related basalts (Manikyamba et al., 2012, 2013). A continental arc in WDC is postulated by the westward subduction of an oceanic crust (Manikyamba et al., 2014). Felsic rocks such as rhyolite, in WDC is interpreted to be a product of ocean-continent subduction while those in EDC is interpreted to be a result of ocean-ocean subduction (**Fig. 1.5c**, Manikyamba et al., 2014). Microcontinental amalgamation and two eastward subducting oceanic plate convergent margin model is proposed for the evolution the entire DC (Li et al., 2018). Multi-stage subduction and associated arc magmatic evolution of volcanic rocks are addressed as continental growth mechanism of DC (Gao and Santosh, 2020, Wang and Santosh, 2020). The same authors considered Sargur Group of rocks as obducted sequence and eastern boundary of CSB as suture zone. Most subduction models in DC are solely based on geochronological and geochemical interpretations.

1.4 Gaps in the area

Regional scale structural studies integrating field and micro-structure have been rarely carried out on any southern Indian terrains. Several

contradicting tectonic models were proposed from Chitradurga Schist Belt. The proposed multiple subduction zones and collisions of smaller island arcs-trench systems (Jayananda et al., 2013), continental plate collision (Chadwick et al., 2000), and sagduction (Chardon et al., 1996, 1998), models are contradicting each other mainly because of the underrating on the detailed large-scale structural information. Such controversies are also due to the confusion in understanding regional stratigraphy. Regional scale study on the composition, stages and timing of metamorphism, magmatic activity, and deformation behavior is required before concluding the tectonic model

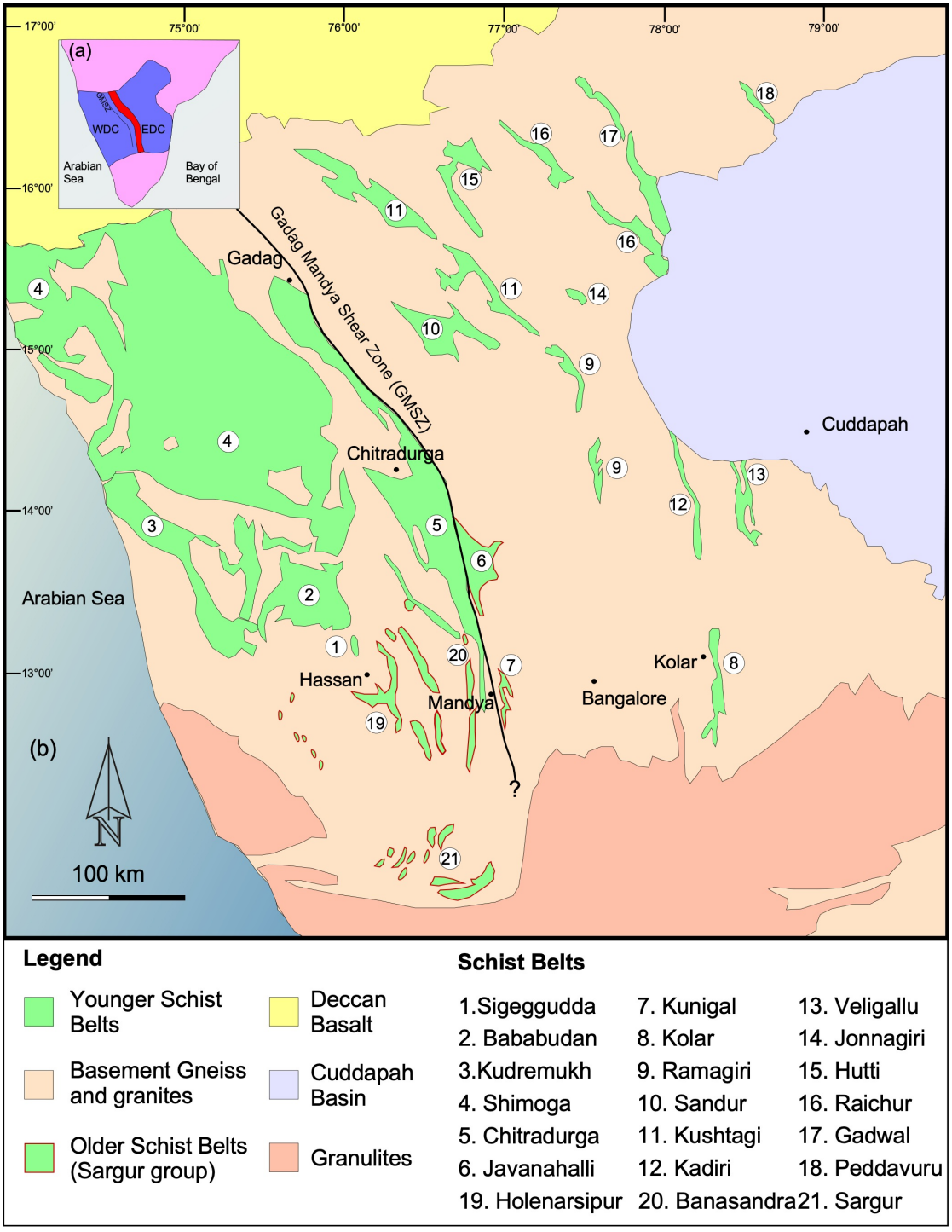

Figure 1.6 *(a) Simplified map of DC (b) Sketch map of schist belts in Dharwar Craton (modified after Jayananda et al., 2013)*

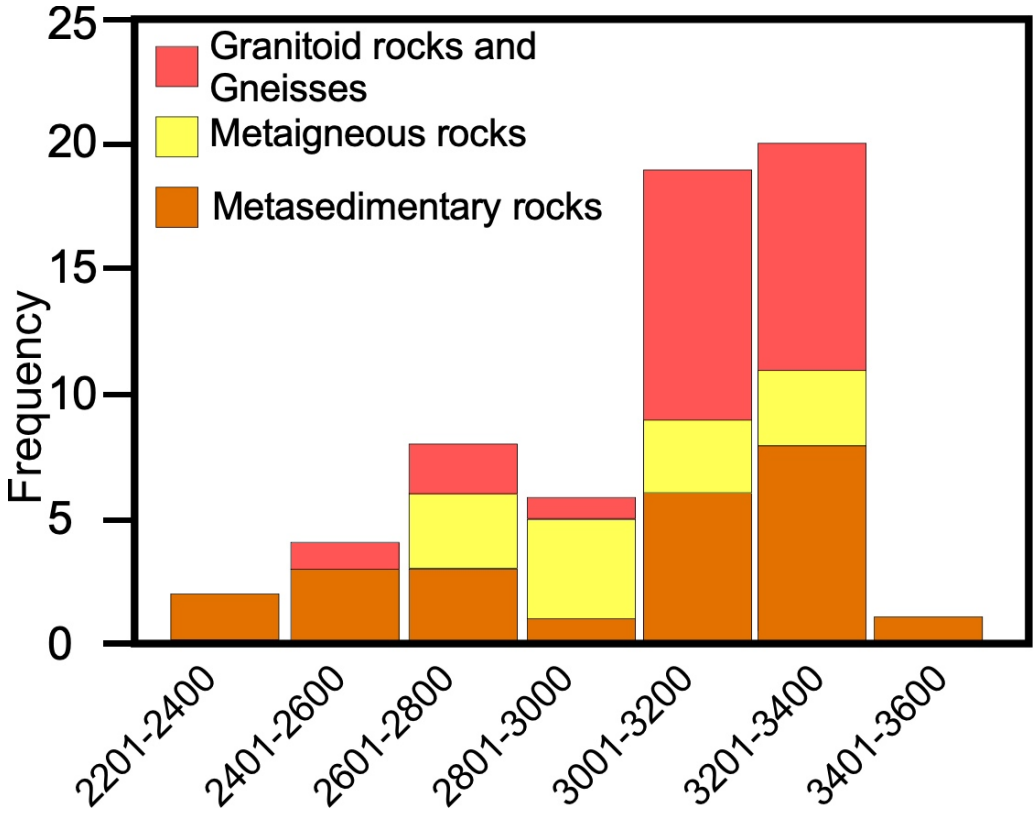

Figure 1.7 *Published ages in Western Dharwar Craton (modified after Patra et al., 2020)*

1.5 Objectives

To showcase the structural and stratigraphic evidences preserved for the 3–2.5 Ga crustal growth process. Based on the field and structural analysis, develop a structural model for Meso-neoarchean crustal growth. To compare these structures with structural relations in the Phanerozoic tectonic regime.

1.6 Layout of the thesis

Schist Belts of WDC and EDC are marked in the **Figure 1.6** and as it is clear from the figure, the volume of schist belts is large in WDC. As I mentioned in section 1.1, theme of my thesis is to evaluate the crustal growth process from 3.0–2.5 Ga. WDC cover ranges of ages from 3.6–2.6 Ga **(Fig. 1.7**). Therefore, in this thesis, I will focus my discussions on schist belts from WDC. Within WDC sketch map of schist belts where I carried out fieldwork are given in **Figure 1.7**. They are Chitradurga Schist belt, Kibbanahalli Schist Belt, Sigeggudda Schist Belt, Bababudan Schist Belt and Shimoga Schist

Belt (**Fig. 1.8**). In next chapters I will present detailed geological map, structural relations, deformation history, metamorphic relation, stratigraphy and geochemistry of the volcanic rocks from these schist belts with giving emphasis to Chitradurga Schist Belt(**Chapter 2**) and Kibbanahalli Schist Belt (**Chapter 3**). Then I will discuss the tectonic origin of these schist belts and tectonic origin of WDC.

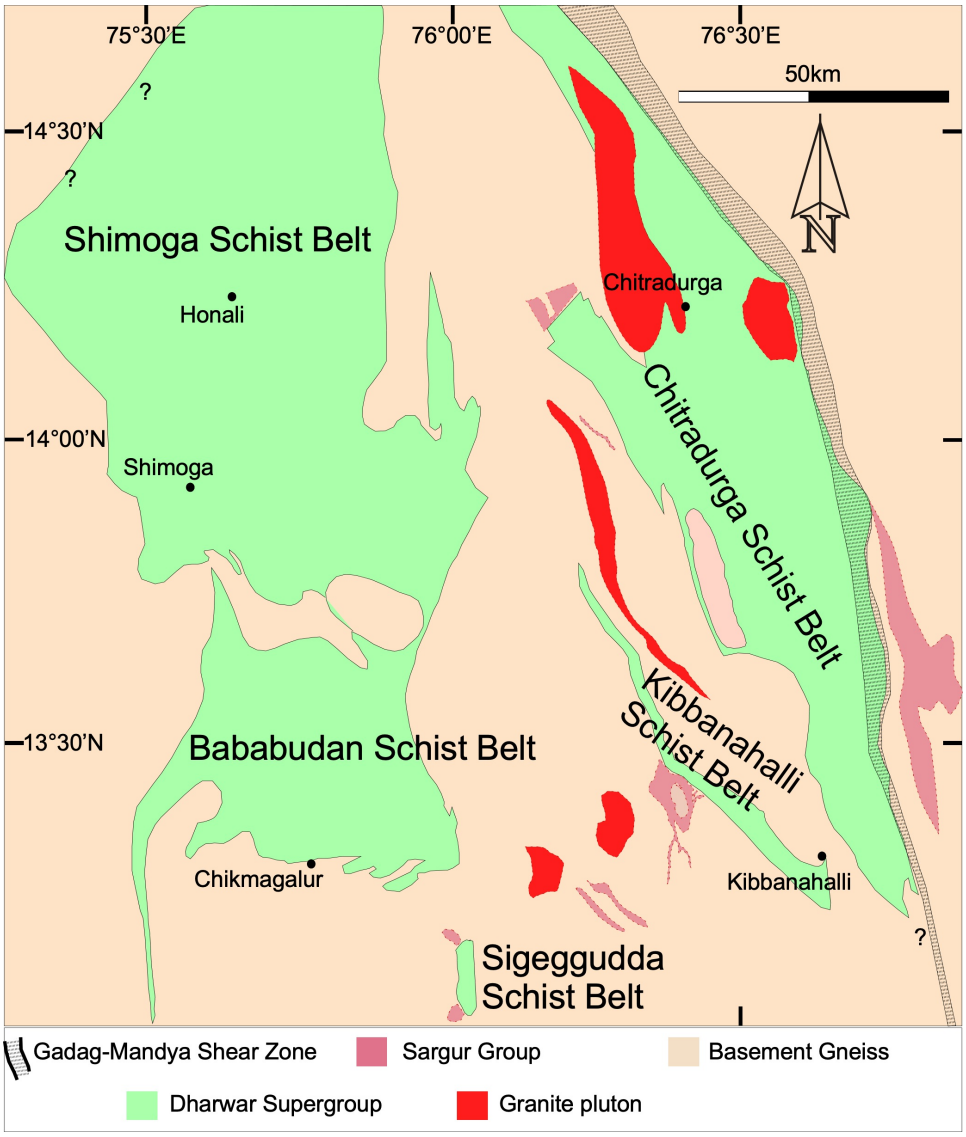

Figure 1.8 *Schist belts of Western Dharwar Craton, mapped and studied in this thesis*

Chapter 2

2 Geological and Structural evolution of southern part of Chitradurga Schist Belt (CSB), Western Dharwar Craton (WDC).

ABSTRACT

Detailed structural mapping in the southern part of Chitradurga Schist Belt (3.0–2.5 Ga) (CSB) distributed around the Chikkanayakanahalli-Kibbanahalli area was carried out. Sargur Group, Basement Gneiss, Bababudan Group, Chitradurga Group and Hiriyur Group of rocks are well preserved in the investigated area. Unconformable relation between Basement Gneiss-Sargur Group and Bababudan Group is defined by oligomict conglomerate with quartzite clast and occasionally preserve granite clast. A polymictic conglomerate separates Bababudan and Chitradurga Groups; similarly, Chitradurga and Hiriyur Groups are also separated by a polymictic conglomerate. A new zone, Akkanahalli Zone, in the eastern margin of the study area is proposed which is belonging to Sargur Group. Zircon grains in the metatuff sample from this zone provide an age of 3313±6 Ma. Six stages of deformation events are recognized in the study area. General trend and megascopic structures in the mapped area have resulted from the earlier two stages of deformations (D_2 and D_3). The D_2 stage structure is distinctly characterized by a fold-and-thrust belt consisting of an NNW–SSE trending fold zone sandwiched between a pair of NNW–SSE trending thrust faults dipping east. Deformation during the D_3 stage resulted in regional-scale sinistral shear zones, such as N–S striking Gadag-Mandya Shear Zone, and narrow N–S and NW trending sinistral 'echelon' shear zones. Based on my structural and field relationship it is proposed that CSB developed in an immature or failed rift setting where shallow marine sequence and shelf deposits are predominant. Sediments and volcanic rocks were unconformably deposited horizontally above Basement Gneiss and later got deformed together in a convergent setting resulted in fold-and-thrust belt along with strike-slip deformations.

2.1 Introduction

In this chapter I will explain the detailed geological and structural data for the southern part of CSB distributed in and around the Chikkanayakanahalli and Kibbanahalli area. Using this I will elucidate the structural and metamorphic evolutionary history of different groups of rocks distributed in the study area. Based on the field and structural evidence, I have interpreted the depositional and deformational history of the CSB and discussed the regional tectonic implications.

2.2 Geological background

CSB is exposed as about 450 km long linear NNW–SSE trending belt from Gadag in the north to Mysore in the south and has a maximum width of around 40 km in the central region (**Fig. 2.1a**). The stratigraphic column in CSB can be summarized in decreasing order of age as Sargur Group, Peninsular Gneiss, Dharwar Supergroup, and the younger granites. Rocks of the Dharwar Supergroup are unconformably overlying older Basement Gneiss with enclaves of the Sargur Group (Ramakrishnan and Vaidyanathan, 2010). Based on the stratigraphic relations the Dharwar Supergroup is divided into older Bababudan and the younger Chitradurga Group. Bababudan Group is separated from the Basement Gneiss by an oligomictic quartz-pebble conglomerate, informally known as 'Neralekatte Conglomerate' (Chadwick et al., 1981). The majority of the CSB is covered by the younger Chitradurga Group, which is separated from the Bababudan Group by a polymictic conglomerate (Ramakrishnan and Vaidyanathan, 2010). Traditionally, the Chitradurga Group is classified into three formations: Vanivilas Formation, Ingaldhal Formation, and Hiriyur Formation (Seshadri et al., 1981). Vanivilas Formation is composed of polymictic conglomerate, chlorite schist, limestone, and Mn-Fe formations. Ingaldhal Formation consists of basic, intermediate to acid volcanic and pyroclastic rocks. A greywacke-argillite sequence with BIF and metabasalts dominate in the Hiriyur Formation (Swaminath and Ramakrishnan, 1981). However, recent studies classified the Chitradurga Group into lower and upper units based on

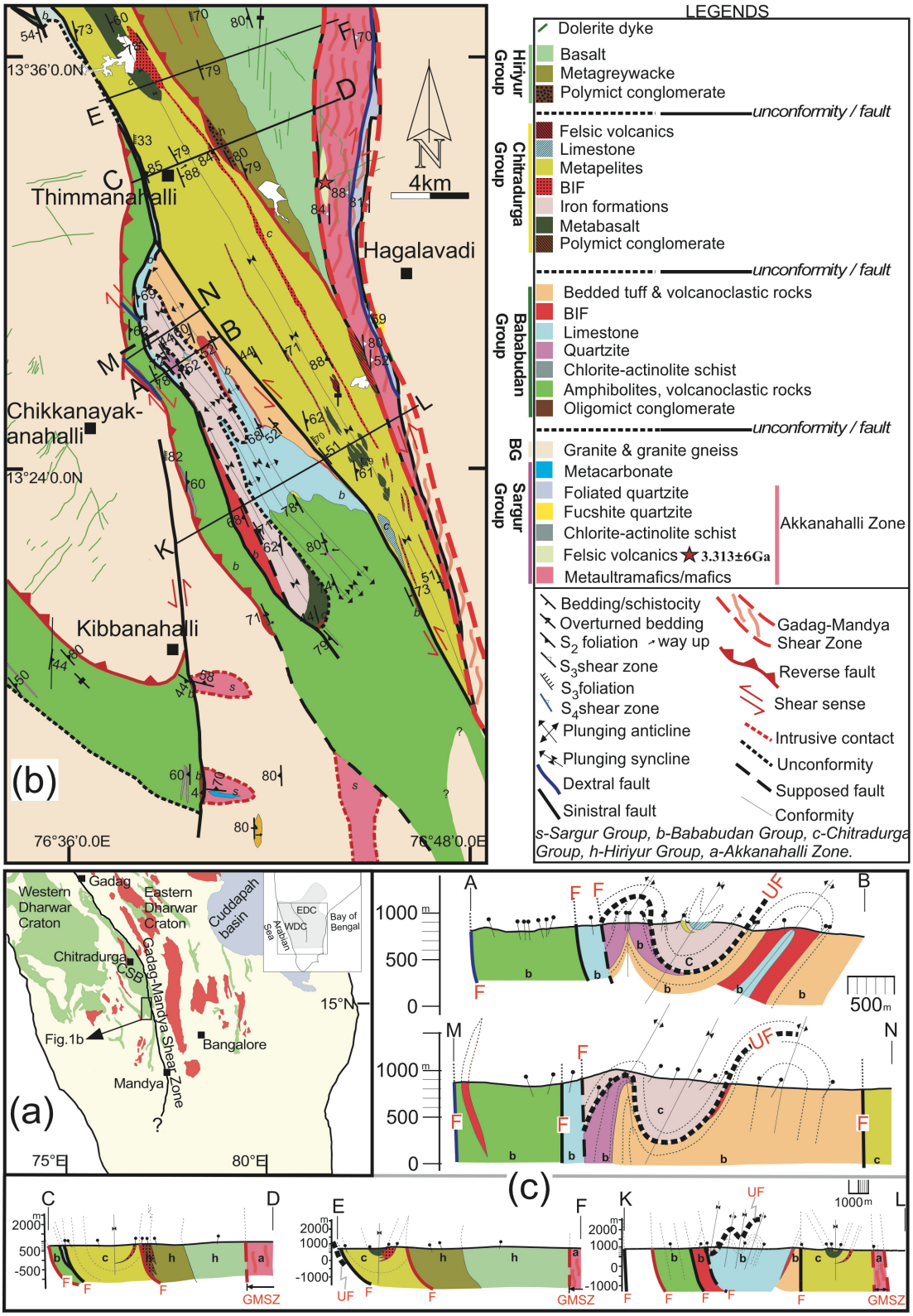

Figure 2.1 *(a) Generalized map, showing distribution of schist belts in Dharwar Craton. Mapped area of Chitradurga Schist Belt is marked in the rectangle. Position of Dharwar craton in south India also shown in the top right corner of the figure. (b) Detailed map of Chitradurga Schist Belt near*

Chikkanayakanahalli and Kibbanahalli area with legends and symbols. GMSZ and Akkanahalli Zone are marked separately. Location of felsic tuff sample analyzed for geochronology is marked by a star (c) Cross-section of marked locations (AB, CD, EF, KL, and MN) in the study area. Note the difference in horizontal length scales of two sets of cross-section (AB, MN and CD, EF, KL). Thin dash lines in the cross-section indicating trace of bedding and thick dash lines represent unconformity. Horizontal and vertical scales of cross-sections are provided. WDC, Western Dharwar craton; EDC, Eastern Dharwar Craton; BG, Basement Gneiss; F, fault; UF, unconformity; GMSZ, Gadag Mandya Shear Zone. Small black dots in cross sections represents sample points.

metamorphic grade and geochronological constraints (Hkada et al., 2013). Hiriyur Formation is separated from lower units (Bababudan Group, Vanivilas Formation, and Ingaldhal Formation) by an unconformity overlain by K.M. Kere conglomerate (Mishima et al., 2017).

My study area is located in the southern part of CSB (**Fig. 2.1a**) in and around Chikkanayakanahalli in the west and Hagalavadi in the east (**Fig. 2.1b**). This part of the schist belt is mentioned as Chikkanayakanahalli schist belt in some earlier studies (e.g. Radhakrishna 1983, Deavraju et al., 1986 and references therein). The detailed structural and geological maps were prepared for Doddaguni and Kondi areas, which are south of Chikkanayakanahalli, where multiple deformation stages were identified (Mukhopadyay et al., 1981). In this study, I prepared detailed geological and structural maps for an area of ca. 300 km^2 (**Fig. 2.1b**). Route maps across AB transect in **Fig. 2.1b** is given in **Appendix A1**

2.3 Field and structural relationship

The stratigraphic division that we followed in this study is mentioned in **Figure 2.2**, along with two other previous studies (Seshadri et al., 1981, Hokada et al., 2013). I propose three divisions for the Dharwar Supergroup of rocks namely Bababudan Group, Chitradurga Group, and Hiriyur Group in

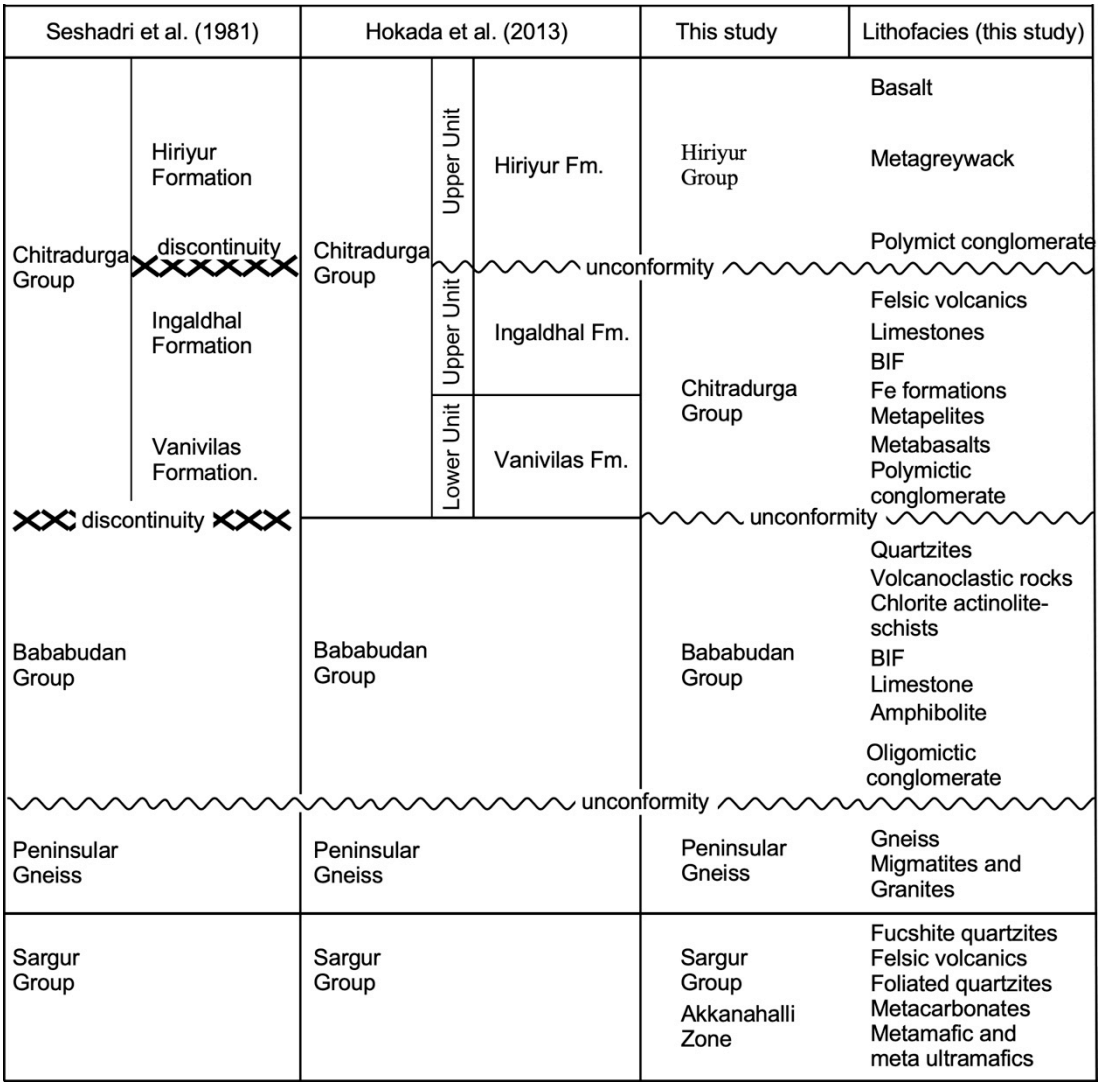

Figure 2.2 *Stratigraphic relations in the study area.*

ascending order of their age. Major lithofacies in each group are also presented in **Figure 2.2.** The field and structural evidence show that Babadudan Group and Chitradurga Group are separated by an unconformity marked by polymictic conglomerate. Similarly based on my fieldwork for the past 4 years I would like to use the terminology 'Hiriyur Group' instead of 'Hiriyur Formation'. This is supported by the fact that Hiriyur Group sediments have younger depositional ages (Hokada et al., 2013, Nasheeth et al., 2016), which demand a separate origin for the Hiriyur Group of rocks. Moreover, a regional-scale unconformity is marked in between Chitradurga and Hiriyur Groups of rocks in previous studies (e.g. Mishima et al., 2017). These criteria demand these rocks should be considered as part of a separate 'Group' than considering as a 'Formation' within the Chitradurga Group.

Field relations and major rock types of the study area are shown in **Figure 2.3**. Planar and linear structural features presented in stereonet are shown in **Figure 2.4**. Microphotographs of the important samples are presented in **Figure 2.5.**

2.3.1 Sargur Group.

Sargur Group identified in the study area is dominated by metamorphosed ultramafic, mafic and sedimentary rocks. Ultramafic and mafic rocks include komatiite, serpentinite, dunite, pyroxenite, gabbro, amphibolite, and chlorite-actinolite schist. Meta-sedimentary rocks are dominated by fuchsite-bearing quartzite, magnetite schist, metacarbonate and metamorphosed sandstone-mudstone successions with well-preserved graded bedding. Sargur group of rocks is preserved as regional-scale enclaves within the Peninsular Gneiss which indicates it is the oldest group of rocks in the DC. Sargur Group separated from younger volcano-sedimentary rocks of Bababudan and Chitradurga Groups, either by unconformity or by strike-slip faults.

2.3.2 Basement Gneiss.

TTG and granites identified from the study area are either massive or foliated in appearance with occasional mafic enclaves. Enclaves are generally amphibolite in nature and in some locations ultramafic enclaves are also present. Foliated TTG has biotite and muscovite along the foliation plane, however, near the GMSZ it generally has chlorite and muscovite aligned along the shear plane. Near Kibbanahalli, migmatites and weakly foliated granites with biotite along their foliation plane are also present. No cross-cutting relationship by granite on the CSB is observed

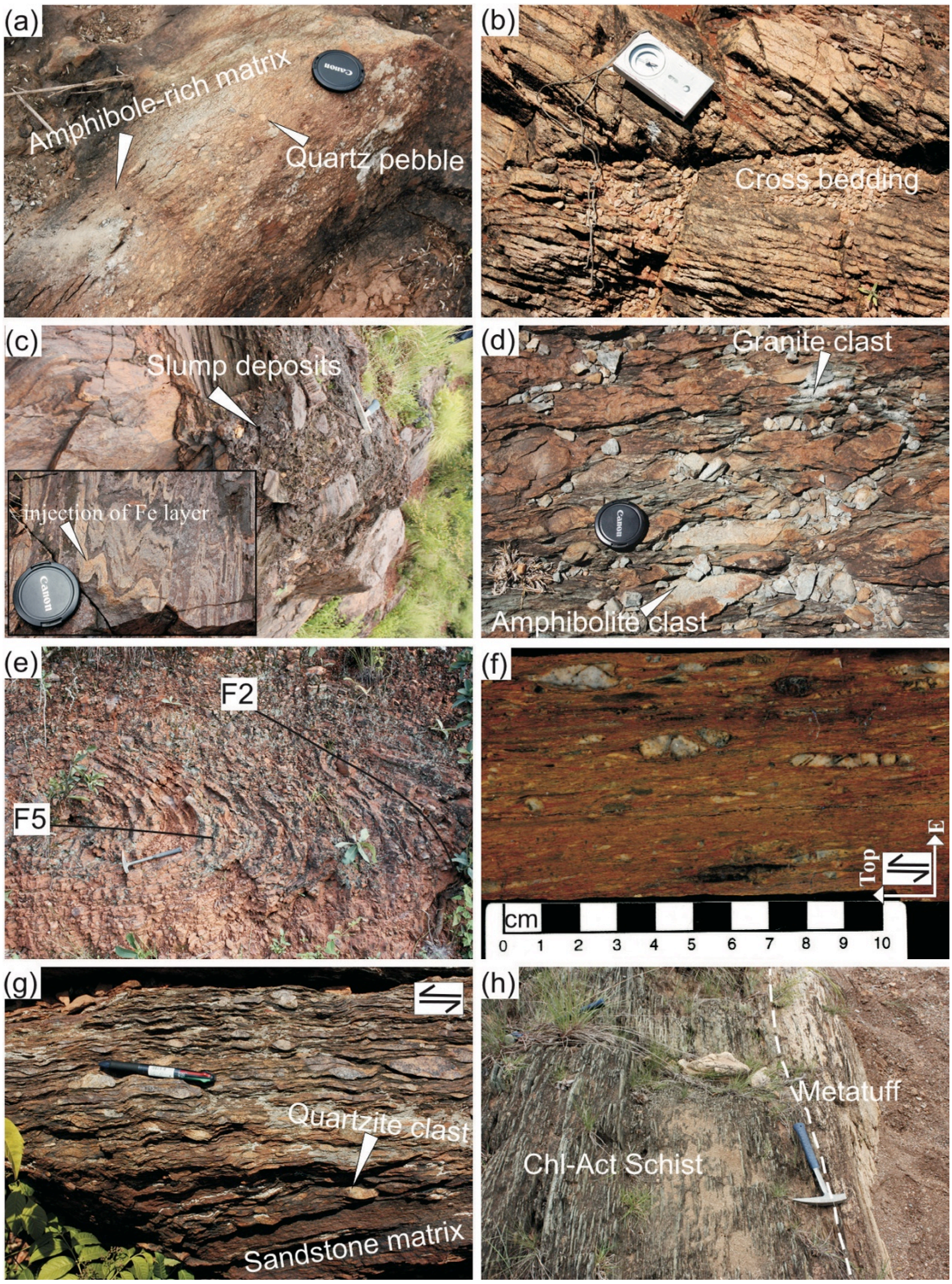

Figure 2.3 *Major rock types in the study area. (a) Deformed quartz pebbbleconglomerate to the east of Kibbanahalli with amphibole-rich matrix represents Basement Gneiss-Babbudan unconformity (b) Cross-bedded quartzite of babbudan Group (c) Slump deposits in BIF of Bababudan Group. Fe rich layer injects into quartz-rich layer indicating soft-sediment deformation is also marked in the bottom left corner. (d) Clast-supported,*

polymictic conglomerate with granite and amphibolite clast. This outcrop exposed to the 8 km east of Kibbanahalli town and represents Bababudan-Chitradurga unconformity. (e) 2 generation folding in Fe-formation of Chitradurga Group, D2 folding with west-dipping axial plane. D5 folding with E–W trending, shallow dipping axial plane, note the refolding of F2 fold around F5 axes (f) Intensely sheared and elongated conglomerate from Chitradurga–Hiriyur Group boundary, showing east-side-up motion sense. (g) Sheared conglomerate in the eastern margin of Chitradurga Group, with quartzite clasts in sandstone matrix showing a sinistral sense of movement (h) Conformable contact relation between metatuff and chlorite-actinolite schist of Akkanahalli Zone.

2.3.3 Bababudan Group.

Two oligomictic conglomerate units are observed towards 6 km south and 6 km east of Kibbanahalli, which form the bottommost layer of the Bababudan Group, rest directly above the Sargur Group and the Basement Gneiss (**Fig. 2.1b**). These oligomictic conglomerate have an amphibole-rich matrix and quartzite clasts (**Fig. 2.3a**) and mark the unconformity betweenSargur Group-Basement Gneiss and Bababudan Group. Fining upward sequence in the clast distribution is evident in the outcrop scale. Bababudan Group of rocks are dominated by metamorphosed volcanic, volcanoclastic and sedimentary rocks. Unlike the Sargur Group, ultramafic rocks are very rare in the Bababudan Group. Meta-volcanic rocks in the Bababudan Group are amphibolite, metabasalt, meta-dolerite and chlorite-actinolite schist. Meta-dolerite cross-cuts amphibolite and metabasalt indicating it is younger. Volcaniclastic rocks in the group are bedded-tuff and volcanic sandstone with randomly oriented amphibole grains (**Fig. 2.5a**). Cross-bedded fuchsite/muscovite-bearing quartzites (**Fig. 2.3b**), sandstone-siltstone/mudstone succession, stromatolite limestone and BIF are major sedimentary rocks in the Bababudan Group exposed in the investigated

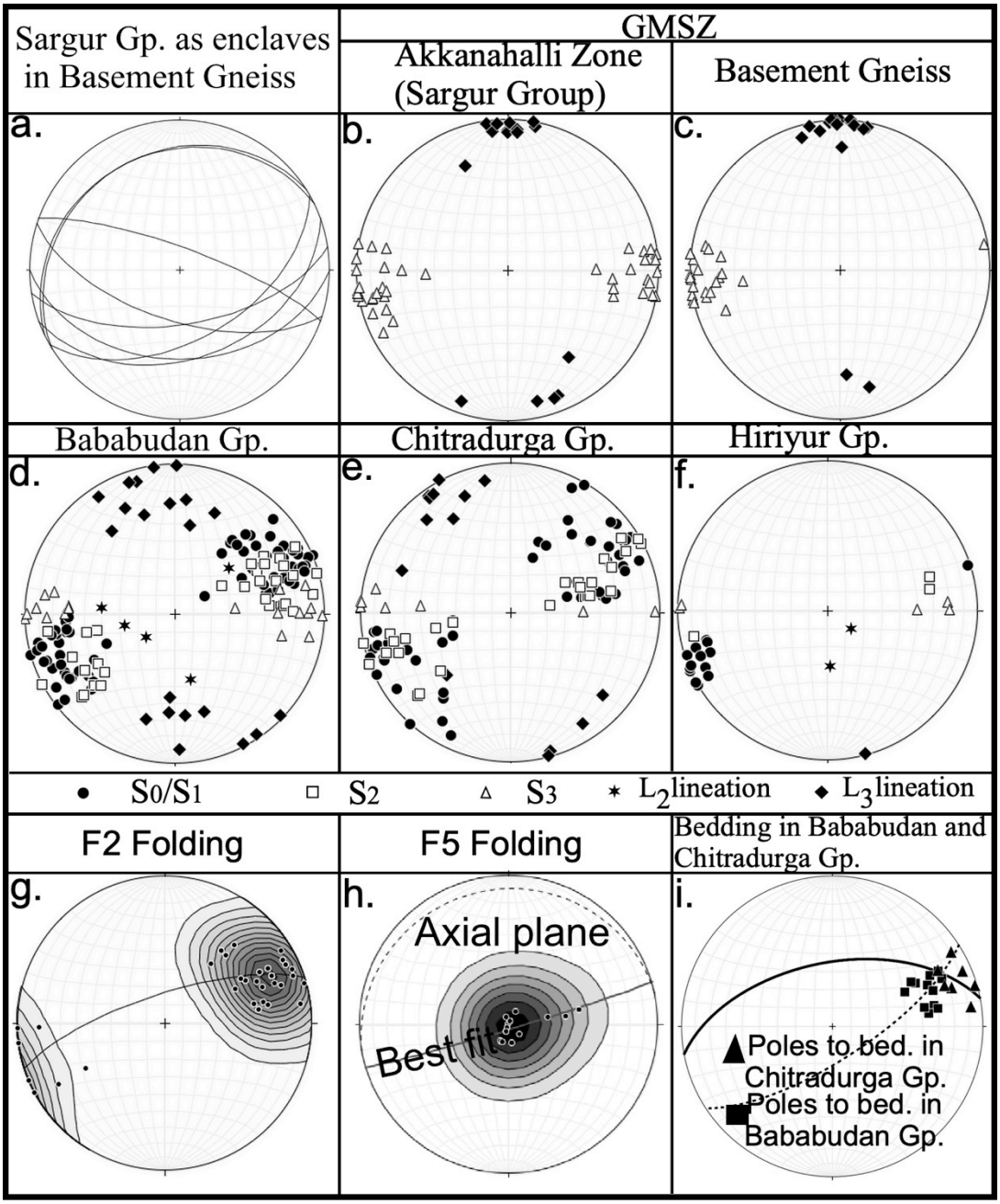

Figure 2.4. *Stereoplots of lineation, foliation and bedding from different parts of the study area classified based on the groups and deformation history. (a) Foliation planes in Sargur Group, as enclaves in basement gneiss (b) Lineation and poles to S_3 foliation in Akkanahalli Zone (Sargur Group) rocks which are part of GMSZ. (c) Lineation and poles to S_3 foliation in Basement Gneiss, part of GMSZ. (d) Poles to S_0, S_1, S_2, and S_3 with L_2 and L_3 lineations in Bababudan Group of rocks. (e) Poles to S_0, S_1, S_2, and S_3 with L_2 and L_3 lineations in Chitradurga Group. (f) Poles to S_0, S_1, S_2, and S_3 with L_2 and L_3 lineations in Hiriyur Group. (g) Poles to the bedding (S_0/S_1) and S_2 foliation of D_2 folding in Bababudan and Chitradurga Group across AB transect in Figure*

1c, data related to angular bedding relation is not included. (g) Poles to the foliations of D_5 folding in the same AB transect. (h) Bedding relation between Bababudan and Chitradurga Group.

area. Quartzite has well-preserved cross-bedding structures indicating a shallow marine depositional environment. Moreover, fuchsite mica in quartzite probably points to the common ultramafic source for them similar to the fuchsite quartzite in the Sargur Group. Limestones in the Bababudan Group have well-preserved stromatolite. These limestones are either calcite-rich or dolomite-rich, and dolomite aggregates are also seen as boudins inside calcite-rich portions. They are also present as alternating bands with quartzite, which are cut across by younger quartz veins. A gradual transition from this banded limestone-quartzite to massive limestone, rich in muscovite is present in some locations to the northwest of Thimmanahalli.

2.3.4 Chitradurga Group.

Unconformable boundary relation between the Bababudan Group and the Chitradurga Group is defined by a polymictic conglomerate located towards 8 km east of Kibbanahalli (**Fig. 2.1b, 2.3d**). This conglomerate is clast-supported in the major part of the exposure. Basaltic fragment-rich matrix is observed in some parts of the outcrop with granite, amphibolite and quartzite clasts. Toward SW of Hagalavadi, there is another conglomerate layer of 100 m-thickness, in the eastern margin of the Chitradurga Group (**Fig. 2.1b**). This conglomerate layer is completely different from the Chitradurga-Hiriyur boundary conglomerate; granite and quartzite clasts are present in them with a siliceous or shaly matrix. This conglomerate is severely sheared and its clasts are strongly elongated (**Fig. 2.3g**). Bedding in Bababudan and Chitradurga Groups shows an oblique contact relation in the western part (**Fig. 2.4i**) and a parallel contact in the eastern part, probably because of their angular to parallel unconformable relation and similar relationship is also present in the geological map (**Fig. 2.1b**). Corresponding to this, cross-sections (AB and MN of **Fig. 1.1c**) also depict the angular and parallel unconformable relation in the west and the east, respectively within the folded zone.

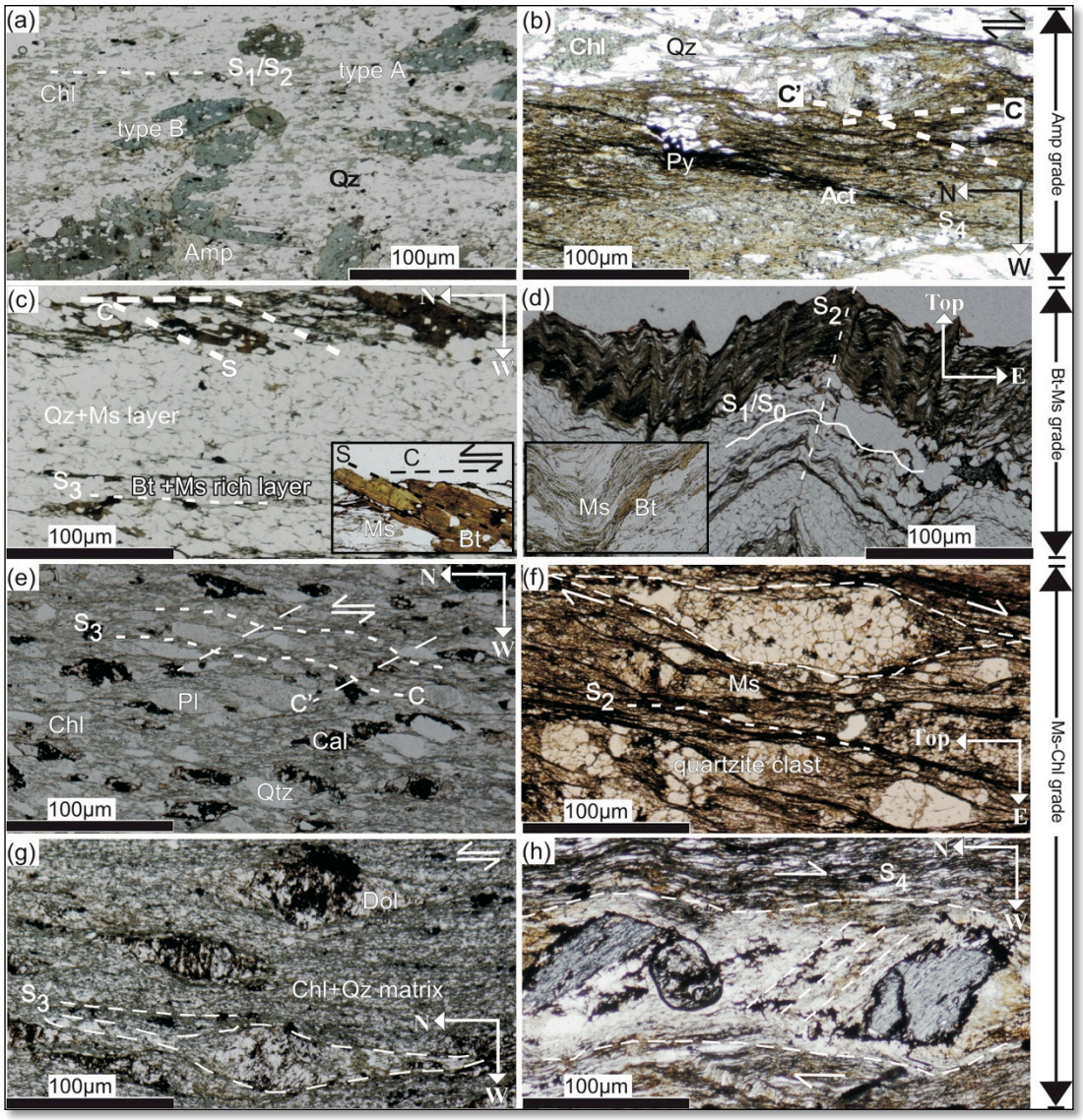

Figure 2.5 *(a) Typical volcanoclastic sandstone of Bababudan Group with foliated matrix composed of chlorite, quartz, and amphibole (type A). Randomly arranged grains of amphibole (type B) are also visible. (b) Sheared chlorite-actinolite schist of Bababudan Group with dextral sense of movement, chlorite is present as crenulated porphyroclast and actinolite is developed along shear plane. (c) Meta-sandstone in Bababudan Group with sinistral shear. Biotite aligned along 'S' plane and muscovite developed in shear planes (S_3). Enlarged view of biotite-muscovite relation in shear plane is also shown in the bottom right corner. (d) Folded schist which shows buckling effect between quartz-rich layer and quartz poor-biotite, muscovite layer. Enlarged view of biotite-muscovite grade maintained during folding shown in the bottom right corner. (e) Metagreywack of Hiriyur Group, show*

C-C' structure indicating sinistral shearing. (f) Thin section photo of the sample shown in figure 2.3f, east-side-up, movement is evident from asymmetrical tail developed around quartzite clast. (g) Metamafic rock from Akkanahalli Zone with abundant chlorite in matrix with dolomite and minor quartz. Muscovite developed along shear planes is also visible. (h) Dextral shear band in schist within sinistral Gadag-Mandya Shear Zone.

Major rock types within the Chitradurga Group of the study area are metabasalt, metapelites, iron formation (both banded magnetite quartzites and Mn-bearing iron formations, **Fig. 2.3e**), felsic volcanics and limestone. Basalt in this group is metamorphosed under the greenschist facies condition. In the study area, these basalts are present above sandstone-mudstone succession and metapelites (see cross-sections EF and KL, **Fig. 2.1c).** Limestone in the Chitradurga Group is seen as lenses in metapelites and Fe-formations.

2.3.5 Hiriyur Group.

Stratigraphically the Hiriyur Group overlies the Chitradurga Group. My detailed field observation near the contact zone shows that both groups are separated by an unconformity to the east of Thimmanahalli (**Fig. 2.1b**). This unconformity is represented by a 600 m-thick conglomerate layer (**Fig. 2.3f**) and has a ferruginous sandstone matrix with clasts of schist, granite, BIF, basalt and quartzite. Also, it is associated with sandstone-mudstone succession. Hiriyur Group is dominated by the presence of metagreywacke with quartz, feldspar, calcite, chlorite and muscovite as the main assemblage (**Fig. 2.5e**). Primary depositional features such as graded bedding are also well-preserved. Near Buddigudda kaval ~6 km northeast of Thimmanahalli, a ~5 km wide mafic volcanic rock unit is observed which is the youngest unit in the Hiriyur Group (See cross-sections CD and EF, **Fig. 2.1c**). This mafic unit generally has fine-grained NW–SE trending, weakly deformed metabasalt. We assume contact between these mafic units and sedimentary rocks is a conformable one, even though clear contact relation is not preserved. Other than metagreywacke, layers of BIF and ferruginous chert are also identified in the Hiriyur Group.

2.3.6 Metamafic to metaultramafic rocks (Akkanahalli Zone).

To the east of the Hiriyur Group and the western edge of GMSZ, a zone of metamafic/metaultramafic rocks along with layers of metatuff and BIF are present. This zone is in fault contact with the Hiriyur Group. While, in the southeastern part of the study area, this zone is in fault contact with the Chitradurga Group. Faults which mark the boundary in this region show a strike-slip sinistral sense of movement. Metamafic and metaultramafic rocks are generally rich in dolomite, chlorite, actinolite, and quartz (**Fig. 2.5g**). Moreover, opaque phases such as magnetite, chromite, rutile, and ilmenite are present as inclusions within chlorite and dolomite. Metatuff is in conformable contact with metamafic rock (**Fig. 2.5h**). All the rock types in this area are strongly foliated and asymmetrical fold and asymmetrical shear structures are also present.

U-Pb analysis in 90 spots on 90 grains of zircon from the metatuff sample in Akkanahalli Zone was carried out using the Agilent 7500a quadrupole ICPMS with laser ablation system of New Wave Research UP-213 in Niigata University. We followed analytical procedures described in Ueda et al. (2018). Calibrations and data quality control were undertaken using the standard silicate glass SRM610 and 91500 standard zircon. The accuracy of my analyses was verified using the Plešovice zircon. The results of the analysis are shown in *Table 1.*

The metatuff sample is rich in quartz and plagioclase, minor quantities of K-feldspar is also present and, muscovite is developed along shear planes (**Fig. 2.6a**). Zircon grains are generally present along grain boundaries and as inclusions in muscovite. Zircon grains in this sample are 50–100 μm long, euhedral, elongated and show oscillatory zoning indicating magmatic crystallization (**Fig. 2.6b**). Nine concordant grains provided a weighted mean of $^{207}Pb/^{206}Pb$ ages as 3313±6 Ma with an MSWD of 1.3 (**Fig. 2.6d**), which is also consistent with an upper intercept age of 3318±13 Ma (**Fig. 2.6c**) for the discordant grains. The weighted mean of $^{207}Pb/^{206}Pb$ of all the analysis including discordant grains (3311±7) is almost identical to that from concordant grains.

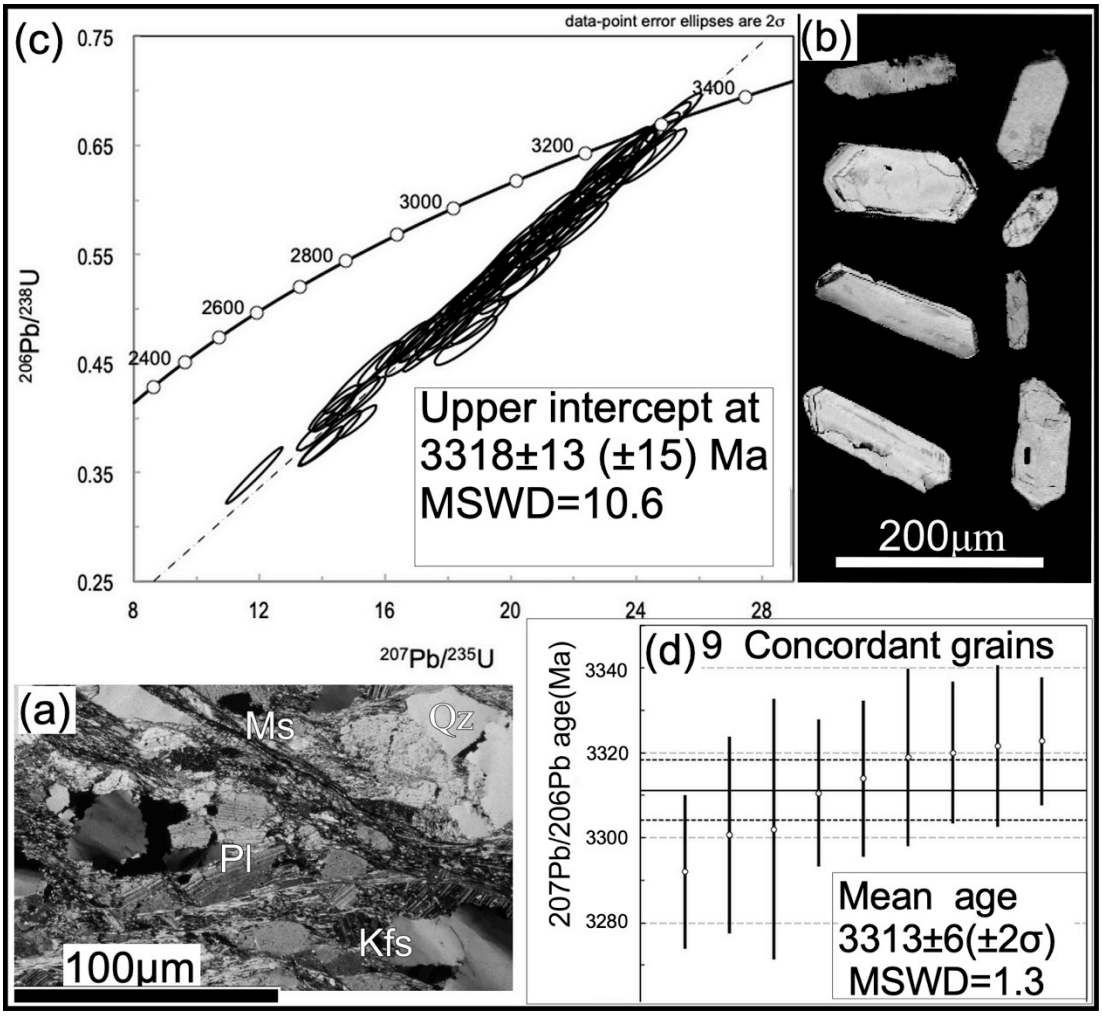

Figure 2.6 *Results of the U-Pb geochronology of metatuff sample from Akkanahalli Zone. (a) Photomicrograph of metatuff sample with zircon grain. (b) Back Scattered Images (BSE) of analyzed zircon grains. (c) Concordia plot of the analytical results. (d) Weighted mean of $^{207}Pb/^{206}Pb$ ages of nine concordant grains*

This result supports that $^{207}Pb/^{206}Pb$ was fairly robust during the lead loss event and based on these facts 3.31 Ga is considered as crystallization age of the felsic tuff sample.

Metatuff is in conformable contact with metamafic rocks (**Fig. 2.3h**) and points to the fact that this entire metamorphosed metavolcanic-metaultramafic association belongs to the older Sargur Group. The presence of a conglomerate layer (**Fig. 2.3g**) to the SW of Hagalavadi implies unconformity between Sargur and Chitradurga Groups. Similar metatuff-mafic rock conformable relation is reported from the Holenarsipur Schist Belt of Sargur Group by Peucat et al. (1995), felsic volcanic (rhyolite flow) in their

study also shows crystallization age of 3298±7 Ma. Since this metamafic/metaultramafic rock zone is lithologically different from other parts of the CSB, we will address it as Akkanahalli Zone (AZ) hereafter.

2.4 Structural relations in CSB

Six events of deformation processes are identified, based on the nature and sequence of deformations in the study area (**Fig. 2.7**). Four early-stage deformations (D_0 to D_3) are of penetrative type, but the later-stages (D_4 and D_5) are of non-penetrative type, forming localized shear zones and minor folds.

D_0 event is characterized by the formation of lithological boundaries, bedding, sedimentary structures, and slump folds (**Fig. 2.3c**). Slump folds, which have no axial plane cleavage, are well-preserved in BIF and limestone formations. In BIF, soft-sediment deformation signatures such as injection of the iron-rich layer into the quartz-rich layer are examined (**Fig. 2.3c**). We interpret this type of structure as developed before the solidification of sediments, i.e. syn-sedimentary deformation. Angular, poorly sorted and fractured BIF distributed in the iron matrix are also associated with this type of folding in BIF. Slump folding and sedimentation followed by the formation of bedding-parallel schistosity (S_1), which has occurred during peak metamorphism (D_1). The observed S_0 and S_1 structures are commonly deformed by the post-D_1-deformations and associating recrystallization of metamorphic minerals, so deformation and tectonics during the D_0 and D_1 are difficult to understand.

The D_2 stage is characterized by an NNW–SSE trending fold zone sandwiched between NNW–SSE trending reverse faults dipping east with dip-parallel lineation (L_2), showing an east-side-up motion sense (**Figs. 2.3f and 2.5f**). Two major reverse faults identified from the study area are in the Basement Gneiss-Bababudan Group and Chitradurga-Hiriyur Group boundary zone (**Figs 2.1b and 2.8c**). A fold zone is made up of five F_2 folds on a geological map-scale (**Fig. 2.8c**). These F_2 folds in the fold zone are tight to isoclinal. They have NNW–SSE trending, vertical to west-dipping

axial planes and 10–20° plunging hinge lines (**Fig. 2.4g**). Their plunging directions vary from the south to the north on a regional scale. These folds exhibit a well-developed NNW–SSE trending axial plane cleavages (S_2). Wavelengths of these folds range from 1–4 km (**Fig. 2.1c**, cross-sections AB and MN). Field and microscopic observations show some typical examples for cleavage refraction and buckling due to the competency contrast between lithologically different layers (**Fig. 2.5d**). Due to the folding and rotation of bedding (S_0) and schistosity (S_1) by D_2 deformation, S_0, S_1, and S_2 generally trend NNW–SSE in the Bababudan Group (**Fig. 2.4d**), Chitradurga Group (**Fig. 2.4e**) and Hiriyur Group (**Fig. 2.4f**). Sargur Group as enclaves in the Basement Gneiss have generally E–W trending foliation (**Fig. 2.4a**). Sargur Group of the Akkanahalli Zone has N–S trending vertical foliation (**Fig. 2.4b**) and minor F_2 folds.

D_3 event is recognized as a regional scale strike-slip sinistral shear. D_3 shear zones ranging from few centimeters to kilometer-scale thickness are identified from the study area. The whole Akkanahalli Zone and Basement Gneiss to the east of Akkanahalli Zone were strongly sheared during D_3 and formed the major sinistral shear zone. This shear zone is 1–2 km wide, N–S striking and nearly vertical dipping GMSZ (**Figs. 2.1b** and **2.8**). In GMSZ, the N– S trending shear planes (S_3) and horizontal lineations (L_3) are strongly developed (**Figs. 2.4b** and **2.4c**). This points to the fact that GMSZ extends into the schist belt rather than restricting in the granitic rocks. N–S or NNW–SSE trending minor D_3 shear zones are sometimes observed across all Groups in the map (**Fig. 2.1c**) and S_3 shear planes are locally developed (**Figs. 2.4b** to **f**). From the geological map in **Figure 2.1c**, it is evident that D_2-related reverse faults are cut across by D_3 sinistral shear zones. Since attitudes and shear sense of D_3 shear zones do not vary between limbs of F_2 fold, D_3 shearing is considered to be unmodified and predated by D_2 folding.

Dextral shear zones are identified from two localities (to the east of Chikkanayakanahalli and to the west of Hagalavadi) with NW–SE strike, dipping to the east and N–S strike with vertical dip, respectively (**Figs. 2.1b** and **2.8**). N–S trending dextral shear zone associated with quartzite to the west of Hagalavadi can be traced at least 20 km along the strike (**Fig. 2.1b**)

Deformation stage	Deformation activity and structures	Structural state of deformation planes
D_5	F_5 folds. localized folding.	E–W trending axial planes.
D_4	Strike-slip dextral shear	NW–SE trending east dipping and N–S trending vertical and steeply east dipping shear planes (S_4). Strike parallel lineation.
D_3	Strike-slip sinistral shear	N–S trending vertical dipping and NNW–SSE trending east and west dipping shear planes and associated foliations (S_3). Strike parallel lineation (L_3)
D_2	F_2 folding, map scale folds.	NNW–SSE trending, west to vertical dipping axial planes, S_2 cleavages trends NNW–SSE direction
	Dip-slip reverse faults	NNW–SSE trending east dipping shear planes. East-side-up shear sense Dip parallel lineation (L_2)
D_1	Layer parallel schistosity S_1	?
D_0	Sedimentation, Slump folding associated with normal faulting (?) S_0	?

Figure 2.7 *Deformation history of the study area*

and is approximately 100 m wide. These strike-slip dextral shear zones, in which strong S_4 foliation developed were resulted from the D_4 event. F_2 folds are refolded by Type 3 interference folding in local scale within some parts of the study area and formed E–W trending folds with almost horizontal axial planes (**Figs. 2.3e** and **2.4h**). In this study, these

minor folds (F_5) are regarded as the resultants of the final, D_5 stage of deformation event even though the spatial relation between D_4 and D_5 events is not clear.

2.5 Microstructural details and metamorphic relations

Metavolcanic rocks of Bababudan Group in the CSB are mainly metamorphosed in the amphibolite grade (**Fig. 2.5a**). Preliminary analysis shows that these amphiboles are Ca-rich, indicating low-grade amphibolite facies condition. Amphiboles are grown in S_1/S_2 foliation planes indicating that the deformation has occurred during amphibolite facies conditions at least in metavolcanic rocks. Volcanoclastic sandstone has more quartz and plagioclase in the matrix with two types of amphiboles. One generation of amphibole grains are aligned parallel to the foliation (type A) and other generation of amphiboles (type B) are randomly aligned (**Fig. 2.5a**). This implies two-generation amphibole growth in the Bababudan Group and the exact reason behind this is not clear yet. In chlorite-actinolite schist, chlorite is seen as the crenulated porphyroclast within a quartz-rich matrix and actinolite is developed along S_4 shear planes (**Fig. 2.5b**). S-C-C' relation shows a dextral sense of movement. Pyrite is also present as an accessory phase in this sample. Quartzites in the Bababudan Group are having muscovite in their S_2/S_3 foliation plane; in some localities presence of fuchsite is also noted.

For samples from Chikkaramapura (13 km NE of Kibbanahalli) within a narrow shear zone in the Bababudan-Chitradurga Group boundary, biotite is seen along 'S' foliation and muscovite is developed along 'C' planes and S-C fabric shows a sinistral sense of motion (**Fig. 2.5c**). Similarly, within folded samples also muscovite is developed along the grain boundaries of biotite, indicating the same retrograde metamorphic condition for both D_2 folding and D_3 shearing (**Fig. 2.5d**). In some samples two generations of biotite are present, the first generation in the matrix is probably detrital in origin. The second generation of biotite is developed along the shear planes along with muscovite.

Hiriyur Group rocks have chlorite and muscovite developed along the shear planes. Typical sandstone from Hiriyur Group has quartz, plagioclase, calcite and muscovite as the main assemblage, with chlorite and muscovite aligned along the S_3 foliation plane (**Fig. 2.5e**). Shear related, S_3 foliation shows a sinistral sense of motion (**Figs. 2.5c** and **5e**). S-C-C' fabric defined by muscovite and asymmetrical tails around quartzite clast in the conglomerate sample of the Chitradurga-Hiriyur boundary shows east-side-up motion sense (**Figs. 2.3f** and **2.5f),** indicating a reverse sense of movement.

Sheared rocks from the Akkanahalli Zone of GMSZ also have chlorite in the shear plane and some samples have muscovite developed along the S_3 shear plane (**Fig. 2.5g**). S-C-C' shear planes are prominent, suggesting a sinistral sense of movement.

It is evident from the above-mentioned fact that, from the lower to upper layer of the stratigraphic column, the metamorphic grade has a transition between Bababudan, Chitradurga and Hiriyur Groups along with the Akkanahalli Zone. Metavolcanic rocks in the Bababudan Group are metamorphosed in amphibolite facies condition. Metasedimentary rocks in both, Bababudan and Chitradurga Groups are metamorphosed in biotite-muscovite grade but the Hiriyur Group, Akkanahalli Zone and GMSZ region are metamorphosed in muscovite-chlorite grade, consistent with the observations in Hokada et al. (2013).

2.6 Discussion

2.6.1 Depositional environment of CSB

The stratigraphic and structural discontinuities across different groups are evident in my field observations, geological map (**Fig. 2.1b**) and structural cross-sections (**Fig. 2.1c**). Previous geochronological data of sedimentary rocks from the CSB also support this notable difference in the age of source rock for different groups. The oldest age of sedimentation of rocks from the Bababudan Group and the Chitradurga Group are well bracketed within the age limit 3.14 Ga and 3.22–2.92 Ga, respectively (Hokada et al., 2013). This indicates that basement rocks including granite and the Sargur Group

probably served as a source for sediments of Bababudan and Chitradurga Groups. Chadwick et al. (1981, 2007) highlighted that the variable uplift of the basement rocks probably initiated the deposition of conglomerate as sedimentary slumps in the basin. The basal conglomerate of the Bababudan Group of my study is composed of coarse fragments of quartzite and a finer-grained clastic matrix. The matrix in sandstone is made up of sand-sized grains of quartz, feldspars, metavolcanic clasts, and mafic and ultramafic mineral particles. Based on this fact, we consider that the basal conglomerate was deposited in a basin close to the mafic volcanic source and quartzite-rich source. The Bababudan Group of rocks which rest above the basal conglomerate is marked by an abundance of cross-bedded quartzites, volcanoclastic sediments, and amphibolites and lack of deep marine formations. Cross-bedded quartzites of the Bababudan Group from the study area are considered as shallow marine tidal deposits, similar to the interpretation made on cross-bedded quartzites and sandstone–mudstone facies association from the western margin of the CSB by Bhattacharya et al. (2015) and Kataoka et al. (2015). Stromatolite limestones also imply a shallow marine depositional environment for the Bababudan Group. Association of BIFs and cross-bedded sandstones within the Bababudan Group points to their shallow marine origin. Slump folding and syn-sedimentary deformation structures in BIFs of the Bababudan Group indicate their deposition in an active tectonic environment. The abundance of amphibolites and volcanoclastic sediments suggests active mafic volcanism during the formation of Bababudan Group. Moreover, my field observations did not show any evidence of accretionary mélanges, deep-marine sediments and ophiolite sequence of oceanic crust within the Bababudan Group. From field and stratigraphic relations, it is clear that sedimentation and basin filling of the Bababudan Group started from basal conglomerate deposited directly above the Basement Gneiss and were followed by shallow-marine sediments.

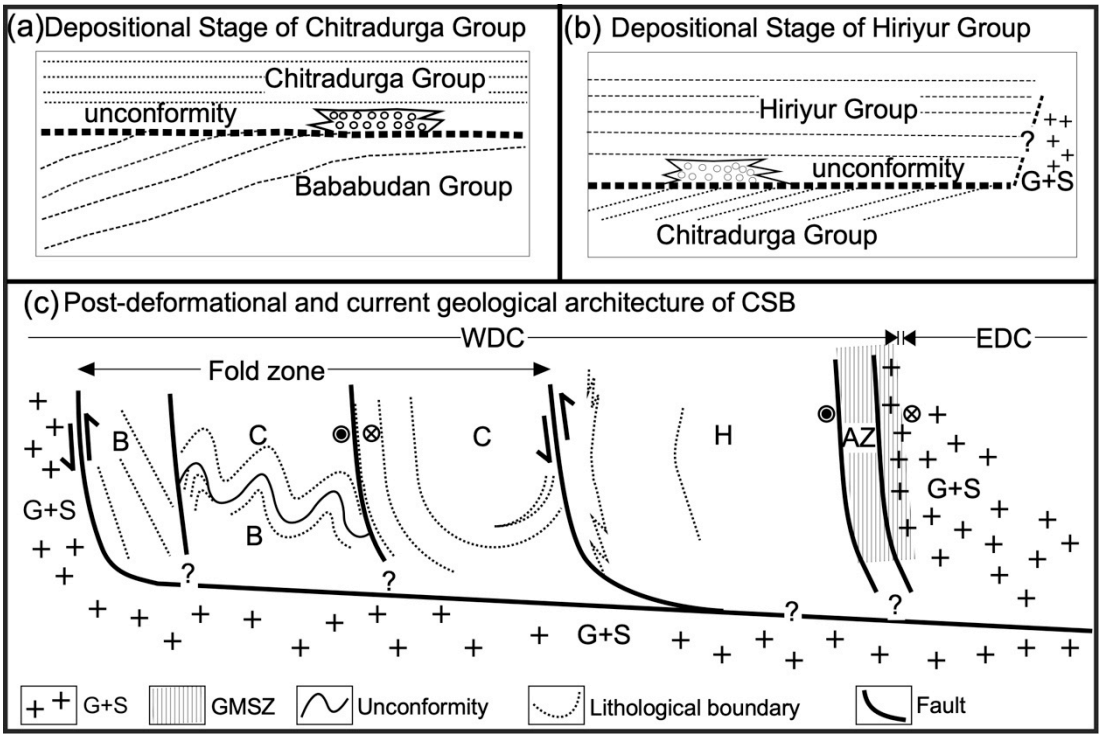

Figure 2.8 *Simplified sedimentation and deformation related structures interpreted on a regional scale for the study area, a view from south (not to scale). (a) Depositional relation between Chitradurga and Bababudan Group, note angular to parallel unconformity between two groups. (b) Depositional relation between Chitradurga and Hiriyur Group. (c) Schematic section of the study area, fold zone is sandwiched between two listric thrust faults and GMSZ post-dates thrust zones. This schematic section resembles a fold-and-thrust belt developed in an inversion tectonic related rift margins. Combination of reverse faults and GMSZ represent sinistral transpression. G, Basement Gneiss; S, Sargur Group; B, Bababudan Group; C, Chitradurga Group; H, Hiriyur Group*

The basal polymictic conglomerate of the Chitradurga Group unconformably covering Bababudan Group have clasts of both amphibolites and granites, showing that the basement and Bababudan Group were the possible source rocks (**Fig. 2.8a**). Chitradurga Group in the study area is rich in iron formations. Mn-bearing iron formations in the Chitradurga Group underlain by orthoquartzite and sandstones have similar stratigraphic relation with Armod-Bisgod region's Mn formation of the WDC (Sethumadhav et al., 2010). Based on this, Mn formations in my study area are also interpreted to be deposited in localized shelf margins or shallow shelf niches similar to the

Armod-Bisgod region. As described earlier, slump folds and deposits dominated in BIF formations of the Chitradurga Group also points to their deposition in an active tectonic, shallow marine environment. The geochemical study of the BIF around the Chitradurga region of CSB also shows deposition in an evolving rift environment (Rao and Naqvi, 1995). An early rift stage to arc-back arc spreading tectonic setting is attributed to the BIF in the Dharwar craton (Mukhopadhyay, 2019). The aforementioned points also support the fact that the BIF was evolved in an immature oceanic environment. As discussed above, similar to the Bababudan Group, shallow-marine sediments dominate the Chitradurga Group. Moreover, my field observations did not produce any evidence of accretionary mélanges, deep-marine sediments and ophiolite sequence of oceanic crust within the Chitradurga Group.

The Hiriyur Group unconformably overlies the Chitradurga Group (cross-sections CD and EF **Fig. 2.1c** and **Fig. 2.8b**). A major population of detrital zircon grains in the Hiriyur Group is having an age of ~2.63 Ga (Hokada et al., 2013). Youngest detrital zircon reported from the Hiriyur group is 2.54 Ga whereas older ones >3.0 Ga are also reported (Nasheeth et al., 2016). The provenance of these zircon grains is interpreted as rocks derived during the second stage of the crustal formation event (2.58–2.54 Ga) as proposed by Jayanada et al. (2013). The above fact implies that sediments of the Hiriyur Group were supplied from the eastern part of the study area, consistent with Nasheeth et al. (2016). Metabasalts including pillow lava is present within the Hiriyur Group in the northern part of the CSB and my study area also. These pillow lavas are chemically similar to be emplaced in shallow marine marginal inter/back-arc basin settings (Duraiswami et al., 2013). We interpret that the Hiriyur Group was formed as a comparatively younger failed rift and thrust upon to existing crustal mass during the final shortening process (**Figs. 2.7b and c**).

Hokada et al. (2013) described the metamorphic grade in Bababudan Group, Chitradurga upper unit and Chitradurga lower unit as low-grade amphibolite, biotite-muscovite, and muscovite-chlorite respectively. My study area, 60 km south of their study area, also has identical metamorphic mineral

assemblages. From this fact, we consider that metamorphic grade variation is regionally preserved throughout the CSB.

2.6.2 Structural evolution of CSB

In the central to the western part of the study area, there is an NNW–SSE trending F_2 fold zone consisting of two anticlines and three synclines with the NNW–SSE trend. The fold zone is sandwiched between two NNW–SSE trending D_2 reverse faults (**Figs. 2.8c and 2.9**). A combination of folds and reverse faults with the same trend characterizes fold-and-thrust belt, inverted back-arc basin and failed rift, in which reverse faults have a listric shape (e.g. Sato and Kato, 2010; Poblet and Lisle, 2011). Considering the competency of granite, it is unlikely that thick granite basement and thin schist layers (thickness of less than several kilometers) form together anticlines and synclines with a wavelength of 1–4 km. To avoid folding of a thick granite and thin schist layers together, the NNW–SSE trending reverse faults bordering the fold zone should have a listric shape passing under the fold zone, and separate the folded schist layers from the basement granite. Moreover, geophysical studies around the southern part of CSB shows the thickness of sediments overlying Basement Gneiss is 0.5–2 km (Bhagya and Ramadass, 2016). From these, it is considered that the NNW–SSE trending reverse faults are thrusts with a listric shape and together with F_2 fold zone form a fold-and-thrust belt in the study area (**Fig. 2.8c**). NNW–SSE regional trend of CSB results from folding, faulting, and rotation of rocks by the D_2 deformation.

Jayananda et al. (2013) pointed out the presence of 3.27 Ga felsic volcanic rocks to the south of Chitradurga town. A 3.32 Ga old felsic volcanic rock occurs in the northwestern part of the Akkanahalli Zone (Fig. 1b), suggesting that both volcanic rocks and the zone belong to the Sargur Group. Tha Akkanahalli Zone is strongly sheared and folded during D_2, D_3, and D_4. Therefore, we consider that the Akkanahalli Zone was juxtaposed to the younger sequences during the shortening/collision events (D_2 to D_3) and modified by strike-slip shear during the D_4 event. A similar model is proposed for the shortening process along the boundary zone in the central part

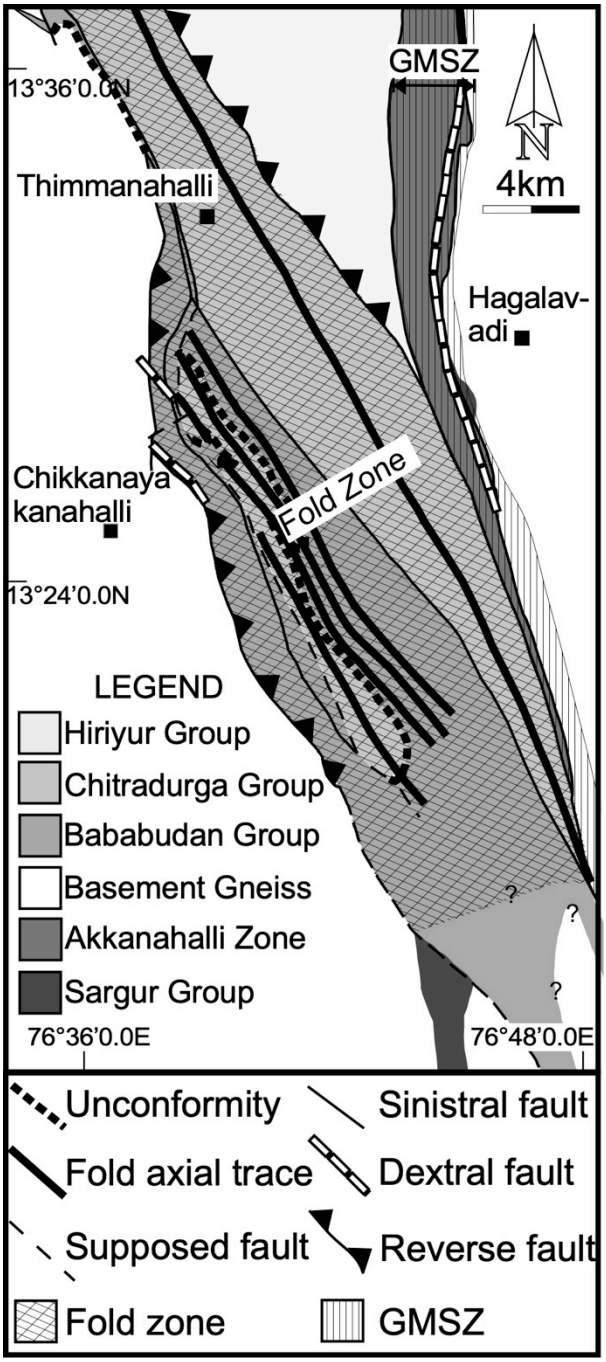

of CSB by Sengupta and Roy (2012). The presence of older rocks of the Sargur Group both in the east and the west of the study area supports the notion of the development of failed-rift by the fracturing of relatively older basement nucleus.

This study indicates sinistral shearing (D_3) after ENE–WSW shortening (D_2) in CSB. Chadwick et al. (2000) proposed sinistral transpression by oblique convergence in DC. Sinistral transpression causes simultaneous zone-normal shortening and zone-parallel (strike-slip) sinistral shearing. Temporal and spatial partitioning between the shortening (folding) and shearing can also take place. It is possible that shortening (D_2) and sinistral shearing (D_3) in the

Figure 2.9 *Simplified map of the study area based on* ***Figure 2.1b****. Traces of strike-slip and reverse faults, along with fold axial traces identified from the study area are marked. Each group of rocks is represented with separate legends. Area between two thrust- faults is marked as fold zone and distribution of GMSZ also shown.*

CSB was caused either by strain partitioning during the transpression or by two separate tectonic events

Previous works explained sinistral transpression was derived from the subduction-related accretionary processes in the Dharwar craton (Chadwick et al., 2000; Jayanada et al., 2013; Manikyamba et al., 2017; Giri et al., 2019). However, my study shows that sedimentary rocks in the study area are not typical of an accretionary prism of subduction origin, but maybe sedimentary rocks that fill a narrow basin, that is, a failed rift zone, created by breaking off a wider granitic continent. The presence of older (>3.0 Ga) Sargur Group rocks on the west and the east (Akkanahalli Zone) of the belt favor this view. Maibam et al. (2011) proposed that WDC and EDC formed as part of a single terrane, using Pb-Pb zircon ages of para- and ortho-gneisses from DC. Their interpretation also supports my idea, a narrow basin (CSB) created by breaking off a stable granitic continent. Therefore, it is considered that the sinistral transpression was created by post-rifting, inversion tectonic related collision events.

The dextral rotation (D_4) after the sinistral event (D_3) is also identified in the study area. This dextral event possibility associated with the evolution of Clospet granite (Moyen et al., 2001).

2.7 Implications for the evolution of DC and Archean crustal growth

Jayananda et al. (2013) explained the Archean crustal growth of DC by the two-stage accretion scenario considering a west-dipping subducting oceanic slab beneath the WDC and then the EDC. They also showed in their figure 20' that during the accretion, huge bodies (juvenile arcs) of mafic and felsic rocks had collided with WDC and DC had grown toward the east. In the previous works, it is mentioned that the Chitradurga Group was formed in the arc or back-arc environments (Chadwick et al., 2000; Jayananda et al., 2013), whilst the Bababudan Group developed in the continental intraplate setting (Chardon et al., 1998). My study shows that CSB is neither arc nor subduction origins, but maybe sedimentary rocks that filled a narrow failed rift zone, created by breaking off a wider granitic continent. Kusky et al. (2018) proposed that the formation of aulacogens played a vital role in 3.0–2.5 Ga crustal growth. Therefore, we consider the formation of failed rifts is one of the important processes of the continental growth of the DC, at least in the

WDC. Moreover, a comparatively thicker oceanic crust in the Archean (Sleep and Windley, 1982) probably get accreted by transpression associated with the strike-slip movement as observed in this study.

2.8 Summary

Detailed field and structural studies in the southern part of CSB were carried out. Unconformable relations between basement rocks, Bababudan Group, Chitradurga Group, and Hiriyur Group are identified. Geological and structural relationships between different rock types show these unconformities developed in a sedimentary setting within a shallow marine environment. A progressive change in the metamorphic grade from the Bababudan Group to the Hiriyur Group is observed. Six stage deformation processes are identified from the study area. Four early stages (D_0 to D_3) deformations were of penetrative type, but those of the later stages (D_4 and D_5) were of a non-penetrative type. D_2 event is characterized by NNW–SSE trending isoclinal folds sandwiched between axial plane trace parallel, NNW–SSE trending east-dipping thrust faults. D_3 event was dominated by sinistral strike-slip faults, represented as 1–2 km wide, N–S trending GMSZ and N–S to NNW–SSE trending minor shear zones/faults. D_2 thrusting and associated folding along with D_3 strike-slip faulting can be explained by the sinistral transpression mechanism. Volcanic and sedimentary rocks of the study area show characteristics evolved in a narrow basin of failed rift zone developed by the fracturing of basement rocks, rather than an accretionary prism evolving during the subduction process. Inversion tectonics related collision events should have resulted in sinistral transpression that post-date rifting events.

Chapter 3

3 Structural and geochemical evidences for a failed rift model of crustal evolution in Western Dharwar Craton, South India.

ABSTRACT

Detailed geological mapping along with structural and geochemical analysis were carried out in Kibbanahalli Schist Belt (KSB) of Bababudan Group in the Western Dharwar Craton (WDC). Repeated sequences of sedimentary rocks and volcanic rocks with conformable contact relation are the major lithological association in KSB. Sedimentary structures and field relations indicate that Bababudan Group begins with basal conglomerate composed of debris (talus) and alluvial fan deposits or fluvial deposits. Volcanic rocks preserve features of explosive volcanism in an aqueous environment.

Based on the field and microstructural observations five stages of deformations (D_0, D_1, D_2, D_3, and D_4) are characterized from the study area. D_0 and D_1 events are related to sedimentation and peak metamorphism respectively. D_2 and D_3 are regional scale events. East dipping NW–SE trending thrust faults and layer parallel F_2 folds that are upright and isoclinal marks D_2 event. These F_2 folds are sandwiched between D_2 thrust faults. D_3 event is a strike-slip sinistral shear observed in the eastern margin of the study area. D_4 deformation is non-penetrative dextral strike-slip shearing event concentrated along the boundary of KSB. These major structures in the study area are pointing to the temporal evolution of a fold-and-thrust belt from a narrow intracratonic basin.

Trace element geochemical analysis of the mafic to intermediate rocks from KSB and Chitradurga Schist Belt (CSB) shows three Types of patterns. Type 1 has Nb-Ta negative anomaly, Type 2 are relatively flat trend similar to E-MORB and Type 3 has Zr-Hf positive anomaly. LREE depleted trend is present in Type 1, whereas relatively flat LREE pattern are observed for Type 2 and 3. HREE pattern in some of the samples are flat with one exception. The geochemical variations are related to the degree of crustal contamination experienced during their eruption in connection with the intracratonic extension.

A pair of thrust faults and folded sequences of volcanic, volcanoclastic and sedimentary rocks summarize the major structural association in the study area. This association is identical to a failed rift structure developed in an intracratonic setting. Geochemical evidence also points to an intracratonic mafic to intermediate volcanism.

KSB thus provides a best-preserved evidence for an Archean failed rift. Post-3.0 Ga crustal growth throughout the Western Dharwar Craton is therefore initiated by similar failed rifting events, which also implies a uniformitarian tectonic evolution for the Dharwar Craton during the Neoarchean.

3.1 Introduction

In this chapter, I present detail geological and structural map of the 'Kibbanahali Schist Belt (KSB), in the southern part of Chitradurga Schist Bet, WDC (**Fig. 3.1a**), along with field, microstructural and geochemical analysis. Based on this I address the questions about tectonic evolution of the Dharwar Craton, the associated discrepancies and mismatches in the previous structural or tectonic models. The role of failed rift in the crustal growth process of Archean Cratons is also discussed.

3.2 Geological background

Kibbanahalli Schist Belt (KSB) is located approximately to the west of the southern part of Chitradurga Schist Belt (CSB) and to the northwest of Kibbanahalli town (**Fig. 3.1b**). KSB can be traced along 80 km in length along the strike. Maximum width of KSB in the mapped area is approximately 6 km and minimum width is 1.5 km. In previous literatures KSB is represented by different names such as Bommanahalli arm of CSB (Srinivasan and Ojkangas, 1985) and Kibbanahalli Arm of CSB (Venkata Dasu et al., 1991, Chardon et al., 1996). The term 'arm' was widely used in the previous works because; KSB appears as a cartographic interdigitation of the CSB (Chardon et al., 1996). Basement Gneiss shares the boundary with KSB in most of the part. This Basement Gneiss surrounding KSB is classified into 3 types (1) tonalitic and trondhjemitic grey gneiss; (2) non-foliated diapiric trondhjemites that includes grey gneiss; and (3) the late-stage Arsikere granite (Meen et al., 1992). Rb–Sr isochron age of the non-foliated diapiric trondhjemites is 3.2 Ga (Rogers and Callahan, 1988), which is mentioned as the Tiptur trondhjemite in their work. Zircon U–Pb age estimated for the Arsikere granite is 2.61 Ga (Jayananda et al., 2006). Another geological unit that shares the boundary between KSB is the Sargur Group of rocks. Locally disrupted and discontinues ultramafic-mafic rocks of the Sargur Group are distributed in the northwestern part of KSB, represented as J.C. Pura belt in the previous literatures (Venkata Dasu et al., 1991, Chardon et al., 1996, Jayananda et al., 2008). Major lithological unit in J.C. Pura belt comprises of cherty quartzite, banded iron formations (BIF)

and komatiitic to tholeiitic volcanic sequence (Venkata Dasu et al., 1991, Jayananada et al., 2008). Sm-Nd whole-rock isochron age for komatiites from WDC is reported as 3.35 Ga after collectively measuring komatiites from Sargur Group distributed at different localities of DC including J.C. Pura belt. Detrital zircons of quartzite in this belt have been dated as ~3.2 Ga old (Ramakrishnan et al., 1994).

Another unit of Sargur Group of rocks is distributed in the southeastern part of the study area represented as Banasandra belt in the map (Fig. 2b). Ultramafic rocks including Komatiite are reported in previous studies around this region (Jayananda et al., 2008, Maya et al., 2017). Sm-Nd whole rock isochron age of Banasandra Komatiite is bracketed around 3.14 Ga (Maya et al., 2017). Venkata Dasu et al. (1991) demonstrated the unconformable relation between Sargur Group and Bababudan Group rocks of J.C. Pura Belt and KSB respectively based on the following features; 1) Fundamental unconformity defined by uraniferous quartz-pebble conglomerate deposited above peneplaned gneissic basement. 2) The angular discordance in the structures; J.C. Pura belt forms a doubly plunging antiform with N–S axis bordered by a rim synform. J.C. Pura belt and Rampura dome abruptly truncated by the NNW–SSE trending synformal structure of KSB. Moreover they also noticed the absence of structures similar to Rampura dome in KSB. 3) Break in the stratigraphy; ultramafic rocks including Komatiite, which is abundant in J.C. Pura belt, on the other hand profusion of amygdular basalts and cross-bedded quartz arenites are reported in KSB. 4) Metamorphic grade; a considerable brake in metamorphic grade between the two belts, middle amphibolite grade in J.C. Pura belt whilst greenish grey greenschist facies to lower amphibolite facies in the KSB. More details about stratigraphy and lithology of KSB are discussed in Srinivasan and Ojkangas, (1986) (Bommenhalli arm in their work). According to their description KSB has twelve-quartzite units, twenty-amygdular flows, seven-mafic sills four-laharic units and minor pelite and iron formations present with a sedimentary rock to volcanic rock ratio of 1:2. Geochemical study of some of these volcanic rocks in KSB indicates a tholeiite affinity (Venkata Dasu et al., 1991).

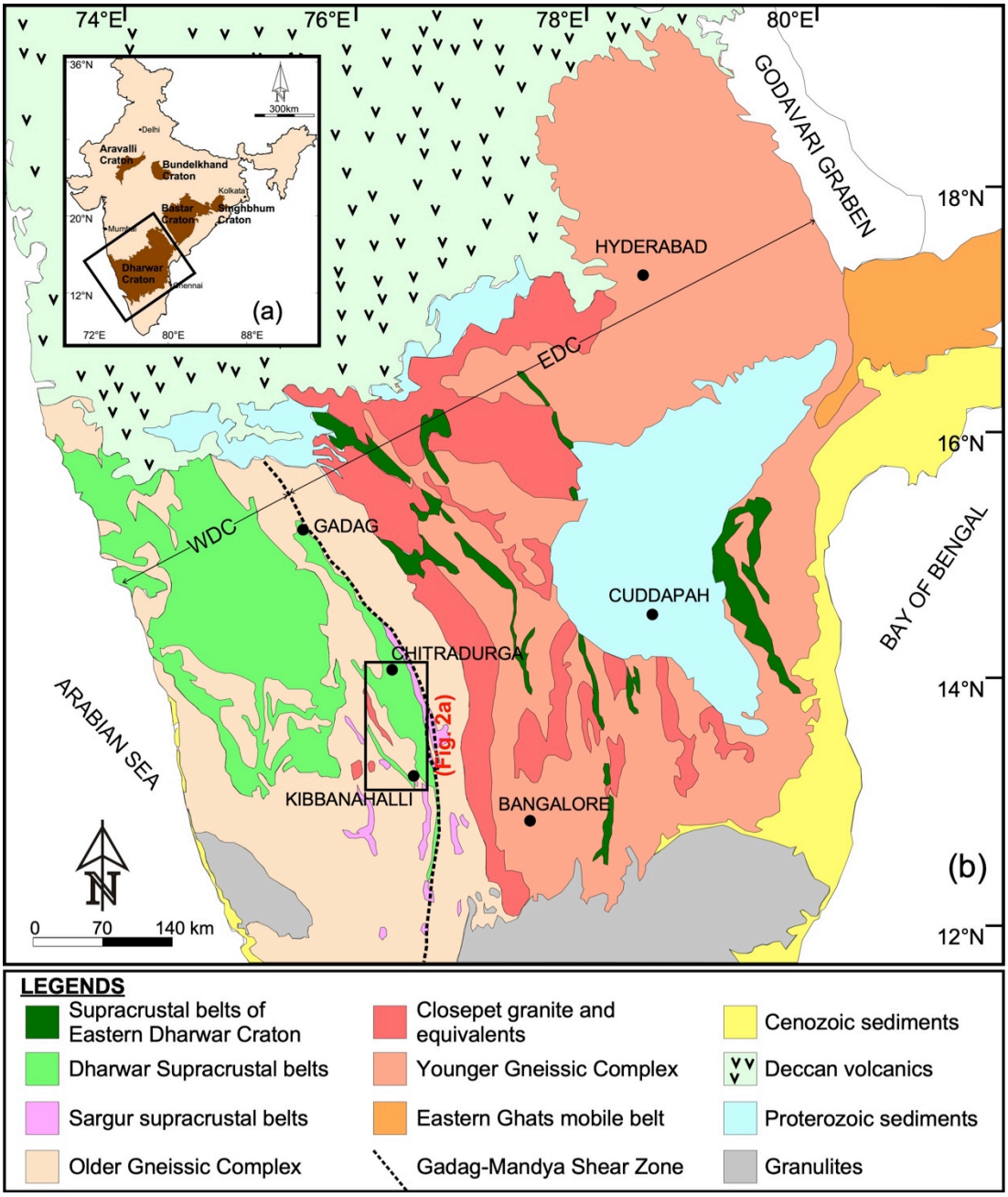

Figure. 3.1. *(a) Distribution of Archean cratons in India, Dharwar Craton is a major litho-tectonic unit in the southern peninsular India. (b) Detailed geological map of Dharwar Craton and associated geological formations (Modified after Ram Mohan et al., 2020, and GSI, 1996).*

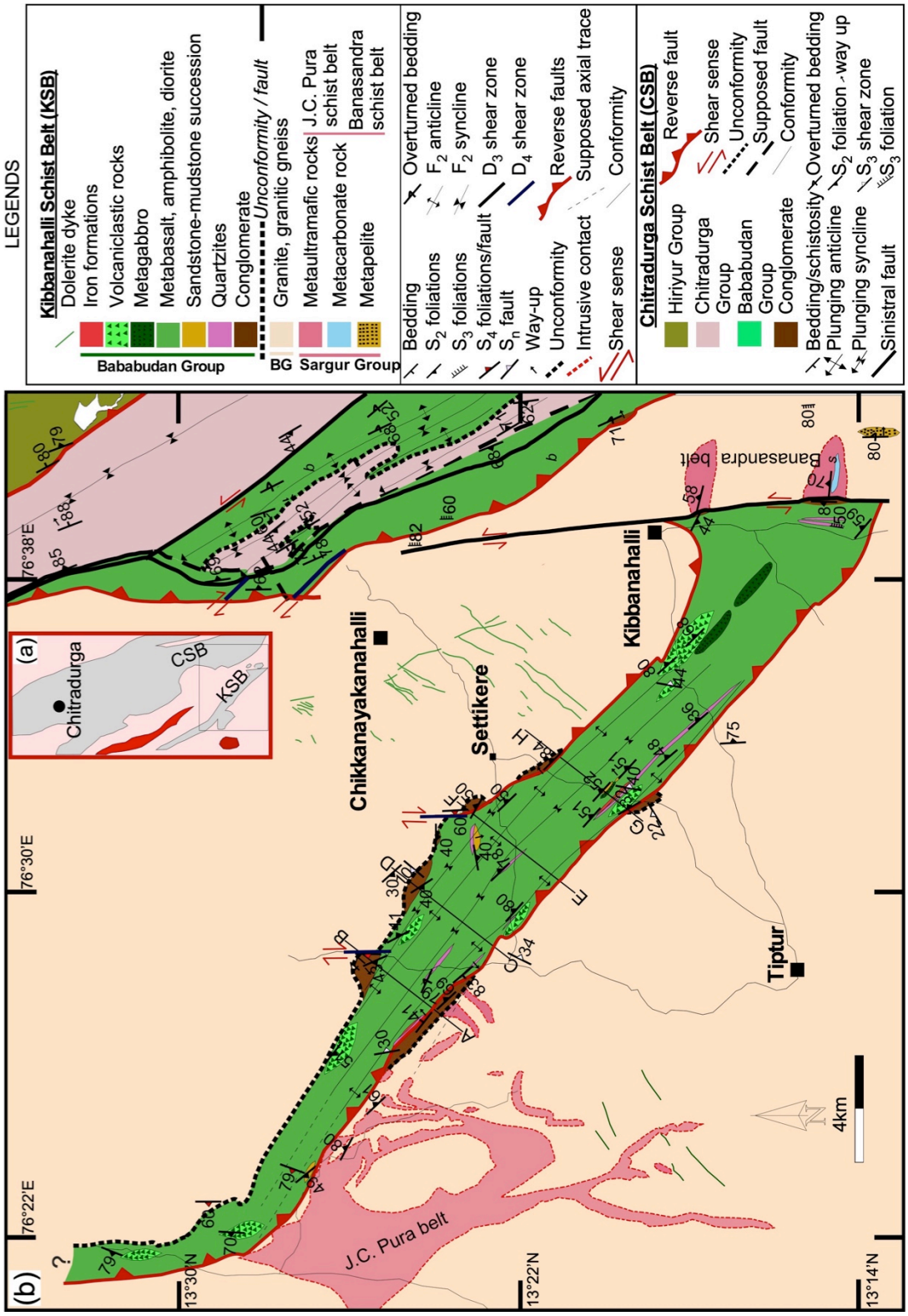

Figure. 3.2. *(a) Geological outline of the Chitradurga Schist Belt (CSB) and Kibbanahalli Schist Belt (KSB). (b) Detailed geological map of Kibbanahalli Schist Belt (KSB) with sturcutural and lithological features. Geological map of southern part of Chitradurga Schist Belt (Modified after, Sreehari and Toyoshima, 2020) is also presented with separate legends and symbols.*

It is a widely held view that KSB is a NW–SE trending synformal structure that resulted from a NE–SW shortening (Venkata Dasu et al., 1991; Chadwick et al., 2000). Contrary to this Chardon et al. (1996) suggested that KSB is resultant of passive sinking of the Dharwar Supergroup into the Basement Gneiss without any crustal shortening.

3.3 Lithology and stratigraphic relations

3.3.1 Gneiss and granites

Granitic gneisses proximal to the contact in the SW and NE margin are foliated and show asymmetrical shear structures in few locations. Foliation planes in them are defined by biotite or amphibole. Granites appears as non-foliated bodies with ~4 cm long plagioclase xenocrysts, or as outcrops with weakly foliated domal shaped bodies. Non-foliated granites with large plagioclase xenocrysts are observed in the SW and NE side of the KSB. Although crosscutting relation of the granite on KSB is not observed, they are in close contact with either conglomerate or amphibolite of KSB. Granite and gneiss will be collectively addressed as Basement Gneiss in this study.

3.3.2 Lithological units in KSB

Detailed geological map of KSB is shown in **Figure 3.2b** and cross sections in **Figure 3.3** Based on this we will discuss structural, lithologic and stratigraphic relations in the KSB. Route maps used to prepare regional scale maps are shown in **Appendix A2.**

Major lithological units identified in KSB are conglomerate, quartzite, metabasalt, metagabbro, volcaniclastics, BIF, metapelites and sandstone.

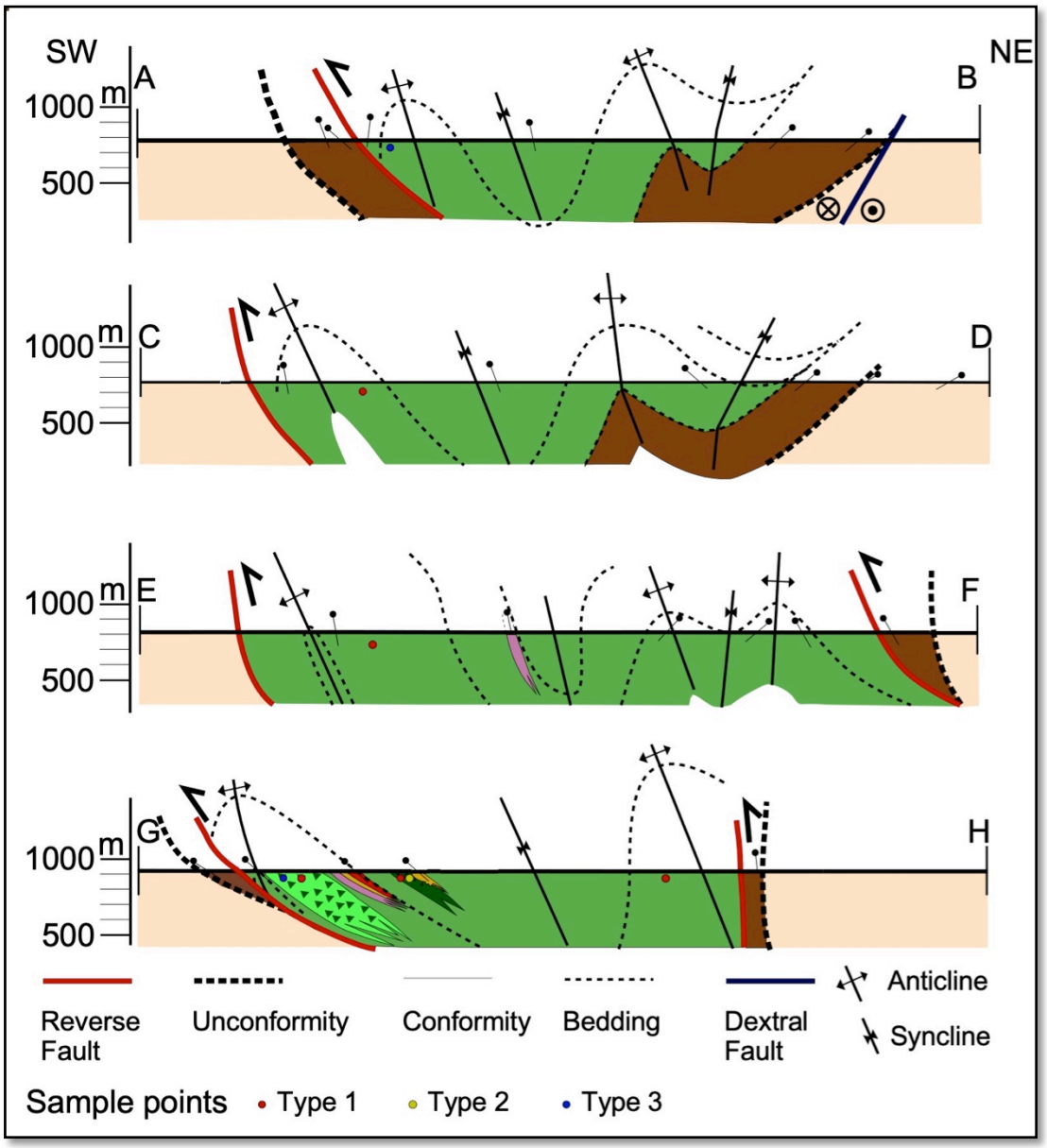

Figure. 3.3. *Cross sections of marked sections AB, CD, EF and GH in* ***Figure 3.2b.*** *Note the west verging isoclinal folds sandwiched between reverse faults. Locations for samples selected for geochemical analysis are also shown*. Small black circles represents

I. Conglomerates

Conglomerates form the basal unit of the stratigraphic column in KSB and are present in the NE, SW and the extreme eastern margin of KSB (**Fig. 3.2b, Fig. 3.3**). Conglomerates with pebble-sized clasts (Quartz Pebble Conglomerate, QPC) and conglomerates with >1m-size quartzite clasts are observed in KSB. QPC is distributed in the NE and SW margin of the KSB. Clasts in this conglomerate are mostly variably sized, pure quartz

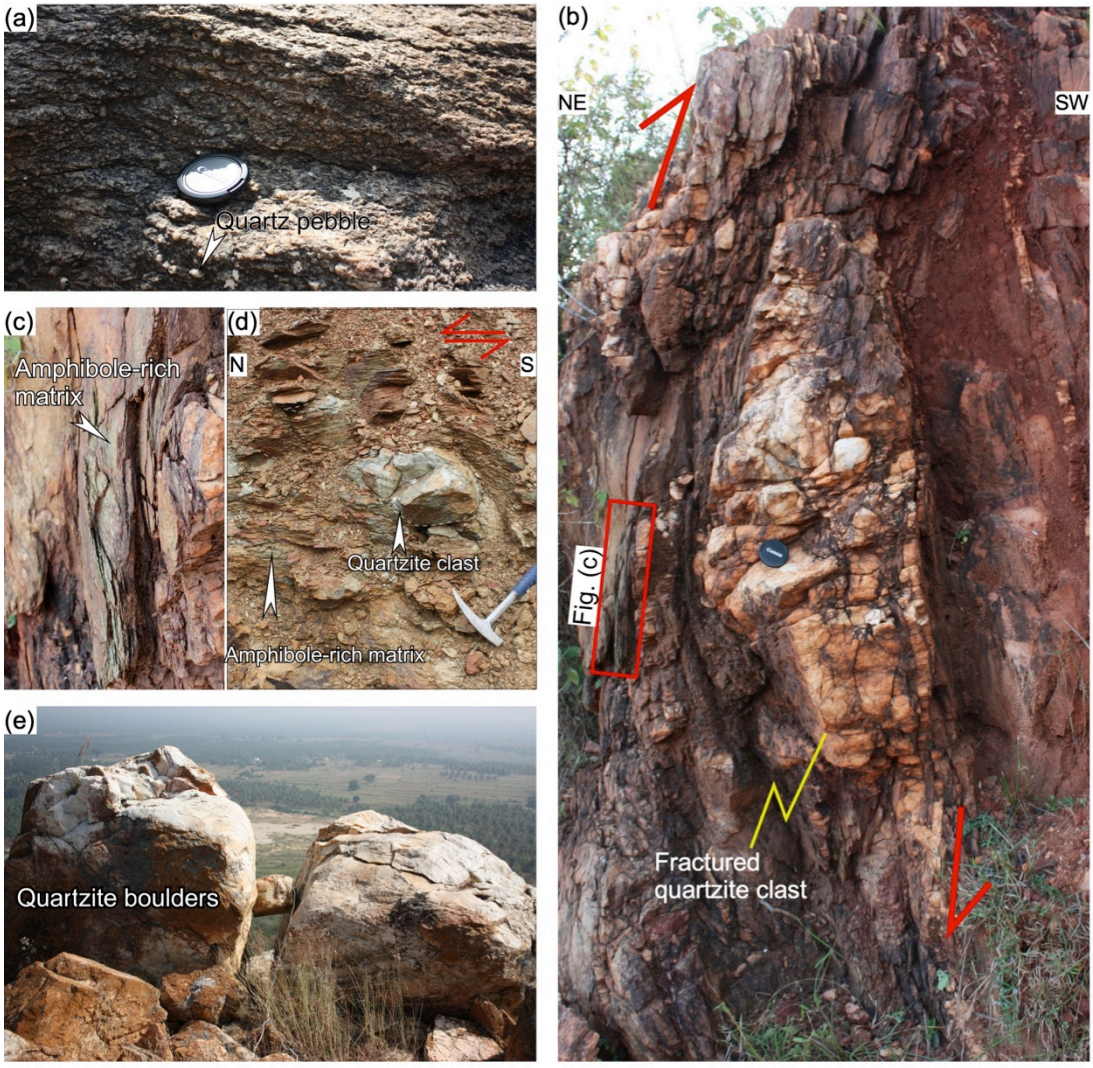

Figure. 3.4. *Types of conglomerates and related structures (a) Quartz Pebble Conglomerate (QPC). (b) Large (>1m) quartzite clast-bearing conglomerate. This quartzite clast is fractured and asymmetrical tailing indicating NE side-to-the top, reverse sense of motion. (c) Enlarged figure of the basaltic matrix in the conglomerate. (d) Conglomerate defining unconformity between KSB and Banasandra belt. Quartzite clast is deposited in amphibole + actinolite rich matrix. The conglomerate has strong foliation and asymmetrical shear structures shows strike-slip sinistral sense of movement. (e) Huge quartzite boulders from NE margin of the KSB representing rift debrites.*

or quartzite that are well rounded and matrix is made up of sand–sized particles (**Fig. 3.4a**). Length of these clasts generally ranges from <1 cm to 6 cm. Conglomerates with larger clasts are identified from NE margin (**Fig. 3.2b**). A 30 m thick conglomerate layer ~3 km southwest of Settikere has

~150 cm long quartzite clasts (**Fig. 3.4b**) representing an extension related deposition environment. Such clasts are brecciated and elongated in the dip direction. Matrix of these conglomerate beds are made up of fragments of basaltic or volcaniclastic rocks (now amphibolite, **Fig. 3.4c**); indicating that the conglomerate was deposited in the proximity of a volcanically active margin. Conglomerate beds in the extreme eastern margin of KSB, separating KSB from Banasandra belt (**Fig. 3.2b**), are also composed of quartzite clasts deposited in matrix framed by quartz, amphibole and actinolite (**Fig. 3.4d**). Oversized 'conglomeratic quartzite' boulders (**Fig. 3.4e**) are observed ~6 km northwest of Settikere. Boulders ranging maximum of 4 m in length are identified. Similar conglomerate beds can be traced as dismembered sequence at least up to 4 km towards the north. In some outcrops of the conglomerate beds in the NE margin, strongly sheared matrix is made of dark-brown colored metapelites with grains of chlorite, biotite and quartz.

II. Quartzite

Quartzite beds are distributed throughout the belt as discrete units with thickness ranging from 300–600 m in a conformable contact with volcanic and volcaniclastic rocks. Some of these quartzites show sedimentary structures like cross bedding indicating their shallow marine origin (**Fig. 3.5a**). Quartzite are either pure without secondary mica or with layers of muscovite or fuchsite in between the bedding/foliation planes.

III. Sandstone-Mudstone

Sandstone is composed of quartz, plagioclase and occasional biotite pointing to granite as the source rocks. Sandstone and mudstone are having a conformable contact with volcanic and volcaniclastic rocks (**Fig. 3.5b**). Outcrops of sandstone often preserve soft sedimentary deformation structures like slump folds (**Fig. 3.5c**), mudstones injected into unevenly fractured sandstone (**Fig. 3.5d)** and sedimentary loading structures (**Fig. 3.5d**). Above mentioned structures are indicative of deformations occurred in unconsolidated/partially-consolidated sedimentary deposits.

Figure. 3.5. *Sedimentary structures (a) Cross-bedding in quartzite (b) Conformable contact between volcaniclastics and sediments. (c) Slump folding in sandstone, mudstone and gravel association. Downslope verging hinge lines and slump absent bedding are present. (d) Uneven fracturing in sandstone. Mudstone injection and sedimentary loading structures are also*

present (e) Silicified lapilli distributed in amphibole-rich matrix. (f) Accretionary lapilli in basaltic matrix. (g) Bedded tuff with alternating amphibole-rich layer and amphibole + quartz-rich layer. (h) Gabbroic sill. (i) Amygdule and quartz clast in the matrix of volcanic rock (j) Basaltic flows with vesicles.

IV. Iron formations

Iron formations are very rare in KSB. Only two units of Iron formations are identified in the mapped area and the maximum thickness of the individual unit is ~1–2 m. Iron formations are generally rich in quartz with thin-layers of magnetite/hematite. These iron formations are in close association with layers of quartzite, tuffaceous sandstone, metapelite and metavolcanic rock, which together constitute a single unit of maximum 20–30 m thickness. Tuffaceous sandstone in this unit is made up of fine-grained quartz, feldspar and occasionally detrital biotite grains.

V. Volcaniclastic rocks

Majority of the KSB is covered with metamorphosed volcaniclastic and volcanic rocks. Metamorphosed volcaniclastic rocks distributed in KSB includes lapilli tuff bedded tuff and volcanic sandstone. Lapilli tuff with rounded to sub rounded accretionary lapilli of >5 cm diameter is identified from ~8 km north of Settikere and close to the contact between Basement Gneiss and KSB (**Fig. 3.5e**). This outcrop has a chlorite and amphibole-rich vesicular matrix and the silicified accretionary lapilli are ferruginous, hard and dense (**Fig. 3.5e**). Accretionary lapilli with ~1 cm felsic lapilli in volcanic matrix (**Fig. 3.5f**) is also distributed in different areas of KSB. Meter size bedded tuff with randomly oriented amphibole grains are also identified from the same location associated with ferruginous beds that we interpreted as altered volcaniclastic material. Similar bedded tuff with >1 cm long and randomly oriented amphibole grains are also well preserved in the western margin of the KSB (**Fig. 3.5g**). Approximately 1 km thick succession of the volcaniclastic rocks are distributed towards the west of the Kibbanahalli town (**Fig. 3.2b**). These volcaniclastic rocks are associated with gabbro sills (**Fig. 3.5h**) and both have a conformable contact relationship. Gabbroic rocks show long elliptical shapes in the regional scale map (dark green color in **Fig.**

3.2b). Volcaniclastic rocks within this succession are tuffaceous sandstone, pyroclastic flow deposits and lahar. Entire NW trending, volcanic and volcaniclastic succession identified from this location is ~50 m long, dipping east, with grain size of amphibole decreasing toward east. These amphibole-rich bedded tuffs are interlayered with fine-grained amphibolite, which we interpret as metamorphosed basalts. Volcanic and volcaniclastic rock successions are in conformable contact with interlayered sedimentary rocks include cross-bedded quartzite, conglomerate, sandstone, mudstone and iron formations.

VI. Volcanic rocks

Metabasites in the KSB are amphibolite/metabasalt, gabbro, and dolerite dyke, along with this; ultramafic rocks are also observed in few locations. Amphibolite (metabasalt) is observed as massive sills and dyke. Layers of foliated amphibolite schists are also observed throughout the study area. Pillow like features and amygdules (**Fig. 3.5i**) are observed in few metabasalts/amphibolite indicating their extrusive nature. Basaltic flows with vesicles and amygdules (**Fig. 3.5j**) are often intercalated with sedimentary rocks also. E–W, N–S and NW–SE trending dolerite dykes that intrude surrounding Basement Gneiss are not observed in KSB.

3.3.3 Bababudan Group of rocks in CSB

Bababudan Group of southern part of CSB has similar volcanic and volcaniclastic rocks with KSB, but possess a thicker stratigraphic column. The stratigraphic column of the Bababudan Group in CSB includes kilometer scale thick limestone, prominent BIF and volcanic rock associations. Based on the structural and stratigraphic analyses of the Bababudan Group in the southern part of CSB an intracratonic rift setting has been assigned to their evolution (Sreehari and Toyoshima, 2020). Moreover sandstone with bedded felsic tuff is also identified from the Bababudan Group of CSB. This provides evidence that more matured bimodal volcanism was active in CSB compared to KSB.

3.3.4 Bababudan Group of rocks in Shimoga Schist Belt (SSB) and Bababudan Schist Belt (BSB)

Route maps of the studied locations in SSB are shown in **Appendix A3**. The samples distributed in contact locations of Basement Gneiss and volcanic rocks are conglomerates and sandstones. Conglomerate with >80cm long quartzite clast are identified within amphibole-rich basaltic matrix (**Fig. 3.6a**). Occasionally, basalt clast is also present in them. Sheared clast in conglomerates shows east-side-up reverse sense of motion (**Fig. 3.6a**). Angular to sub-angular quartzite clast are also present (**Fig. 3.6b**) indicating non-fluvial origin of the conglomerates. Conglomerates from the eastern margin of the BSB, (mentioned as Kadurga conglomerate by Chadwick et al., 1985) show granite, quartzite and basalt clast (**Fig. 3.6c**). Major portion of the matrix in conglomerate is made up of amphibole-rich volcaniclastic rocks. Similar to CSB and KSB, slump folds in sedimentary rocks are present in SSB also. **Figure 3.6d** shows wide exposure of slump folds, characterized by the presence of uneven axial planes and sedimentary load structures.

Basal unit in BSB are Quartz Pebble Conglomerate (QPC). QPC are widely distributed around Chikkumagaluru (**Fig. 3.7a, 3.7b** and **3.7c**). Sedimentary structures likes of graded bedding (**Fig. 3.7b**), cross bedding (3.3**b**), and stratification, are well preserved in the study area. Quartz pebble with size ranges from 1–3cm are present in most of the observed conglomerate (**Fig. 3.7a, b, c**). Cobble sized quartz pebbles are also observed in few locations (**Fig. 3.7d**). Alternate layers of quartz pebble-rich layer and sand-sized quartz rich layer are present in most of the locations (**Fig. 3.7a**, **b**). These structures are belived to be fluvial in origin (Chadwick et al., 1985, Srinivasan and Ojkangas, 1985), and possibly resulted from the river level variations. Typical soft sedimentary deformation structures are preserved in BIF's of BSB (**Fig. 3.7e**)

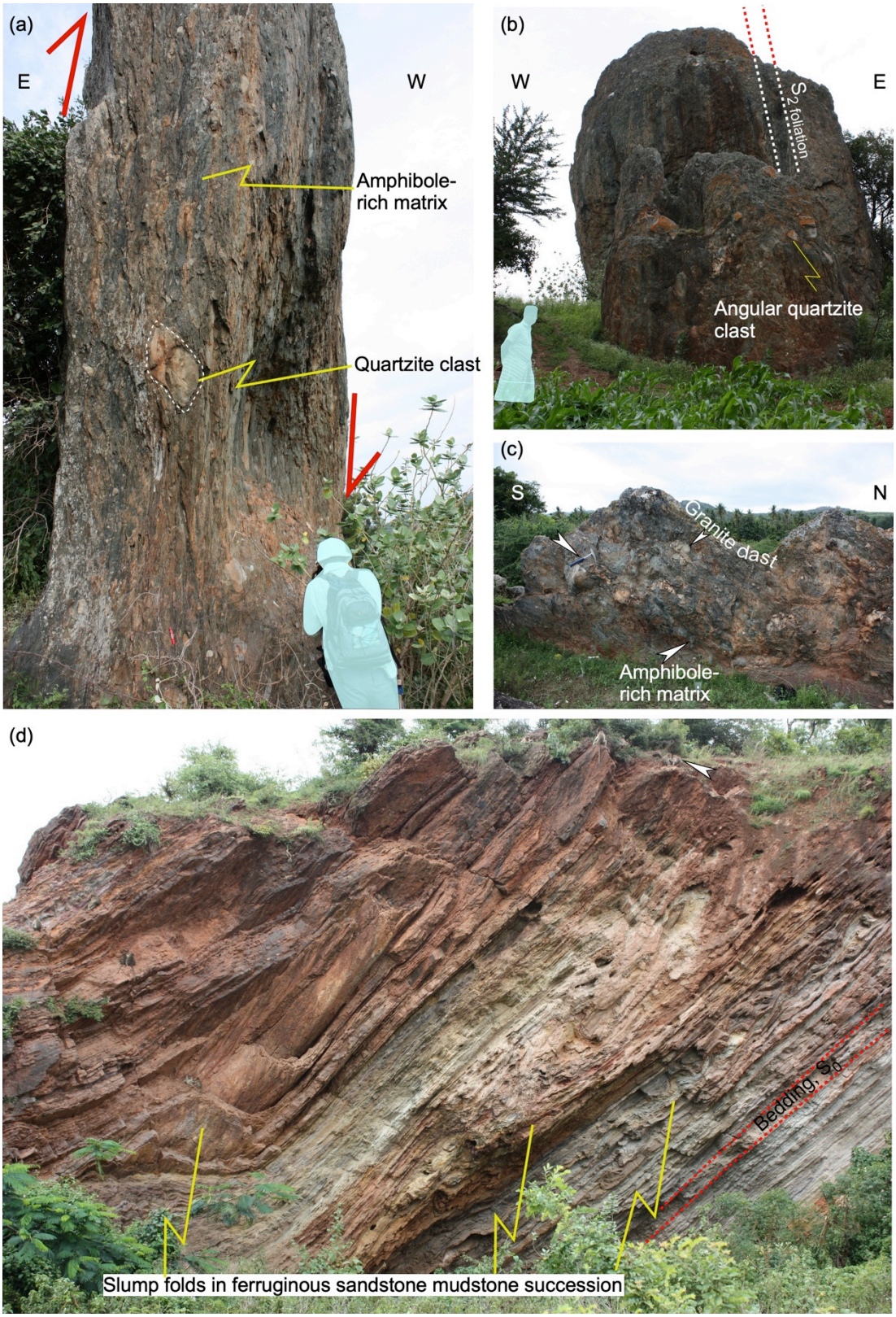

Figure 3.6 *(a), (b) and (c)Typical rift debrites-type conglomerates in Shimoga Schist Belt. (d)Slump folds in sandstone-mudstone succession*

Figure 3.7 *(a), (b), (c), (d). Conglomerates in Bababudan Schist Belt (e) Sedimentary load structures in BIF of Bababudan Schist Belt.*

Sedimentary loading of quartz-rich layer into Fe-rich layer (**Fig. 3.7e**) is indicating soft sedimentary deformation i.e. before the solidification of the sediments.

3.3.5 Stratigraphic relation of KSB with Sargur Group and Basement Gneiss

Structural and stratigraphic discontinuity between Sargur Group of rocks in J.C. Pura belt and Bababudan Group of rocks in KSB are well established in previous works (Section 3.2). My field observation shows a clear stratigraphic break in the southeastern margin of the KSB also (**Fig.**

3.2b). An abrupt change in the lithology is noticeable towards the southeast of the Kibbabahalli town. Majority of the rocks exposed here are altered ultramafic rocks including serpentinite, chlorite-actinolite schist, talc schist, komatiite and pyroxenite associated with metacarbonate rocks and a unit of overturned sandstone-mudstone succession. Previous literatures included these

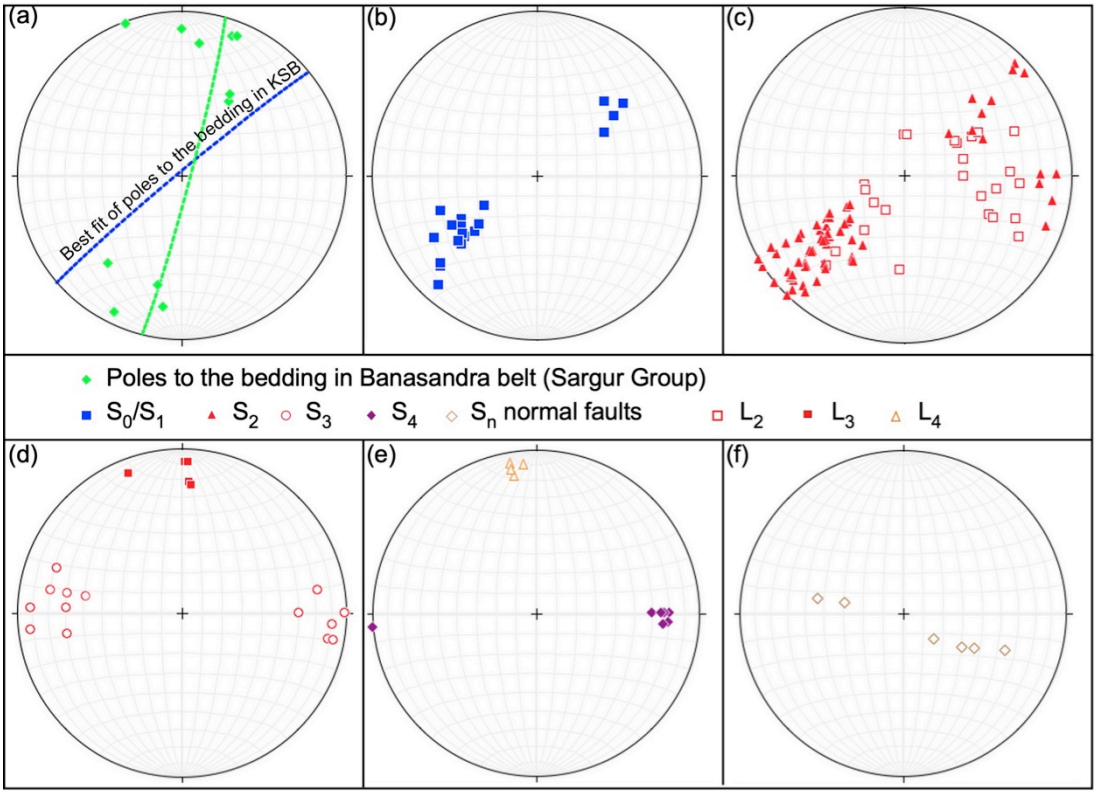

Figure. 3.8. *Linear and planar structures from the study area. (a) Unconformable relation between bedding in Banasandra belt and Kibbanahalli Schist Belt (KSB). (b) Poles to S_0/S_1 structures in KSB (c) Poles to S_2 and L_2 structures in KSB (d) Poles to S_3 and L_3. (e) Poles to S_4 and L_4 structures (f) Poles to D_n normal faults.*

ultramafic units as part of Banasandra belt of Sargur Group (Maya et al., 2017), but clear relation of these ultramafic rocks with KSB and CSB is not well documented. My detailed fieldwork in contact region between Banasandra belt and KSB showed an unconformity represented by ~25m thick sheared conglomerate layer with sinistral sense of movement (**Fig. 3.4d**). This conglomerate is composed of quartzite clasts, size ranging from 2–50 cm, deposited in a matrix made up of fragments of amphibole, quartz

and actinolite. To the west of this conglomerate layer fuchsite mica-bearing sheared quartzite beds are present, together representing westward younging conglomerate-quartzite succession. Structural relation also shows a discontinuity/unconformity between Banasandra belt and KSB, the former has E–W trending bedding and folds with horizontal hinge lines, but the later has NW–SE foliation and vertical to oblique bedding (**Fig. 3.8a, b**). Lithology, structure and field relation show that KSB is not continuously extending to Bababudan Group of rocks deposited in CSB. Interlaying Banasandra belt is stratigraphically and structurally different from the Bababudan Group of rocks in CSB and KSB. Therefore, we propose that KSB and CSB represent separate and isolated volcano-sedimentary basins.

3.4 Deformation history

3.4.1 Large scale geological structures

Five generations (D_0, D_1, D_2, D_3 and D_4) of structural events are reported from the rocks of KSB. Planar and linear feature identified from the study area are shown in stereonet (**Fig. 3.8**). Deformation sequences identified from KSB are shown in **Figure 3.9**. Field photographs of the major structures are given in **Figure 3.10**

First stage deformation, D_0, is allied to initial rifting related processes like normal faulting, slump folding and soft-sediment deformation (**Fig. 3.5c** and **5d**) and formation of bedding (S_0). Slump folds in quartzite and sandstone have uneven axial planes and down slope verging and facing hinge lines associated with undeformed beds, typical of slump folds (**Fig 3.5c;** Alsop et al., 2016).

D_1 event is connected to the development of bedding parallel schistosity (S_1) and associated peak metamorphism. Post-D_1 deformations affected initial depositional and metamorphic features of S_0 and S_1 structures, because of this only limited S_0/S_1 features are preserved. Observed S_0/S_1 planes are NW–SE trending and variably dipping east/west (**Fig. 3.8b**).

Deformation event	KSB	Structural state of deformation planes
D_n	Localised normal faulting	NNE–SSW to NE–SW trending shallow to oblique dipping normal faults
D_4	Strike-slip dextral shear, F_4 asymmetrical folds in local scale.	N–S shear planes, S_4 foliation and strike-parallel lineation L_4 lineation.
D_3	Strike-slip sinistral shear F_3 asymmetrical folds.	N–S trending, vertical to steep east and west dipping shear planes, N–S trending S_3 foliation and strike parallel L_3 lineation
D_2	F_2 folding, map scale folds. Dip-slip reverse faults.	Upright, layer-parallel and isoclinal, S_2 foliations, NW–SE striking east dipping reverse faults, East-side-up motion sense, Dip-parallel L_2 lineation.
D_1	Layer parellel schistosity, S_1, Peak metamorphism.	
D_0	Sedimentation and slump folding.	

Figure. 3.9. *Deformation sequence in the Kibbanhalli Shist Belt (KSB)*

D_2 event is the major regional-scale deformation activity recorded in KSB. D_2 event is characterized by the NW–SE to NNW–SSE trending reverse faults dipping to NE (Fig. 2b, 3 and 4a), NW–SE to NNW–SSE trending S_2

foliations (**Fig. 3.8c**), dip-parallel lineation (L_2; **Fig 3.8c**), and upright folds, F_2. Crenulation foliations (S_2) associated with F_2 folds (**Fig. 3.10a**) are also well preserved in the study area (**Fig. 3.10e**). Regional scale D_2 reverse faults (**Fig. 3.4b and 10b**) are present in both NW and SE margin of the KSB (**Fig. 3.2b**). Northern part of NE contact has a well-preserved unconformity defined by conglomerates, but in other places it is either modified or removed by D_2 structures. So D_2 structures are well preserved in conglomerates (**Fig. 3.4b**) in the boundary. Cross sections show regional scale NW–SE trending F_2 folds genetically connected to the D_2 reverse faults (**Fig. 3.3**). These F_2 folds are layer-parallel, tight, upright horizontal, and maximum half wavelength around ~830 m. (**Fig. 3.3**, cross section CD). It is also noted that southwest-dipping limb of the fold showing southwest-side-up sense of asymmetrical structures (**Fig. 3.10a and 3.10e**) and the northeast-dipping limb northeast-side-up motion sense. Opposite sense of bedding-parallel shear on opposite limbs indicates flexural-slip or flexural-flow folding, suggesting that F_2 fold is a buckling fold. Measured L_2 lineation is dip-parallel (**Fig. 3.8c**), both mineral lineation, and discrete lineation such as the dip-parallel arrangement of accreted lapilli (**Fig. 3.5f**) are also identified. Amphiboles are aligned as stretched minerals in metavolcanic rocks, whereas muscovite or biotite is aligned in the metasediments.

Sinistral strike-slip shearing is identified as the major deformation event during D_3 stage. ~20 km long and ~500 m thick D_3 shear zone is observed in the N-S trending easternmost boundary, that is boundary separating Banasandra belt and KSB. Conglomerate separating Banasandra belt and KSB are strongly sheared indicating left-lateral sense of movement (**Fig. 3.4d**). Sinistral shear zone is also exposed in Basement Gneiss ~4 km SE of Chikkanayakanahalli town. D_3 shear zones strike N–S and dip near vertical. S_3 foliations associated with D_3 event are also >60° to vertical dipping (Fig. 6d). Lineation in the shear zone is strike-parallel (**Fig. 3.8d**) and both intersection lineation and mineral lineation are identified. Mineral lineation is defined by muscovite and chlorite.

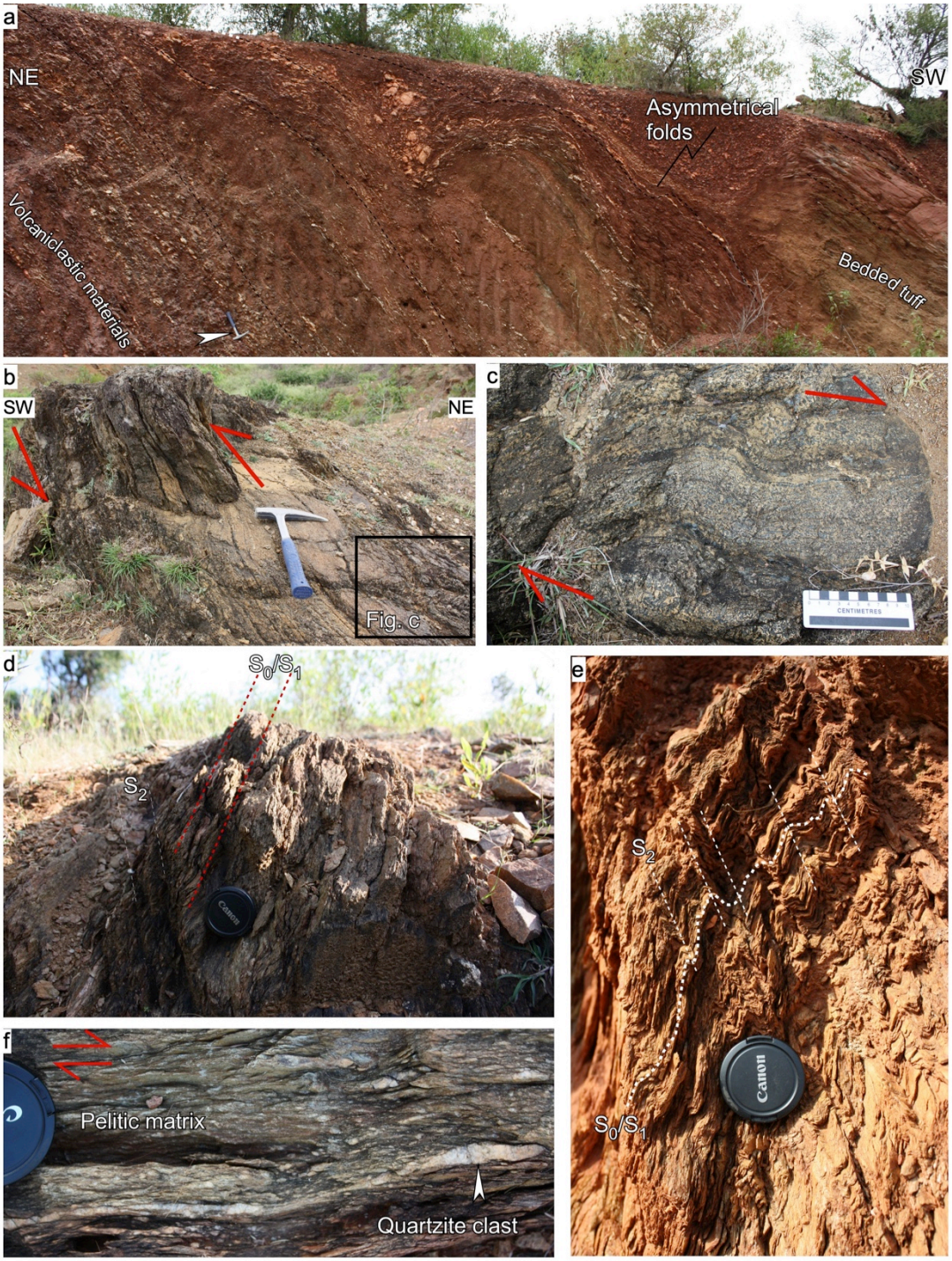

Figure. 3.10. *Major structural features. (a) Southwest dipping formations volcaniclastic sediments and bedded tuff. Asymmetrical folds indicating west-side-up motion sense are also present. (b) Northeast-side-up, D_2 structure in bedded tuff, (c) Enlarged views of asymmetrical fold showing strike-slip dextral movement in the Figure 8b. (d) Crenulation foliations showing S_2 and S_0/S_1 foliations in sandstone. (e) Crenulation foliations showing asymmetrical folding in matrix of conglomerates (f) Strike-slip dextral motion in conglomerate in NE margin.*

Major event during D_4 deformation is the localized dextral strike-slip faults with S-C-C' shear planes. Dextral strike-slip movements are also evident from small-scale asymmetrical folds (F_4 folds) in both NE and SW boundary (**Fig. 3.2b**). Unconformity and D_2 reverse faults are locally folded by F_4 folds (**Fig. 3.2b**). Typical example for this is preserved in volcaniclastic deposits in SW margin (**Fig. 3.10b and 10c**). Movements associated with these D_4, locally dragged existing S_0, S_1 and S_2 foliations to E–W direction. From two localities from the NE margin, N–S striking dextral faults are identified, cross cutting the matrix of the basal conglomerate (**Fig. 3.10f**). S_4 foliations associated with D_4 events are striking N–S and vertical dipping (**Fig. 3.8e**). Lineation (L_4) is parallel to the strike of the fault planes (S_4, **Fig. 3.8e**).

Another set of locally developed faults has a NE–SW to NNE–SSW striking and moderate to shallow dipping fault planes (**Fig. 3.8f**). These faults showing normal senses of movement are considered as localized extensional faults probably associated with post-Dharwar extension processes (D_n).

N–S and E–W trending bedding or foliations are identified in the Sargur Group and Basement Gneiss are interpreted as a result of the pre-D_0 deformation, these E-W trending foliations or bedding are preserved in the Banasandra belt and J.C. Pura belt.

3.4.2 Microstructures and their relation with metamorphism

Fine-grained amphibolite with a S_2 foliation defined by plagioclase and amphibole is interpreted as metamorphosed basaltic rock (**Fig. 3.11a**). Volcaniclastic rocks similar to lahar, with quartz (~50 μm), amphibole and ~100 μm long pumice clasts distributed in fine-grained matrix is also observed, having a weak S_2 foliation (**Figs. 3.11b and 5f**). Bedded tuff in Figure 9a has a S_2 foliation and asymmetrical structures indicating apparent southwest-side-up motion sense and defined by amphibole and quartz with minor amounts of elongated K-feldspar (**Fig. 3.11d**). In a folded amphibole-

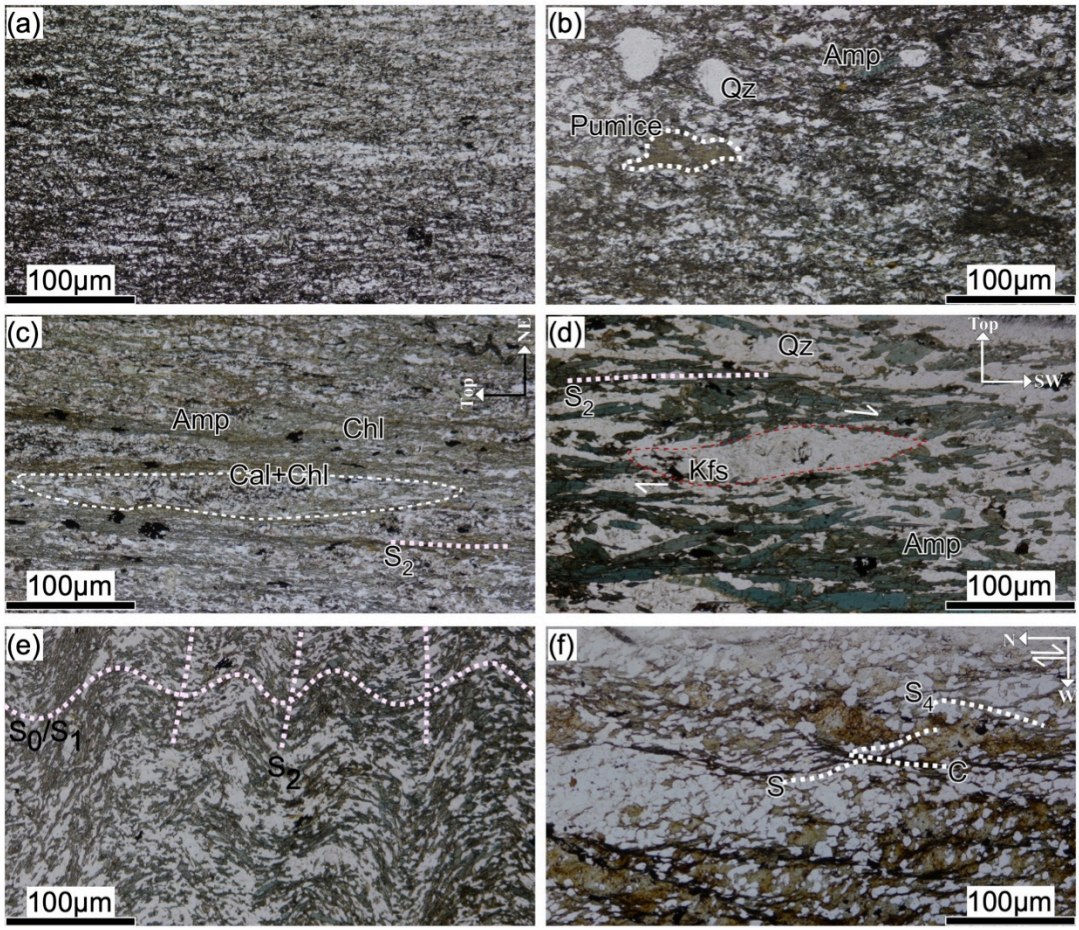

Figure. 3.11 *Photomicrographs (a) Fine-grained amphibolite. (b) Volcaniclastic rocks with pumice clasts. (c) Thin section of accretionary lapilli in Figure 3.5f. Well-developed foliation with amphibole and chlorite as stable phases in shear planes are observed. (d) Photomicrograph of bedded tuff in Figure 3.10a. Asymmetrical structures showing southwest-side-up motion sense. Note the stability of amphibole during D_2 deformations. (e) Layer-parallel F_2 folding associated with D_2 deformation. (f) Strike-slip dextral sense movement in metapelite. Chlorite along shear planes.*

rich volcaniclastic layer, S_0/S_1 foliation defined by alignment of amphibole is folded by F_2 fold with S_2-axial foliation defined by recrystallized fine-grained amphibole (**Fig. 3.11e**). These S_2-forming amphiboles indicate that amphibole is stable during the D_1 and D_2 deformations and metavolcanic rocks in the KSB were metamorphosed in the amphibolite grade.

Metavolcaniclastic rocks such as lapilli tuff have often two types of S_2 foliation: weaker and stronger S_2 foliations defined by amphibole and chlorite, respectively (**Fig. 3.11c**). Chlorite-defining strong S2 foliation develops in

narrow shear zones in amphibolite matrix of meta-lapilli tuff (**Fig. 3.11c**). The narrow shear zones are also characterized by strongly elongated lapilli consisting of fine-grained chlorite and calcite. These microstructural features suggest that change in metamorphic grade of KSB from amphibolite to greenschist facies occurred during D_2 and retrograde metamorphism initiated at the later D_2.

S_4 plane associated with N–S striking D_4 faults in the NE margin of the KSB are marked by chlorite (**Fig. 3.11g**). This confirms that D_4 deformation occurred locally under the retrograde greenschist facies conditions.

3.5 Geochemistry

3.5.1 Analytical Procedures

Major element compositions were determined by X-ray fluorescence (XRF) spectrometry using RIGAKU ZSX Primus II at the Research Institute for Natural Hazards & Disaster Recovery, Niigata University. In this analysis, we used the semi-quantitative analysis program installed in an XRF, and analytical quality was examined by comparing my results for GSJ reference materials (JB-2 and JA-2; **Table 2**). Glass beads were prepared by fusing rock powder sample (0.5 g) with lithium tetraborate ($Li_2B_4O_7$, 5.0 g). Detailed preparation procedures have been described by Takahashi and Shuto (1997).

Rare earth element (REE) and Rb, Sr, Ba, Y, Zr, Nb, Hf and Th abundances were determined using inductively coupled plasma-mass spectrometer (ICP-MS; Agilent 7500a) at the Faculty of Science, Niigata University. For all the samples alkali fusion method was used. Rock powder samples (0.1 g) were decomposed by HF in the Pt crucible, and then sample solutions were evaporated on the hotplate. Residues of samples were fused with Na_2CO_3 (0.5 g) at 1050ºC. The fused samples were dissolved with HNO_3 + HCl and diluted by a factor of 70,000 with a mixture of HF-HNO_3-HCl. Detailed preparation procedures have been described by Senda et al. (2014). A single solution of USGS reference material (BHVO-2) was used as an external calibration standard, using reference values of Eggins et al.

(1997). Sensitivity variation during the analytical runs was corrected using three internal standards (In, Re, Bi). Analytical quality was examined by comparing my results for USGS reference material, W-2a with literature values (Eggins et al., 1997).

3.5.2 Results

Geochemical analyses of fifteen least altered mafic volcanic/volcaniclastic rocks were carried out. Twelve samples were from Bababudan Group and one sample each from Chitradurga Group, Hiriyur Group and Sargur Group are also analyzed. Out of 12 Bababudan Group samples, 8 samples are from KSB and remaining ones are from CSB. Sample locations from KSB are plotted in cross section (**Fig. 3.3**). CSB samples are from basal section of Bababudan Group; Chitradurga Group sample is from top most part of the stratigraphic succession and Hiriyur Group sample is from middle of the top most basalt strata. All these samples have been metamorphosed to low-grade amphibolite facies to greenschist facies condition. Results of major, trace and rare-earth element (REE) geochemical analyses are listed in **Table 2.**

Alkali elements especially Na and K are mobile during the greenschist to low-grade amphibolite facies metamorphism. Moreover, in volcaniclastic rocks, the silica content varies during alteration. Other than that, if the eruption is accompanied by pyroclastic flow, country rocks or previous volcanic materials can also be mixed together to change the original composition. Based on these facts we use immobile elements such as high field strength elements (HFSE) and REE for further geochemical characterization and interpretations, although mixture of different generations of volcaniclastic/volcanic rocks could not be differentiated in the present scale of investigation.

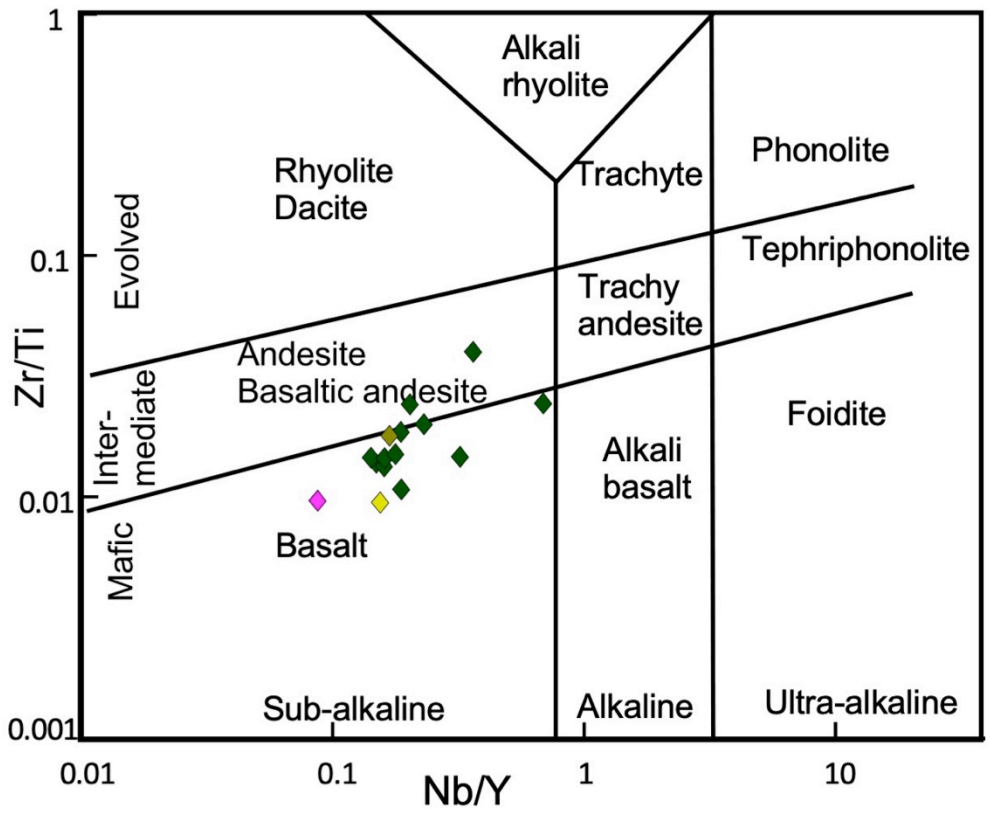

Figure. 3.12. *Discrimination diagram of volcanic rocks. Trace element classification diagram of Winchester and Floyd (1977), modified by Pearce (1996).*

All samples plot within the field of basalt to basaltic andesite in Zr/Ti vs. Nb/Y diagram (**Fig. 3.12**). They have sub-alkaline compositions (Nb/Y<0.8). Even though there is no evident bimodal distribution, some samples plot in the intermediate field, owing to their high Zr/Ti ratio. The range of SiO_2 in the sample (**Table 2**) is between 44–62%, which is in agreement with the mafic to intermediate clusters, as observed in **Figure 3.12**.

Trace elements are normalized with primitive mantle values from McDonough and Sun, (1989, **Fig. 3.13**). Trace elements show parallel to sub-parallel trend with 10 to 100 times enrichment of the sample compared to the primitive mantle. Based on normalized trace element and REE patterns, samples have been divided into three types, Type 1 (**Fig. 13a, d**), Type 2 (**Fig. 3.13b, e**) and Type 3 (**Fig. 3.13c, f**). Type 1 samples have Nb-Ta negative anomaly with slightly enriched Th, La, Ce, Pr and Nd. Type 2 samples have almost flat trend with slightly depleted HFSE (Nb, Ta, and Th)

in two samples (1808205A and 1808211A). Type 3 samples have positive Zr-Hf anomaly for 4 out of five samples. Some of the samples show Th enrichment.

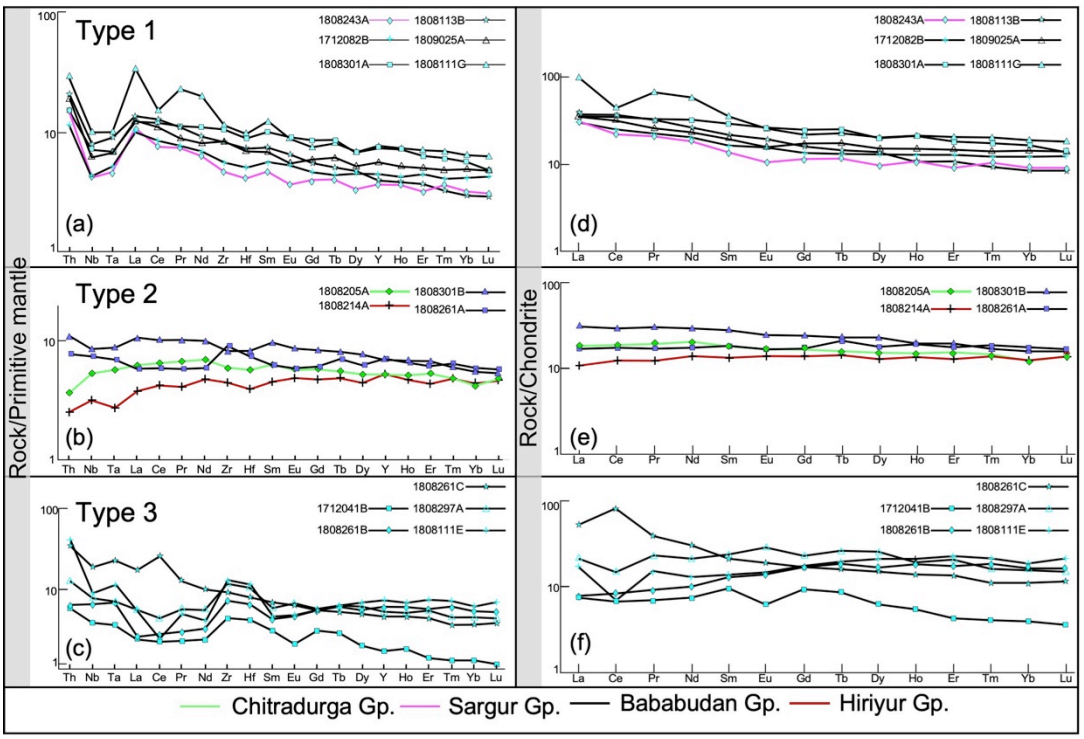

Figure 3.13. *Multi-element spider diagrams normalized to primitive mantle and chondrite normalized REE diagrams. Primitive mantle values and Chondrite values are from Sun and McDonough (1989).*

REE's are normalized to chondrite values from McDonough and Sun, (1989) Type 1 sample shows slight LREE enrichment (Fig. 11d, $(La/Yb)_N$ = 2.1 to 5.2). Type 2 REE shows flat trend (**Fig. 3.13e**) with negligible LREE enrichment ($(La/Yb)_N$ = 0.8–1.8). 3 samples from Type 3 group show flat LREE pattern (**Fig. 3.13f**) with two samples (1808111E and 1808297A) has Ce anomalies, whereas one sample (1808261C) has LREE enrichment ($(La/Yb)_N$ = 4.68). HREE's in Type 1, Type 2 and Type 3 show identical flat pattern except one sample (1712041B).

3.6 Discussion

3.6.1 Volcanic and sedimentary structures

Krapez et al. (2020) presented a detailed review on the evolution of DC and mentioned the tectonic, stratigraphic and geochronological constrains of the Bababudan Group. According to their findings, the Bababudan Group is an intracontinental rift developed between 2765–2720 Ma. Similar views about the tectonic setting, i.e, an intracontinental rift, were presented in Chadwick et al., (1985) based on their field, structural and stratigraphic understanding of the Bababudan basin. They interpreted an eastward deepening-extensional setting as an evolutionary mechanism for the Bababudan Group. Sedimentary and stratigraphic analysis in the Bababudan Group rocks exposed in Bababudan, Sigeggudda and KSB have also revealed intracontinental rift setting as the possible evolutionary mechanism (Srinivasan and Ojkangas, (1986).

Sedimentary and volcanic structures preserved in KSB are giving direct insights into the depositional environment of the terrain. Soft sediment deformation features such as slump folds (**Fig. 3.5c**), fractures filled by mudstone injection (**Fig. 3.5d**), and sedimentary loading are identified in my own field studies in KSB. Chadwick et al., (1985) also pointed out the liquefaction structures including convolute bedding and water escape structures in Bababudan basin, interpreted to have been developed in seismic activities associated with volcanism and initial basin growth. We interpret that, slump folding and soft sediment deformation points to a tectonically active, aqueous environment of deposition, moreover sediments must be in an unconsolidated/partially-consolidated state during the deformation. Adding to this, cross bedding in sandstone and quartzite (**Fig. 3.5a**) throughout KSB implies a possible shallow water/marine environment for their deposition, consistent with what has been reported from Bababudan Group in previous studies (Chadwick et al., 1985, Bhattacharya et al., 2015). Shallow marine, rapidly subsiding, sub-aqueous to aqueous environment has been attributed to several Formations (Kalasapura, Allampur, Santaveri, Mulaingiri, Jagar and Mundre) in the Bababudan Group (Chadwick et al., 1985). It is important to note that the contact between sedimentary rocks and volcanic rocks in KSB are conformable (Fig. 5b), which provides a hint that the volcanism was simultaneously occurring during active deposition.

Conglomerates in KSB show variations in their clast size and matrix composition. Conglomerate with >1m-clast size is preserved in KSB (**Fig. 3.4b, 4e**) mainly in NE margin of KSB. This type of conglomerate is poorly sorted, matrix-supported, and massive without stratification. These are characteristics of debris flow related deposits (Reading, 2009). Rift basins generally bounded by normal fault scraps on both sides, a foot of which slope debris are accumulated as debris aprons or fans (Haughton et al., 2003). Based on this, we speculate that conglomerate with oversized clast (**Fig. 3.4b, 4e**) are produced as rift debrites rimming the KSB. This may be produced as a result of extension of stable quartzite platforms. Matrix of some conglomerates, made up of basaltic materials (**Fig. 3.4c**), is pointing to the fact that the deposition was close to a volcanic edifice. Conglomerate with centimeter sized quartz pebble as clast is distributed mainly on SW margin of KSB. These conglomerates have either sandstone-rich matrix (**Fig. 3.4a**) or amphibole-rich matrix (**Fig. 3.5i**). They are possibly formed by the fluvial action or by sedimentary sorting at the toe end of rift debrites. Some of fragment-supported conglomerates may be of alluvial fan deposits. The rift debrites type conglomerate concentrates on NE side of the KSB. This fact indicates appearance of steep slopes or cliffs on NE side of KSB and the eastward deepening of the basin consistent with interpretation of Chadwick et al., (1985).

Rare outcrops of deformed pillow basalts, amygdular flows, and the flow structures depict the extrusive nature of basaltic rocks. Presence of lapilli tuff also indicates the ancient explosive volcanic activity. Variable size of accretionary lapilli are probably linked to their evolutionary mechanism (Schumacher and Schimincke, 1995). Lahars are reported from KSB (Srinivasan and Ojkanjas, 1992) and also identified in my fieldwork, they are generally products of water-rock interactions during volcanic activity or post-volcanic processes that occurred near crater lake or river (Vallance and Iverson, 2015). Volcaniclastic rocks with elongated amphibole grains (**Fig. 3.5g**) are interpreted as altered volcaniclastic materials. Abundant quartz present in matrix within this rock signifies the contribution from Basement Gneiss during the sedimentation. Similar amphibole-rich, pyroclastic rock

were reported from Proterozoic Cudappah Basin, and lithologically described as feebly stratified lapilli-tuff facies, developed through laminar pyroclastic flow mechanism in an intracratonic rift setting (Goswami et al., 2010).

Striking difference in the stratigraphic sections of KSB and CSB is the absence of limestone and rarity of BIF in KSB. My own field observation shows that ~700m thick limestone formation and ~500m thick BIF layers in southern part of CSB (Sreehari and Toyoshima, 2020). BIF and limestone layers are placed above the volcanic and volcaniclastic rocks (Sreehari and Toyoshima, 2020). This implies that basin development has been more prolonged in CSB even though sedimentary conditions (slump folds in BIF and stromatolites in limestone) indicate shallow-marine signatures. Based on this we infer that KSB was an intracontinental immature/failed rift basin in which, rifting processes had sustained only for a comparatively short span of time. As mentioned previously a fining upward section from conglomerate via quartzite (sandstone) to BIF with limited thickness are also compatible with development of a narrow rift basin.

Sedimentary and volcanic features preserved in KSB points to the fact that active tectonic, shallow water and extrusive mafic volcanism occurred contemporaneously in KSB. These are in agreement with my proposed model of intracontinental rift setting for the evolution of KSB. A similar structure in Bababudan basin and CSB of WDC implies a coeval intracratonic rifting related shallow marine volcanism and sedimentation throughout the Craton.

3.6.2 Structural and tectonic evolution

Detailed geological map (**Fig. 3.2b**) and structural cross sections (**Fig. 3.3**) show that D_2 reverse fault and associated F_2 isoclinal folds are the major/regional scale deformation events in the study area. A pair of reverse faults in the NE and SW margins, and ~2000 m thick association of tightly folded volcanics and the sediments shortened between these reverse faults are present in KSB. This co-existence of reverse faults with thick succession of volcanics and sediments packaged between these faults are typical

features of an inverted rifted continental margin (Stein et al., 2018). A regional scale NE–SW shortening was explained as a major deformation

event in DC (Chadwick et al., 1997). We speculate that during the NE–SW compressive regime, NW–SE reverse faults and simultaneously parallel folds with NW–SE trending axial planes are developed. The same metamorphic grade (low-grade amphibolite) preserved in volcanic rock during folding and reverse faults are in support with this speculation. This reverse fault and layer-parallel fold association is identical to a fold-and-thrust-belt (Poblet and Lisle, 2011), as shown in the southern part of CSB (Sreehari and Toyoshima, 2020).

Contrary to the above interpretation, passive sinking of the cover rocks to the Basement Gneiss without any crustal shortening is proposed as the evolutionary mechanism of KSB (Chardon et al., 1996). Normal faults in the NE and SW margin, shallower cleavages than bedding associated with these normal faults were presented as the prime evidence for the passive or 'sagduction' tectonics. But these cleavages are identified as crenulation cleavages (S_2; **Fig. 3.10d** and **3.10e**) distributed throughout the belt rather than the boundary. My field investigation also shows reverse faults in the conglomerate (**Fig. 3.4b**) and volcanic rocks (**Fig. 3.10b**), from the boundary, which is not explained in the 'sagduction' model. Moreover, overall west verging structures in the folds (**Fig. 3.3**) are consistent with the east-side-up motion sense. In the opposite verging fold limbs apparent reverse sense of movements defined by asymmetric folds (**Fig. 3.10a** and **3.10e**) are also consistent with my fold-and-thrust belt model. Normal faults that we observed in KSB are localized rather than a regional event and these faults trends NE–SW.

D_3 event is a sinistral strike-slip event that observed in the eastern margin of the study area and we interpret this as contemporaneous with the evolution of Gadag-Mandya-Shear-Zone (GMSZ; Sreehari and Toyoshima, 2020) in the eastern margin of CSB (**Fig. 3.1b**). The N–S striking regional scale structure of the eastern margin shear zone is consistent with the N–S trend of GMSZ (**Fig. 3.1b**).

D_4 deformation is not a penetrative deformation in the study area; strike-slip motion in the later stage of the evolution of DC is documented as dextral sense (Krapez et al., 2020, Sreehari and Toyoshima, 2020). We interpret, weaker zones/previous shear zones including unconformities and D_2 shear zones, got rejuvenated during the D_3 and D_4 strike-slip events. Comparatively low-grade microstructures such as alignment of chlorite in shear planes are consistent with our interpretations.

My findings on structures conclude that the superimposition of D_2, D_3, and D_4 deformations are responsible for the elevation and overall structural architecture of KSB, If NW–SE thrusting during D_2 and N–S sinistral strike-slip faulting during D_3 occurred simultaneously in the same event, a sinistral transpression setting would have truly happened in the WDC as shown by Chadwick et al., (1989, 1997, 2000). But based on our evidence, the strike slip deformations (D_3 and D_4) are probably younger event than the NW–SE thrusting (D_2), and so it may be difficult to prove a sinistral transpression setting in the WDC.

3.6.3 Geochemical implications of intracratonic rifting.

In Th/Yb vs. Nb/Yb plot (**Fig. 3.14**) basalts from this study demonstrate a gradational trend initiating from primitive mantle (PM) array towards the continental crust (CC) indicating a significant role of crustal contamination during their evolution. Two samples plotting within the mantle array are from Chitradurga and Hiriyur Groups implies their mantle affinity with less crustal contamination. For comparison we plotted data from Manikyamba et al., (2012, 2013; **Fig. 3.15**) from Sigeggudda schist belt (see **Fig. 1.6b**) of Bababudan Group which also gave a comparable trend with my data. Data from Archean Murmac Bay Group, Canadian shield (~2.7 Ga), a well-studied example of intracontinental Archean rift (Hartlaub et al., 2007) is also matching with my data set. All these lines of evidences suggest to a continental crust-plume derived magma interaction during the earliest stages of evolution of Bababudan Group as if in an intracratonic rift setting.

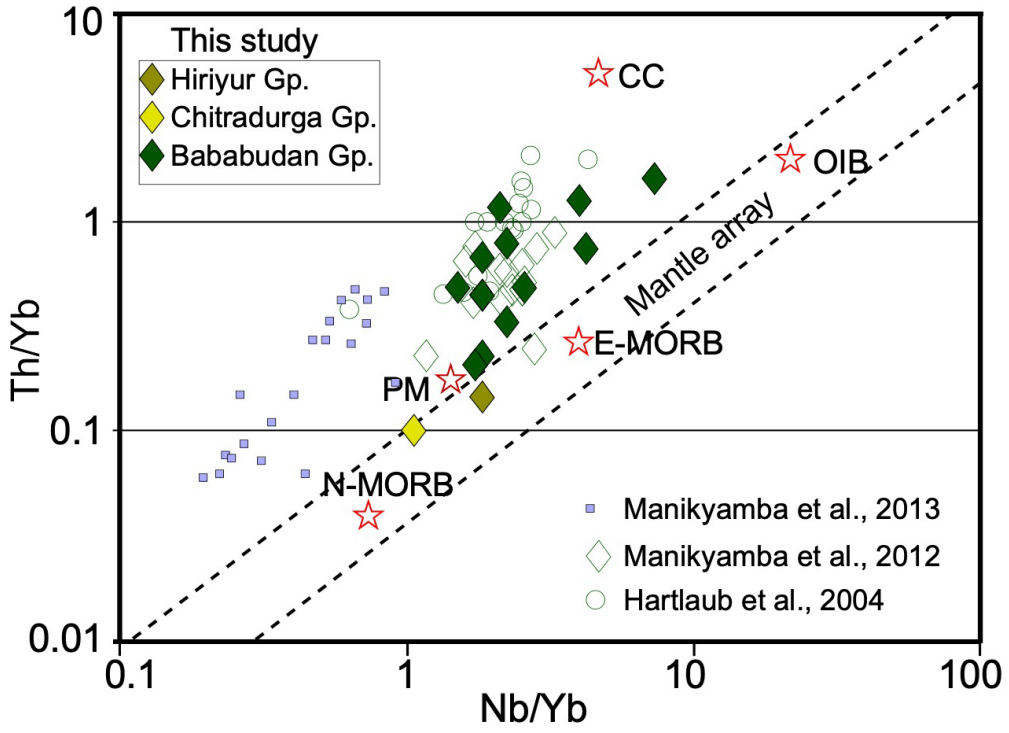

Figure 3.14. *Th/Yb vs. Nb/Yb diagrams after Pearce (2008).*

Type 1 samples in my study shows Nb-Ta negative anomalies, and enriched LREE (**Fig. 3.13a**). This is a typical feature of crustally contaminated basalts (Hollings and Kerrich, 1999). Contaminated lithospheric mantle that has evolved through a subduction related TTG generation (Hollings and Kerrich, 1999) could also be able to generate Nb-Ta depleted basalt. Subduction related TTG generation is postulated in WDC prior to the formation (> 3.0 Ga) of Bababudan Group (Jayananda et al., 2008; Tushipokla and Jayananda, 2013). Also, Type 1 basalts are showing similarities in trace element pattern with basalts from Murmac Bay Group (**Fig. 3.15a**, Hartlaub et al., 2007) and one group of basalts from Sigeggudda belt of WDC (**Fig. 3.15a**, Manikyamba et al., 2012). Type 2 samples HREE pattern similar to the previous studies and slight LREE depletion in this group are identical to E-MORB trend (**Fig. 3.15b**). HREE depleted pattern in Type 3 (**Fig. 3.15c**) is because of one sample (1712041B), otherwise they also follow similar HREE pattern of previous studies (**Fig. 3.15c**). Type 3 samples show positive Zr-Hf anomalies (**Fig. 3.13c**). Zr-Hf positive anomalies in basalts are generally related to the assimilation with TTG type crust or assimilation from zircon-rich domains or by the interaction with zircon rich

felsic melt (Said et al., 2010). Contrary to Type 1 and 3, Type 2 basalts are showing no evidence of crustal contamination; moreover it is showing a trend similar to E-MORB pattern. It is also found that, except for one sample (1712041B), all of the analyzed samples show flat MREE and HREE pattern (**Fig.3.13 d, e and f**). This is probably linked to a single parental magma source. REE patterns of three samples (1808297A, 1808111E, and

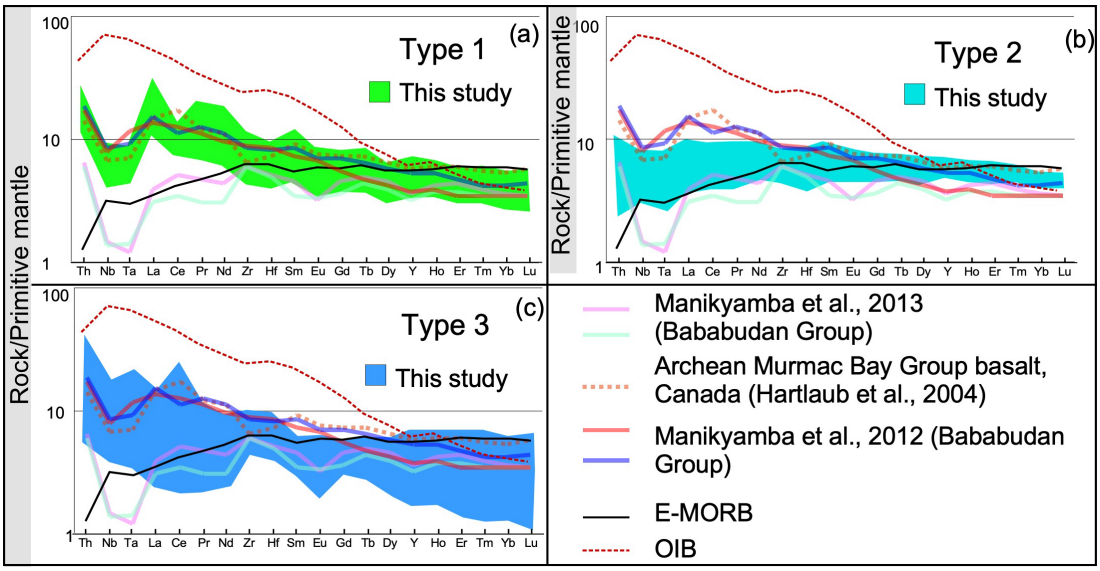

Figure 3.15. *(a), (b), (c) Comparison of trace element geochemical data in this study with representative data from previous studies.*

1808261B) showing identical trend of Type 2 samples. But these samples also showing Zr-Hf positive anomalies probably points to the fact that samples are contaminated versions of Type 2. In conclusion Type 1, Type 2 and Type 3 samples probably generated within a limited span of time from a single source with varying amounts of crustal contamination. Higher silica content (>50%) in Type 1 and Type 3 can be linked to the degree of contamination. Basalts with or without crustal contamination are recorded from intracontinental rift setting in the Archean terrains (Said et al., 2010, Said and Kerrich, 2010). Similar geochemical variations in the volcanic rocks are also reported in the intercontinental, East African Rift system (Rooney, 2020) and therefore the continental rifting processes undergoing in Archean may not be different from present day.

3.6.4 Implications for the tectonic evolution of Bababudan Group and WDC

Age of felsic ash fall deposit from Mulaingiri formation in Bababudan basin was reported as 2719 ± 7 Ma (Trendall et al., 1997). Based on this, Krapez et al. (2020) argued that the rifting event in Bababudan Group might have started at least by 2756 Ma. This argument was based on the fact that ~45 m.y. thermal time constant determines the rate of lithospheric extension. Previous geochronological studies in quartzite and conglomerate of Bababudan Group show that maximum depositional age is in the range of 3136 ± 7 – 3205 ± 21 Ma (Hokada et al., 2013, Lancaster et al., 2015, Maibam et al., 2016, Krapez et al., 2020). The older age spectrums in the sedimentary rocks are consistent with the published age of the granites in the DC (Lancaster et al., 2015), which implies that Basement Gneiss is the source of these sediments. Sedimentary analysis by Srinivasan and Ojkanjas, (1992) also showed that Basement Gneiss are the source for conglomerates, and importantly they have a fluvial origin.

Youngest age of Basement Gneiss in WDC is 2988 ± 9 Ma (Bukkapatna augen gneiss, Chardon et al., 2011). This implies that there is ~200 m.y. of time gap between rift initiation and temporary cessation of granite genesis. So ~200 m.y long time gap probably resulted in peneplanation and quartzite platforms above a stable continent (**Fig. 3.16a**). This was succeeded intracontinental rift related explosive volcanic activities in a shallow water depth environment. This resulted in deposition of volcanic, volcaniclasic and sedimentary rocks (**Fig. 3.16b**) with succession staring with rift debrite type conglomerate passing through volcaniclastic and volcanic rocks. The NE–SW shortening reported throughout the DC (Chadwick et al., 2008, Sreehari and Toyoshima, 2020) shaped the structural architecture of KSB similar to an ‘inverted failed rift/fold-and-thrust belt (**Fig. 3.16c, d**). Simultaneous rapid rifting events probably developed intracratonic basin in different locations within the WDC. These resulted in the formation of Bababudan Group of rocks, some of which are preserved in Bababudan, Chitradurga, Sigeggudda and KSB schist belts. Similarities in stratigraphic succession (Chadwick et al., 2000) and age relation in these schist belts (Krapez et al., 2020) provide supporting evidence for my interpretation of development of multiple rift basins. After the termination of rifting, granitic

plutons intruded into the Bababudan Group probably indicating the initiation of convergence event. This convergence mechanism may act as a barricade

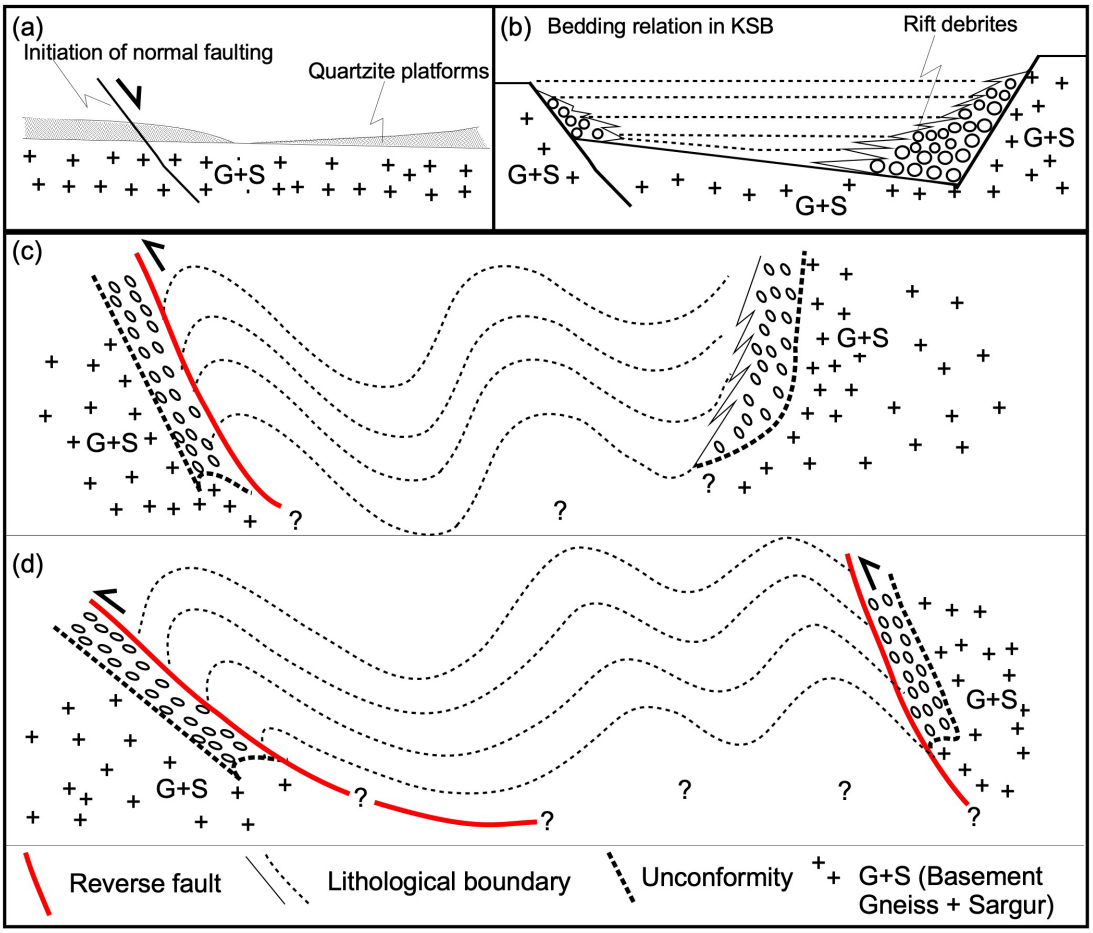

Figure 3.16. *(a) Development of quartzite platforms above Basement Gneiss (b) Syn-rift sedimentation in KSB (c) and (d) Schematic section of present structural architecture of KSB. G+S – Granite and Sargur Group.*

for continuous growth of rifts into larger oceans and results in multiple aborted rifts in DC. Above-mentioned factors accentuate the role of failed rifts in the initiation of crustal growth process in DC. This also highlights the fact that, plate tectonics were active at least from the beginning of 3 Ga, although it has not attained the present-day style until Archean-Proterozoic boundary.

3.7 Summary

Detailed field and microstructural observations in KSB pointed out five stages of deformations in KSB. First two stages (D0 and D1) are related to sedimentation and schistocity formation. D2 event is the major deformation

event in KSB with NW–SE trending and east dipping thrust faults, NW–SE trending S2 foliation and F2 folds. F2 folds are upright, bedding parallel and positioned between east dipping thrust faults. D3 is a regional scale strike-slip sinistral sense of faulting event. D4 event is non-penetrative with localized dextral strike-slip faults distributed along the boundary of the schist belt. Sedimentary and volcanic structures and their mutual relations show a shallow marine, explosive volcanic activity in a failed rift type tectonic setting. Trace and REE patterns of mafic to intermediate rocks from KSB shows both crustally contaminated and uncontaminated volcanic rocks similar to be evolved in an intracratonic rift setting. Based on the detailed field observation, structural geology and geochemical analysis we conclude that KSB is a well-preserved Archean intracontinental failed rift/aulocogen that formed in the initial stages of rifting of post 3.0 Ga DC.

Chapter 4

4 DISCUSSION

4.1 Introduction

I presented detailed structural analysis and tectonic evolution of CSB and KSB in Chapter 2 and Chapter 3 respectively. A failed rift model of crustal evolution is evident in the WDC from the discussions presented in above-mentioned chapters. So I would like to clarify two more aspects, 1) Why schist belts in WDC are not accretionary complexes and 2) the tectonic model and temporal evolution of failed rift in WDC. For above-mentioned purpose, I will present this discussion as three sections; in first part (section 4.2) I will discuss the detailed structural and field relations of a Cenozoic accretionary complex, Hiroo Complex, Hokkaido, Japan. Based on this I will compare the structures and stratigraphic relations in Hiroo Complex and WDC to raise my arguments against accretionary complex models in WDC. In sections 4.3 and 4.4, Geochronological relation between different units and temporal evolutions of failed rifts in WDC and their tectonic implications will be highlighted. Based on this I will present my findings on role of aborted/failed rifts in crustal growth mechanism throughout the earth history (Section 4.5).

4.2 Comparison of structural architecture of a Cenozoic accretionary complex with structures in WDC: Why WDC's schist belts are not mélanges?

4.2.1 Introduction to Hiroo Complex, Hokkaido Japan.

Hokkaido is located in the northern part of Japan and triple junction of the Pacific, the North America and the Eurasia plate is situated in the south of Hokkaido (**Fig. 4.1a**). Geologically Hokkaido is classified into three main tectonic units; Western Hokkaido, Central Hokkaido and Eastern Hokkaido (**Fig. 4.1b**).

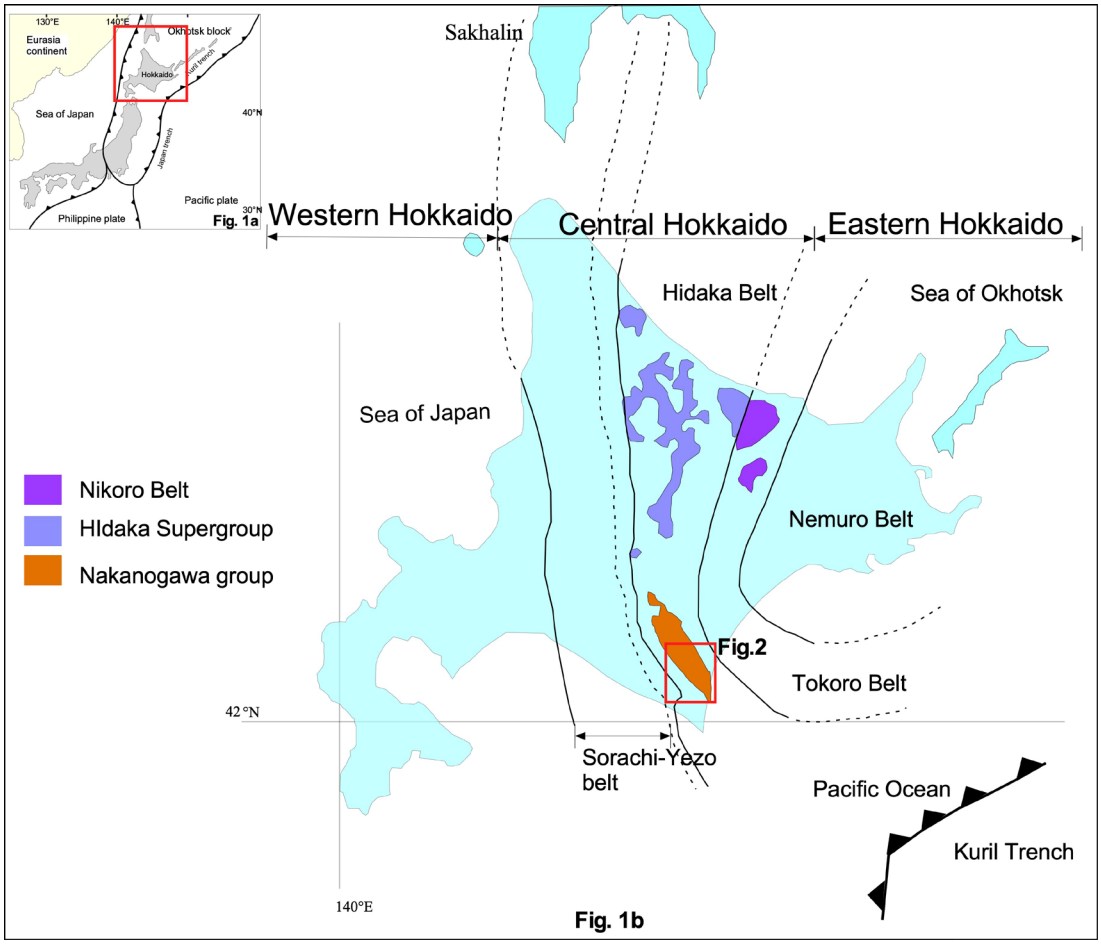

Figure 4.1: *(a) Generalized tectonic setting of Japan, red box shows Hokkaido, (b) Tectonic division of Hokkaido (after Nanayama et al., 2017; Yamasaki and Nanayama, 2018 and references there in) simplified geology of Central Hokkaido is also marked.*

Hidaka Supergroup in the southern part of Hidaka metamorphic belt (HMB) is considered as Nakanogawa Group. On the basis of lithofacies it is divided into Satsunaigawa Formation and Yaoromappugawa Formation that are stratigraphically lower and upper respectively and separated by a strike-slip Nupinaigawa fault (Nanyama 1992a, 1992b). Nanayama et al. (2017) also considered Nakanogawa Group as a part of Hidaka Group and divided it into northern and southern tectonic unit bounded by Nupinaigawa fault. Nanayama and Ganzawa (1997) reported the detailed lithofacies and sedimentary analysis of northern unit of Nakanogawa Group. According to that study northern unit is classified into three sedimentary formations, from east to west, Oda mélange, Sakashita Formation and Yaoromappugawa Formation respectively and are bounded by fault contacts. Southern unit of

Nakanogawa Group is further classified into Hiroo complex and Kamitoyoni formation, former is a deformed mélange facies of rocks along with exotic blocks of basalt and limestone and later is a separate turbidite facies rock formation (Nanayama 1992a, Nanayama et al., 2017, 2018).

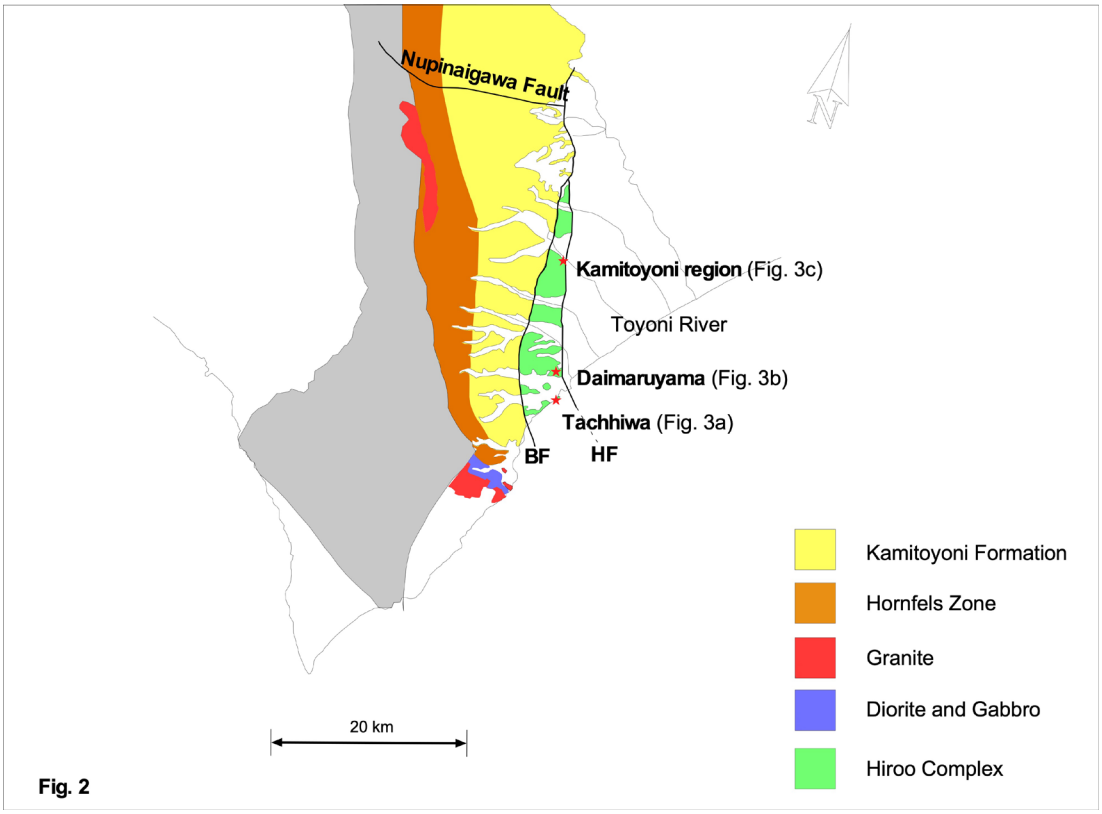

Figure 4.2 *Geological map of southern unit of Nakanogawa Group (after Nanayama et al., 2017), starred locations are studied regions within Hiroo Complex. HF:Hiroo Fault, BF:Bihoro Fault. Locations for the route maps in Figs 3a,3b and 3c are also marked.*

Previous studies explained detailed lithology of northern and southern unit of Nakanogawa group along with radiometric and fossil age data (Owada et al., 1992, Nanayama 1992a,b, Kontani 1978,1980, Nanayama et al., 2017,2018, Nanayama and Ganzawa 1997). Yaoramappugawa formation and Satsunaigawa formation of northern unit are majorly composed of turbidite facies of rock and minor component of inter-bedded acidic tuff layers within them. Oda mélange of the same northern unit has red and green mudstones of hemipelagic origin as main rock types. On the other hand in southern unit, the Kamitoyoni formation has less or no exotic component in it and major part of the formation is covered by turbidite facies of rocks. The

Hiroo complex in southern unit along the eastern part of the Kamitoyoni formation is lithologically described as deformed turbidite facies (mélange facies) rocks along with blocks of bedded limestone, micritic limestone and red mudstone as exotic blocks. The Hiroo Complex is separated from other formations by NNW trending sinistral faults Bihoro fault and Hiroo fault in the west and the east respectively (Nanayama, 1992a). The Hiroo complex also has several allochthonous blocks of greenstones within this mélange facies of rocks. One of them is the Daimaruyama formation, which is largest (800 m × 200 m.) among these greenstone formations. The Daimaruyama greenstones are described as coarse volcaniclastic rocks with lesser amount of lava and recent geochemical study in this rocks emphasized that they are geochemically comparable with Nikoro group greenstones of the Tokoro belt in the Eastern Hokkaido (Yamasaki and Nanayama, 2018). Another well-studied greenstone formation in Nakanogawa Group is Tachiiwa body, which is on the other hand reported as alkaline volcanic rock and they are also compared with Nikoro Group greenstones based on geochemical study (Owada et al., 1992). The turbidite facies rocks in Tachiiwa region are 1000m thick and characterized by tectonic deformation features (Nanayama 1992b). Depositional age of Nakanogawa group is discussed in different studies using both fossil ages and radiometric ages. Paleocene (66-56 Ma.) radiolarian fossils are reported from Yaoromappugawa Formation in northern unit; Kamitoyoni Formation and Hiroo Complex in southern unit (Nanyama and Ganzawa 1997). Nanayama and Ganzawa (1997) indicated fission track (FT) ages for vitric acidic tuff in Sakashita Formation in northern unit as 47.9 ± 2.6 Ma (2 σ error) and 50.4 ± 2.4 Ma (2 σ error) for Kamitoyoni Formation in northern unit. Reported sandstone ages using FT method from southern unit are 58.6 ± 28.2 and 67.1 ± 24.2 with 2σ error (Ono, 2002). K-Ar ages of biotite hornfels from Meguro-Shoya area have been reported as 35–32Ma (Saeki et al., 1995) and Ono (2002) indicated 40-39 Ma FT ages of hornfels from Hiroo area and these authors indicated depositional ages Nakanogawa group should be older than the hornfels age. Three age group of detrital zircon population are identified through U-Pb analysis of turbidite sandstone and acidic tuff from

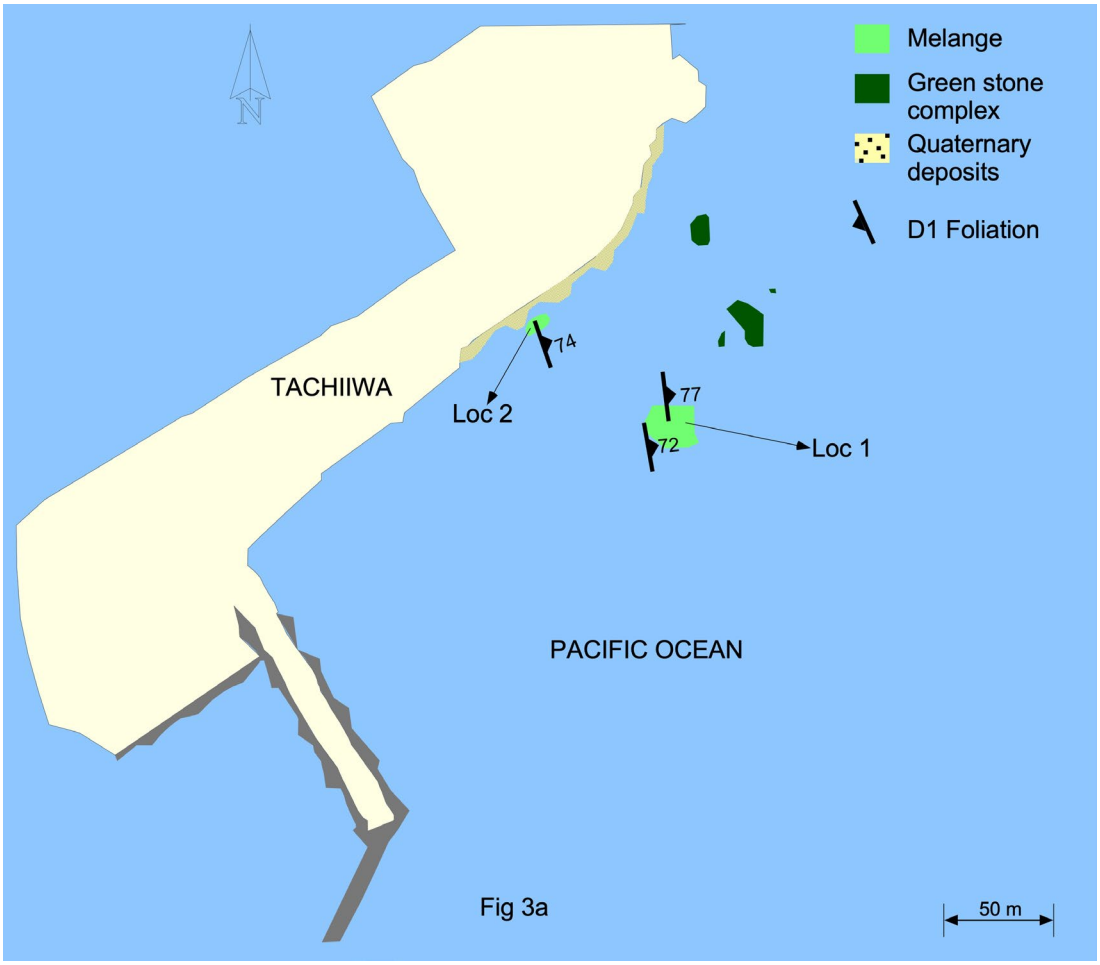

Figure 4.3a*: Route map of Tachiiwa region.*

Nakanogawa Group – 1) Youngest group with age ranges from 80-53Ma, 2) Second group of zircons has three different age group; 120–180Ma, 180–140Ma, 340–220Ma which are mentioned as intermediate group and 3) Oldest group of Precambrian zircons are dated as 2700Ma, 2200Ma and 1900Ma (Nanayama et al., 2017). Youngest group of zircons from northern unit and southern unit have different age range, 58–48 Ma and 66–56 Ma respectively. Sandstone petrology and paleocurrent direction analysis of sandstone sequence in Nakanogawa Group is carried out by Nanayama (1992a,b), Nanayama and Ganzawa (1997). Based on these results and along with spinel chemistry, these authors discussed the possibility of three zones within Nakanogawa Group (Zone 1, Zone 2 and Zone 3). This classification is based on the source of sediments and paleo-direction analysis of those sediments. According to their interpretation Zone 1 and Zone 2 sediments are from Paleo Kuril Arc region and Zone 3 is from Paleo Japan Arc region. On the basis of this authors argued that Nakanogawa

group is deposited in an Arc-Arc junction of Paleo Japan Arc and Paleo Kuril Arc. They also pointed out that the Hiroo Complex and exotic blocks of green stones are accreted during subduction process associated with Kuril Arc evolution. Contrary to this view Kimura (1994) suggested that mélange facies rocks such as chert and limestones are olistolith of Idonnapu belt and hence part of westward subducting paleo- NE Japan arc system. Konatani (1978) reported that Nakanogawa Group has conical to curved conical type folds with axes tends to converge south direction and diverge in N–NE direction, in southern part of Nakanogawa Group the folds are generally normal with wavelength 2 to 4 kilometers. General trending of fold axes is reported as NNW–SSE. In contrast to this northern part have isoclinal folds with wider wavelength. Fold axis trend generally change from NNW–SSE towards NE–SW in the northern part of Nakanogawa group. Kontani (1978,1980) also noticed that HMB with NNW–SSE trend is obliquely crossed by Nakanogawa group and sediments in close proximity to HMB has been thermally metamorphosed which emphasis that Nakanogawa group of sediments are protolith for meta-sedimentary rocks in HMB. Some preliminary structural studies are conducted in Hiroo complex, and result show eastward subduction as the evolutionary mechanism (Toyoshima and Nanyama, 1993).

4.2.2 Distribution of mélange type of rocks in Tachiiwa, Daimaruyam and Toyonigawa region in Hiroo Complex

Tachiiwa rock body is occupied in the southern most part of Nakanaogawa Group and Hiroo Complex. It is distributed in Tachiiwa along the Pacific Ocean coastline nearby the Tokachi port (**Fig. 4.3a**). Major parts of the mélange outcrops are situated in Ocean side around 100m away from the coastline, which is accessible during low tide. Along the coastline quaternary sediments cover the outcrops but few are visible around the beach. Outcrops in the Ocean side are mainly with dark brown colored chert, red mudstone and green mudstone. Basaltic green stones also present in few part of the outcrop. Owada et al., (1992) reported lamprophyre

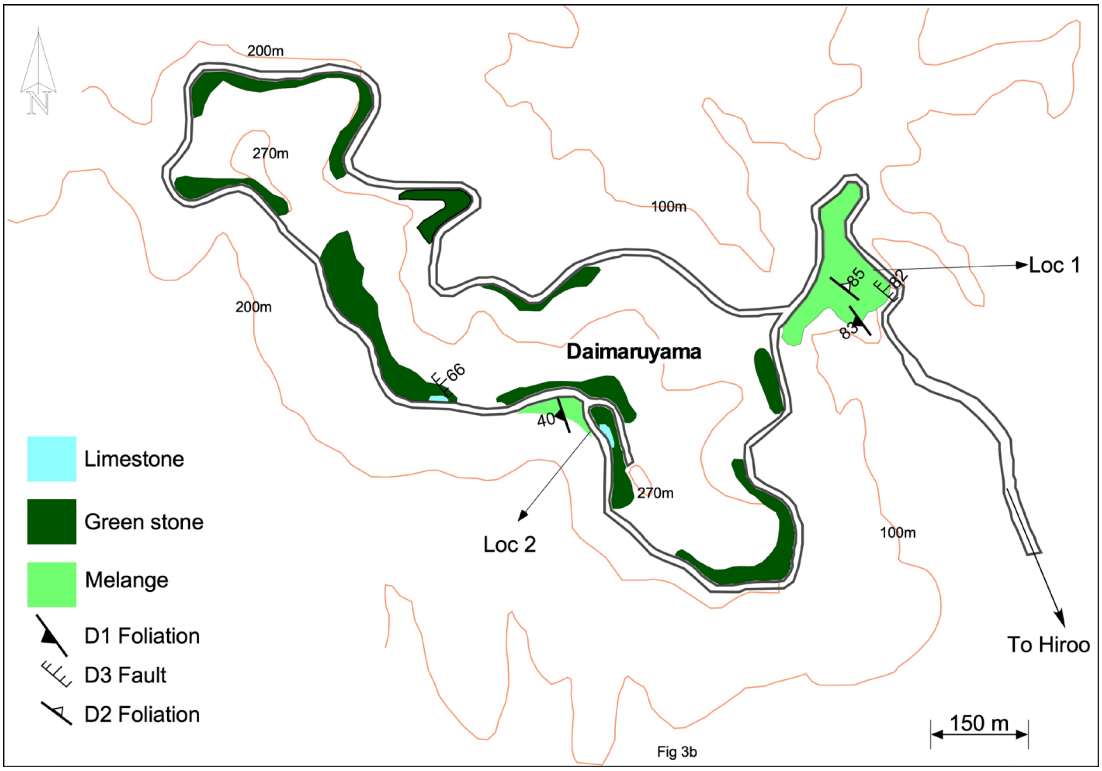

***Figure 4.3b**. Route map of Daimaruyama region.*

(camptonite) from Tachiiwa body which is present as a dyke in pelagic sediments surrounded by basic tuff matrix with K-Ar age of 95 Ma. Along the beach side, greywackes with volcanic sandstone as clast in them are also exposed. Calcite and zeolite veins are also present as intrusions in Loc 1 (**Fig. 4.3a**). Daimaruyama is located in the southeastern part of Hiroo Complex and in the northern part of Tachiiwa region. We carried out investigation in Daiamruyama region around a forest road in the Daimaruyama Park in Hiroo town. Main lithologies in the route include limestone, red chert, red shale and green stones. Nanayama, (1992b) has reported a formation age of 125–101 Ma for Daimaruyama greenstone on account of radiolarian fossils in chert embedded within the greenstones. Even though major rock type exposed along this study area is greenstones, some parts of the Daimaruyama region also have other mélange type of rocks including turbidite with well-preserved deformation structures (eg: Loc 1 and Loc 2 in **Figure 4.3b**. Loc 1 (**Fig. 4.3b**) has alternating beds of deformed turbiditic sandstone and mudstone in which graded bedding is also preserved. Similarly the Toyonigawa region in the northern part of the Hiroo

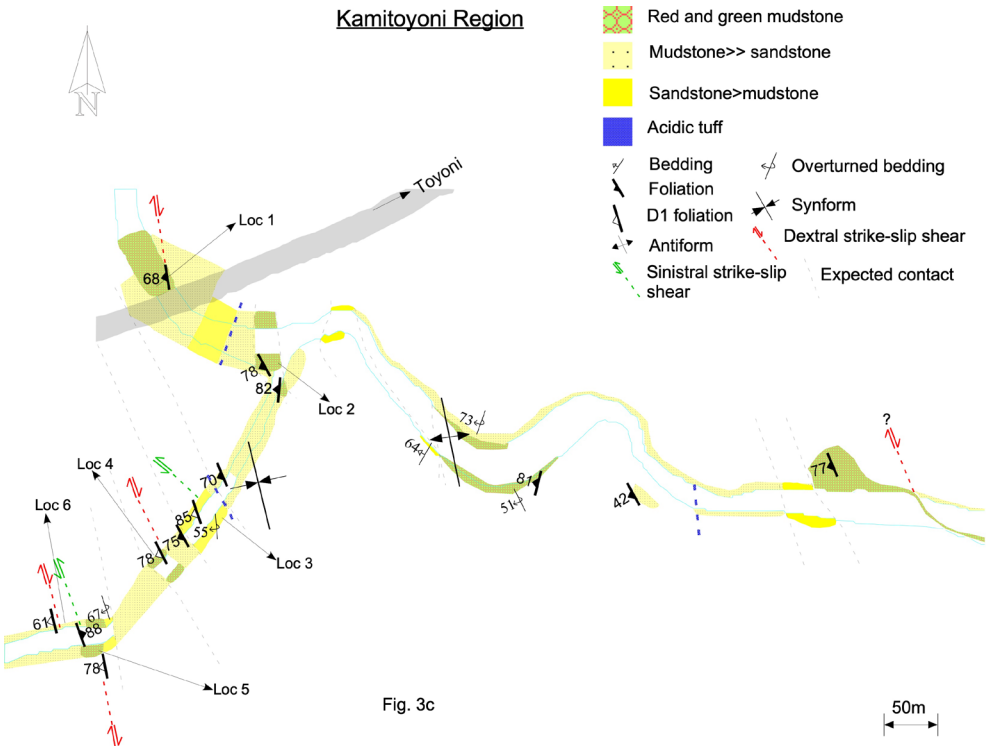

Figure 4.3c. *Route map of Kamitoyoni region. Loc: locations*

Complex also has well-preserved mélange type of rocks (**Fig. 4.2a**). Outcrops are mainly occupied along the two sides of the river around Kamitoyoni bridge (**Fig. 4.3c**). Main lithotypes are turbiditic sandstone-mudstone, red mudstone and green mudstone that are accompanied by thin layers of acidic tuff. Sandstone mudstone succession are overturned and folded, fold axis trending in NNW–NW direction with vertical hinge line. Nanayama and Ganzawa (1997) dated vitric acidic tuff from this location by FT method and reported an age of 50.4 ± 2.4 Ma (with 2σ error).

4.2.3 Deformation structures and their mutual relation in the study area

Four different deformation events are identified in the evolutionary history of Hiroo Complex (see Table 1). Based on chronological order they can be listed as 1) East-side-up sense dip-slip deformation (D_1), 2) Right-lateral strike-slip deformation (D_2) 3) Left-lateral strike-slip to oblique-slip deformation (D_3) and 4) West-side-down dip-slip deformation (D_4).

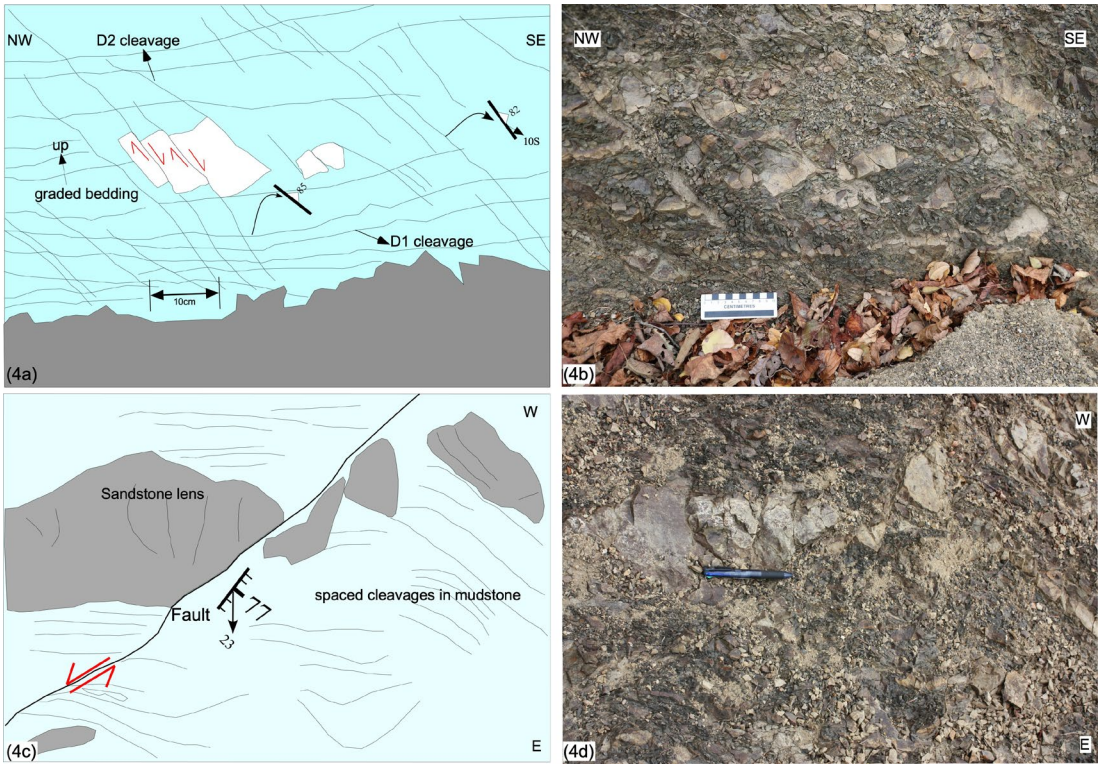

Figure 4.4: *Field relationship in Daimaruyama region. (a) Sketch diagram and (b) Field photograph from the study location showing bedding parallel cleavage (D_1) and oblique cleavage (D_2) with later showing dextral sense of movement which is clear from the displacement of sandstone blocks. (c) Approximate sketch and (d) field photograph of D_3 event observed in Daimaruyama region. Deflection of foliation around the fault zone shows sinistral sense of movement. Pen in the figure is around 15cm long.*

Field relation shows that, D_1 event is most penetrative and regional tectonic event and later events are of non-penetrative type, at least in the studied locations. D_2, D_3 and D_4 events are concentrated in narrow cataclastic type shear or faults, while D_1 shear zones in Tachiiwa, Daimaruyama and Toyonigwa region are identified in wide and strongly foliated shear zones with typical 'block in matrix' tectonic mélange structures. The 'matrix' of these shear zone are strongly foliated mudstone (black, green or red mudstone), and in three of the studied locations these foliation trend strikes in N–NNW direction. The sandstone and chert blocks within this foliated mudstone matrix are lens shaped and elongated in dip direction. Stretching lineation in the D_1 shear zone identified from Toyonigawa, Daimaruyama and Tachiiwa region are parallel to dip direction of the

foliation, which indicating a dip-slip motion along the shear plane. Tectonic deformation features like composite planar structures (P-Y-R shear), asymmetric sigma structures, extensional veins in sandstone blocks, mesoscopic asymmetric folding and pressure solution cleavages identified from different parts of the study area indicating the east-side-up movement direction for D1 event. Microstructure observation of D_1 event in thin-section also shows tectonic mélange structures. Development of P-Y-R shear by extensional shearing is evident in thin-section from Toyonigawa and Tachiiwa locations along with asymmetric structures. Low-grade metamorphic minerals like muscovite/chlorite are aligned along shear planes also identified in thin-section. These field and microscopic observations of D1 event are well in agreement with the general features of the mélange developed through tectonic process rather than by a sedimentary mass-transport chaotic means (Festa et al., 2010, Festa et al., 2012, Yamamoto et al., 2012).

A cataclastic shear zone in the ocean side outcrop within Tachiiwa region (Loc 1, **Fig. 4.3a**) that is 2 m wide and 3 m long is identified. This shear zone had red mudstone and green mudstones as matrix and within them fractured chert and sandstone is occupied as clast/block (**Fig. 4.5d**), representing a typical 'block in matrix structure' (definition after Festa et al., 2012). Matrix of this shear zone is strongly foliated and composite planar structures such as P foliation (P) (**Fig. 4.5d**), Y foliation (Y) and Riedel shear (R) (Logan, 1979; Rutter et al., 1986) are well developed. The trend of main foliation (Y) in the shear zone strikes in N–NNW direction, with dip angle in between 75**–**85° and dipping towards the east (**Fig. 4.5b**). Stretching lineation is observed on this shear plane (Fig. 5a) which are aligned almost parallel to the dip direction and their plunge ranges in between 55°N–85°N. Trend for P foliation strikes in between 40°W–25**°**W and dipping in between 70–73**°** towards west. Some parts of the shear zone also have calcite veins filling R2 shear planes which strikes between N19°W and N36°W and dipping towards west. Obliquity of P foliation to Y shear (P-Y fabric) and mutual relation field and microscopic observation (**Fig. 4.6a, 6c, 6d**). These spaced cleavages trend strikes in N–NNW direction as similar to Daimaruyama and

Tachiiwa location and in microscopic observations also these cleavages are between P, R1 and R2 shear (P-R1-R2 fabric) are used to understand the shear sense in study area (Snoke et al., 1998). In Tachiiwa region this P-Y-R mutual relationship shows east-side-up dip-slip movement (D_1). At Loc-2 in Tachiiwa (**Fig. 4.3b**.), elongated volcanic sandstones are present as clast in greywacke in shear zone with lineation plunging parallel to the dip-direction. Here also shear plane has strikes in N– NNW direction. Moreover the volcanic sandstone inclusions in greywacke have typical tectonic mélange structures like 'elongate neck' and 'asymmetrical tailing' (**Fig. 4.5e**). Penetrative nature of D_1 deformation is more evident in Daimaruyama region in the studied location. Within this outcrop two sets of shear cleavages (foliation) with different attitudes of strike are observed. First set of shear cleavages are parallel to the attitude of bedding and strikes in N40–45°W direction. Second set of shear cleavages strike in N20–30°W which is slightly oblique to the attitude of bedding.

I consider these bedding parallel cleavages are related to D_1 deformation event, which are resulted from east-side-up dip-slip deformation. Bedding parallel cleavages have a dip towards the east and bedding oblique cleavages has a varying dip to both in the east and the west. First set of cleavages (bedding parallel cleavages) are more penetrative in nature and the second set of cleavages (bedding oblique cleavages) cut the bedding parallel cleavage. Therefore, the bedding parallel cleavages are older than bedding oblique cleavages (**Fig. 4.4a, 4b**).

The bedding oblique cleavage has a lineation which is plunging 10–24° towards south and it is sub-parallel to the strike of the cleavage- Both type of cleavages -bedding parallel and oblique cleavages- mainly concentrated in mudstones, whereas sandstone is occupied as block within them.

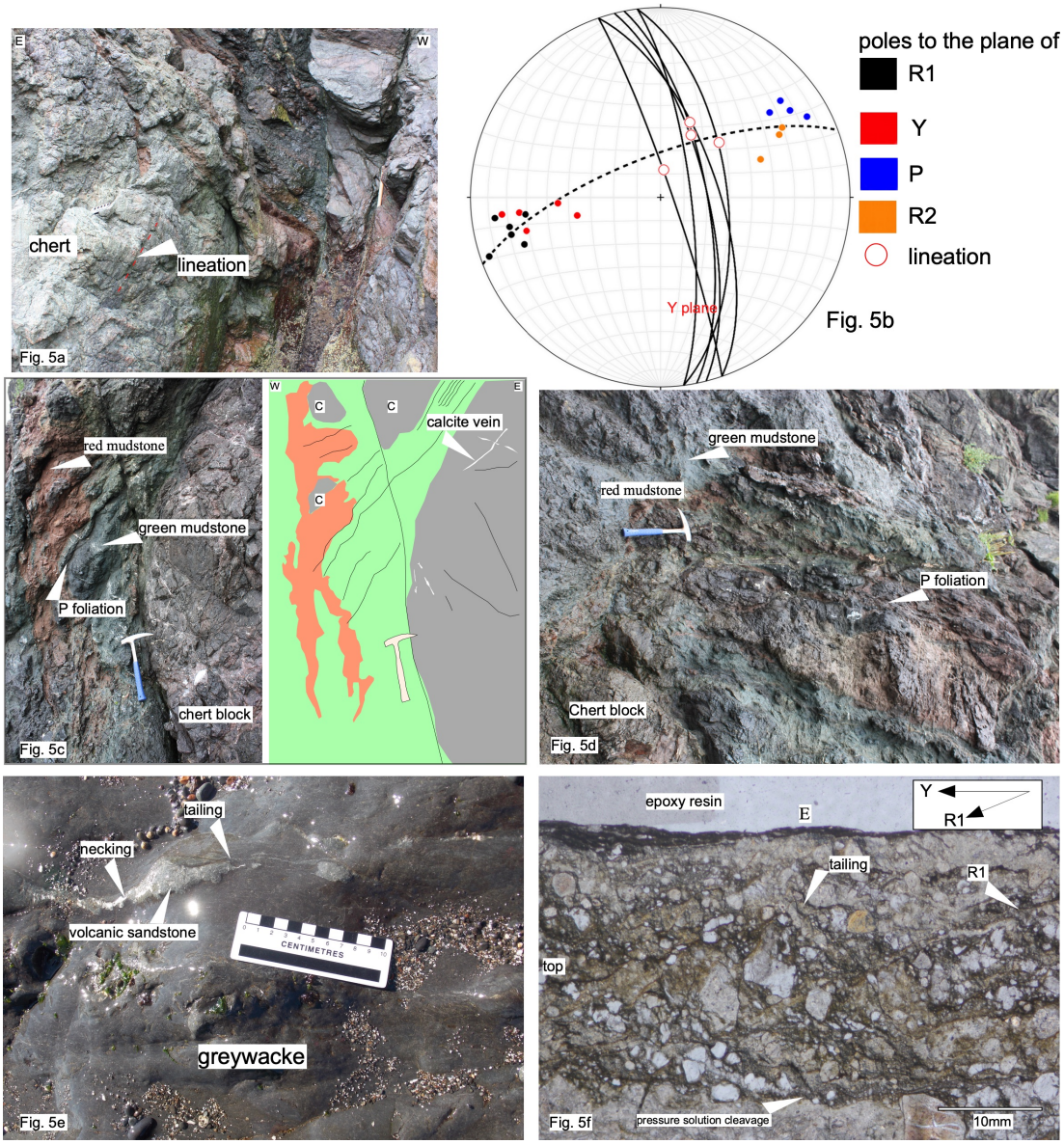

Figure 4.5: *Field and microstructural details of Tachiiwa region. (a) Chert block showing stretching lineation plunging north direction on chert block. (b) Lower hemisphere projection of structural data collected from Tachiiwa region, Y shear are plotted as both planes and poles to those planes (red circles), mutual relationship indicating east-side-up motion sense. (c) Red and green mudstone foliated and fractured chert block, field photo in the left and its approximate sketch in the right side. P foliation is visible in mudstone and chert fragments are located within them. This is clear evidence for continues deformation in partially consolidated sediments. East-side-up sense of movement. (5d) Chert as clast within foliated mudstone matrix, P foliation direction indicating east-side-up motion sense. (5e) Volcanic sandstone in greywacke matrix, sandstone shows necking and tailing. (5f)*

Microphotograph of thin-section prepared parallel to lineation in Fig. 5a shows east-side-up sense of motion. Pressure solution cleavage along grain boundaries and asymmetric tails around clasts are also visible. C: Chert. Hammer in the photographs is around 35cm long.

These sandstone blocks with size ranging between ~10cm to ~2m are exposed as blocks in sheared mudstone matrix, which is described as typical tectonic mélange structure (Yamamoto et al., 2012 and references there in). We interpret these structures are evolved during D1 deformation, which is more penetrative and widely distributed. Along the bedding oblique cleavage the sandstone blocks show clear evidence for shear displacement in centimeter scale (**Fig. 4.4a, 4.b**) and its asymmetry indicates a dextral (right-lateral) sense of movement. This strike-slip dextral movement concentrated as narrow fault zones is termed as D_2 deformation. Eastern part of Loc 1 (**Fig. 4.3b**) the bedding parallel cleavages (D_1) and bedding oblique cleavages (D_2) are cut by an NNW–NW striking fault that dip 77° in east direction (Fig. 4b & Fig. 4bb). Slicken line type of lineation in fault plane plunging 23°–37° towards SE indicates a strike-slip to oblique-slip movement. Deflections of previous shear cleavages in this fault plane indicate sinistral sense of movement (left-lateral). This strike-slip to oblique-slip deformation event cut D_1 and D_2 in deformation in the Daimaruyama outcrop and hence termed as later D_3 event. Other than these three-deformation events, younger D_4 deformation is also identified in Toyonigawa region. This deformation generally identified as fault gouge zones, which are approximately 10cm–80cm wide and cut D_3 deformation zones in Loc 3 and Loc 5 (**Fig. 4.6h**). These fault gouge zones strike N–S and dip vertical to steep west. Slicken-line lineations are parallel to the dip direction and step faults on the shear planes indicate normal faulting with west-side-down sense. We also identified P-Y-R shear in D_4 zone that confirms west-side-down sense of movement. D_1, D_2 and D_3 deformation events also well preserved in Toyonigawa region. D_1 shear zones are observed with approximate dimension of 5m wide and 2m long in Loc 3, Loc 4, Loc 5, and Loc 6 (**Fig. 4.3c**). Shear zones are observed with typical mélange structure;

spaced shear cleavages (foliation) in mudstones and sandstones as clast ('block in matrix' structure) within them, both in

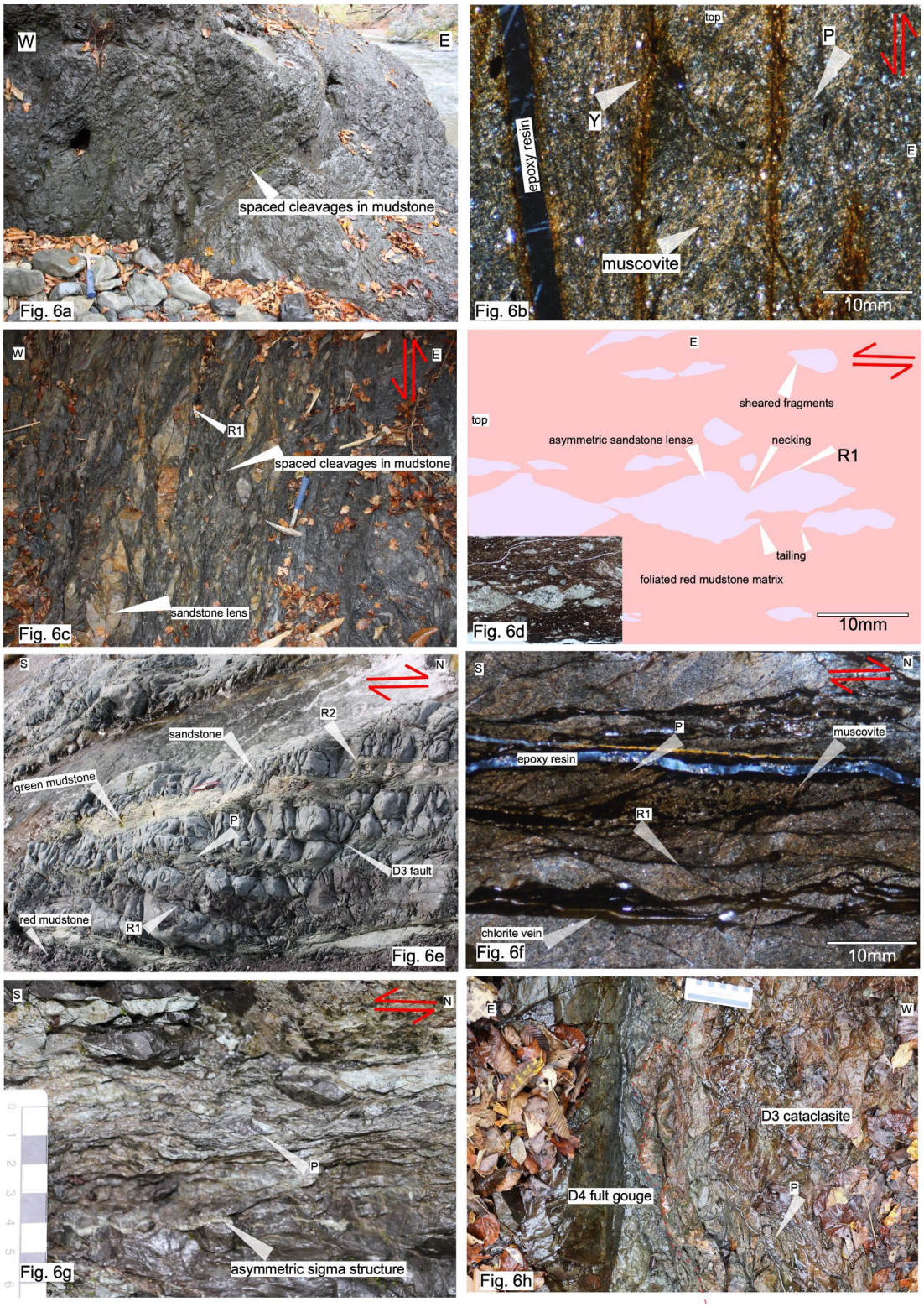

P.T.O for captions

Figure 4.6: *Field and microstructural observations in Kamaitoyoni region. (Fig. 6a) Spaced cleavages in mudstone rich region, these cleavages or*

foliation strikes in N-NNW direction. (Fig. 6b) Microphotograph of thin-section prepared parallel to the dip-parallel lineation in Fig.6a sample. Muscovite is aligned along foliation plane. P-Y relation shows east-side-up sense. (Fig. 6c) Lens shaped sandstone in foliated mudstone matrix, with Y-R1 relation shows east-side-up sense of movement. (Fig. 6d) Sketch of the insect microphotograph of thin-section prepared parallel to dip-parallel lineation of d1 deformation. Micro sandstone clast with asymmetric tail and necking, are distributed in foliated red mudstone matrix. Fragments of large sandstone clast are also visible in the matrix, which are also sheared; indicating continues deformation in partially consolidated sediments. East-side-up motion sense. (Fig. 6e) Field photo of D2 deformation event, indicating dextral sense of movement. P foliation concentrated in green mudstone layer. Note sinistral sense of movement along R2 shear. D3 sinistral fault cut foliations, shows it is the latest event among the two. (Fig. 6f) Thin-section prepared parallel to the strike-parallel lineation in mudstone shows dextral sense of movement. Muscovite aligned along foliation and chlorite intruded as later vein. (Fig. 6g) D3 cataclastic sinistral deformation. Field photograph shows asymmetrical structures with sinistral sense indicator, P foliation also shows same sense of movement. (Fig. 6g) Contact between D3 catacalstic sinistral shear zone and D4 fault gouge.

clearly visible (**Fig. 4.6b**). Mutual relation between D_2 and D_3 deformations are also preserved in Toyonigawa region. An outcrop near Kamitoyoni Bridge with red and green mudstone exposed is sheared, foliated and deformation related structures are well preserved in field (**Fig. 4.6e)** and microscopic scale (**Fig. 4.6f**). Foliation of the deformed rocks in this location trends in N10–25°W and dips to the west. A slicken-line like lineation plunging 1–10° towards the south is also visible on the foliation plane. Contact zone between adjacent layers of green and red mudstone is more strongly foliated when compared to other parts. This strongly foliated area has well preserved P-Y-R foliations. Mutual relationship between this P-Y-R shear indicates dextral sense of movement (D_2). Along with this vertical dipping R2 shear is also identified, and displacement along R2 shear indicates a sinistral sense, which is antithetic to the imposed shear direction (Twiss and Moores, 1992).

D3 fault, which strikes N54°-30W and dips 66-70° to the west, cuts dextral shear system (D_2). Displacement along fault plane and step faults indicates strike-slip to oblique-sip sinistral sense of movement (**Fig. 4.6e**).

4.2.4 Microstructural observation

I. Tachiiwa region

Thin-section of sandstone from shear zone (Loc 1) shows typical cataclastic type features, angular to sub-angular fragments in fine-grained matrix (Snoke et al., 2014). Size of this quartz fragments ranges from 1mm to 7mm. Along the grain boundaries pressure solution seams are also present (**Fig. 4.5f**). Quartz fragments with asymmetric tails are aligned along P foliation, indicating east-side-up sense of motion. The composite planar fabric (P-Y-R relation) observed from thin-section also indicates east-side-up movement (**Fig. 4.5f**). Calcite, chlorite, and zeolite are precipitated within extension veins in sandstone along R2 shear planes are also identified.

II. Kamitoyoni Region

Thin-section parallel to lineation from Loc 3, Loc 4, Loc 5, and Loc 6 shows east-side-up shear sense, in agreement with field observation. In thin-section of mudstone sample from Loc 3, fine-grained quartz, plagioclase, and calcite are present in matrix and muscovite is aligned along Y plane (**Fig. 4.6b**). Thin-section of red mudstone sample from Loc 4 shows typical tectonic mélange-type micro fabrics such as asymmetrical extensional shear (Festa et al., 2012) indicating east-side-up motion sense (**Fig. 4.6d**). Matrix of the sample is entirely made up of red mudstone, which is foliated and chlorite/muscovite are aligned along this foliation. Within red mudstone matrix sandstone clasts of varying size (0.01–1mm), which include quartz, plagioclase and calcite as major minerals and have undergone strong asymmetrical extension shear evident from P-Y-R relations. Asymmetric boudinage structures are developed in sandstone clast and some of them separated into small fragments of millimeter size. Both, the clast and fragments sheared asymmetrically. Tails and necks are developed in these small fragments also. P-Y-R shear and asymmetrical structures in sandstone clsats, both show east-side-up shear sense. Similar kind of sheared sandstone clasts in a foliated mudstone matrix structures is observed in thin-

sections of samples from Loc 5 and Loc 6 also. Thin-section prepared from mudstone sample with strike parallel lineation in Loc 6 shows dextral sense of shear as indicated by P-Y-R relations (**Fig. 4.6f**). Muscovite is aligned along the P foliation in this mudstone sample and ~0.1mm thick chlorite vein is intruded parallel to the Y foliation. Thin section of mudstone samples from oblique lineation part in Loc 3 has a fine-grained matrix with oblique; around 1mm wide micro shear zones present in them. P-Y-R relation in this micro shear zones shows sinistral sense of movement. Thin section of sinistral-cataclastic rocks in Loc 3, Loc 5, and Loc 6 have angular to sub-angular quartz fragments of varying sizes ranging from 0.1–2mm. Pressure solution seems are distributed along fine-grained matrix. Some of the quartz fragments have asymmetric tails around them showing sinistral sense. P-Y-R shear also indicates sinistral sense of motion.

4.2.5 Features of a tectonic mélange, evidences from Hiroo Complex.

Recent compilation of characteristic features of tectonics of mélange formation around the globe pointed out some fact about progressive stratal disruption leading to mélange/broken formations and their decisive factors (Festa et al., 2010, 2012, 2019). According to them major controlling factors are (1) consolidation and lithification of sediments, (2) magnitude of shear stress, and (3) structural domain in which tectonic activity is taking place. On the basis of this, my observations from Hiroo Complex - scaly matrix foliation with asymmetric brittle boudinaged (P-Y-R shear) sandstone in it, pressure solution seams along grain boundaries, extensional veining in sandstone/chert blocks etc.- can be used to interpret following points about mélange tectonics in the Hiroo Complex; (1) the structures from Hiroo Complex are comparable to those evolved in a deeper structural domain than shallow domains (2) deformation took place in moderately lithified-to completely lithified sediments, and (3) structures are developed through non-coaxial shear deformation. Typical features of sedimentary mélange like, soft sediment deformation, presence of sandstone dikes, absence of shear deformation indicators, etc. (Osazawa et al., 2009; Festa et al., 2010; Festa et al., 2012; Yamamoto et al., 2011) are not present in the studied location

which also confirms that D_1 structures are developed by progressive tectonic deformation on moderately consolidated to consolidated sediments in an accretionary complex setting.

More than emphasizing on the tectonic evolution of the Hiroo Complex, points I would like to highlight here are the features of a tectonic mélange. Following features can be listed as field and structural features of an accretionary complex.

Presence of blocks of sedimentary or volcanic rocks in both map-scale and outcrop scale (eg: **Fig. 4.3b**, Limestone blocks in greenstones in Daimaruyama, Greenstone blocks in Tachiiwa **Fig. 4.3a**).

'Block in matrix' structure. As mentioned through out the section 4.2, one striking feature of the tectonic mélange is the presence of blocks of sandstone in mudstone matrix with spaced cleavage.

In Hiroo Complex, soft sediment deformation structures are absent, points to the fact that subduction related accretion took place when sediments were partially consolidated or in consolidated state. Afore mentioned features is suppose to be preserved in most of the tectonic mélange originated through subduction-accretion process.

4.2.6 Why DC's Schist Belts are not subduction related accretionary complexes?

As mentioned in section 1.4.3, there are numbers of models considering sedimentary and volcanic rocks in WDC as part of subduction related accretionary complexes. Most of these explanations are based on geochemical (Manikyamaba et al., 2014) or geochronology based approach (Gao and Santosh, 2020). Field or structural evidence for an accretionary complex is not yet identified. For example Komiya et al., (1999) and Peng et al., (2020) presented detailed field based evidence for accretionary complexes in the Archean Isua Complex and North China Craton respectively. These evidences include blocks of mafic rocks in metasediments, fault contact between sedimentary and volcanic units etc. So there are clear field evidences present at least in some of the cratons around

the globe. But my fieldwork in DC shows no field/structural evidence for an Archean accretionary complex. Instead few points are straight foreword against accretionary complex models (1) Absence of 'allochthonous units in the stratigraphy, (2) Conformable contact relation between sediments and volcanic rocks indicating their simultaneous origin. (3) No deep-marine facies of sedimentary rocks identified in my fieldwork in DC. Instead sedimentary rocks preserved shallow-marine origin signatures. (4) No 'block in matrix ' feature preserved in sandstone-mudstone successions especially in the contact zone or proposed suture zones.

Gao and Santosh, (2020) and Li et al., (2019) presented arguments about Sargur Group in the eastern margin of the CSB are 'obducted' sequence. Their arguments based on the age and metamorphic relations of few rock types from Sargur Group. In this context it easy to misinterpret Akkanahalli Zone in the eastern margin of CSB (Chapter 2, Section) as an accretionary prism. But in my observation Sargur Group is distributed both in the east and west of CSB. Moreover Sargur Group of rocks is observed in the east of GMSZ also (eg: Javanahalli Belt, Kunigal Belt, Fig. 1.7b). More than that Sargur group evidently shows an intrusive relation with Basement Gneiss. Last two sentences are evidently indicating Sargur group was part of a cratonic nucleus prior to the formation of failed rifts. Probably because of this reason Sargur Group of rocks are present as dismembered sequence on either side of the GMSZ. Moreover Sargur group of rocks is present in both east and the west of CSB and KSB (Fig. 2.1b and 3.2b) also agrees with my hypothesis.

Another approach towards understanding arc magmatism and associated accretionary complex formation in the DC is based on geochemical studies (Giri et al., 2019, Manikyamba et al., 2012, 2013, 2014). But in conclusion of recent review on geochemical evolution of basaltic rocks Xia, 2014, mentioned "*Contamination by continental crust or lithosphere can impart subduction-like signatures (e.g., low Nb, low Ta and low Ti) and lead to the misidentification of contaminated continental intra- plate basaltic lavas as arc related".* So, I would suggest it is important to consider proper

stratigraphic and structural analysis prior to geochemical and geochronological interpretations in DC.

In conclusion both structure and stratigraphy observed in this thesis are not successfully matches with structural and stratigraphy observations from a Cenozoic accretionary complex. So I would suggest more cautious approach while considering an accretionary complex models in DC purely rooted on geochemical and geochronological studies.

Discussion on Cenozoic accretionary complexes and obvious mismatches with WDC geology confirm my discussions on failed rift model mentioned in Chapter 2 and Chapter 3. So another vital task is to understand the temporal significance of failed rift events in WDC.

4.3 Geochronological relation between stratigraphic units in WDC.

I compiled available geochronological information from WDC and scrutinized in Table 4.1. Ages are grouped based on their stratigraphic relation and references are also mentioned within the table. Based on the age distribution further discussions on tectonic evolution of the schist belts in WDC are presented.

4.3.1 Basement Gneiss

As mentioned in Chapter 2 and 3, Basement Gneiss is the oldest unit in the stratigraphic column of the DC. Oldest reported Basement Gneiss age is 3410.8 ± 3.8 Ma (Guitreau et al., 2017) from Holanarsipur area. The same authors also pointed out ~3600 Ma old inherited zircons within Basement Gneiss. Presence of older inherited zircons points to the vanished older crustal blocks in DC (Guitreau et al., 2017). Jayananda et al., (2018) postulated two events of accretion in WDC based on the published ages. Initial event is ca. 3450–3300 Ma and second event is 3230–3200 Ma (Jayananda et al., 2018). But, ages <3200 Ma also reported from WDC in zircon U-Pb analysis, examples include, Bhukkapatna granite (2988 ± 9 Ma, Chardon et al., 2011), KMK pluton (2973 ± 2 Ma, Korfu and Hedge, 2020) and Sargur trondhjemite (2972 Ma (Zircon Pb-Pb), Gao and Santosh, 2020). Above-mentioned ages close to 3000 Ma probably represent another event

of magmatism/accretion in WDC. In summary Basement Gneiss in WDC shows an episodic crustal growth. Published age data show, minimum of three episodes of crustal growth had been occurred in Basement Gneiss within WDC.

4.3.2 Sargur Group

Age peaks in Sargur Group shows komatiite volcanism ranges between ~3400–3100 Ma and felsic volcanic peaks ~3300 Ma (Table 4.1). Recent ages from Holenarsipur and Nuggihalli show relatively younger age of 2934 ± 88 Ma for ultramafic intrusives (Sm-Nd age, Patra et al., 2020). There is a striking correlation between the ages of volcanic rocks in Sargur Group and Basement gneiss. This factor implies a possible relation in evolutionary process between Basement Gneiss and Sargur Group (Jayananda et al., 2008, Maya et al., 2017 etc.).

4.3.3 Bababudan Group

Felsic volcanic ages in Bababudan Group are very limited. Only two ages are reported from metatuffs in the Bababudan Group (Trendall et al., 1997a). U-Pb ages of zircons from this ash fall tuffs are 2720 ± 7 Ma and 2718 ± 6 Ma. As I mentioned in Chapter 3, Krapez et al., (2020) synthesized this age relation to explain the initiation of the Bababudan rifting from 2756 Ma. Kalsapura volcanic ages (2848 ± 70 Ma, Kumar et al., 1996) with broad error limits are also fit into the time frame mentioned by Krapez et al., (2020). In age relation proposed by Baskar Rao et al., (2008), zircons in Sigeggudda basal conglomerate have a 2713 ± 13 Ma rim around 3348 ± 1o Ma core. Pointing to a ~2.7 Ga thermal event possibly associated with Bababudan Group mafic magmatism. Another event giving direct evidence to the age relation of Bababudan Group is 2614.4 ± 9.7 Ma, high-K Chitradurga granites. This granite cross cuts Bababudan Group of rocks in CSB (Jayananda et al., 2006), implies that Bababudan Group is younger than ~2.6 Ga.

4.3.4 Chitradurga Group

Unlike Bababudan Group, U-Pb analyses of zircons in volcanic rocks, especially rhyolites show peak near 2.6 Ga in Chitradurga Group. Daginkatte

rhyolite of SSB shows volcanic age of 2601 ± 6 Ma (Trendall et al., 1996). Quartz-feldspar porphyry of Chitradurga Group shows 2588 ± 10 Ma (Sarma et al., 2011). Felsic schist in in Ranibennur also has similar age (2614 ± 8 Ma, Nutman et al., 1996). Recent data from Talya conglomerate which separates Chitradurga and Bababudan Group shows age distribution betwenn 3384–2597 (Middle Talya conglomerate, Krapez et al., 2020). Age from lower section within the Talya conglomerate shows range between 3386–2610 Ma (Krapez et al., 2020). But another set of data from Ingaldhal volcanics of Chitradurga Group shows age of felsic volcanics like rhyolite shows as 2676 ± 20 Ma (U-Pb age in zircon, Hokada et al., 2013). Felsic schist (probably altered rhyolite) shows volcanic age of 2665 ± 15 Ma (Jayananda et al., 2013a,b). But Krapez et al., (2020) mentioned, "*Sample H1102E of Hokada et al. (2013) is of a rhyolite that intrudes the Ingaldhal Formation at Ingladahalu. A SHRIMP U- Pb zircon age of 2676 ± 20 Ma was presented for the sample, but the age-spectrum is bimodal with modes at 2667 Ma and 2789 Ma (Fig. 9c) confirming that the rhyolite contains xenocrysts".* Krapez et al., (2020) also commented on the reliability of felsic schist dated 2665 ± 15 Ma (U-Pb Zircon, Jayananda et al., 2013a, b) from Kadhalu because; only three analyses were used for calculating the mean age. Other than above mentioned points, factors in favor of ~2.61 initiation of Chitradurga Group are, 1) Chitradurga granite not cross cutting Chitradurga Group and 2) presence of ~2.6 Ga zircons in basal section of Talya conglomerate and 3) unimodal age spectrum of zircons in rhyolites such as Daginkatte rhyolite.

4.3.5 Hiriyur Group

Zircon U-Pb age of felsic volcanic rocks in Hiriyur Group was calculated as 2576 ± 20 Ma (Jayananda et al., 2013a,b). Major lithological unit of Hiriyur Group is metagreywacke and it has youngest age spectrum in detrital zircon grains ranging from 2547 ± 5 Ma to 2578 ± 8 Ma (Sarma et al., 2012 and Nasheeth et al., 2016). Krapez et al., 2020 considered Chitradurga-Hiriyur boundary has a very narrow gap (<1Ma) or no gap (see their figure 19, Krapez et al., 2020). But In my fieldwork it is evident that there is a regional-scale, thick conglomerate layer separating two Groups.

Moreover the regional scale thick conglomerate layers are marked in Mishima et al., (2017) also. Conglomerate layer implies an event of uplift and erosion at least for few million years before Hiriyur volcano sedimentary basin formation. But these precise ages for this conglomerate are not constrained yet, so exact age constrain of initiation of Hiriyur Group is difficult.

4.3.6 Age spectrum of granites <3.0 Ga in WDC

After the younger granite genesis events in Basement Gneiss (Bhukkapatna granite (2988 ± 9 Ma), KMK pluton (2973 ± 2 Ma) and Sargur trondhjemite (2972 Ma)), there is no granite intrusion in WDC until 2623 ± 5 Ma intrusion of granite in Gadag duplex (Corfu and Hedge, 2020). Similar ~2.62 events are Chitradurga granite (2614.4 ± 9.7, Jayananda et al., 2006), Arsikere plutons (2617 ± 3 Ma, Jayananda et al., 2006), and Uchangidurga Granite (2648 ± 40 Ma, Chadwick et al., 2007). Multiple events of granite intrusion starting from ~2555 Ma is also reported in WDC (Table 4.1). Dated gold mineralization events in WDC are close to these granitic events (2520 ± 9 Ma, Sarma et al., 2011), probably pointing to their temporal connection.

4.3.7 Metamorphic ages in WDC

Metamorphic age relation of samples from WDC implies two thermal peaks (Hokada et al 2013), c.a. 2.5–2.3 Ga and c.a. 3.2–3.1 Ga. But the same authors also mention one monazite date of c.a. 2.7 Ga in Sargur Group of rocks. Similarly as mentioned in section 4.3.2, same (c.a. 2.7 Ga) metamorphic overprint preserved in zircons of basal sections of Bababudan Group. Jayananda et al., (2013) reported 2.6 Ga peak near eastern part of WDC. In summary these peaks (c.a. 3.1, 2.7, 2.6 and 2.5) are within error limits of the ages reported in granites and felsic volcanic rocks. Thus the thermal events in WDC are possibly associated with extension or convergence occurred within or around WDC.

4.4 Secular evolution of multiple failed rift basin in WDC

In CSB three different rifting events and associated basins of Bababudan, Chitradurga and Hiriyur Groups are constrained based on field and structural relations in Chapter 2 and 3. These basins, each separated by an unconformity and preserved shallow marine conditions are already explained in last two chapters. Last section (section 4.3) shows considerable age gap between three rifting events. Highlighting the age and field observations a summary of tectonic events in WDC is shown **figure 4.7**. The evolutionary history of WDC can be broadly classified into Pre-Dharwar evolution (> 3.0 Ga) and Dharwar Supergroup evolution. This classification is based on the fact that after c.a. 3.0 Ga or before the evolution of Dharwar Supergroup most of the Basement Gneiss is already formed and basement units (Sargur and Basement Gneiss) undergone a considerable peneplanation.

Pre-Dharwar evolutionary history mainly includes multiple episodes of granitoid (mainly TTG's) generation and evolution of Sargur group (**Fig. 4.7**). As explained in section 4.3.1 three episodes of granite generation is evident in WDC during pre-Dharwar evolution. Sargur Group's age range I marked in the **Figure 4.7** is conspicuous; this is expected because of the lack of precise volcanic age in the belt. Available data is limited to constrain the initiation and termination of the Sargur Group. I suppose ~3.3 Ga felsic volcanic/metatuff (Peucat et al., 1996, Sreehari and Toyoshima, 2020) marks the initiation of volcanic activity in Sargur Group. But based on Sm-Nd age of komatiite and associated Basement Gneiss, Jayananda et al., (2008) a multi-stage plume and arc growth model for the Sargur Group and pre-Dharwar rock types. According to Jayananda et al., (2008, 2018) these events are marked between time period 3400–3200 Ma.

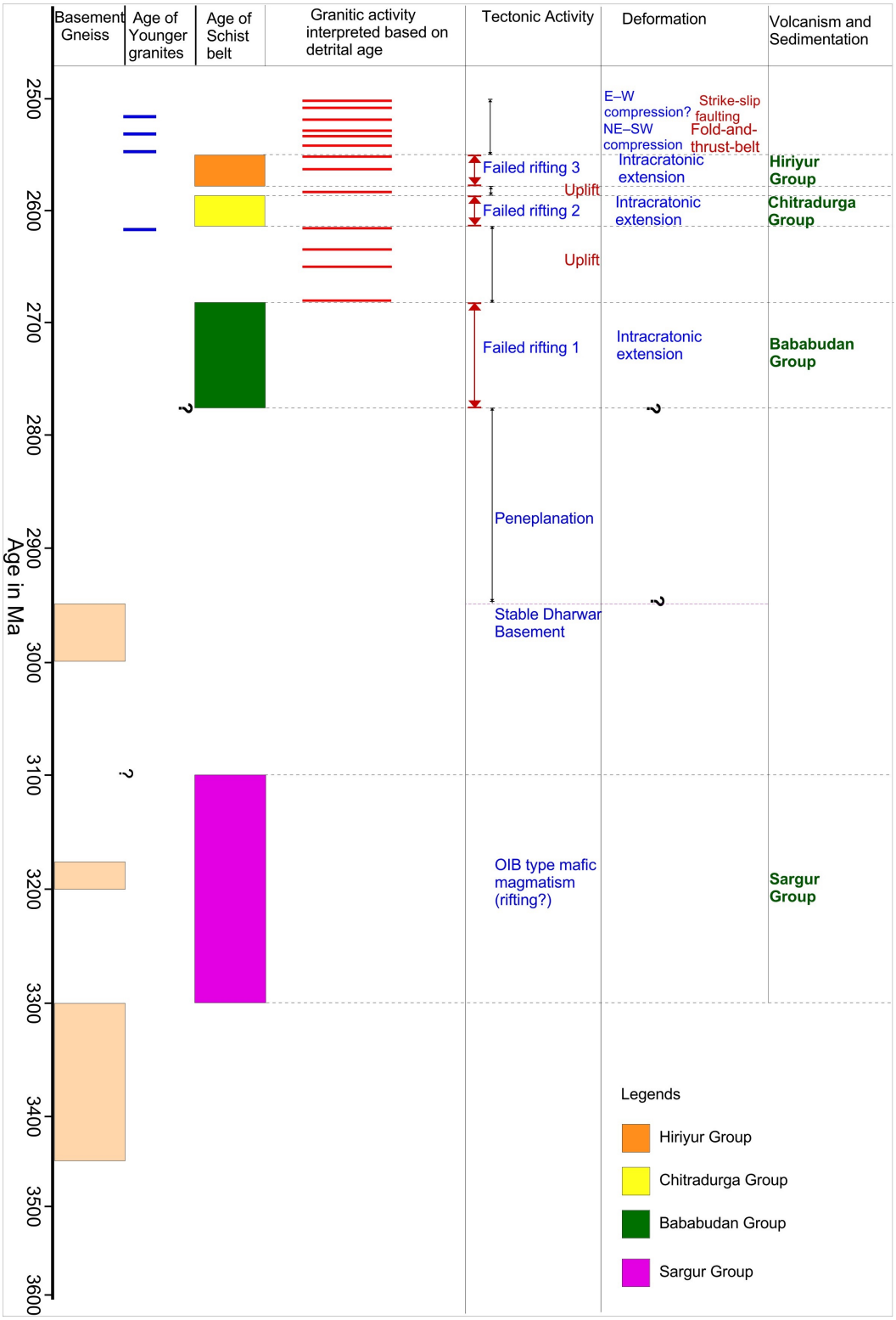

Figure 4.7 *Summary of the tectonic evolution of WDC. Age relations from table 4.1 and revised age relations of Krapez et al., 2020 and Jayananda et al., 2018 are incorporated.*

As I mentioned in chapter 3 after c.a. 3.0 Ga granite activities in WDC the next major tectonic activity is the initiation of Bababudan rifting that approximated to started in 2756 Ga. This ~200 Myr gap in the tectonic activity in WDC is marked as peneplanation event in the **Figure 4.7.** This time period probably resulted in continues erosion and weathering activities resulted in conglomerates or palaeosol above the basement only few of which is preserved in the present DC. The above-mentioned scenario is addressed in section 3.6 of chapter 3.

Bababudan Group of rocks, as mentioned in Chapter 2 and 3, are formed in a shallow-marine condition implying the immature nature of the rifting event. Rift debrite type conglomerate shown in Chapter 3 are marking the intiation of this event (**Fig.3.4b** and **Fig.3.6a, b, c**). The rifting probably lasted up to ~2718 Ma since it is the youngest age in felsic volcanic of Bababudan. Even though further geochronological analysis rooted on stratigraphy is required to understand the exact age relations in the Bababudan group. Krapez et al., (2020) based on comparing detrital zircon ages and ages of granites and felsic volcanic rock inferred granitic activity in DC beginning from 2.68 Ga (**Fig. 4.7**). They mentioned it as indication of initiation of convergence. So in this context it is important to mention the Post-Bababudan and pre-Chitradurga deformation in the study area. As I shown in the model in Chapter 2, **Figure 2.8a**, Bababudan Group and Chitradurga Group have no parallel bedding relation. Instead the unconformity is slightly oblique which we deducted from bedding relation in the field. So it is clear that Bababudan Group has experienced a weak shortening/convergence before the evolution of Chitradurga Group. I suppose, this convergence event probably resulted in the termination of rifting in Bababudan Group.

After the termination of Bababudan rifting, another gap is visible when observing major granitic events in WDC. ~40 Myr gap is present between first two granite event record after the termination of Bababudan rifting. But the direct granites cross cutting Bababudan Group such as Chitradurga granite are ~2.6 Ga old. This also implies another ‘hibernation’ period in

terms of volcanic or plutonic activities in WDC. This inactive period again span ~40–70Myrs.

Chitradurga basin (Chitradurga Group) probably initiated after the Chitradurga granite event. Krapez et al., (2020) mentioned an exact age of initiation as 2615 ± 3 Ma. Similar to Bababudan Group, I characterized the lithology and structure to conclude the failed rift nature of the basin. Before the initiation of Hiriyur Group a convergence event probably occurred and resulted in slight tilting of the bedding (**Fig. 2.8b**) resulted in an angular unconformity between Hiriyur and Chitradurga Groups. In the **Figure 4.8** the basin formation of Chitradurga Group clearly occurred within the intervals of two granitic events, this is also evident in the field as no granite cross cuts the Chitradurga Group of rocks. But Hokada et al., (2013) pointed an older age for Ingaldhal felsic volcanic (2676 ± 20 Ma). This age implies ~80–90 Myr long basin formation, which is long period for a basin, if this is true basin should have deep marine facies in them which is not evident in the field. Another possibility is that the time will be spend for local unconformities within the basin, but In my observation no such local unconformities are located within Chitradurga Group. Based on this I propose a narrow basin in Chitrdaurga Group probably lasted <20–30 Myr.

Hiriyur Group also followed same style as other basins, but Krapez et al., (2020) considered Hiriyur and Chitradurga Groups as basins associated with arc magmatism. This was based on the granitic peaks interpreted from detrital zircon ages. The detrital zircons in Hiriyur Group are also interpreted to supply from EDC (Nasheeth et al., 2016), thus younger ages spikes not always represent granitic activity in WDC. A thick conglomerate layer in separating Hiriyur Group and Chitradurga Group are shown in **Figure 2.1b** that is totally unmarked in most of the previous literatures. As I mentioned in last chapters this conglomerate also represent rift debrite deposits.

Ram Mohan et al., (2014) identified four stages of granitic activity in WDC, they are 2.61 Ga, 2.54 Ga, 2.56 Ga and 2.52 Ga. It is obvious from table 4.1 the felsic volcanic activity in schist belts is not exactly simultaneous with the granitic activity in WDC. So as it is evident from the **Figure 4.7** mafic magmatism or rifting and granitic activities are episodic in WDC. Granite

generation episodes and mafic magmatism are not contemporaneous. Their evolutionary history and geochemistry showing that granites are evolved during the episodic convergence events (Jayanada et al., 2006). I suppose the rift basins in the Dharwar Supergroup are failed because of the same reason. This means that extension stopped and convergence started along with granite intrusions in multiple times within WDC. The final stage fold-and-thrust belt and associated strike-slip movements also contributed to the enormous volume of granite intrusions in the DC (Chadwick et al., 2000, Chardon et al., 2011). So in conclusion this episodic extension and shortening events played a crucial role in the present architecture of the WDC (**Figure 4.8**). Present day architecture shows tight folds and strike slip shear zone in the eastern margin of the WDC implying strong deformation. On the other hand western margin of WDC is weakly folded according to previous literatures (Chadwick et al., 1985). Different schist belts represent single stage (KSB, chapter 3) or multistage (CSB, chapter 2) failed rift basins later faulted and folded through regional shortening.

Figure 4.8 indicate that CSB, KSB, BSB and SSB are isolated narrow failed rifts and evolved and deformed together. Based on my observations it is clear that three stages of rifting events are only preserved in CSB and in other schist belts it is either single stages of rifting or two stages of rifting probably preserved. Strong deformation in CSB and KSB indicate along GMSZ, WDC and EDC were collided and this event resulted in formation of fold-and-thrust belt (D_3). This may be the same reason for weak deformation in the western part of WDC. The randomly arranged fold axes are probably indicate the initial failed rift related synclines. Thus overall present day architecture of WDC supports the failed rift hypothesis I presented through out this thesis.

Korenaga et al., (2006) mentioned that more higher mantle temperature in the Archean means more sluggish plate movement in the Archean. Based on this concept Herzberg et al., (2010) pointed out basalts in the Archean-Proterozoic transition are erupted along rifts and adjacent areas from ambient mantle and mantle plumes. This also implies that rifting events might have played important role in balancing the thermal budget of the early

earth. Similar to my observations in DC, brief but voluminous episodes of diverse magmatism followed by period of quiescence and derivation of partially molten granites are also addressed in Yilgarn province (Hill et al., 1996). Thus I suppose the failed rift mechanism might have played a key role in the Archehan crustal growth process at least in some cratons around the globe.

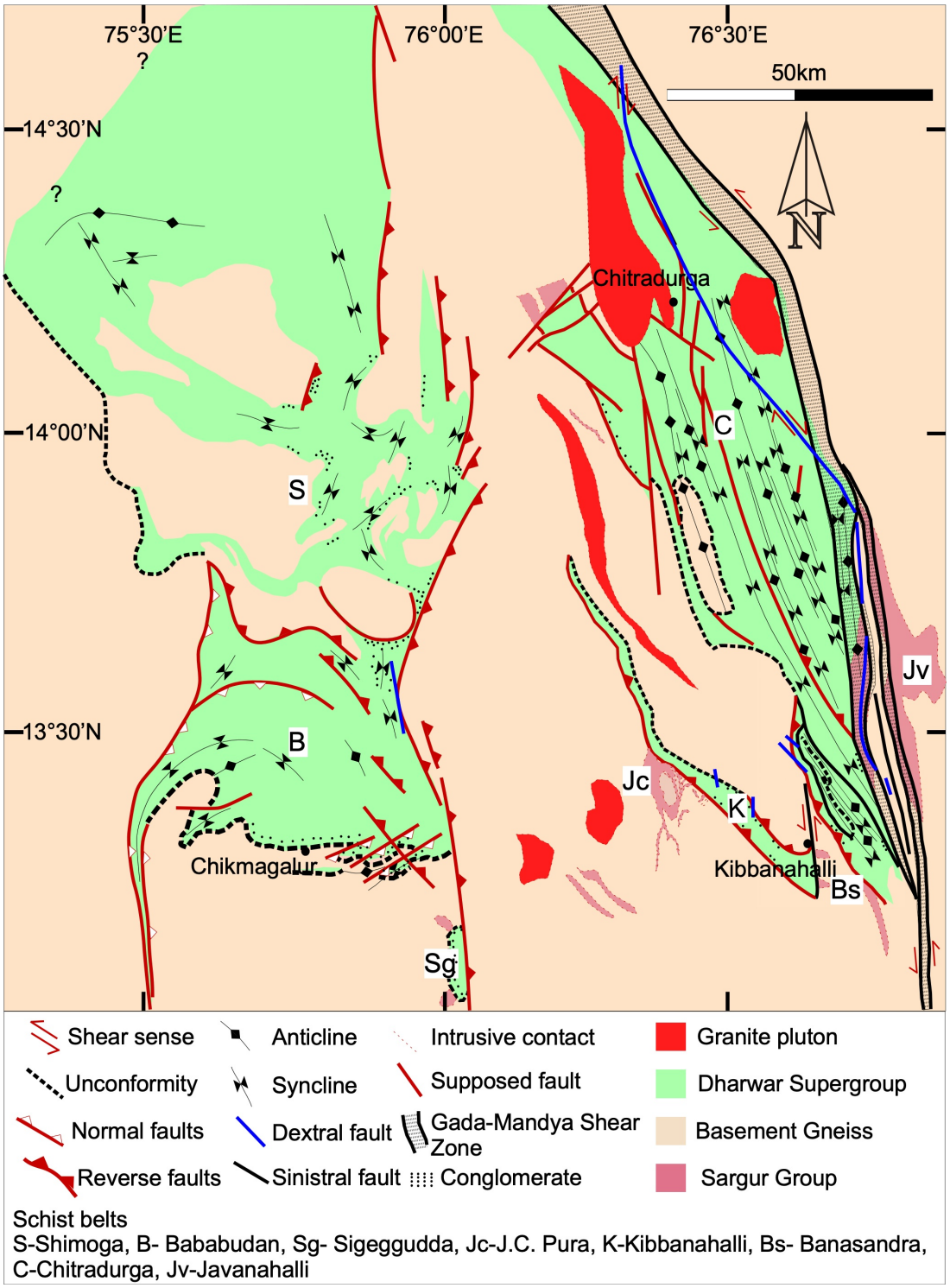

Figure 4.8 *Regional scale structural map of WDC. Compiled by information from my own fieldwork and previous studies (Chadwick et al., 1985, GSI 1996, Mishima et al., 2017). C-Chitradurga Schist Belt, Jv- Javanahalli Schist Belt, Jc-J.C.Pura Schist Belt, K- Kibbanahalli Schist Belt, Bs-Banasandra Schist Belt, Sg-Sigeggudda Schist Belt, B-Bababudan Schist Belt, S-Shimoga Schist Belt.*

4.5 Role of failed rifts in the crustal growth process.

Classical term used for failed rifts was 'aulacogens'. Aulacogens are explained as paleorifts which never reached crustal separation nor formed deep oceans (Khain, 1992). This term evolved from the Greek word 'aulax' means furrows (Twiss and Moores, 1992). Ernst and Buchan (2001) explained failed rifts as '*infants passed away before reaching maturity*'. Failed rifts are basically explained related to plume models and during the extensional activities associated with super continental cycle (Stein et al., 2018).

Based on my field observation and summary of tectonic activities presented in last section it is clear that the mafic crust evolution had directly promoted by failed rift events. By maintaining the thermal cycling of Archean mantle it again played a vital role in the evolution of felsic magmas. Even though aforementioned statement require further geochemical validation, it is clear that failed rifts have a control over the granite generation in DC. The episodic growth of convergence related granite genesis is connected to failed rift event prior to it. Similarly mafic magmatism possibly through intracontinental OIB type mafic magmatism in Sargur Group is also played an important role in generation of TTG (Jayananda et al., 2008). Another scenario mentioned by Hill et al., (1992) was that the weathering products of mafic rocks are clays and these clays are light and hence protected from subduction. These clays thus add to the overall continental mass, a significant contribution to the crustal volume. On the basis of this thesis, it is difficult to make an argument that failed rifts directly contributed to crustal growth process. Instead, I will argue that failed rifts played a proper 'catalysts' role in the crustal growth processes. Failed rifts initiated the episodic crustal growth events, increased the sediment supply and improved

thermal balancing between crust and mantle thus contributed significantly to the crustal growth processes.

There are other examples for large failed rift basin around the globe. One such example is preserved in the eastern flank of EDC called Cuddapah Basin. Paleoproterozoic Cuddapah Basin is a bounded by different basins separated by unconformities and deposited above continental crust of DC (Saha and Tripathy, 2012). Boundary thrust faults, inverted basin sequences and volcanic and sedimentary rock rich basins are all pointing to the intracontinental rifting (Saha et al., 2010, Lakshminarayana et al., 2019). Shalllow marine sediment-rich succession and presence of excessive bimodal volcanic rock in basins are typical of failed rift basins similar to WDC.

Failed intracontinental rift in North America, Midcontinental Rift (MCR) is a 3000m long ‘U’ shaped igneous and sedimentary rock-rich basin (Stein et al., 2018). Major rifting event in MCR is recorded at ~1.1 Ga (Grenvile orogeny) and this rift failed to split Precambrian core of the North American continent and consequently leaving behind a failed rift behind (Merdith et al., 2017). Similar to DC, the MCR also later undergone compression and resulted in the uplifting of the volcanic rocks (Hoffman, 1991).

The Japan sea back-arc basin is also considered as a failed rift in literatures (Sato and Kato, 2010). Thick piles of sedimentary and volcanic rocks in Niigata and Akita Basins associated with Early to Middle Miocene failed rifts (Ishiyama et al., 2017). These sediments are undergone Pliocene basin inversion (Sato and Kato, 2017).

Geological and geophysical evidence are present for failed rifts originated associated to East African rift system. Rirbara rift associated with Ethiopian rift was identified as aborted rift in geophysical analyses (Corti et al., 2019).

In conclusion, failed rifts are preserved throughout the evolutionary history of the Earth. They are also preserved in major intracontinental rift systems, back-arc basins and supercontinental margins as aborted volcano-sedimentary basins. They played crucial role in initiating the crustal growth processes, maintain the geochemical and thermal cycle between crust-

mantle systems, and balancing the sediment supply. Thus failed rifts can be considered as an important tectonic process contributed to crustal growth process in the Archean to Phanerozoic tectonic settings.

Chapter 5

5 CONCLUSIONS

Structural geology and stratigraphic relations in Archean Western Dharwar Craton (WDC) is studied. Geological maps are prepared for the southern part of Chitradurga Schist Belt (CSB) and Kibbanhalli Schist Belt (KSB) in WDC. Based on geological history and structural analysis evolutionary models for WDC are developed.

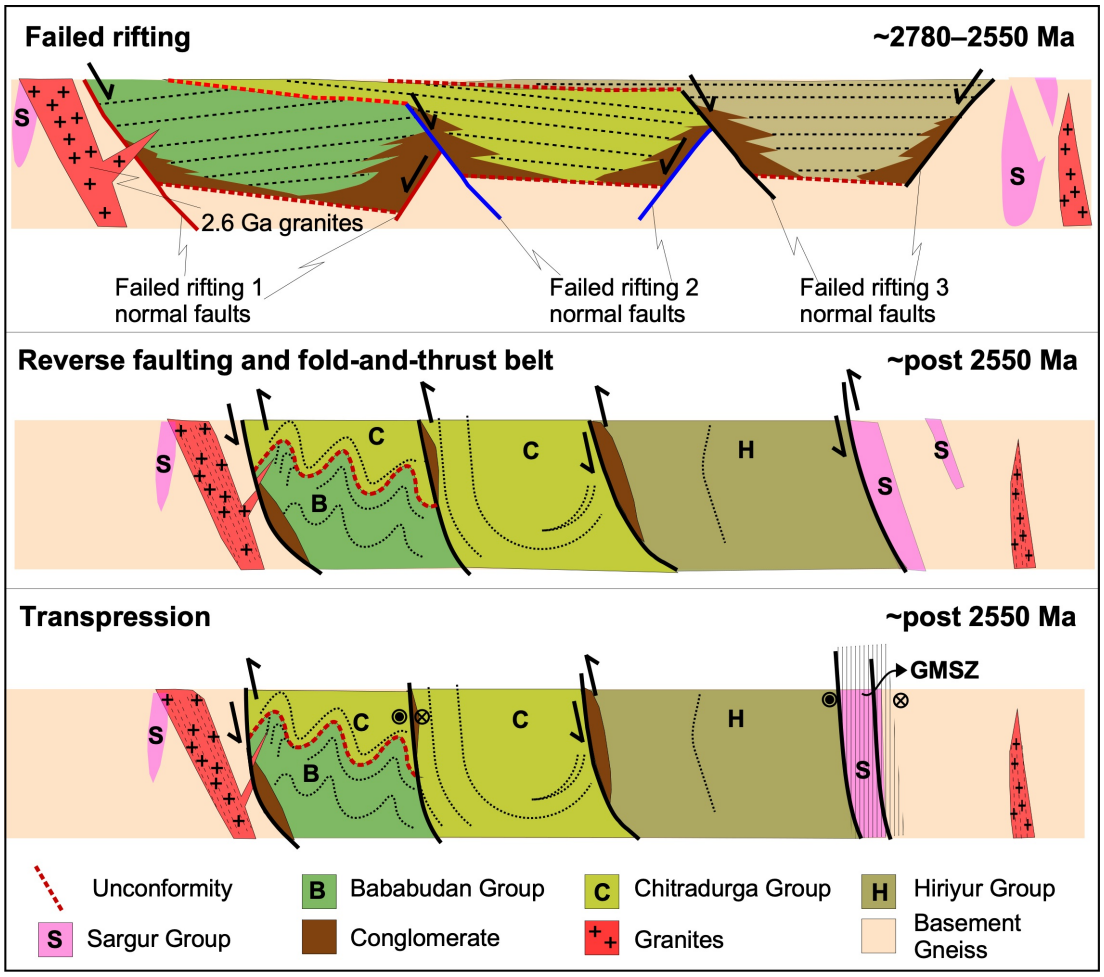

Figure 4.9 *Schematic model (not to scale) of three sages of failed rifting and evolution of fold-and-thrust belt in Western Dharwar Craton. Each rifting event followed by successive granite intrusions and this produced an angular unconformity between bedding in each Groups. Collision between Eastern and Western Dharwar Cratons produced initial thrust faulting and fold-and-thrust belt architecture. Last stage of deformation is progressed as transpression associated with intrusion of large volume of granites.*

On the basis of geological relationship and structural analysis it is concluded that Dharwar Supergroup of rocks deposited in different schist belts of WDC can be subdivided into three; Bababudan Group, Chitradurga Group and Hiriyur Group. Each of these Groups is separated by an unconformity defined by conglomerate. Characteristics of this conglomerate are similar to a rift debrites, deposited in the basal section of an intracratonic rift.

Sedimentary structures in WDC give an indication of fluvial to shallow marine origin for the rocks preserved in Bababudan, Chitradurga and Hiriyur Groups. Three shallow marine successions of WDC each separated by unconformity represent different episodes of failed intracratonic extension.

Structural analyses provided evidence for six stages of deformation process in WDC. Major D_2 episode is reverse faulting and simultaneous isoclinal folding of volcano-sedimentary rocks. The association of reverse fault bounded, folded, narrow volcano-sedimentary associations represent an inverted failed rift. Regional scale strike-slip sinistral shear (D_3) marks the major terrain boundary (Gadag Mandya Shear Zone, GMSZ). Narrow zones of strike-slip dextral shear (D_4) zone are also identified from WDC. Reverse faults are slightly pre-dating strike-slip faults or evolved together as if in a transpression setting.

Geochemical analyses show indication of crustally contaminated and uncontaminated metabasites in the study area. These variations in the chemical properties are resultant of crust-magma interactions in connection to intracratonic extension.

Field and structural relations of schist belts in WDC is not identical to a Cenozoic accretioanry Complex of Hiroo, Hokkaido Japan. The key structures and field association in schist belts of WDC support an aborted rift setting than an accretionary complex.

Secular evolution of WDC indicates multiple episodes of short-lived volcanic activity resulted in the formation of three failed rift basins. The Bababudan Group formed after long-lived (~200 Myr) cessation of granitic activity. Convergence related granitic activities resulted in failure of

Bababudan rifting. Similarly episodes of volcanic activities in Chitradurga and Hiriyur failed rifts are not contemporaneous with granite evolution. Post 3.0 Ga granites in WDC are product of convergence/shortening acted as a barricade for continues rifting. The final event of fold-and-thrust belt resulted in most extensive magmatic activities in the Dharwar Craton.

Failed rifts are identified in different part of the globe and reported in Archean to Phanerozoic time period. Failed rifting contributed to the crustal growth mechanism by initiating the convergence related magmatic activities, maintain thermo-chemical balancing between crust and mantle and providing sedimentary inputs. Failed rifts are reported in back-arc basins, intracontinental and intracratonic rifts around the globe beginning from the Archean.

This study concludes that schist belts of WDC are best-preserved examples for Archean failed rifts. These failed rifting events played important role in the crustal growth processes of WDC.

Chapter 6

6 Future plans and perspectives

Structural Evolution and Tectonic Setting of EDC

As part of this thesis project, preliminary fieldworks were carried out in EDC. These preliminary data shows some differences in the structural association and field relation in EDC. Further detailed fieldworks are needed to improve the maps and structural analysis. I think detailed mapping and geochronological analysis in schist belt s such as, Kolar Schist Belt will give vital clues towards the docking of EDC and WDC.

Geochronological Analyses In WDC

If I can check the detrital zircon ages in sedimentary rock based on stratigraphic relations that will give important insight into the depositional history of the basin. Some of the felsic tuff I tried hasn't preserved any zircons in it; this problem will also need to be addressed. The age relations from of Bababudan Group will be an important question to answer.

Boundary Shear Zone Problem

The extent of GMSZ and the relation between granites and schist belts are not properly constrained yet; this will be an interesting project to work on. Similarly the proposed shear zone in the central part of DC is not identified, nor mapped in the field. Detailed mapping in the eastern part of Kolar Schist Belt will give proper lead in this topic. The southern extension of GMSZ into granulite terrain is also needs to be addressed.

7 REFERENCES

Alsop, G. I., Marco, S., Weinberger, R., & Levi, T. (2016). Sedimentary and structural controls on seismogenic slumping within mass transport deposits from the Dead Sea Basin. *Sedimentary Geology*, *344*, 71-90.

Anhaeusser, C. R. (2014). Archaean greenstone belts and associated granitic rocks–a review. *Journal of African Earth Sciences*, *100*, 684-732.

Barker, F., & Arth, J. G. (1976). Generation of trondhjemitic-tonalitic liquids and Archean bimodal trondhjemite-basalt suites. *Geology*, *4*(10), 596-600.

Belousova, E. A., Kostitsyn, Y. A., Griffin, W. L., Begg, G. C., O'Reilly, S. Y., & Pearson, N. J. (2010). The growth of the continental crust: constraints from zircon Hf-isotope data. *Lithos*, *119*(3-4), 457-466.

Bhagya, K., & Ramadass, G. (2016). Sub–surface structural configuration of the Chitradurga Schist Belt as inferred from Bouguer Gravity data analysis. *IOSR Journal of Applied Geology and Geophysics*, *4*, 21-32.

Bidyananda, M., Deomurari, M. P., & Goswami, J. N. (2003). 207 Pb–206 Pb ages of zircons from the Nuggihalli schist belt, Dharwar craton, southern India. *Current Science*, 1482-1485.

Brown, M., Johnson, T., & Gardiner, N. J. (2020). Plate tectonics and the Archean Earth. *Annual Review of Earth and Planetary Sciences*, *48*.

Burke, K., Kidd, W. S. F., & Kusky, T. M. (1985). The Pongola structure of southeastern Africa- The world's oldest preserved rift?. *Journal of Geodynamics*, *2*(1), 35-49.

Chadwick, B., Ramakrishnan, M., & Viswanatha, M. N. (1981). The stratigraphy and structure of the Chitradurga region: an illustration of cover-basement interaction in the late Archaean evolution of the Karnataka craton, southern India. *Precambrian Research*, *16*(1-2), 31-54.

Chadwick, B., Ramakrishnan, M., Vasudev, V. N., & Viswanatha, M. N. (1989). Facies distributions and structure of a Dharwar volcanosedimentary basin: evidence for late Archaean transpression in southern India?. *Journal of the Geological Society*, *146*(5), 825-834.

Chadwick, B., Vasudev, V. N., & Hegde, G. V. (1997). The Dharwar craton, southern India, and its Late Archaean plate tectonic setting: current interpretations and controversies. *Proceedings of the Indian Academy of Sciences-Earth and Planetary Sciences*, *106*(4), 249-258.

Chadwick, B., Vasudev, V. N., & Hegde, G. V. (2000). The Dharwar craton, southern India, interpreted as the result of Late Archaean oblique convergence. *Precambrian Research*, *99*(1-2), 91-111.

Chadwick, B., Vasudev, V. N., Hegde, G. V., & Nutman, A. P. (2007). Structure and SHRIMP U/Pb zircon ages of granites adjacent to the Chitradurga schist belt: implications for Neoarchaean convergence in the Dharwar craton, southern India. *Journal of the Geological Society of India*, *69*(1), 5-24.

Chardon, D., Choukroune, P., & Jayananda, M. (1996). Strain patterns, décollement and incipient sagducted greenstone terrains in the Archaean Dharwar craton (south India). *Journal of Structural Geology*, *18*(8), 991-1004.

Chardon, D., Choukroune, P., & Jayananda, M. (1998). Sinking of the Dharwar basin (South India): implications for Archaean tectonics. *Precambrian Research*, *91*(1-2), 15-39.

Chardon, D., Jayananda, M., & Peucat, J. J. (2011). Lateral constrictional flow of hot orogenic crust: Insights from the Neoarchean of south India, geological and geophysical implications for orogenic plateaux. *Geochemistry, Geophysics, Geosystems*, *12*(2).

Chardon, D., Jayananda, M., Chetty, T. R., & Peucat, J. J. (2008). Precambrian continental strain and shear zone patterns: South Indian case. *Journal of Geophysical Research: Solid Earth*, *113*(B8).

Choukroune, P., Ludden, J. N., Chardon, D., Calvert, A. J., & Bouhallier, H. (1997). Archaean crustal growth and tectonic processes: a comparison of the Superior Province, Canada and the Dharwar Craton, India. *Geological Society, London, Special Publications*, *121*(1), 63-98.

Collins, W. J., Van Kranendonk, A. M., & Teyssier, C. (1998). Partial convective overturn of Archaean crust in the east Pilbara Craton, Western Australia: driving mechanisms and tectonic implications. *Journal of Structural Geology*, *20*(9-10), 1405-1424.

Condie, K. C. (1981). *Archean greenstone belts*. Elsevier.

Condie, K. C. (2018). A planet in transition: the onset of plate tectonics on Earth between 3 and 2 Ga?. *Geoscience Frontiers*, *9*(1), 51-60.

Corfu, F., & Hegde, V. S. (2020). U–Pb systematics of the western Dharwar Craton-Glimpses of a billion year history of crustal evolution and relations to ancient supercratons. *Journal of South American Earth Sciences*, 102659.

Corti, G., Cioni, R., Franceschini, Z., Sani, F., Scaillet, S., Molin, P., ... & Erbello, A. (2019). Aborted propagation of the Ethiopian rift caused by linkage with the Kenyan rift. *Nature communications*, *10*(1), 1-11.

Devaraju, T. C., Anantha Murthy, K. S., & Khanadali, S. D. (1986). Iron-formation of the Chiknayakanhalli greenstone belt, Karnataka, India. *Journal of the Geological Society of India*, *28*(2-3), 201-217.

Devaraju, T. C., Huhma, H., Sudhakara, T. L., Kaukonen, R. J., & Alapieti, T. T. (2007). Petrology, geochemistry, model Sm-Nd ages and petrogenesis of the granitoids of the northern block of Western Dharwar Craton. *JOURNAL-GEOLOGICAL SOCIETY OF INDIA*, *70*(6), 889.

Dhuime, B., Hawkesworth, C. J., Cawood, P. A., & Storey, C. D. (2012). A change in the geodynamics of continental growth 3 billion years ago. *Science*, *335*(6074), 1334-1336.

Dhuime, B., Hawkesworth, C. J., Delavault, H., & Cawood, P. A. (2018). Rates of generation and destruction of the continental crust: implications for

continental growth. *Philosophical Transactions of the Royal Society A: Mathematical, Physical and Engineering Sciences*, *376*(2132), 20170403.

Dhuime, B., Hawkesworth, C. J., Delavault, H., & Cawood, P. A. (2017). Continental growth seen through the sedimentary record. *Sedimentary Geology*, *357*, 16-32.

Duraiswami, R. A., Inamdar, M. M., & Shaikh, T. N. (2013). Emplacement of pillow lavas from the~ 2.8 Ga Chitradurga Greenstone Belt, South India: A physical volcanological, morphometric and geochemical perspective. *Journal of volcanology and geothermal research*, *264*, 134-149.

Eggins, S., & Martin, J. R. (1997). Genres and registers of discourse.

Ernst, R. E., & Buchan, K. L. (Eds.). (2001). *Mantle plumes: their identification through time* (Vol. 352). Geological Society of America.

Festa, A., Dilek, Y., Pini, G. A., Codegone, G., & Ogata, K. (2012). Mechanisms and processes of stratal disruption and mixing in the development of mélanges and broken formations: Redefining and classifying mélanges. *Tectonophysics*, *568*, 7-24.

Festa, A., Pini, G. A., Dilek, Y., & Codegone, G. (2010). Mélanges and mélange-forming processes: a historical overview and new concepts. *International Geology Review*, *52*(10-12), 1040-1105.

Furnes, H., de Wit, M., & Dilek, Y. (2014). Precambrian greenstone belts host different ophiolite types. In *Evolution of Archean Crust and Early Life* (pp. 1-22). Springer, Dordrecht.

Gao, P., Santosh, M., Nakagawa, M., & Li, S. S. (2020). Ocean island basalts and sedimentary units in the accretionary complex of Kochi, SW Japan: Implications for convergent margin tectonics and arc subduction. *Geological Journal*, *55*(1), 533-552.

Giri, A., Anand, R., Balakrishnan, S., Dash, J. K., & Sarma, D. S. (2019). Neoarchean magmatism in Shimoga greenstone belt, India: Evidence for subduction-accretion processes in the evolution of the western Dharwar stratigraphy. *Lithos*, *330*, 177-193.

Gokarn, S. G., Gupta, G., & Rao, C. K. (2004). Geoelectric structure of the Dharwar craton from magnetotelluric studies: Archean suture identified along the Chitradurga-Gadag schist belt. *Geophysical Journal International*, *158*(2), 712-728.

Goswami, S., Dey, S., Zakaulla, S., & Verma, M. B. (2020). Active rifting and bimodal volcanism in Proterozoic Papaghni sub-basin, Cuddapah basin (Andhra Pradesh), India. *Journal of Earth System Science*, *129*(1), 1-31.

Guitreau, M., Mukasa, S. B., Loudin, L., & Krishnan, S. (2017). New constraints on the early formation of the Western Dharwar Craton (India) from igneous zircon U-Pb and Lu-Hf isotopes. *Precambrian Research*, *302*, 33-49.

Hartlaub, R. P., Heaman, L. M., Ashton, K. E., & Chacko, T. (2004). The Archean Murmac Bay Group: evidence for a giant archean rift in the Rae Province, Canada. *Precambrian Research*, *131*(3-4), 345-372.

Hoffman, P. F. (1991). Did the breakout of Laurentia turn Gondwanaland inside-out?. *Science*, *252*(5011), 1409-1412.

Hokada, T., Horie, K., Satish-Kumar, M., Ueno, Y., Nasheeth, A., Mishima, K., & Shiraishi, K. (2013). An appraisal of Archaean supracrustal sequences in Chitradurga schist belt, western Dharwar Craton, southern India. *Precambrian Research*, *227*, 99-119.

Hollings, P., & Kerrich, R. (1999). Trace element systematics of ultramafic and mafic volcanic rocks from the 3 Ga North Caribou greenstone belt, northwestern Superior Province. *Precambrian Research*, *93*(4), 257-279.

Humbert, F., Agangi, A., Massuyeau, M., Elburg, M. A., Belyanin, G., Smith, A. J., ... & Wabo, H. (2020). Rifting of the Kaapvaal Craton during the early Paleoproterozoic: Evidence from magmatism in the western Transvaal subbasin (South Africa). *Precambrian Research*, 105687.

Ishiyama, T., Sato, H., Kato, N., Koshiya, S., Abe, S., Shiraishi, K., & Matsubara, M. (2017). Structures and active tectonics of compressionally reactivated back-arc failed rift across the Toyama trough in the Sea of Japan, revealed by multiscale seismic profiling. *Tectonophysics*, *710*, 21-36.

Jayananda, M., Aadhiseshan, K. R., Kusiak, M. A., Wilde, S. A., Sekhamo, K. U., Guitreau, M., ... & Gireesh, R. V. (2020). Multi-stage crustal growth and Neoarchean geodynamics in the Eastern Dharwar Craton, southern India. *Gondwana Research*, *78*, 228-260.

Jayananda, M., Chardon, D., Peucat, J. J., & Capdevila, R. (2006). 2.61 Ga potassic granites and crustal reworking in the western Dharwar craton, southern India: tectonic, geochronologic and geochemical constraints. *Precambrian Research*, *150*(1-2), 1-26.

Jayananda, M., Chardon, D., Peucat, J. J., & Fanning, C. M. (2015). Paleo-to Mesoarchean TTG accretion and continental growth in the western Dharwar craton, Southern India: Constraints from SHRIMP U–Pb zircon geochronology, whole-rock geochemistry and Nd–Sr isotopes. *Precambrian Research*, *268*, 295-322.

Jayananda, M., Kano, T., Peucat, J. J., & Channabasappa, S. (2008). 3.35 Ga komatiite volcanism in the western Dharwar craton, southern India: constraints from Nd isotopes and whole-rock geochemistry. Precambrian Research, 162(1-2), 160-179.

Jayananda, M., Peucat, J. J., Chardon, D., Rao, B. K., Fanning, C. M., & Corfu, F. (2013). Neoarchean greenstone volcanism and continental growth, Dharwar craton, southern India: constraints from SIMS U–Pb zircon geochronology and Nd isotopes. *Precambrian Research*, *227*, 55-76.

Jayananda, M., Santosh, M., & Aadhiseshan, K. R. (2018). Formation of Archean (3600–2500 Ma) continental crust in the Dharwar Craton, southern India. *Earth-Science Reviews*, *181*, 12-42.

Jayananda, M., Tsutsumi, Y., Miyazaki, T., Gireesh, R. V., Kapfo, K. U., Hidaka, H., & Kano, T. (2013). Geochronological constraints on Meso-and Neoarchean regional metamorphism and magmatism in the Dharwar craton, southern India. *Journal of Asian Earth Sciences*, *78*, 18-38.

Johnson, T. E., Brown, M., Gardiner, N. J., Kirkland, C. L., & Smithies, R. H. (2017). Earth's first stable continents did not form by subduction. *Nature*, *543*(7644), 239-242.

Khain, V. Y. (1992). The role of rifting in the evolution of the Earth's crust. *Tectonophysics*, *215*(1-2), 1-7.

Khelen, A. C., Manikyamba, C., Tang, L., Santosh, M., Subramanyam, K. S. V., & Singh, T. D. (2020). Detrital zircon U-Pb geochronology of stromatolitic carbonates from the greenstone belts of Dharwar Craton and Cuddapah basin of Peninsular India. *Geoscience Frontiers*, *11*(1), 229-242.

Kontani, Y. (1978). Geological study of the Hidaka Supergroup distributed on the east side of the Hidaka metamorphic belt (Part 1)-Stratigraphy and geological structure. *J. Geol. Soc. Japan*, *84*, 1-14.

Kontani, Y., & Kiminami, K. (1980). Petrological study of the sandstones in the pre-Cretaceous Yubetsu Group, northeastern Hidaka Belt, Hokkaido, Japan. *Earth Science (Chikyu Kagaku)*, *34*(6), 307-319.

Korenaga, J. (2018). Crustal evolution and mantle dynamics through Earth history. *Philosophical Transactions of the Royal Society A: Mathematical, Physical and Engineering Sciences*, *376*(2132), 20170408.

Kranendonk, M. J. V., Hickman, A. H., Smithies, R. H., Nelson, D. R., & Pike, G. (2002). Geology and tectonic evolution of the archean North Pilbara terrain, Pilbara Craton, Western Australia. *Economic Geology*, *97*(4), 695-732.

Krapež, B., Sarma, D. S., Mohan, M. R., McNaughton, N. J., Rasmussen, B., & Wilde, S. A. (2020). Tectonostratigraphy of the Late Archean Dharwar Supergroup, Dharwar Craton, India: defining a tectonic history from spatially linked but temporally distinct intracontinental and arc-related basins. *Earth-Science Reviews*, *201*, 102966.

Kumar, A., Rao, Y. B., Sivaraman, T. V., & Gopalan, K. (1996). Sm□ Nd ages of Archaean metavolcanics of the Dharwar craton, South India. *Precambrian Research*, *80*(3-4), 205-216.

Kusky, T. M., Windley, B. F., & Polat, A. (2018). Geological evidence for the operation of plate tectonics throughout the Archean: Records from Archean paleo-plate boundaries. *Journal of Earth Science*, *29*(6), 1291-1303.

Lakshminarayana, G., Kumar, D. V., Kumar, S. K., & Raghavendra, G. (2019). Extension related magmatism and basin evolution in northwestern part of the Cuddapah rift, India. *Journal of the Geological Society of India*, *94*(2), 149-161.

Lancaster, P. J., Dey, S., Storey, C. D., Mitra, A., & Bhunia, R. K. (2015). Contrasting crustal evolution processes in the Dharwar craton: insights from detrital zircon U–Pb and Hf isotopes. *Gondwana Research*, *28*(4), 1361-1372.

Li, S. S., Santosh, M., & Palin, R. M. (2018). Metamorphism during the Archean–Paleoproterozoic transition associated with microblock amalgamation in the Dharwar Craton, India. *Journal of Petrology*, *59*(12), 2435-2462.

Maibam, B., Gerdes, A., & Goswami, J. N. (2016). U–Pb and Hf isotope records in detrital and magmatic zircon from eastern and western Dharwar craton, southern India: Evidence for coeval Archaean crustal evolution. *Precambrian Research*, *275*, 496-512.

Maibam, B., Goswami, J. N., & Srinivasan, R. (2011). Pb–Pb zircon ages of Archaean metasediments and gneisses from the Dharwar craton, southern India: implications for the antiquity of the eastern Dharwar craton. *Journal of Earth System Science*, *120*(4), 643-661.

Maibam, B., Sanyal, P., & Bhattacharya, S. (2015). Geochronological study of metasediments and carbon isotopes in associated graphites from the Sargur area, Dharwar craton: Constraints on the age and nature of the protoliths. *Journal of the Geological Society of India*, *85*(5), 577-585.

Manikyamba, C., & Ganguly, S. O. H. I. N. I. (2020). Annals of Precambrian lithospheric evolution and metallogeny in the Dharwar Craton, India: Recent paradigms and perspectives.

Manikyamba, C., Ganguly, S., Santosh, M., & Subramanyam, K. S. V. (2017). Volcano-sedimentary and metallogenic records of the Dharwar greenstone terranes, India: Window to Archean plate tectonics, continent growth, and mineral endowment. *Gondwana Research*, *50*, 38-66.

Manikyamba, C., Kerrich, R., Polat, A., & Saha, A. (2013). Geochemistry of two stratigraphically-related ultramafic (komatiite) layers from the Neoarchean Sigegudda greenstone terrane, Western Dharwar Craton, India: evidence for compositional diversity in Archean mantle plumes. *Lithos*, *177*, 120-135.

Manikyamba, C., Kerrich, R., Polat, A., Raju, K., Satyanarayanan, M., & Krishna, A. K. (2012). Arc picrite–potassic adakitic–shoshonitic volcanic association of the Neoarchean Sigegudda Greenstone Terrane, Western Dharwar Craton: transition from arc wedge to lithosphere melting. *Precambrian Research*, *212*, 207-224.

Manikyamba, C., Saha, A., Santosh, M., Ganguly, S., Singh, M. R., Rao, D. S., & Lingadevaru, M. (2014). Neoarchaean felsic volcanic rocks from the Shimoga greenstone belt, Dharwar Craton, India: geochemical fingerprints of crustal growth at an active continental margin. *Precambrian Research*, *252*, 1-21.

Martin, H. (1986). Effect of steeper Archean geothermal gradient on geochemistry of subduction-zone magmas. *Geology*, *14*(9), 753-756.

Maya, J. M., Bhutani, R., Balakrishnan, S., & Sandhya, S. R. (2017). Petrogenesis of 3.15 Ga old Banasandra komatiites from the Dharwar craton, India: Implications for early mantle heterogeneity. *Geoscience Frontiers*, *8*(3), 467-481.

Meen, J. K., Rogers, J. J., & Fullagar, P. D. (1992). Lead isotopic compositions of the Western Dharwar Craton, southern India: evidence for distinct Middle

Archean terranes in a Late Archean craton. *Geochimica et Cosmochimica Acta*, *56*(6), 2455-2470.

Mishima, K., Yamazaki, R., Satish-Kumar, M., Ueno, Y., Hokada, T., & Toyoshima, T. (2017). Multiple sulfur isotope geochemistry of Dharwar Supergroup, Southern India: Late Archean record of changing atmospheric chemistry. *Earth and Planetary Science Letters*, *464*, 69-83.

Mohan, M. R., Asokan, A. D., & Wilde, S. A. (2020). Crustal growth of the Eastern Dharwar Craton: a Neoarchean collisional orogeny?. *Geological Society, London, Special Publications*, *489*.

Mohan, M. R., Sarma, D. S., McNaughton, N. J., Fletcher, I. R., Wilde, S. A., Siddiqui, M. A., ... & Kamo, S. L. (2014). SHRIMP zircon and titanite U-Pb ages, Lu-Hf isotope signatures and geochemical constraints for~ 2.56 Ga granitic magmatism in Western Dharwar Craton, Southern India: Evidence for short-lived Neoarchean episodic crustal growth?. *Precambrian Research*, *243*, 197-220.

Moyen, J. F., & Martin, H. (2012). Forty years of TTG research. *Lithos*, *148*, 312-336.

Moyen, J. F., Nédélec, A., Martin, H., & Jayananda, M. (2001). Contrasted granite emplacement modes within an oblique crustal section: the Closepet Granite, South India. *Physics and Chemistry of the Earth, Part A: Solid Earth and Geodesy*, *26*(4-5), 295-301.

Mukherjee, S. (2012). Simple shear is not so simple! Kinematics and shear senses in Newtonian viscous simple shear zones. *Geological Magazine*, *149*(5), 819-826.

Mukhopadhyay, D. H. R. U. B. A., Baral, M. C., & Ghosh, D. E. B. A. S. H. I. S. H. (1981). A tectono-stratigraphic model of the Chitradurga schist belt, Karnataka, India. *Journal of the Geological Society of India*, *22*, 22-31.

Nanayama, F. (1992). Stratigraphy and facies of the Paleocene Nakanogawa Group in the southern part of central Hokkaido, Japan. *Chishitsugaku Zasshi*, *98*(11), 1041-1059.

Nanayama, F. (1992). Three petroprovinces identified in the Nakanogawa Group, Hidaka Belt, central Hokkaido, Japan, and their geotectonic significance. *Chishitsugaku ronshū*, *38*, 27-42.

Nanayama, F., & Ganzawa, Y. (1997). Sedimentary stratigraphy, environment and age of the northern unit of Nakanogawa Group in the Hidaka belt, central Hokkaido, Japan. *Mem. Geol. Soc. Japan*, *47*, 279-293.

Nanayama, F., Takahashi, Y., Yamasaki, T., Nakagawa, M., Iwano, H., Danhara, T., & Hirata, T. (2018). U–Pb zircon ages of the Nakanogawa Group in the Hidaka Belt, northern Japan: Implications for its provenance and the protolith of the Hidaka metamorphic rocks. *Island Arc*, *27*(2), e12234.

Nasheeth, A., Okudaira, T., Horie, K., Hokada, T., & Satish-Kumar, M. (2016). U-Pb SHRIMP ages of detrital zircons from Hiriyur Formation in Chitradurga greenstone belt and its implication to the Neoarchean evolution of Dharwar craton, south India. *Journal of the Geological Society of India*, *87*(1), 43-54.

Neo, N., Yamazaki, S., & Miyashita, S. (2009). Data report: bulk rock compositions of samples from the IODP Expedition 309/312 sample pool, ODP Hole 1256D. In *Proceedings of the Integrated Ocean Drilling Program* (Vol. 309, p. 312).

Nicoli, G., Moyen, J. F., & Stevens, G. (2016). Diversity of burial rates in convergent settings decreased as Earth aged. *Scientific Reports*, *6*, 26359.

Nutman, A. P., Chadwick, B., Krishna Rao, B., & Vasudev, V. N. (1996). SHRIMP U/Pb zircon ages of acid volcanic rocks in the Chitradurga and Sandur groups, and granites adjacent to the Sandur schist belt, Karnataka. *Journal of the Geological Society of India*, *47*(2), 153-164.

Nutman, A. P., Chadwick, B., Ramakrishnan, M., & Viswanatha, M. N. (1992). SHRIMP U-Pb ages of detrital zircon in Sargur supracrustal rocks in western Karnataka, southern India. *Journal of the Geological Society of India*, *39*(5), 367-374.

Osozawa, S., Morimoto, J., & Flower, M. F. (2009). “Block-in-matrix” fabrics that lack shearing but possess composite cleavage planes: A sedimentary mélange origin for the Yuwan accretionary complex in the Ryukyu island arc, Japan. *Geological Society of America Bulletin*, *121*(7-8), 1190-1203.

Patra, K., Anand, R., Balakrishnan, S., & Dash, J. K. (2020). Geochemistry of ultramafic–mafic rocks of Mesoarchean Sargur Group, western Dharwar craton, India: Implications for their petrogenesis and tectonic setting. *Journal of Earth System Science*, *129*(1), 26.

Pearce, J. A. (1996). A user’s guide to basalt discrimination diagrams. *Trace element geochemistry of volcanic rocks: applications for massive sulphide exploration. Geological Association of Canada, Short Course Notes*, *12*(79), 113.

Peucat, J. J., Bouhallier, H., Fanning, C. M., & Jayananda, M. (1995). Age of the Holenarsipur greenstone belt, relationships with the surrounding gneisses (Karnataka, South India). *The Journal of Geology*, *103*(6), 701-710.

Peucat, J. J., Jayananda, M., Chardon, D., Capdevila, R., Fanning, C. M., & Paquette, J. L. (2013). The lower crust of the Dharwar Craton, Southern India: Patchwork of Archean granulitic domains. *Precambrian Research*, *227*, 4-28.

Peucat, J. J., Mahabaleswar, B., & Jayananda, M. (1993). Age of younger tonalitic magmatism and granulitic metamorphism in the South Indian transition zone (Krishnagiri area); comparison with older Peninsular gneisses from the Gorur–Hassan area. *Journal of Metamorphic Geology*, *11*(6), 879-888.

Pichamuthu, C. S. (1946). Cycles in Dharwar Sedimentation. *Current Science*, *15*(10), 273-274.

Poblet, J., & Lisle, R. J. (2011). Kinematic evolution and structural styles of fold-and-thrust belts. *Geological Society, London, Special Publications*, *349*(1), 1-24.

Radhakrishna, B. P. (1983). Archaean granite-greenstone terrain of the south Indian Shield in Precambrian of south India. *Geol. Soc. Ind. Mem.*, *4*, 1-46.

Radhakrishna, B. P., & Naqvi, S. M. (1986). Precambrian continental crust of India and its evolution. *The Journal of Geology*, *94*(2), 145-166.

Raju, P. S., & Mazumder, R. (2020). Archean sedimentation on Dharwar Craton, India and its implications. *Earth-Science Reviews*, *202*, 102999.

Ramakrishnan, M. Vaidyanathan 2008 Geology of India; Vol. 1. *Geol. Soc. India, Bangalore*.

Ramakrishnan, M., & Nath, J. S. (Eds.). (1981). *Early Precambrian supracrustals of southern Karnataka* (Vol. 112). Geological Survey of India.

Ramakrishnan, M., Venkata Dasu, S. P., & Kröner, A. (1994). Middle Archaean age of Sargur Group by single grain zircon dating and geochemical evidence for the clastic origin of metaquartzite from JC Pura Greenstone belt, Karnataka. *Journal of the Geological Society of India*, *44*(6), 605-616.

Rao, B. R. (1962). *A handbook of the geology of Mysore state, southern India*. Bangalore Printing and Publishing Company.

Rao, T. G., & Naqvi, S. M. (1995). Geochemistry, depositional environment and tectonic setting of the BIF's of the late Archaean Chitradurga schist belt, India. *Chemical Geology*, *121*(1-4), 217-243.

Rao, V. V., Murty, A. S. N., Sarkar, D., Rao, Y. B., Khare, P., Prasad, A. S. S. S. R. S., ... & Sen, M. K. (2015). Crustal velocity structure of the Neoarchean convergence zone between the eastern and western blocks of Dharwar Craton, India from seismic wide-angle studies. *Precambrian Research*, *266*, 282-295.

Rao, Y. B. (2008). The emerging pattern of crust-formation and recycling history in the Precambrian Dharwar craton and the southern granulite terrain, southern India: constraints from recent geochronological and isotopic results. In *National Symposium on Geodynamics and evolution of Indian Shield–through time and space* (p. 10).

Rao, Y. B. (2008). The emerging pattern of crust-formation and recycling history in the Precambrian Dharwar craton and the southern granulite terrain, southern India: constraints from recent geochronological and isotopic results. In *National Symposium on Geodynamics and evolution of Indian Shield–through time and space* (p. 10).

Rao, Y. B., Kumar, A., Vrevsky, A. B., Srinivasan, R., & Iyer, G. A. (2000). Sm-Nd ages of two meta-anorthosite complexes around Holenarsipur: Constraints on the antiquity of Archean supracrustal rocks of the Dharwar craton. *Journal of Earth System Science*, *109*(1), 57-65.

Rogers, J. J., & Callahan, E. J. (1989). Diapiric trondhjemites of the western Dharwar craton, southern India. *Canadian Journal of Earth Sciences*, *26*(2), 244-256.

Rooney, T. O. (2020). The Cenozoic magmatism of East Africa: part V–magma sources and processes in the East African Rift. *Lithos*, *360*, 105296.

Rudnick, R. L. (1995). Making continental crust. *Nature*, *378*(6557), 571-578.

Saha, D., & Tripathy, V. (2012). Palaeoproterozoic sedimentation in the Cuddapah Basin, south India and regional tectonics: a review. *Geological Society, London, Special Publications*, *365*(1), 161-184.

Saha, D., Chakraborti, S., & Tripathy, V. (2010). Intracontinental thrusts and inclined transpression along eastern margin of the East Dharwar Craton, India. *Journal of the Geological Society of India*, *75*(1), 323-337.

Said, N., & Kerrich, R. (2010). Elemental and Nd-isotope systematics of the Upper Basalt Unit, 2.7 Ga Kambalda Sequence: Quantitative modeling of progressive crustal contamination of plume asthenosphere. *Chemical Geology*, *273*(3-4), 193-211.

Said, N., Kerrich, R., & Groves, D. (2010). Geochemical systematics of basalts of the Lower Basalt Unit, 2.7 Ga Kambalda Sequence, Yilgarn craton, Australia: plume impingement at a rifted craton margin. *Lithos*, *115*(1-4), 82-100.

Sappin, A. A., Guilmette, C., Goutier, J., & Beaudoin, G. (2018). Geochemistry of Mesoarchean felsic to ultramafic volcanic rocks of the Lac Guyer area, La Grande Subprovince (Canada): Evidence for plume-related magmatism in a rift setting. *Precambrian Research*, *316*, 83-102.

Sarma, D. S., Fletcher, I. R., Rasmussen, B., McNaughton, N. J., Mohan, M. R., & Groves, D. I. (2011). Archaean gold mineralization synchronous with late cratonization of the Western Dharwar Craton, India: 2.52 Ga U–Pb ages of hydrothermal monazite and xenotime in gold deposits. *Mineralium Deposita*, *46*(3), 273-288.

Sarma, D. S., McNaughton, N. J., Belusova, E., Mohan, M. R., & Fletcher, I. R. (2012). Detrital zircon U–Pb ages and Hf-isotope systematics from the Gadag Greenstone Belt: Archean crustal growth in the western Dharwar Craton, India. *Gondwana Research*, *22*(3-4), 843-854.

Sato, H., & Kato, N. (2010). Crustal structure and earthquake source faults on the backarc side of northern Honshu, Japan. *J Geol Soc Jpn*, *116*, 592-601.

Schumacher, R., & Schmincke, H. U. (1995). Models for the origin of accretionary lapilli. *Bulletin of Volcanology*, *56*(8), 626-639.

Senda, R., Kimura, J. I., & Chang, Q. (2014). Evaluation of a rapid, effective sample digestion method for trace element analysis of granitoid samples containing acid-resistant minerals: Alkali fusion after acid digestion. *Geochemical Journal*, *48*(1), 99-103.

Sengupta, S., & Roy, A. (2012). Tectonic amalgamation of crustal blocks along Gadag-Mandya Shear Zone in Dharwar Craton of southern India. *Journal of the Geological Society of India*, *80*(1), 75-88.

Sethumadhav, M. S., Gunnell, Y., & Ahmed, M. M. (2010). Late Archean manganese mineralization and younger supergene manganese ores in the Anmod–Bisgod region, Western Dharwar Craton, southern India: Geological characterization, palaeoenvironmental history, and geomorphological setting. *Ore Geology Reviews*, *38*(1-2), 70-89.

Sleep, N. H., & Windley, B. F. (1982). Archean plate tectonics: constraints and inferences. *The Journal of Geology*, *90*(4), 363-379.

Sreehari, L., & Toyoshima, T. (2020). Structural architecture and geological relationships in the southern part of Chitradurga Schist Belt, Dharwar craton, South India. *Journal of Mineralogical and Petrological Sciences*, 191120.

Srinivasan, R., & Ojakangas, R. W. (1986). Sedimentology of quartz-pebble conglomerates and quartzites of the Archean Bababudan Group, Dharwar Craton, South India: evidence for early crustal stability. *The Journal of Geology*, *94*(2), 199-214.

Stein, S., Stein, C. A., Elling, R., Kley, J., Keller, G. R., Wysession, M., ... & Moucha, R. (2018). Insights from North America's failed Midcontinent Rift into the evolution of continental rifts and passive continental margins. *Tectonophysics*, *744*, 403-421.

Sun, S. S., & McDonough, W. F. (1989). Chemical and isotopic systematics of oceanic basalts: implications for mantle composition and processes. *Geological Society, London, Special Publications*, *42*(1), 313-345.

Takahashi, T. (1997). Major and trace element analysis of silicate rocks using X-ray fluorescence spectrometer RIX 3000. *The Rigaku Journal*, *28*, 25-37.

Trendall, A. F., De Laeter, J. R., Nelson, D. R., & Bhaskar Rao, Y. J. (1997b). Further zircon U-Pb age data for the Daginkatte formation, Dharwar Supergroup, Karnataka craton. *Journal of the Geological Society of India*, *50*(1), 25-30.

Trendall, A. F., De Laeter, J. R., Nelson, D. R., & Mukhopadhyay, D. (1997a). A precise zircon U-Pb age for the base of the BIF of the Mulaingiri Formation,(Bababudan Group, Dharwar Supergroup) of the Karnataka Craton. *Journal of the Geological Society of India*, *50*(2), 161-170.

Twiss, R. J., Twiss, R. J., & Moores, E. M. (1992). *Structural geology*. Macmillan.

Ueda, H., Takazawa, E., Kato, R., & Adachi, Y. (2018). Evaluation of time-resolved mean-of-ratios reduction for laser ablation zircon U-Pb dating using quadrupole ICPMS. *Geochemical Journal*, *52*(3), 241-254.

Vaidyanadhan, R., & Ramakrishnan, M. (2010). *Geology of India*. Geological Society of India.

Vallance, J. W., & Iverson, R. M. (2015). Lahars and their deposits. In *The Encyclopedia of Volcanoes* (pp. 649-664). Academic Press.

Valley, J. W., Lackey, J. S., Cavosie, A. J., Clechenko, C. C., Spicuzza, M. J., Basei, M. A. S., ... & Peck, W. H. (2005). 4.4 billion years of crustal maturation: oxygen isotope ratios of magmatic zircon. *Contributions to Mineralogy and Petrology*, *150*(6), 561-580.

Van Kranendonk, M. J., Collins, W. J., Hickman, A., & Pawley, M. J. (2004). Critical tests of vertical vs. horizontal tectonic models for the Archaean East Pilbara

granite–greenstone terrane, Pilbara craton, western Australia. *Precambrian Research*, *131*(3-4), 173-211.

Venkata Dasu, S. P., Ramakrishnan, T. M., & Mahabaleswar, B. (1991). Sargur-Dharwar relationship around the komatiite-rich Jayachamarajapura greenstone belt in Karnataka. *Journal of the Geological Society of India*, *38*(6), 577-592.

Winchester, J. A., & Floyd, P. A. (1977). Geochemical discrimination of different magma series and their differentiation products using immobile elements. *Chemical geology*, *20*, 325-343.

Yamasaki, T., & Nanayama, F. (2018). Immature intra-oceanic arc-type volcanism on the Izanagi Plate revealed by the geochemistry of the Daimaruyama greenstones in the Hiroo Complex, southern Hidaka Belt, central Hokkaido, Japan. *Lithos*, *302*, 224-241.

8 TABLES

ID	$^{206}Pb/^{238}U$	err	$^{207}Pb/^{235}U$	err	207Pb-206Pb age	error (2se)
SL0363	1922	102	2592	58	3181.82	18.89
SL0300	2336	121	2832	61	3219.52	25.37
SL0326	2210	78	2775	42	3229.94	25.54
SL0306	2395	72	2870	36	3236.49	20.09
SL0435	2193	66	2775	37	3244.73	24
SL0284	2466	81	2910	40	3247.73	22.75
SL0350	2109	64	2741	37	3259.74	23.93
Sl0432	2506	74	2939	37	3264.91	20.75
SL0436	2476	74	2926	36	3266.49	17.9
SL0287	2239	83	2813	44	3268.86	24.58
SL0411	2588	60	2979	29	3269.4	15.16
SL0375	2633	86	3004	40	3276.14	18.61
SL0430	2711	98	3039	44	3277.67	15.68
SL0458	2698	67	3034	31	3278.8	16.66
SL0454	2986	67	3157	29	3281.01	18.24
SL0281	2872	96	3110	43	3281.26	23.53
SL0309	2814	98	3089	44	3287.01	24.56
SL0370	2259	66	2835	36	3287.65	23.51
SL0410	2751	72	3063	33	3288.51	17.63
SL0322	2707	76	3044	36	3288.97	22.36
SL0394	2750	79	3063	36	3289.4	16.76
SL02823	2514	93	2959	45	3290.78	25.19
SL0414	2672	64	3031	30	3292.27	17.52
SL0275	2807	106	3090	47	3293.73	24.43
SL0420	2476	61	2944	30	3294.38	16.53
SL0347	2732	82	3060	39	3297.15	26.08
SL0279	2447	84	2932	43	3297.72	25.71
SL0386	3012	78	3178	33	3297.88	16.11
SL0451	2818	65	3098	29	3298.7	16.92
SL0366	2623	77	3014	37	3299.51	20.66
SL0307	2916	80	3140	36	3299.52	21.91
SL0329	2704	73	3050	34	3299.97	19.35
SL0442	2958	70	3158	31	3300.59	17.9
SL0388	3089	77	3211	33	3302.32	18.4
SL0463	2801	65	3094	29	3303.95	16.61
SL0364	3077	76	3208	32	3304.21	15.59
SL0429	2852	78	3117	34	3306.68	16.11
SL0441	2987	69	3175	30	3310.08	17.06
SL0397	2520	67	2974	33	3311.12	16.96
SL0328	2984	74	3176	32	3313.63	18.98
SL0285	3052	94	3204	40	3314.5	22.8

SL0331	3090	83	3220	36	3316.08	23.79
SL0367	2661	67	3042	31	3318.36	16.13
SL0372	2740	72	3078	33	3320.02	19.91
SL0460	3054	73	3209	32	3320.32	18.94
SL0297	2048	69	2748	39	3324.88	18.72
SL0395	2908	71	3152	31	3325.32	15.17
SL0408	2084	94	2768	52	3327.08	26.5
SL0389	2889	70	3147	31	3329.09	16.54
SL0345	2716	81	3074	39	3330.32	26.75
SL0319	2552	83	3001	40	3331.52	19.88
SL0278	2891	94	3149	42	3331.9	24.42
SL0385	2486	101	2972	48	3332.79	18.32
SL0376	3076	78	3227	33	3336.62	18.32
SL0354	2510	80	2986	40	3338.9	25.78
SL0407	3131	76	3254	33	3343.88	20.9
SL0464	2787	80	3114	37	3345.04	24.3
SL0452	2869	75	3149	33	3345.4	18.44
SL0348	3023	76	3212	33	3346.41	20.11
SL0392	2978	78	3196	34	3350.38	19.15
SL0438	2898	104	3164	45	3351.82	21.87
SL0344	2151	56	2821	32	3356.37	22.15
SL0413	2931	77	3190	34	3371.45	20.75
SL0320	2553	80	3027	40	3371.54	27.78
SL0461	2687	75	3088	36	3373.33	23.4
SL0323	2755	78	3121	36	3379.57	23.16
SL0342	2729	68	3112	32	3382.24	18.35
SL0373	2565	75	3042	38	3388.68	25.69
SL0353	2488	80	3019	42	3409.14	29.7

Table 1: Result of U-Pb analysis in zircons from metatuff sample

ID	$^{206}Pb/^{238}U$	err	$^{207}Pb/^{235}U$	err	$^{208}Pb/^{232}Th$	err
SL0009	1270	36	1940	29	1885	73
SL0010	1851	60	2401	37	2168	118
SL0012	967	31	1846	31	2377	96
SL0013	1675	50	2250	34	1793	85
SL0015	1112	34	1858	32	1081	60
SL0016	2476	59	2974	30	2746	162
SL0018	2537	62	2584	31	2428	91
SL0019	1297	55	1961	42	2069	110
SL0021	2970	81	2989	36	2694	113
SL0022	1238	39	2045	33	2608	116
SL0031	2115	61	2588	38	2699	145
SL0032	1027	35	1873	33	2132	107
SL0034	1038	40	2210	40	5417	249
SL0035	2322	60	2506	32	2187	98
SL0037	2179	65	2445	37	2038	98
SL0038	1152	35	1896	32	2224	114
SL0040	1359	49	1984	37	1639	82
SL0041	1801	50	2308	31	1745	81
SL0043	1455	57	2108	42	1737	134
SL0044	1462	51	2203	38	1873	107
SL0053	1227	45	1981	38	1708	81
SL0054	1315	46	1989	36	1417	86
SL0056	1481	44	2240	33	2083	87
SL0057	1152	36	2010	35	2393	121
SL0059	1446	53	2163	41	2758	264
SL0060	1343	45	2021	36	2189	105
SL0062	1619	56	2518	42	3179	160
SL0063	869	41	1833	47	2862	178
SL0065	1096	53	1948	48	1785	103
SL0066	1140	45	1942	40	1103	60
SL0075	3972	344	3982	142	18751	2073
SL0076	1212	48	1960	40	1745	95
SL0078	1549	118	2419	88	1645	185
SL0079	767	42	1747	50	1563	102
SL0081	1632	129	2487	106	3067	392
SL0082	1064	68	1867	61	1171	103
SL0084	478	20	1381	35	580	34
SL0085	1596	44	2284	31	1950	83
SL0087	2553	70	2564	36	2486	119
SL0088	993	39	1824	39	1422	86
SL0097	1808	52	2356	33	3229	143
SL0098	1711	53	2747	39	3478	183

P.T.O

SL0100	1223	40	1983	34	2290	108
SL0101	2092	63	2462	36	2725	141
SL0103	1685	59	2325	41	1879	121
SL0104	836	32	1619	35	1833	92
SL0106	1622	59	2188	40	1760	145
SL0107	1364	52	2342	48	2198	117
SL0109	672	23	1871	35	6431	288
SL0110	2272	137	2901	76	4723	594
SL0119	1086	41	1819	38	1476	108
SL0120	1262	58	2125	48	1556	108
SL0122	2516	74	3028	37	3253	291
SL0123	1332	42	2097	33	1629	76
SL0125	749	30	1744	37	2060	104
SL0126	1345	51	2110	40	2656	141
SL0128	927	34	1737	35	1797	82
SL0129	1478	53	2432	39	5784	332
SL0131	2392	107	3022	55	3639	260
SL0132	1271	55	2155	46	1969	106
SL0141	1417	41	2071	30	1938	76
SL0142	1257	41	1997	33	1985	87
SL0144	1033	42	1978	41	1118	59
SL0145	1498	55	2147	39	2508	121
SL0147	1202	39	1967	33	1667	102
SL0148	1439	46	2120	35	2787	122
SL0150	1738	61	2289	55	2451	129
SL0151	1273	37	2058	31	2170	88
SL0153	889	29	1916	33	2740	121
SL0154	1309	42	2178	34	2362	99
SL0163	1134	45	1889	39	2515	137
SL0164	912	45	1885	47	2192	174
SL0166	1215	43	1887	35	1432	81
SL0167	1069	37	1821	35	2170	115
SL0169	968	60	1950	60	3048	303
SL0170	1308	45	1951	35	1234	61
SL0172	2105	61	2792	34	2964	143
SL0173	1439	45	2129	33	2560	119
SL0175	2279	69	2574	37	2787	131
SL0176	1559	47	2353	34	2606	142
SL0185	1437	46	2094	33	2039	86
SL0186	1552	52	2462	39	2575	153
SL0188	1658	47	2231	31	2338	86
SL0189	1691	38	2266	27	2300	83
SL0191	1817	45	2309	28	2278	110
SL0192	1414	50	2024	36	1916	85
SL0194	1660	47	2271	31	2177	93
SL0195	874	59	1692	60	1393	108

P.T.O

SL0197	2303	58	2671	31	3050	113
SL0198	1362	35	1932	26	1814	60
SL0207	1156	77	1907	64	1813	140
SL0208	1312	44	2403	36	3726	217
SL0210	1220	54	2025	44	950	75
SL0211						
SL0213	2023	48	2448	28	2641	87
SL0214	1476	39	2056	31	2354	131
SL0216	928	38	1644	37	985	71
SL0217	1663	42	2273	28	2873	99
SL0219	1299	37	2106	30	2140	99
SL0220	1302	46	2059	37	1542	79
SL0229	1379	58	2092	43	1981	101
SL0230	2563	60	2625	29	2751	114
SL0232	2143	56	2775	30	2624	140
SL0233	2393	79	2507	41	2630	164
SL0235	936	32	1981	34	1520	74
SL0236	1081	53	2033	49	2563	169
SL0238	1491	52	2217	38	2631	124
SL0239	1538	46	2250	36	2232	132
SL0241	927	31	1697	32	905	42
SL0242	2426	62	2613	32	3085	131
SL0251	1998	71	2447	45	2398	126
SL0252	1899	51	2444	32	2559	153
SL0254	2053	89	2567	53	3663	258
SL0255	1057	37	2069	37	4182	192
SL0257	1203	41	1950	35	1529	70
SL0258	890	33	1774	36	1718	79
SL0260	1157	51	2122	47	1841	112
SL0261	2116	77	2466	44	3162	173
SL0263	1157	40	1949	36	1907	92
SL0264	1576	51	2189	36	2231	100

Table 2: Zircon U-Pb analysis results in metagreywacke of Hiriyur Group.

Table 3. Major (wt %) and trace element concentration in metavolcanic rocks TFe_2o_3–total Fe_2O_3

	Type 1						Type 2				Type 3				
Sample name	1808243A	1808301A	1808113B	1712082B	18083111G	1809025A	**Sample name**	1808205A	1808301B	1808214A	1808261A	1712041B	1808111E	1808297A	1808261B	1808261C
Major elements							**Major elements**					**Major elements**				
SiO2	54.5023	52.994	53.8999	62.5394	54.3129	57.2359	SiO2	48.8696	51.7096	48.9445	50.8983	45.9345	57.0412	55.5847	52.1257	50.5674
TiO2	0.6194	1.4579	1.1497	0.7719	0.9926	0.9541	TiO2	1.2147	1.5056	0.8941	1.2475	0.2416	1.4149	1.1985	1.0856	0.804
Al2O3	11.7786	12.3851	9.1723	12.7056	14.8894	14.2002	Al2O3	13.8979	13.3745	15.6899	14.9104	16.3886	12.7188	14.3713	15.7418	7.1717
Fe2O3	10.621	16.2648	12.6553	8.9941	12.7138	11.3056	Fe2O3	13.9356	14.7154	14.1736	12.7016	9.7716	16.3701	10.0868	12.5461	14.4997
MnO	0.1921	0.2181	0.1871	n.d.	0.177	0.1301	MnO	n.d.	0.2092	0.1947	0.1688	0.1533	0.1553	n.d.	n.d.	0.2214
MgO	8.9217	4.5926	10.7026	4.5418	5.6265	6.713	MgO	7.1708	5.7606	7.4732	7.7398	17.8483	3.0135	6.5311	6.3771	15.6291
CaO	11.4238	9.1555	9.9954	10.3587	8.2267	9.1706	CaO	12.1035	10.3294	10.328	9.397	8.9908	6.7617	8.1796	8.4896	10.4946
Na2O	1.7719	2.481	1.8422	n.d.	2.7184	n.d.	Na2O	2.6515	1.9176	2.0346	2.5763	0.576	2.0492	3.4609	3.3092	0.4364
K2O	0.1051	0.2968	0.2726	0.0449	0.2034	0.1751	K2O	0.0754	0.3448	0.1752	0.2051	0.0952	0.2972	0.4671	0.1943	0.076
P2O5	0.0642	0.1543	0.1228	0.0436	0.1393	0.1155	P2O5	0.0811	0.1332	0.0922	0.1552	n.d.	0.1782	0.1201	0.1305	0.0997
Total	100.0001	100.0001	99.9999	100	100	100.0001	Total	100.0001	99.9999	100	100	99.9999	100.0001	100.0001	99.9999	100
Trace and Rare Earth Elements							**Trace and Rare Earth Elements**					**Trace and Rare Earth Elements**				
Cs	0.05292171	0.02975279	0.12398918	0.02671367	0.02025901	0.2597633	Cs	0.07888058	0.16414305	0.08368004	0.02644076	0.04441276	0.04542068	0.11013657	0.02314958	0.02843473
Rb	2.15538681	3.0373202	7.16967898	0.37326172	1.50901128	4.30303077	Rb	1.16763456	14.588828	4.61928698	1.45046692	1.12268513	1.77843456	6.59838492	1.34550705	0.23613067
Ba	10.9002807	38.4942086	60.5090031	21.6680644	28.2969194	40.3374753	Ba	25.4892489	55.2781915	44.4532531	15.1662813	5.78102502	20.3570831	121.786722	12.9832412	1.73477847
Th	1.31317286	1.27778255	1.80953312	0.99337874	2.52147893	1.64052664	Th	0.30716143	0.9214826	0.21157518	0.65327613	0.50331143	3.49790969	1.07892717	0.54716792	2.9283917
U	0.26466339	0.27820437	0.31937911	0.27551049	0.20167799	0.45053484	U	0.10717605	0.25125635	0.04279844	0.08414108	0.27495674	0.37021025	0.11785804	0.04165761	0.33304344
Nb	3.03946874	5.12867697	5.75007597	3.08727125	7.1370171	4.43045857	Nb	3.77033199	6.06136917	2.2243348	5.33703525	2.76318833	6.40849639	5.67467893	4.63307987	13.3487095
Ta	0.19108641	0.28380282	0.37404001	0.21226747	0.41222833	0.28096077	Ta	0.23506506	0.36044368	0.1105141	0.28667538	0.15209296	0.46853437	0.29438819	0.28564973	0.91923118
La	7.43461653	8.40899346	9.3654226	7.13295774	23.42819	8.41983337	La	4.28943673	7.212765	2.57271094	4.00383022	1.68917694	3.91988314	3.83220223	1.78164266	11.8753596
Ce	14.0249259	21.4907287	22.6127211	15.2342234	27.2594677	19.6449131	Ce	11.3613697	17.8407478	7.3830612	10.5450205	4.01862225	4.34197208	7.85652411	4.96596956	46.297646
Pb	9.89551788	2.07451073	3.41411381	2.93870883	4.45963864	3.30350091	Pb	0.41819839	1.5726057	0.89762483	2.84395585	0.2936077	5.95352563	2.23479137	2.27049513	1.15416605
Pr	2.0680648	3.10521904	3.0437251	2.13909953	6.40892542	2.47230433	Pr	1.85362753	2.81659784	1.14496869	1.59948275	0.6410414	1.35736631	1.60538631	0.84215383	3.54553323
Sr (86)	258.244063	146.68878	175.453228	43.2466381	204.102062	32.7759516	Sr (86)	132.63227	127.74772	168.216917	112.465529	30.9636885	134.787834	308.60514	95.1177352	6.06895558
Nd	8.81061158	15.0763039	12.4835834	9.41409691	27.0668832	11.0693153	Nd	9.30975271	13.5463889	6.43846883	8.04965862	3.37168186	5.71290238	7.50436848	4.49745389	13.5873361
Zr	52.4598971	119.325293	93.582253	62.2522338	129.614939	94.2088868	Zr	65.5481289	91.0888125	49.8407079	100.932722	49.5183477	145.698298	132.734079	81.2160077	103.807681
Hf	1.27516686	2.74107534	2.27206407	1.56374729	3.01206442	2.1383725	Hf	1.7510161	2.52931933	1.21375196	2.2799268	1.29840952	3.52957845	3.26812665	2.02115351	2.48241211
Sm	2.09513073	4.52551891	3.30786997	2.46790687	5.5138424	3.01591973	Sm	2.76669886	4.21914162	2.00043946	2.75848237	1.39885337	2.04809902	2.6022609	1.91073824	3.11124919
Eu	0.62073876	1.52531616	1.10813682	0.8993515	1.48922905	0.92591957	Eu	0.96663572	1.43364473	0.80717381	0.98498265	0.35061019	0.81325943	1.13171855	0.77654295	1.06255712
Gd	2.34865797	5.11239001	3.33160662	2.76504974	4.44798306	3.50199634	Gd	3.47964707	4.93340314	2.81405356	3.55266366	1.86660728	3.37767651	3.44442928	3.24088489	3.3238059
Tb	0.43551484	0.93101244	0.55245968	0.48005587	0.85715755	0.65847984	Tb	0.5911001	0.87039275	0.5245712	0.76203939	0.31137251	0.69853629	0.68258409	0.6485433	0.58114679
Dy	2.43888019	4.98702051	3.50547262	3.29181851	5.08106583	3.80686223	Dy	3.83917427	5.73929015	3.27925234	4.5477977	1.53497056	5.12302543	4.54440682	4.14782471	3.69693747
Y	16.8905476	33.7698699	18.1061656	20.3575392	34.7541305	25.2189645	Y	23.5662683	31.6617637	23.5912039	32.318189	7.95452474	33.7483434	24.4543022	27.8739219	21.0508785
Ho	0.60449121	1.1789919	0.62666672	0.6994245	1.19198013	0.85679865	Ho	0.84181916	1.1171612	0.77193346	1.08631649	0.30445338	1.1408803	0.84383014	0.98756619	0.75646263
Er	1.53527955	3.01576231	1.77521247	2.16941691	3.39856616	2.41367508	Er	2.52097527	3.20458328	2.10115923	2.92534534	0.69475211	3.5800635	2.62322967	2.77688288	2.13513515
Tm	0.26620369	0.44944301	0.23994416	0.30546196	0.5143282	0.35712997	Tm	0.36010637	0.44582309	0.35227699	0.4688116	0.10053978	0.53408456	0.34019524	0.44635796	0.27261718
Yb	1.57096783	2.81298144	1.45474569	2.03933816	3.20583656	2.40982057	Yb	2.07444966	2.72455686	2.12445114	2.9318845	0.66463146	3.07338697	2.22585868	2.65996981	1.82028382
Lu	0.22584587	0.35628599	0.21293973	0.31623987	0.46524633	0.35232474	Lu	0.35359867	0.39353078	0.33966917	0.41927439	0.08951573	0.5086273	0.32513161	0.39013352	0.28466305

Summary of Published age data in Western Dharwar Craton (WDC)

Lithology	Method	Age	Reference
Basement Gneiss			
Grey Gneiss	Feldspar Pb-Pb	3078–3408 Ma	Meen et al.,1992
Diapiric Trondhjemites	Feldspar Pb-Pb	3031 ± 12 Ma	Meen et al.,1992
TTG(Gorur)	Zr single grain evaporation	3309 ± 7 Maand 3212 ± 76 Ma	Peucat et al., 1993
Halekote(TTG)	Zr single grain evaporation	3242 ± 15 Ma and 3210 ± 5 Ma	Peucat et al., 1993
Chickmagaluru	Zr single grain evaporation	3251 ± 33 Ma	Peucat et al., 1993
Sigeggudda TTG	Zr single grain evaporation	3328 ± 10 Ma and 3234 ± 8 Ma	Peucat et al., 1993
Gorur Gneiss	SHRIMP U-Pb	3342 ± 6 Ma 3329 ± 7 Ma	Jayananda et al., 2015
Intrusive to Gorur Gneiss	SHRIMP U-Pb	3146 ± 26 Ma	Jayananda et al., 2015
Eastren Gneiss	SHRIMP U-Pb	3276 ± 4 Ma	Jayananda et al., 2015
Eastern Leucocratic Gneiss	SHRIMP U-Pb	3100 ± 4 Ma	Jayananda et al., 2015
Trondhjemite plutons	SHRIMP U-Pb	3203 ± 6 to 3200 Ma	Jayananda et al., 2015
Chickmagalur Gneiss	SHRIMP U-Pb	3350 ± 9 to3280 Ma	Jayananda et al., 2015
Chickmagaluru Granite	SHRIMP U-Pb	3153 ± 4 Ma	Jayananda et al., 2015
Goruru Gneiss	U-Pb Zircon	3346 ± 10 Ma	Baskar Rao et al., 2008
Grnaite Gneiss (Holanarsipur)	U-Pb Zircon	3410.8 ± 3.8Ma	Guitreau et al., 2017
Trondhjemite gneiss (Holanarsipur)	U-Pb Zircon	3178 ± 10 Ma	Guitreau et al., 2017
KMK Pluton	U-Pb Zircon	2973 ± 2 Ma	Corfu and Hedge, 2020
Gadag augen gneiss	U-Pb Zircon	3089 ± 18	Corfu and Hedge, 2020
Trondhjemite (Anmod ghat)	Sm-Nd Model age	3300 Ma	Devaraju et al., 2007
Tonalite (Ramnagar)	Sm-Nd Model age	3300 Ma	Devaraju et al., 2007
Monozogranite	Sm-Nd Model age	3300 Ma	Devaraju et al., 2007
Chandranath, Dudhsagar, Ramnagar Granite	Sm-Nd Model age	2.83-2.95 Ga	Devaraju et al., 2007
Bhukkaptna Granite	SHRIM U-Pb and SIMS U-Pb Zircon	2988 ± 9 Ma	Chardon et al., 2011
Nuggehalli Gneiss	SIMS Pb-Pb Zircon	3091 ± 8 Ma	Maibam et al., 2003
Sargur Trondhjemite	Zircon Pb-Pb	2972 Ma	Gao and Santosh, 2020
Sargur Group, sediments and volcanics			
Sargur quartzite	U-Pb detrital Zircon	3600–2750 Ma	Lancaster et al., 2015
Sargur metasediments	SHRIMP U-Pb	2497 ± 12 Ma	Peucat et al., 2013
Rhyolite (Holenarsipur)	SHRIMP U-Pb	3298 ± 7 Ma	Peucat et al., 1995
Psammopelite and quartzite	Lu-Hf	2.66–2.81 Ga	Maibam et al., 2016
Nuggehalli supracrustals	SIMS Pb-Pb	3204 ± 24 Ma	Maibam et al., 2003
Metatuff, Akkanahlli Zone	U-Pb Zircon	3313 ± 6 Ma	Sreehari and Toyoshima, 2020
Metamorphosed pssamopelite	Detrital Zircon	2519 ± 9 Ma	Maibam et al., 2015
Komatiites (J.C. Pura)	Sm-Nd whole rock	3352 ± 110 Ma	Jayananda et al., 2008
Komatiites (Banasandra)	Sm-Nd whole rock	3137 ± 190 Ma	Maya et al., 2017
JC Pura Spracrustals	SHRIMP U-Pb	3230 ± 5 Ma	Ramakrishnan et al., 1994
Holenarsipur anorthosite	Sm-Nd whole rock	3285 ± 170 Ma	Bhaskar Rao et al., 2000
Chromiferous ultramafic-mafic rocks	Sm-Nd whole rock	3125 ± 120 Ma	Mukherjee et al., 2012
Metasediment	U-Pb detrital Zircon	3482–2862 Ma	Gao and Santosh, 2020
Chromite bearing serpentinite	U-Pb detrital Zircon	2863–2463 Ma	Gao and Santosh, 2020
Garnet amphibolite	U-Pb Zircon	2511 ± 14	Li et al., 2018
Nuggihalli and Holenarsipur ultrmafic intrusives	Sm-Nd	2934 ± 88 Ma	Patra et al., 2020
Granite (<3.0 Ga)			
Arsikere granite	Feldspar Pb-Pb	2539 ± 72 Ma	Meent et al., 1992
Turchilal Granite	U-Pb Zircon	2555 ± 22	Chadwick et al., 2007
Chabbi Granite	SHRIMP U-Pb (Zircon)	2565 ± 9 Ma	Mohan et al., 2014
Chabbi Granite	SHRIMP U-Pb (Titanite)	2568 ± 5 Ma	Mohan et al., 2014
Chabbi Granite	SHRIMP U-Pb	2555 ± 6 Ma	Sarma et al., 2011
Doni intrusive Granite	SHRIMP U-Pb (Titanite)	2556 ± 11	Mohan et al., 2014
Harapanahalli Granite	U-Pb Zircon	2598 ± 19 Ma	Chadwick et al., 2007
Uchangidurga Granite	U-Pb Zircon	2648 ± 40 Ma	Chadwick et al., 2007
Annigeri-Majjigudda Granite	Sm-Nd Model age	2.68 Ga	Devaraju et al., 2007
Arsikere Granite	SIMS U-Pb	2617 ±3 Ma	Jayananda et al., 2006
Chitradurga Granite	SIMS U-Pb	2614.4 ± 9.7	Jayananda et al., 2006
Granite dyke, Gadag duplex	U-Pb Zircon	2623 ± 5 Ma	Corfu and Hedge, 2020
Bababudan Group , sediments and Volcanics			
Bhimasamudra stromatalite	Detrital Zircon U-Pb	3426–2928 Ma	Khelan et al., 2020

P.T.O

Kalsapura metavolcanics	Sm-Nd	2848 ± 70 Ma	Kumar et al., 1996
Kalsapura metavolcanics	Sm-Nd	2911 ± 49 Ma	Kumar et al., 1996
Katrikere conglomerate	Detrital Zircon U-Pb	3.14-3.24 Ga	Maibam et al., 2016
Metatuff	SHRIMP	2720 ± 7 Ma	Tredall et al., 1997a
Metatuff	SHRIMP	2718 ± 6 Ma	Tredall et al., 1997a
Neralekatte conglomerate	SHRIM U-Pb	3282–3162	Krapez et al., 2020
Quartzite	SHRIM U-Pb	3137 ± 7 to 3283 Ma	Hokada et al., 2013
Quartzite	SHRIM U-Pb	3140-3280 Ma	Hokada et al., 2013
Quartzite	Zircon U-Pb	3248 ± 92 Ma	Lancaster et al., 2015
Sigeggudda basal conglomerate	U-Pb Zircon	3348 ± 10(core) and 2713 ± 20 Ma(rim)	Bhaskar Rao et al., 2008
Chitrdurga Group, sediments and volcanics			
Felsic schist	SHRIMP U-Pb	2665 ± 15 Ma	Jayananda et al., 2013a,2013b
Rhyolite	SHRIMP U-Pb	2676 ± 20Ma	Hokada et al., 2013
Middle Talya conglomerate	SHRIM U-Pb	3384–2597 Ma	Krapez et al., 2020
Metasandstone	SHRIM U-Pb	<2612 ± 7 Ma	Sarma et al., 2012
Ingaldhal volcanics	Sm-Nd whole rock	2747 ± 15 Ma	Kumar et al., 1996
Felsic schist, Ranibennur	SHRIMP U-Pb	2614 ± 8 Ma	Nutman et al., 1996
Daginkatte Rhyolite	SHRIMP U-Pb	2601 ± 6 Ma	Trendall et al., 1997b
Chitradurga Psammite	SHRIM U-Pb	33260–2984 Ma	Hokada et al., 2013
Chitradurga Pelte	SHRIM U-Pb	2919–3283 Ma	Hokada et al., 2013
Basal Talya conglomerate	SHRIM U-Pb	3386–2610 Ma	Krapez et al., 2020
Hiriyur Group, sediments and volcanics			
Felsic volcanic	SHRIMP U-Pb	2576 ± 20 Ma	Jayananda et al., 2013a,2013b
Quartz feldspar porphyry	SHRIMP U-Pb	2588 ± 10 Ma	Sarma et al., 2011
Metsandstone	SHRIM U-Pb	<2548 ± 5 Ma	Krapez et al., 2020
Metasandstone	SHRIM U-Pb	<2632 ± 9 Ma	Hokada et al., 2013
Metagreywacke	SHRIM U-Pb	<2565 ± 10 Ma	Nasheeth et al., 2016
Metagreywacke	SHRIM U-Pb	<2578 ± 8 Ma	Nasheeth et al., 2016
Metagreywacke	SHRIM U-Pb	<2547 ± 5 Ma	Sarma et al., 2012
Aimanagala conglomerate	SHRIM U-Pb	2549 ± 7 Ma	Krapez et al., 2020
Gold mineralization age			
Ajjanahalli gold deposit	Monazite and Xenotime	2520 ± 9 Ma	Sarma et al., 2011
Gadag gold mineralization	Xenotime, SHRIMP U-Pb	2523 ± 6 Ma	Sarma et al., 2011

Table 4: Summary of Published ages in WDC.

Sample name :1712082A (Amphibolite, Bababudan Group)

K2O	CaO	Al2O3	SiO2	TiO2	FeO	Cr2O3	MnO	ZnO	Na2O	MgO	Total
0.117	12.134	8.684	50.148	0.113	13.472	0.005	0.07	0.056	0.44	11.771	97.01
0	23.249	26.76	38.505	0	8.167	0.051	0	0	0.033	0.016	96.781
0	23.645	26.533	38.41	0.011	6.669	0.072	0	0.023	0.028	0.081	95.472
0	23.276	28.425	38.774	0.04	5.991	0.048	0.003	0	0.011	0.032	96.6
0	0.034	20.296	25.611	0	22.146	0.034	0.043	0	0	16.376	84.54
0.002	23.692	27.617	38.423	0	6.559	0.066	0.023	0	0	0.139	96.521
0	23.312	27.116	38.627	0	8.214	0.062	0.017	0.032	0.018	0.054	97.452
0	23.725	26.669	38.349	0.024	7.432	0.066	0.025	0.1	0	0.14	96.53
0	23.528	28.092	39.052	0.015	7.025	0	0.027	0.063	0.013	0.043	97.858
0.147	12.047	6.234	50.453	0	14.578	0	0.085	0.014	0.497	12.859	96.914
0.001	0.025	0	99.906	0	0.025	0.015	0.013	0.024	0	0.031	100.04
0	0	0.004	99.901	0.049	0	0.036	0.022	0.024	0.015	0.011	100.062
0.005	0.014	0.015	100.184	0.004	0.064	0.009	0	0.043	0	0.01	100.348
0	0.023	0	101.722	0	0.015	0.009	0.046	0	0	0.024	101.839
0	0.031	0.028	99.967	0	0.191	0	0.027	0	0.011	0	100.255
0.005	0.082	0.048	101.026	0	0.181	0.006	0.033	0	0.006	0	101.387
0	0.075	0	100.124	0.033	0.221	0.002	0	0.009	0	0.017	100.481
0.004	0.03	0.02	100.98	0	0.078	0.024	0	0.021	0	0.017	101.174
0.441	0.446	10.606	52.024	0	9.678	0.032	0.028	0.033	0.071	9.251	82.61
0	0.021	0	100.251	0	0.034	0.004	0	0	0	0.009	100.319
0.006	0.013	21.463	25.043	0.026	23.468	0.086	0.122	0.007	0.021	15.094	85.349
0.02	0.127	20.307	24.995	0	22.74	0.035	0.049	0.053	0.045	15.102	83.473
0	0.045	21.289	24.926	0.017	23.972	0.05	0.093	0.099	0.056	14.561	85.108
0.004	0.105	20.459	24.923	0	23.262	0.059	0.099	0.002	0.052	15.309	84.274
0	0.072	21.074	25.745	0	22.973	0.071	0.058	0.018	0.048	15.459	85.518
0	0.027	21.229	25.295	0.003	22.311	0.068	0.12	0.018	0.026	15.174	84.271
0	0.103	21.097	25.024	0.016	23.279	0.044	0.068	0	0.075	15.057	84.763
0	0.087	6.246	77.306	0	7.51	0.045	0.033	0	0.018	4.706	95.951
0.008	0.148	21.461	25.493	0.021	23.996	0.067	0.091	0.014	0.067	14.917	86.283
0	0.056	21.489	25.39	0	23.051	0.067	0.033	0.062	0.003	15.148	85.299
0.497	11.531	15.248	43.738	0.048	17.054	0.105	0.04	0.009	1.303	7.463	97.036
0	21.874	26.417	43.474	0.024	5.227	0.057	0.028	0.081	0	0.036	97.218
0	22.892	28.016	38.647	0	7.049	0.048	0.048	0	0	0.4	97.1
0	23.737	28.661	39.268	0.009	5.244	0.044	0.078	0.012	0.015	0.035	97.103
0.013	23.841	28.46	38.774	0.002	5.74	0.068	0.038	0	0	0.069	97.005
0.004	23.738	28.568	39.294	0.031	5.832	0.017	0	0.007	0	0.041	97.532
0	23.595	28.75	39.227	0	6.179	0.068	0.061	0.002	0	0.049	97.931
9.553	0.099	17.504	37.015	0.127	17.99	0.096	0.018	0.099	0.18	10.35	93.031
9.447	0.166	17.413	37.069	0.141	18.141	0.072	0.097	0.032	0.174	10.468	93.22
0	23.448	28.236	39.086	0.024	6.414	0.033	0.019	0.063	0	0.034	97.357
0	0.017	0.023	99.581	0.024	0.02	0	0	0	0.019	0.006	99.69
0.003	0.023	0	98.886	0.004	0.034	0	0.002	0.05	0	0.003	99.005
0	0.015	0.021	100.881	0.035	0.044	0	0	0.052	0	0.001	101.049
0	0.011	0.007	100.824	0	0.034	0.013	0.021	0	0	0.026	100.936
0.02	0	0.018	99.971	0	0.034	0	0.009	0	0.016	0.005	100.073
0	23.577	28.512	38.985	0	6.072	0.035	0.03	0.072	0.013	0.004	97.3
0	23.603	28.571	39.335	0	6.136	0.02	0.014	0	0.009	0.022	97.71
0.002	23.801	28.535	39.23	0	6.025	0.044	0.009	0	0.014	0.05	97.71
0.1	12.078	5.545	51.395	0	14.369	0.066	0.118	0	0.437	12.967	97.075
0.384	11.817	11.818	45.024	0.068	16.226	0.057	0.111	0.039	0.942	9.76	96.246
0.122	10.926	7.043	48.962	0.036	15.038	0.082	0.124	0.146	0.41	13.125	96.014
0.424	11.522	14.349	43.437	0.014	17.178	0.069	0.073	0.083	1.286	8.158	96.593
0	23.4	27.933	39.358	0.038	6.861	0.031	0.048	0.028	0.01	0.015	97.722
0.01	23.622	28.489	38.612	0.046	5.812	0.015	0	0.03	0	0.012	96.648
0	23.609	28.32	39.07	0.002	6.732	0.062	0.02	0.035	0.019	0.033	97.902
0.512	11.549	13.877	44.051	0.046	15.716	0.082	0.073	0	1.108	8.199	95.213
0.005	23.616	28.356	38.973	0.011	5.909	0.074	0.023	0	0.018	0.021	97.006
0	23.585	27.681	38.908	0.015	6.415	0	0.034	0.03	0.004	0.055	96.727
0	22.149	26.612	41.971	0	6.45	0.006	0.042	0.033	0	0.09	97.353
0.009	19.482	22.78	48.938	0.022	5.433	0	0.042	0.047	0.022	0.035	96.81
0.003	0.035	21.225	25.013	0.029	24.049	0.052	0.068	0.126	0.051	15.403	86.054
0	0	21.579	25.169	0.028	23.496	0.056	0.134	0.025	0.037	15.509	86.033
0	0.05	21.57	25.136	0	23.196	0.045	0.04	0	0.019	15.239	85.295
0.004	0.007	21.312	25.506	0	23.295	0.071	0.094	0.018	0.053	15.444	85.804
0	0.046	20.579	25.25	0	23.525	0.015	0.105	0	0	15.843	85.363
0	0.009	20.29	26.404	0.017	22.106	0.024	0.093	0.023	0.022	16	84.988
0	0.037	21.344	25.637	0.059	23.286	0.069	0.087	0.051	0.012	15.412	85.994
0	0.099	21.644	25.25	0	22.778	0.054	0.053	0	0.012	14.923	84.813
0.009	0.053	21.63	25.485	0	23.85	0.044	0.062	0	0.025	14.885	86.043
0.011	0.061	20.636	26.053	0.017	23.164	0	0.058	0.103	0	15.34	85.443
0	0.002	21.289	24.952	0	22.989	0.034	0.049	0.053	0.018	15.059	84.445
0.018	0.034	21.563	25.489	0.034	23.746	0.089	0.094	0.002	0.012	14.766	85.847
0	0.035	21.763	25.269	0.066	22.307	0.061	0.097	0	0	15.379	84.977
0	0.041	21.367	25.562	0	23.709	0.044	0.047	0	0	15.083	85.853
0.013	0.015	21.482	25.55	0	22.78	0.079	0.084	0	0	15.138	85.141
0	0.037	20.511	25.92	0	22.439	0.015	0.03	0.051	0	16.33	85.333
0	23.478	28.002	38.62	0	6.009	0.098	0.038	0.077	0	0.011	96.333
0	23.481	29.151	39.001	0.015	5.658	0	0.019	0	0	0.037	97.362
0	0.185	21.776	25.385	0	22.114	0.063	0.076	0.023	0.082	14.8	84.504
0.002	22.458	24.312	38.806	0.04	8.651	0.02	0.039	0	0.038	1.031	95.397
0	23.769	28.558	39.177	0.077	6.14	0.007	0.02	0.04	0	0.031	97.819
0.11	11.784	4.913	51.787	0.011	13.986	0	0.082	0	0.345	13.532	96.55
0	23.406	27.548	38.834	0	6.719	0.057	0	0	0	0.081	96.645
0	23.507	28.324	38.779	0	6.645	0	0	0.053	0.002	0.019	97.329
0	22.949	28.051	38.517	0.009	7.064	0.05	0.033	0	0	0.246	96.919
0	23.381	28.346	38.808	0.04	6.351	0.028	0.028	0.074	0.006	0.006	97.068
0	0.03	21.388	25.374	0.003	23.534	0.051	0.11	0.021	0.02	15.379	85.91
0.005	0.153	20.578	27.128	0	21.887	0.066	0.059	0.078	0.022	15.457	85.433
0.01	0.02	20.616	25.416	0.003	23.102	0.074	0.043	0.037	0.055	15.586	84.962
0	0	21.955	25.611	0	23.885	0.059	0.023	0.057	0.002	15.186	86.778
0.019	0.091	21.077	25.839	0.019	23.307	0.066	0.1	0	0.046	15.373	85.937
0.01	0.051	21.109	25.323	0	23.204	0.108	0.076	0.041	0	15.555	85.477
0	0.073	21.754	25.195	0	23.515	0.061	0.085	0	0.008	15.168	85.859
0.017	0.069	21.121	24.861	0	23.431	0.005	0.059	0	0	15.192	84.755
0.022	0.049	21.163	25.733	0.022	22.786	0.019	0.129	0	0.013	15.39	85.326

Table 5: Mineral chemistry based on EPMA analysis in amphibolite of Bababudan Group

1712085A Amphibolite(Bababudan Group)

K2O	CaO	Al2O3	SiO2	TiO2	FeO	Cr2O3	MnO	ZnO	Na2O	MgO	Total
0.038	4.502	23.218	62.879	0	0.156	0.041	0.014	0	8.896	0.015	99.759
0.045	4.689	23.706	62.302	0.007	0.097	0.037	0.022	0.026	8.782	0.014	99.727
0.052	4.604	23.769	62.296	0	0.263	0	0	0	8.681	0.01	99.675
0.043	4.823	23.558	62.347	0	0.341	0	0.006	0.066	8.796	0.003	99.983
0.058	4.649	23.458	62.463	0.016	0.316	0	0	0.04	8.989	0.008	99.997
0.048	4.735	23.547	62.334	0.004	0.409	0.002	0	0	8.711	0.005	99.795
0.033	4.571	23.249	62.445	0.016	0.292	0.002	0	0	9.021	0	99.629
0.048	4.751	23.659	62.285	0	0.243	0	0.028	0	8.862	0	99.876
0.043	4.545	23.301	62.792	0	0.19	0	0	0	8.841	0.009	99.721
0.053	4.672	23.461	62.903	0	0.122	0.007	0	0	8.685	0.002	99.905
0.146	11.24	9.732	47.119	0.036	16.292	0.004	0.082	0	1.01	10.608	96.269
0.288	11.31	14.279	42.658	0.021	17.437	0.065	0.069	0.074	1.248	7.756	95.205
0.291	11.07	15.377	42.328	0.016	17.75	0.048	0.102	0.042	1.521	7.281	95.826
0.274	11.025	14.609	43.004	0.057	17.742	0.049	0.042	0	1.183	7.588	95.573
0.283	10.692	15.122	42.542	0.067	18.558	0.085	0.091	0.023	1.512	7.084	96.059
0.466	11.141	15.551	42.326	0.062	17.922	0.057	0.085	0	1.439	7.528	96.577
0.284	11.257	15.079	42.902	0.039	17.904	0.044	0.069	0.122	1.426	7.844	96.97
0.283	11.377	14.53	42.859	0.066	17.488	0.05	0.066	0	1.232	7.542	95.493
0.257	11.276	13.862	43.813	0.046	17.235	0.012	0.022	0	1.308	8.294	96.125
0.252	11.187	14.678	42.971	0.004	16.937	0.073	0.026	0	1.319	7.61	95.057
0	0.054	0	100.251	0.016	0.358	0	0	0.038	0.013	0.019	100.749
0	0.033	0	99.649	0.005	0.25	0.015	0	0	0.007	0.042	100.001
0.014	0.069	0.014	100.351	0.042	0.284	0.028	0	0.064	0.022	0.035	100.923
0	0.037	0.018	99.959	0	0.196	0	0	0.038	0.003	0	100.251
0	0.04	0.028	99.604	0	0.26	0.054	0.003	0	0.024	0	100.013
0.046	4.242	23.164	63.403	0.005	0.175	0.024	0.027	0	8.885	0.012	99.983
0.061	4.586	23.606	62.517	0	0.117	0.004	0.014	0.031	8.719	0	99.655
0.049	4.491	23.356	62.514	0	0.127	0	0	0	8.905	0	99.442
0.011	0.03	0.005	99.93	0	0.074	0.019	0.008	0	0	0.051	100.128
0.048	4.509	23.527	62.679	0	0.088	0	0	0.04	8.818	0.002	99.711
0.023	4.876	23.896	62.369	0	0.292	0	0	0.094	8.807	0	100.357
0.033	4.717	23.061	62.066	0.015	0.078	0	0.011	0	8.662	0	98.643
0.031	4.462	23.144	63.319	0	0.058	0.02	0.023	0.019	8.863	0	99.939
0.046	4.625	23.774	62.661	0.035	0.316	0	0	0.002	8.749	0	100.208
0.049	4.713	23.839	62.858	0	0.253	0.015	0	0	8.785	0	100.512
0.328	11.02	15.873	42.114	0.011	17.584	0	0.086	0.051	1.55	7.123	95.74
0.239	10.873	14.996	42.697	0.025	17.37	0.065	0.051	0.053	1.532	7.466	95.367
0.393	11.254	16.025	41.858	0.064	17.611	0.041	0.026	0.12	1.516	7.205	96.113
0.283	11.435	14.939	44.081	0.002	17.211	0.044	0.089	0	1.2	7.733	97.017
0.25	11.348	14.465	43.237	0.08	17.641	0.067	0.063	0	1.305	7.922	96.378
0.281	11.245	15.279	43.332	0.014	17.564	0.051	0.091	0.012	1.45	7.279	96.598
0.264	11.212	14.781	42.672	0.041	17.661	0.03	0.045	0.025	1.467	7.853	96.051
0.381	10.997	15.903	42.385	0.057	17.667	0.049	0.091	0.141	1.621	7.319	96.611
0.252	10.994	14.637	43.323	0.064	17.474	0	0.045	0.039	1.443	7.896	96.167
0.3	10.891	14.589	43.3	0.018	18.07	0.012	0.083	0	1.224	7.232	95.719
0	0.031	0.029	100.085	0.018	0.196	0	0	0	0.03	0.025	100.414
0	0.058	0.016	100.018	0.029	0.309	0	0.03	0.118	0	0.001	100.579
0	0.034	0	100.604	0.033	0.26	0	0.019	0.05	0.004	0.033	101.037
0	0.022	0.001	100.29	0	0.211	0.004	0.017	0.026	0	0.008	100.579
0	0.025	0	100.405	0	0.23	0.006	0.024	0	0	0.008	100.698
0.056	4.769	23.799	62.985	0	0.112	0	0	0.016	8.605	0	100.342
0.067	4.754	23.435	63.021	0	0.073	0	0	0.063	8.676	0	100.089
0.056	4.279	23.682	63.105	0.002	0.044	0.017	0	0.033	9.065	0	100.283
0.046	4.467	23.355	62.552	0.004	0.068	0	0	0.021	8.949	0	99.462
0.055	4.705	23.74	62.677	0	0.068	0.004	0.008	0	8.902	0	100.159
0.021	4.832	23.989	62.531	0	0.204	0.017	0.008	0	8.769	0.014	100.385
0.034	4.633	23.53	62.69	0.015	0.112	0	0.003	0.035	8.918	0	99.97
0.049	4.435	23.522	63.398	0	0.117	0.007	0.03	0	8.912	0.013	100.483
0.051	4.669	23.588	62.772	0.038	0.146	0.017	0	0.042	8.813	0.01	100.146
0.049	4.663	23.648	62.558	0	0.117	0	0.006	0	8.673	0	99.714
0.267	11.112	8.577	48.423	0.023	16.27	0.068	0.142	0.102	0.837	11.157	96.978
0.362	10.913	14.388	42.554	0.018	17.283	0.025	0.012	0	1.5	7.877	94.932
0.302	11.067	15.164	42.67	0.045	16.928	0.065	0.114	0.002	1.517	7.39	95.264
0.26	11.121	15.291	42.437	0.018	17.79	0.069	0.082	0	1.593	7.4	96.061
0.247	11.172	14.406	42.965	0	16.347	0.059	0.074	0	1.315	7.738	94.323
0.276	11.139	12.162	45.387	0.1	16.586	0.048	0.071	0	1.173	9.246	96.188
0.366	10.991	15.993	41.693	0.012	17.076	0.019	0.086	0	1.627	7.381	95.244
0.317	11.148	15.275	42.536	0.048	17.321	0.005	0.062	0	1.518	7.423	95.653
0.56	11.234	15.485	42.004	0.009	17.705	0.057	0.08	0	1.42	7.457	96.011
0.201	10.927	15.021	43.242	0.025	18.004	0.104	0.092	0.069	1.566	7.817	97.068

Table 6: Mineral chemistry based on EPMA analysis in amphibolite of Bababudan Group

12041B- Amphibolite (Bababudan Group)

K2O	CaO	Al2O3	SiO2	TiO2	FeO	Cr2O3	MnO	ZnO	Na2O	MgO	Total
0.355	11.056	15.203	43.243	0.255	15.082	0.091	0.012	0.037	1.335	9.293	95.962
0.327	11.208	15.186	42.714	0.204	14.682	0.057	0	0.069	1.372	9.17	94.989
0.308	10.958	13.151	42.099	0.208	17.218	0	0.003	0	1.343	9.022	94.31
0.31	10.772	14.305	43.544	0.285	16.155	0	0	0	1.387	9.166	95.924
0.343	10.694	13.798	41.103	0.196	16.782	0	0.003	0.044	1.431	8.842	93.236
0.378	11.167	15.054	41.652	0.296	15.936	0	0.019	0.039	1.365	9.267	95.173
0.317	11.093	13.648	42.81	0.157	17.5	0.028	0.011	0	1.377	9.03	95.971
0.303	11.319	15.527	42.401	0.164	14.617	0.025	0.005	0.042	1.378	9.338	95.119
0.306	10.926	13.971	42.907	0.23	15.732	0.027	0	0.016	1.436	9.125	94.676
0.326	11.241	15.289	43.078	0.22	14.348	0.002	0.019	0.093	1.286	9.374	95.276
0.323	11.207	15.059	43.018	0.123	14.701	0.023	0.005	0	1.175	9.354	94.988
0.365	11.23	15.451	43.233	0.193	15.225	0.032	0.008	0.009	1.273	8.937	95.956
0.351	11.17	15.152	42.441	0.223	14.757	0.018	0.011	0.046	1.321	9.081	94.571
0.334	11.261	15.403	43.637	0.247	14.867	0.027	0.006	0	1.259	8.819	95.86
0.332	11.169	15.079	43.213	0.166	15.213	0.044	0.014	0	1.213	9.182	95.625
0.331	11.065	14.263	41.563	0.196	16.103	0.014	0	0.085	1.473	9.321	94.414

171204-4 (Amphibolite, Bababudan Group)

K2O	CaO	Al2O3	SiO2	TiO2	FeO	Cr2O3	MnO	ZnO	Na2O	MgO	Total
0.256	10.221	14.338	41.363	0.177	18.072	0	0.008	0	1.639	7.658	93.732
0.291	10.366	14.027	41.849	0.145	18.069	0.053	0	0.023	1.652	7.463	93.938
0.24	9.996	12.935	41.232	0.2	18.16	0	0.014	0.051	1.779	7.643	92.25
0.272	10.379	13.974	41.14	0.172	17.671	0.056	0.043	0	1.649	7.437	92.793
0.265	10.267	13.934	41.219	0.22	17.692	0.025	0.055	0.044	1.589	7.487	92.797
0.232	10.135	13.725	41.641	0.197	18.071	0.021	0.011	0	1.646	7.413	93.092
0.191	10.068	13.447	41.72	0.149	17.885	0.137	0.006	0	1.634	7.917	93.154
0.239	10.246	14.04	41.922	0.268	16.957	0.021	0	0	1.588	7.833	93.114
0.242	10.354	13.531	42.467	0.193	17.663	0.033	0.034	0.039	1.579	7.849	93.984
0.218	9.443	15.212	45.253	0.286	17.153	0.051	0.017	0	0.965	4.682	93.28
0.218	10.225	13.141	42.262	0.129	17.857	0.06	0.035	0.074	1.456	7.954	93.411
0.058	0.444	0.813	51.562	0.059	25.645	0.017	0	0	0.159	14.02	92.777
0.236	10.304	13.86	41.876	0.249	17.376	0.018	0.046	0.055	1.602	7.659	93.281
0.244	10.303	14.06	41.577	0.227	17.064	0.021	0	0.088	1.607	7.427	92.618
0.266	10.107	13.335	41.123	0.151	18.028	0.039	0.023	0.067	1.672	7.435	92.246
0.247	10.136	13.607	41.768	0.19	17.048	0	0	0	1.635	7.463	92.094
0.263	10.113	13.815	41.627	0.17	17.486	0.049	0.046	0.065	1.63	7.547	92.811
0.259	10.091	13.681	40.801	0.202	18.155	0.012	0.014	0	1.568	7.337	92.12
0.262	10.127	13.596	41.06	0.218	17.783	0	0.015	0.088	1.552	7.369	92.07
0.25	10.043	13.605	41.054	0.186	17.462	0.025	0.023	0	1.461	7.425	91.534
0.223	10.014	13.43	41.424	0.256	16.83	0.042	0.005	0	1.592	7.484	91.3
0.214	9.841	13.646	41.722	0.272	16.913	0.011	0.048	0.055	1.508	7.743	91.973
0.19	9.96	13.275	41.711	0.295	15.944	0	0	0.127	1.522	8.07	91.094
0.203	9.839	12.874	42.031	0.115	16.32	0.03	0.002	0.046	1.374	7.964	90.798
0.199	9.761	12.547	42.173	0.154	18.25	0.054	0	0.018	1.556	7.753	92.465
0.185	10.29	12.821	42.512	0.227	17.909	0.023	0.017	0.021	1.497	8.52	94.022
0.23	10.335	13.54	41.884	0.209	17.45	0.039	0	0.016	1.629	8.036	93.368
0.188	10.269	13.129	42.519	0.227	17.871	0.016	0.058	0.009	1.519	8.466	94.271
0.249	10.339	14.456	42.152	0.169	17.147	0.037	0	0.124	1.665	7.744	94.082
0.214	10.39	12.991	42.66	0.217	17.211	0.072	0	0	1.502	8.339	93.596
0.179	10.097	11.982	43.08	0.22	17.654	0.04	0	0	1.295	8.843	93.39
0.22	10.254	13.787	42.179	0.188	17.347	0.002	0.026	0.032	1.614	7.981	93.63
0.191	10.293	13.302	42.188	0.22	16.674	0.041	0.009	0.074	1.468	8.058	92.518
0.18	10.262	13.192	42.761	0.225	17.821	0.07	0	0	1.448	8.293	94.252
0.21	10.349	13.175	42.911	0.172	17.365	0.009	0.048	0.039	1.576	8.442	94.296
0.192	10.358	13.352	41.9	0.144	17.452	0.04	0	0.099	1.511	8.017	93.065
0.186	9.757	12.634	42.377	0.161	17.925	0.004	0	0	1.399	8.425	92.868
0.211	10.184	13.317	42.329	0.2	17.578	0.065	0.018	0	1.547	8.056	93.505
0.224	10.229	13.58	42.032	0.126	17.179	0	0	0.007	1.494	7.974	92.845

Table 7: Mineral chemistry based on EPMA analysis in amphibolite of Bababudan Group

1712041C (Amphibolite, Bababudan Group)

K2O	CaO	Al2O3	SiO2	TiO2	FeO	Cr2O3	MnO	ZnO	Na2O	MgO	Total
0.06	5.051	23.8	61.7	0	0	0	0	0	8.59	0.019	99.138
0.052	5.24	23.9	61.2	0	0	0.04	0.01	0	8.52	0	98.988
0.03	5.624	24.2	60.9	0	0.102	0	0	0	8.18	0.003	99.044
0.044	5.233	24	61.2	0	0.039	0.03	0.02	0	8.27	0	98.847
0.038	6.185	24.7	59.8	0.07	0.078	0	0	0	7.98	0.015	98.872
0.034	5.156	24	61.5	0.02	0.063	0	0	0	8.56	0	99.278
0.039	5.253	24	61.6	0.03	0.029	0.01	0.03	0	8.62	0.019	99.608
0.046	4.967	23.9	62.1	0	0.029	0	0	0	8.55	0.013	99.537
0.039	4.816	23.4	62	0.01	0.034	0	0.01	0.1	8.82	0	99.175
0.045	4.935	23.7	61.6	0	0	0.01	0	0.1	8.53	0	98.968
0.037	4.98	23.8	61.4	0	0	0	0	0	8.54	0.01	98.719
0.046	4.971	23.7	61.7	0.01	0.034	0	0.01	0	8.81	0.005	99.247
0.04	4.901	23.8	61.4	0.02	0.005	0	0	0	8.59	0	98.843
0.041	4.883	23.7	61.9	0	0.039	0	0	0	8.65	0	99.219
0.037	4.871	23.8	61.9	0	0.019	0.01	0	0	8.79	0	99.407
0	0.026	0	99.8	0	0.029	0	0.05	0	0.02	0.022	99.985
0.003	0.024	0.02	99.6	0	0.073	0	0.02	0	0	0	99.746
0.011	0.027	0.01	98.6	0	0	0	0	0	0.02	0.014	98.719
0.003	0.04	0.01	99.6	0.01	0.024	0	0	0	0.01	0.019	99.721
0.043	5.014	23.6	61.6	0	0	0	0	0	8.73	0.008	98.956
0.023	5.264	23.8	61.4	0	0.039	0	0	0	8.47	0.001	99.01
0.031	5.003	23.8	61.6	0.06	0	0	0	0	8.41	0.006	98.955
0.032	4.975	23.8	61.6	0	0.015	0.04	0.03	0	8.42	0	98.82
0.054	5.082	23.6	61.1	0	0.049	0	0.02	0	8.54	0.006	98.489
0.009	0.017	0	99.5	0	0	0	0	0.1	0	0.002	99.674
0.059	4.956	23.8	61.5	0	0	0	0.04	0	8.66	0	98.959
0.275	11.32	14.3	42.5	0.31	14.77	0.02	0.02	0.1	1.39	9.78	94.729
0.241	11.46	14.3	43.3	0.32	13.86	0.01	0.02	0	1.31	9.89	94.788
0.248	11.29	14.2	43.2	0.18	14.25	0.03	0	0	1.35	9.779	94.547
0.259	11.26	14.7	42.5	0.22	14.71	0.01	0	0	1.44	9.698	94.786
0.013	0.586	0.46	96	0	0.196	0.02	0	0	0.05	0.664	97.988
0.027	2.165	1.98	85.6	0.04	0.836	0	0.02	0	0.2	2.201	93.123
0	0.482	0.25	95.5	0	0.201	0.03	0.02	0	0.04	0.393	96.897
0.283	11.15	14.7	42.8	0.27	14.48	0.05	0	0	1.49	9.808	95.063
0.241	11.25	13.5	43.8	0.26	14.17	0.02	0	0	1.28	10.55	95.07
0.237	11.28	14.4	42.8	0.25	14.97	0.05	0	0	1.42	9.593	95.04
0.284	11.23	13.6	43.5	0.29	14.68	0.02	0	0.1	1.31	10.03	95.058
0.243	11.34	14	43.2	0.23	14.79	0.02	0	0.1	1.34	10	95.18
0.252	11.32	14.4	43	0.24	15.05	0.06	0.01	0.1	1.31	9.872	95.623
0.123	11.86	8.83	47.5	0.12	12.37	0	0.05	0	0.86	13.07	94.848
0.31	11.15	12.2	44.3	0.21	15.53	0.02	0.06	0.1	1.3	10.33	95.472
0.302	11.09	12	44	0.22	16.29	0.06	0	0.1	1.27	10.25	95.543
0.269	11.43	13.9	43.3	0.29	15.09	0	0.03	0	1.3	9.726	95.269
0.162	11.49	10.8	46.2	0.21	13.14	0.04	0	0	1.03	11.84	94.915

Table 8: Mineral chemistry based on EPMA analysis in amphibolite of Bababudan Group

Akkanahalli Zone (Sargur Gp.)

Sl No	Sample name	Rock type	Shear sense	Minerals	Foliation plane mineral	Comment
1	1808256AH	metaultramfic	Sinistral	Chl+Act	Chl	10x photos, conjugate crenulation axis.
2	1808252AH	Metaquartzite/sandstone	sinistral followed by dextral	Ms+Qtz+Chl	Ms	2x photo
3	1808252D	metamafic	sinistral	Chl+Act+Qz+pl+Albite	Chl	Radial growth structur earound albite
4	1808256BH	metaultramfic	Sinistral	Chl+Act	Chl	.
5	1808246AH	metamafic?	Sinistral?	Cal/Dol+Chl+Qtz	Chl	Calcite/dol grown around opaque minerals (2x photo)
6	1808242CH	metamafic?	Sinistral?	Cal/Dol+Chl+Qtz	Chl	Calcite/dol grown around opaque minerals
7	1808246A FA perp.	metamafic	?	Cal/Dol+Chl+Qtz	Chl	2x photo, folded chlorite
8	1808257A	metatuff	?	Plg+Qtz+Ms+KFeld	Ms	
9	1808244B	Metasandstone?	Dextral	Qtz+Ms+Chl	Chl	2x photos
10	1808242BLpar	metamafic?	Sinistral?	Cal/Dol+Chl+Qtz	Chl	Calcite/dol grown around opaque

11	1808243AH	metagabbro	?	Plg+Chl+Act+pyx	Chl	More clear in the field
12	1808246AH	metamafic	Dextral	Chl+Cal/Dol+Qtz	Chl	probably an earlier sinistral sense of movement.
13	18008244BV	metasandstone	East-side- up	Qtz+Ms+Chl	Chl	2x photos
14	1808252AH	Metaquartzite/sandstone	sinistral followed by dextral	Ms+Qtz+Chl	Ms	2x photo
15	1808246A FA perp.	metamafic	?	Cal/Dol+Chl+Qtz	Chl	2x photo, folded chlorite
16	1808254AHR Cr perp.	mudstone	folded	Qtz+Chl+Ms	Chl+Ms	Layer-parallel folds (2x photos)
17	1808254AH.	mudstone	folded	Qtz+Chl+Ms	Chl+Ms	Layer-parallel folds
18	1808255B	sandstone	sinistral	Qtz+Chl+Ms+Pl	Ms+Chl	Sandstone as clast also present.
19	1808254AHR Cr perp.	mudstone	folded	Qtz+Chl+Ms	Chl+Ms	Layer-parallel folds
20	1808255CH	Metamafic	sinistral	Qtz+Chl_Act	Chl	Act+Chl rich qtz looks like clast in it , probably volcano clastic rock.

Table 9: Details of the representative thinsections in Akkanahalli Zone

Hiriyur Gp.						
Sl No	Sample name	Rock type	Shear sense	Minerals	Foliation plane mineral	Comment
1	1808234BH	Conglomerate	NIL	Qtz+Ms+Bt+Chl+Pl	Ms	Sandstone, Quatrzite, basalt clasts, strike parallel crenulations.(2xphotos)
2	1808233AV	Conglomerate	East side up	Qtz+Ms+Bt	Ms	Reverse fault
3	1808227AHR	Metagreywacke	Sinistral	Qtz+Cal+Chl+Pl	Chl	Strike-parallel sinistral shear(Zircon photo 40x)
4	1808234AH	Conglomerate	NIL	Qtz+Ms+Bt	Ms	Sandstone, Quatrzite, basalt clasts, strike parallel crenulations.
5	18082333DHR	Mudstone/shale	Sinistral	Qtz+Bt+Ms+Chl	Ms+Chl	Strike-parallel sinistral shear (10x photos).
6	1808211BHR	Metagreywack	Sinistral	Qtz+Cal+Chl+Pl+Ms	Chl+Ms	Strike-parallel sinistral shear
7	1808234BH	Conglomerate	NIL	Qtz+Ms+Bt+Chl+Pl	Ms	Sandstone, Quatrzite, basalt clasts, strike parallel crenulations.(2xphotos)
8	18082333DH	Mudstone/shale	NIL	Qtz+Bt+Ms+Chl	Ms+Chl	Strike-parallel sinistral shear. Weak folding
9	1808227BH	Metagreywacke	NIL	Qtz+Cal+Chl+Pl	Chl+Ms	Strike-parallel sinistral shear(Zircon photo 40x)
10	1808203BHR	Metabasalt	NIL	Chl+Plg+Act+Ms	?	2x photo
11	1808205A	Metadyke?	NIL	Chl+Pl+Qtz	?	Pl+Chl phenocrysts, 2x photos
12	1808203A	Metadyke?	NIL	Act+Pyx+Chl+Pl	?	2x photos
13	1808204A	Metadyke	NIL	Pyx+Chl+Pl	?	2x photos
14	1808203A	Metadyke?	NIL	Act+Pyx+Chl+Pl	?	2x photos
15	1808205B	Metadyke?	NIL	Act+Pyx+Chl+Pl	?	2x photos
16	1808203BH	Metabasalt	NIL	Chl+Plg+Act+Ms	?	2x photo
17	1808233EH	Shale	sinistral	Chl+Qtz+Ms	Chl	2x photo, asymmetrical folds.
18	1808211AHR	Metagreywacke	Sinistral	Qtz+Cal+Chl+Pl	Chl	Strike-parallel sinistral shear.
19	1808233EH	Shale	?	Chl+Qtz+Ms	Chl	Asymmetrical crenulatations , load clasts present. 2x photos

Table 10: Details of the representative thinsections in Hiriyur Group

9 APPENDIX

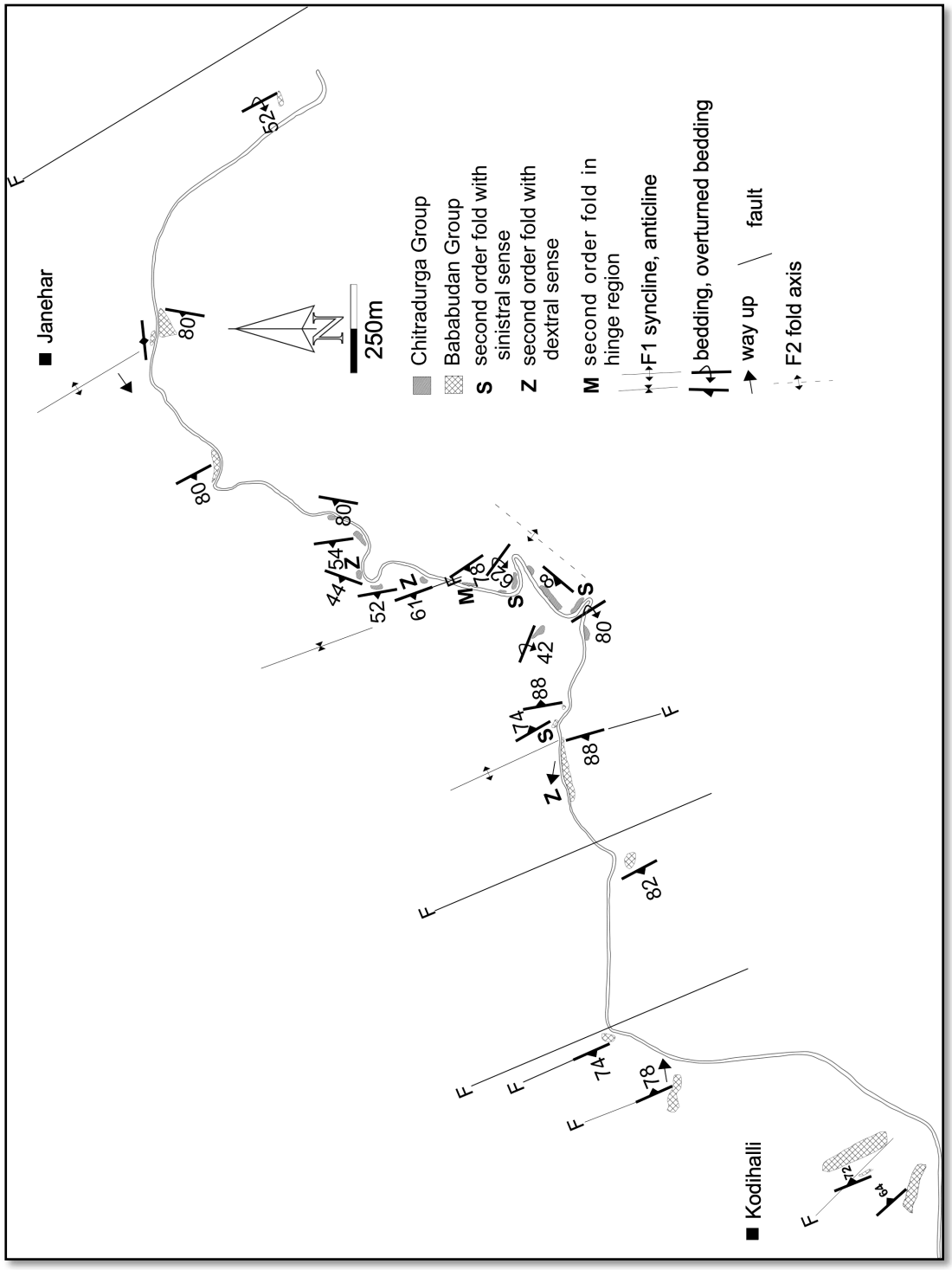

A1: Route map in the folded zone (along AB transect in Figure 2.1) in CSB.

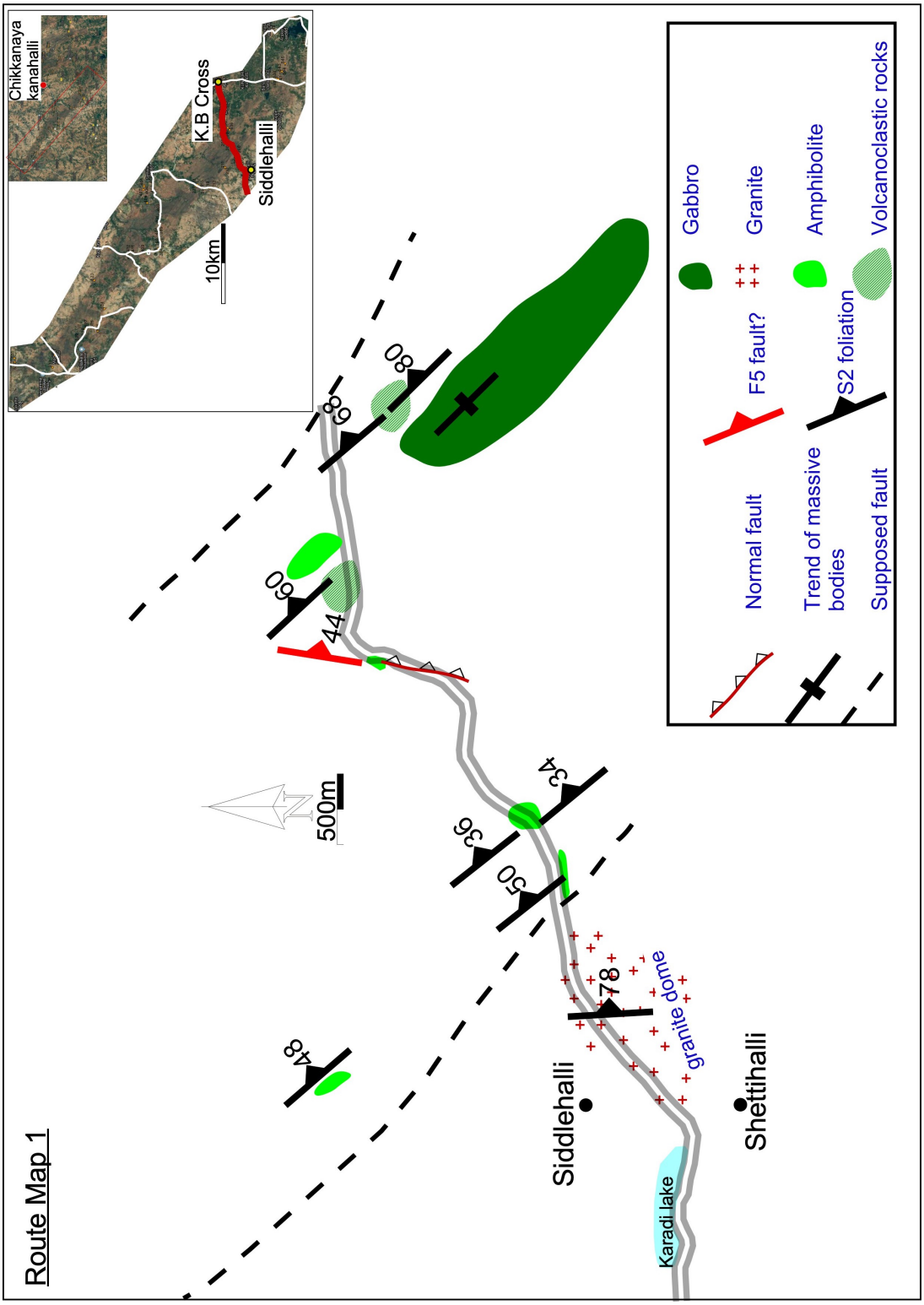

A2. Route map in Kibbanahalli Schist Belt.

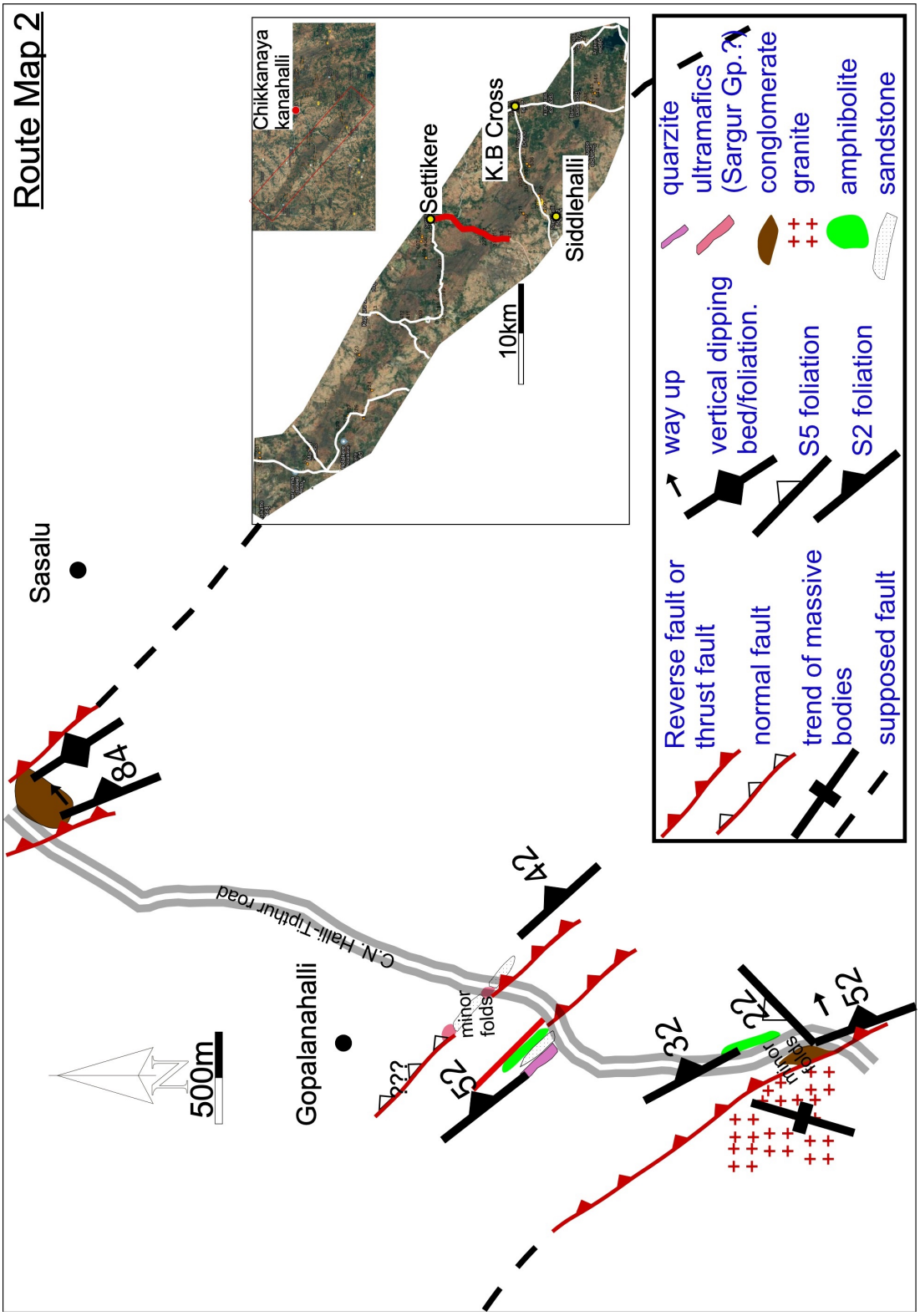

A3. Route map in Kibbanahalli Schist Belt.

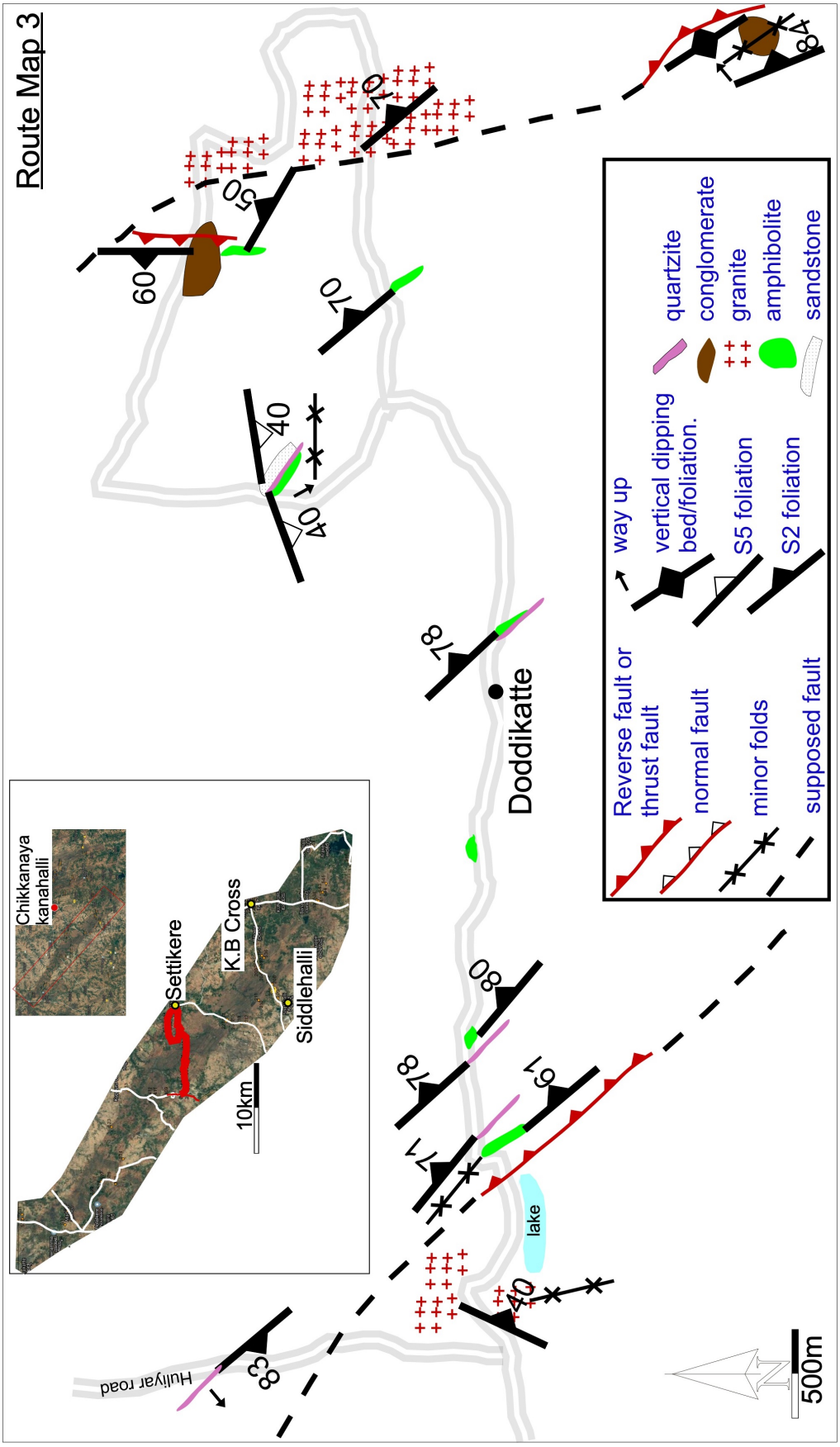

A4. Route map in Kibbanahalli Schist Belt.

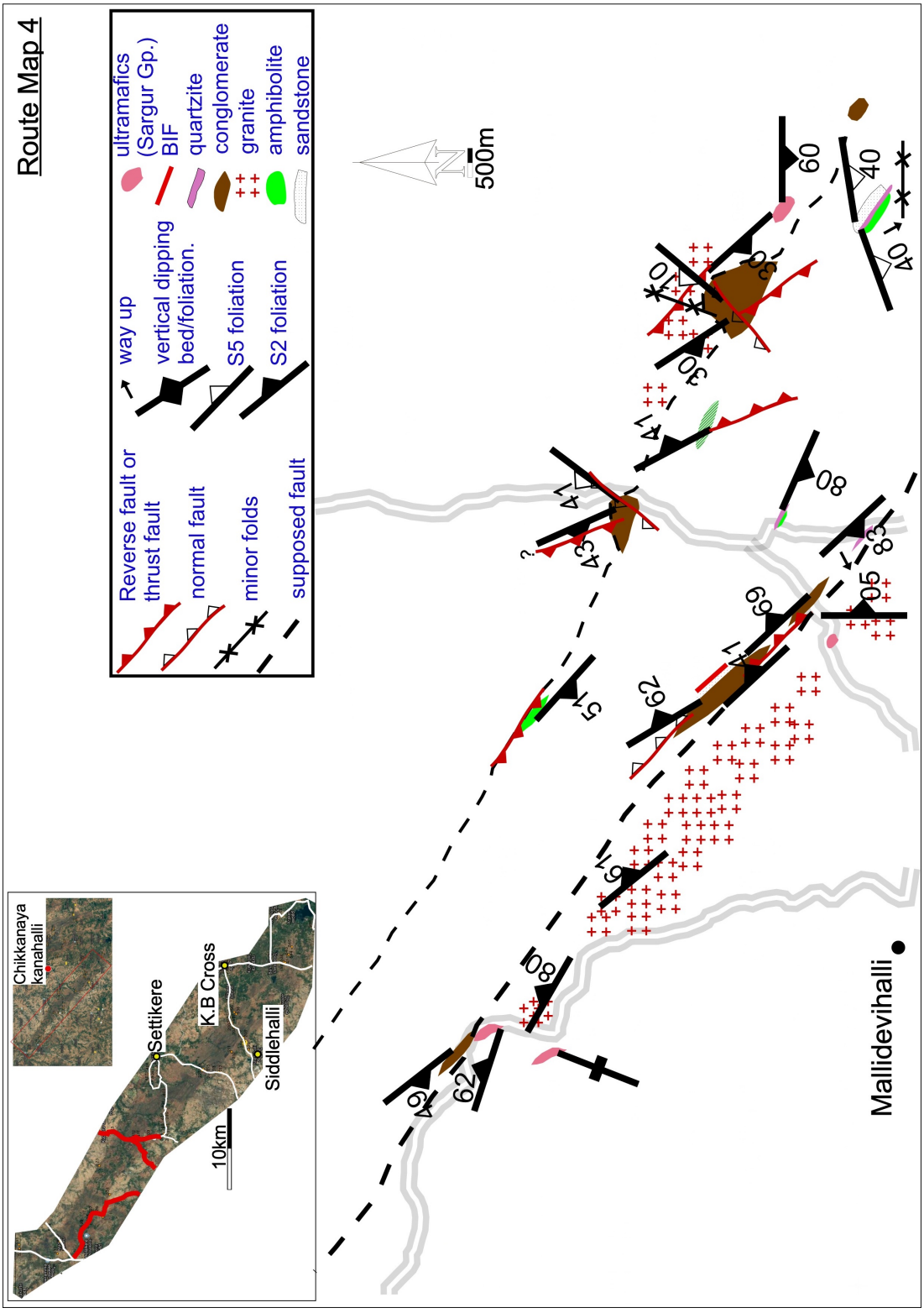

A5. Route map in Kibbanahalli Schist Belt.

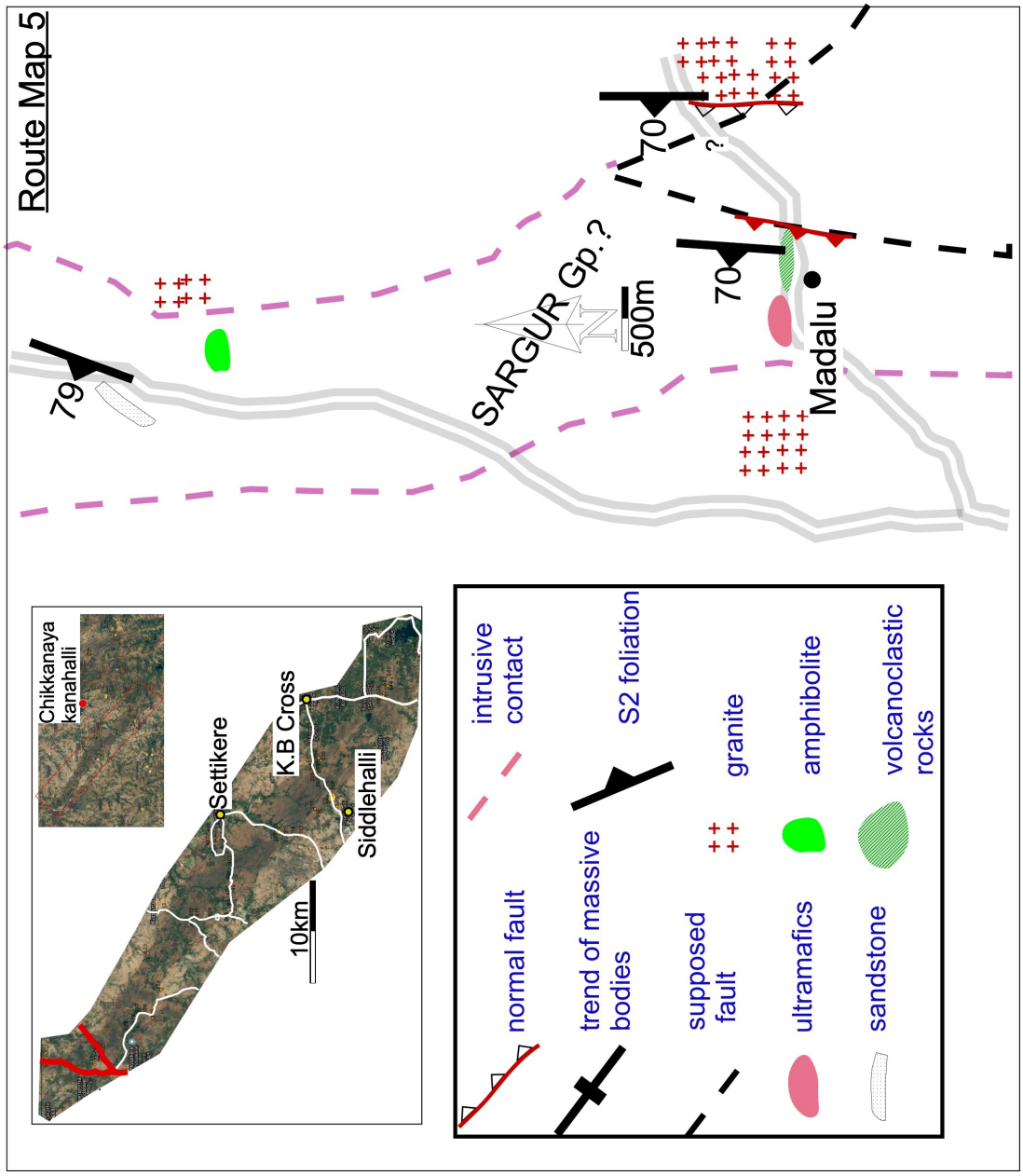

A6. Route map in Kibbanahalli Schist Belt.

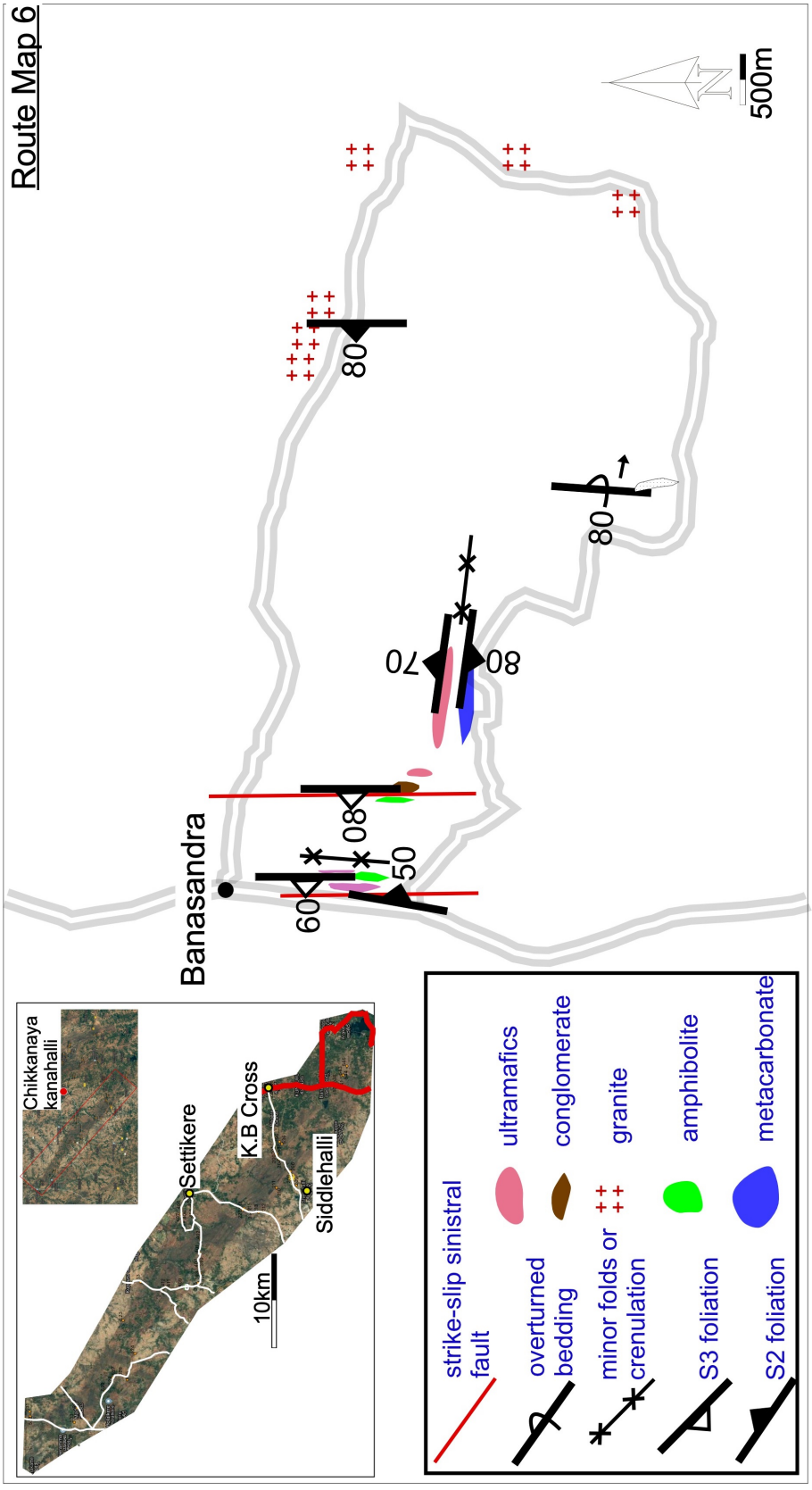

A7. Route maps in Kibbanahalli Schist Belt.

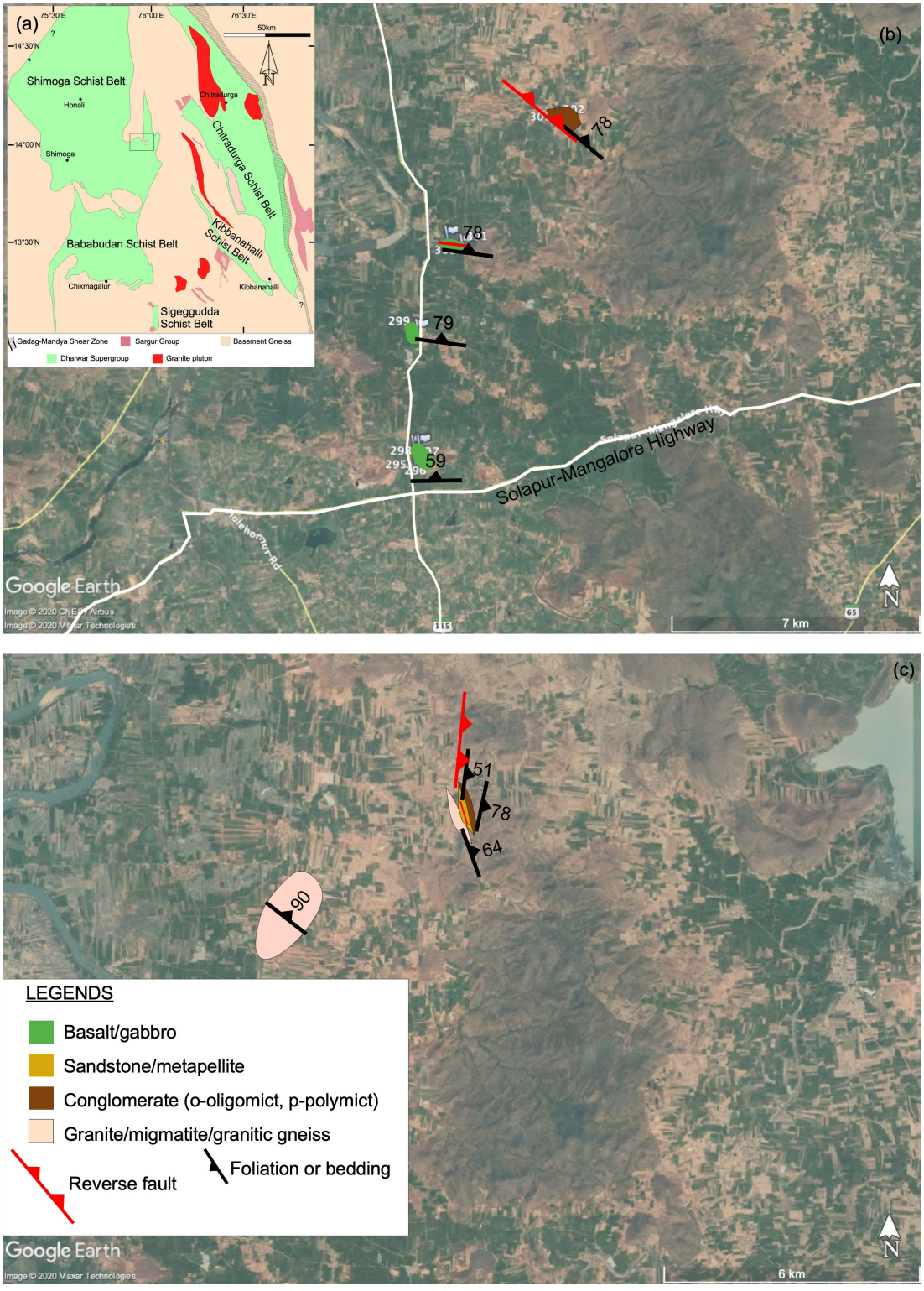

A8. Route maps for Bababudan Schist belt and Shimoga Schist Belts

A9. Route maps for Bababudan Group of rocks distributed near Chikkanayakanahalli

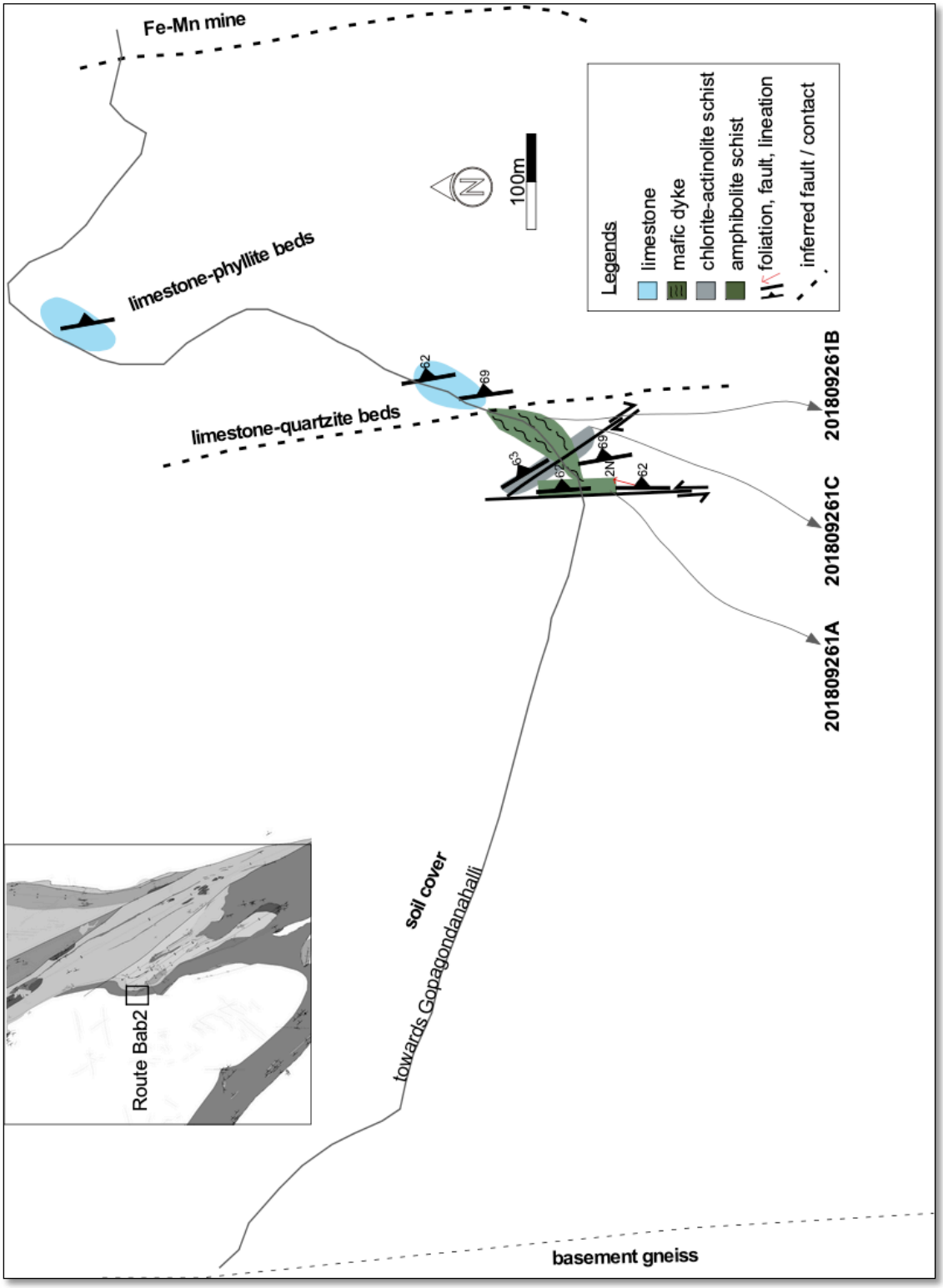

A10. Route map across CSB

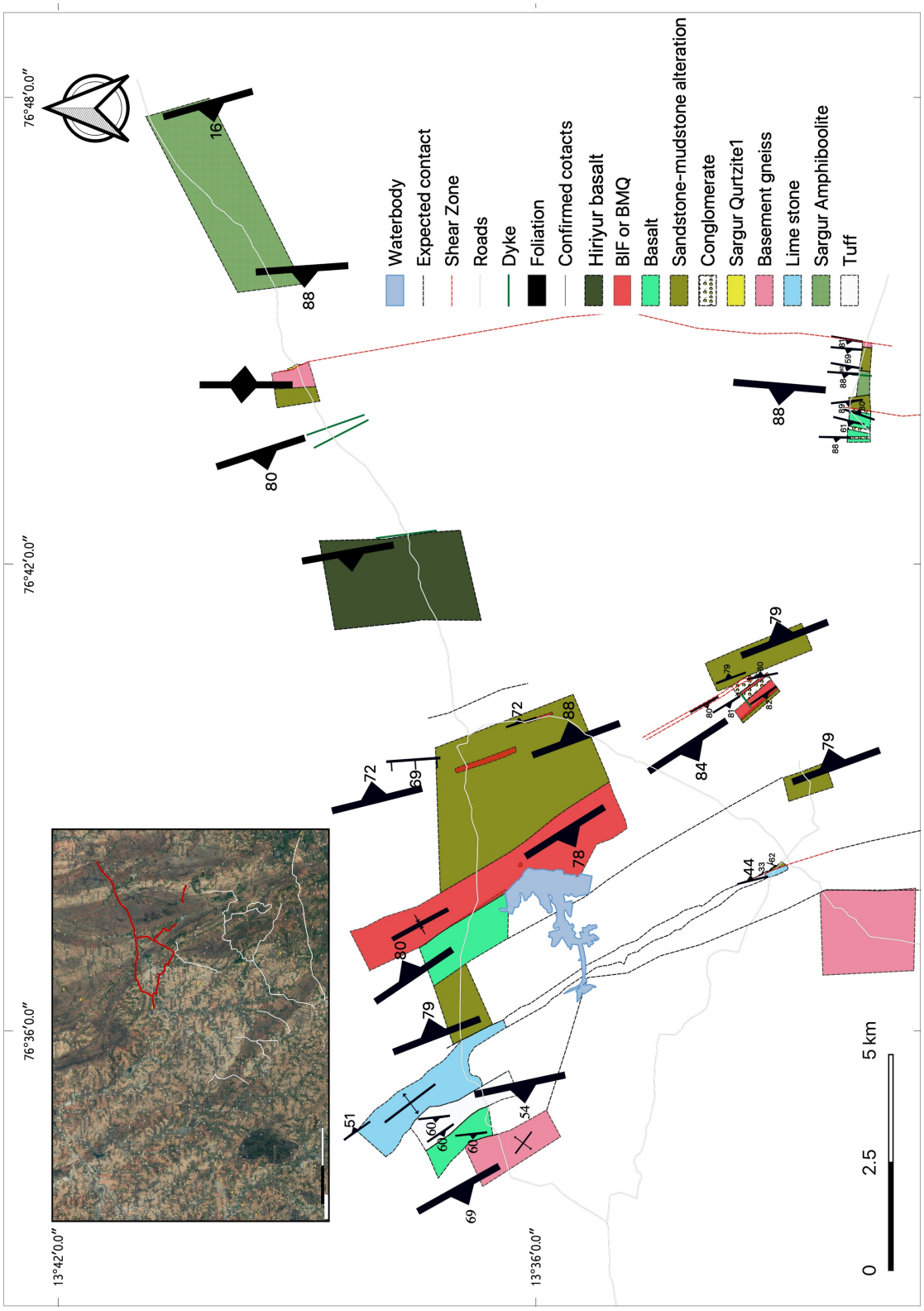

A11. Route map across CSB

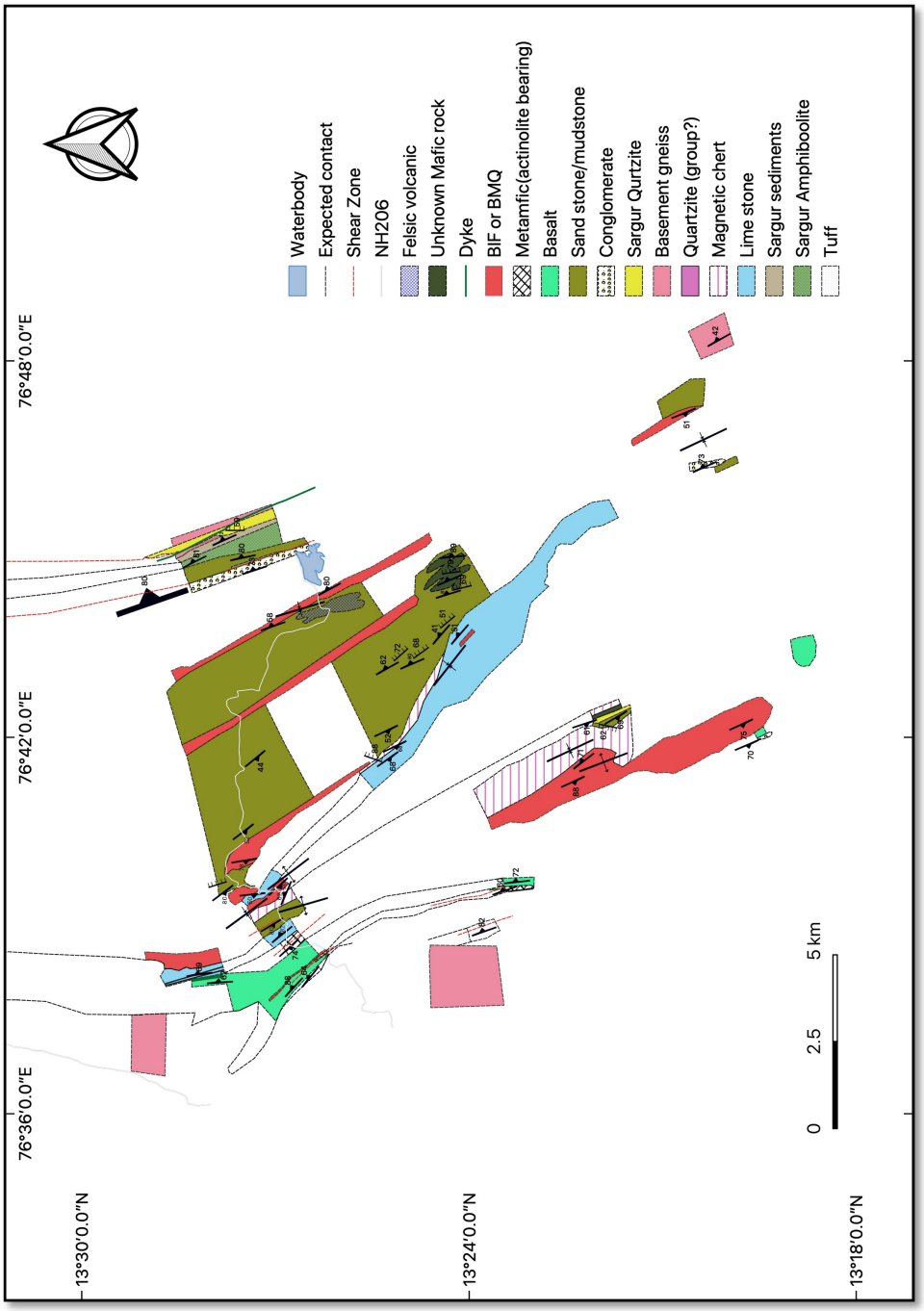

A12. Route map across CSB with structural data, small red circle represents lineation in stereographic equal area projection.

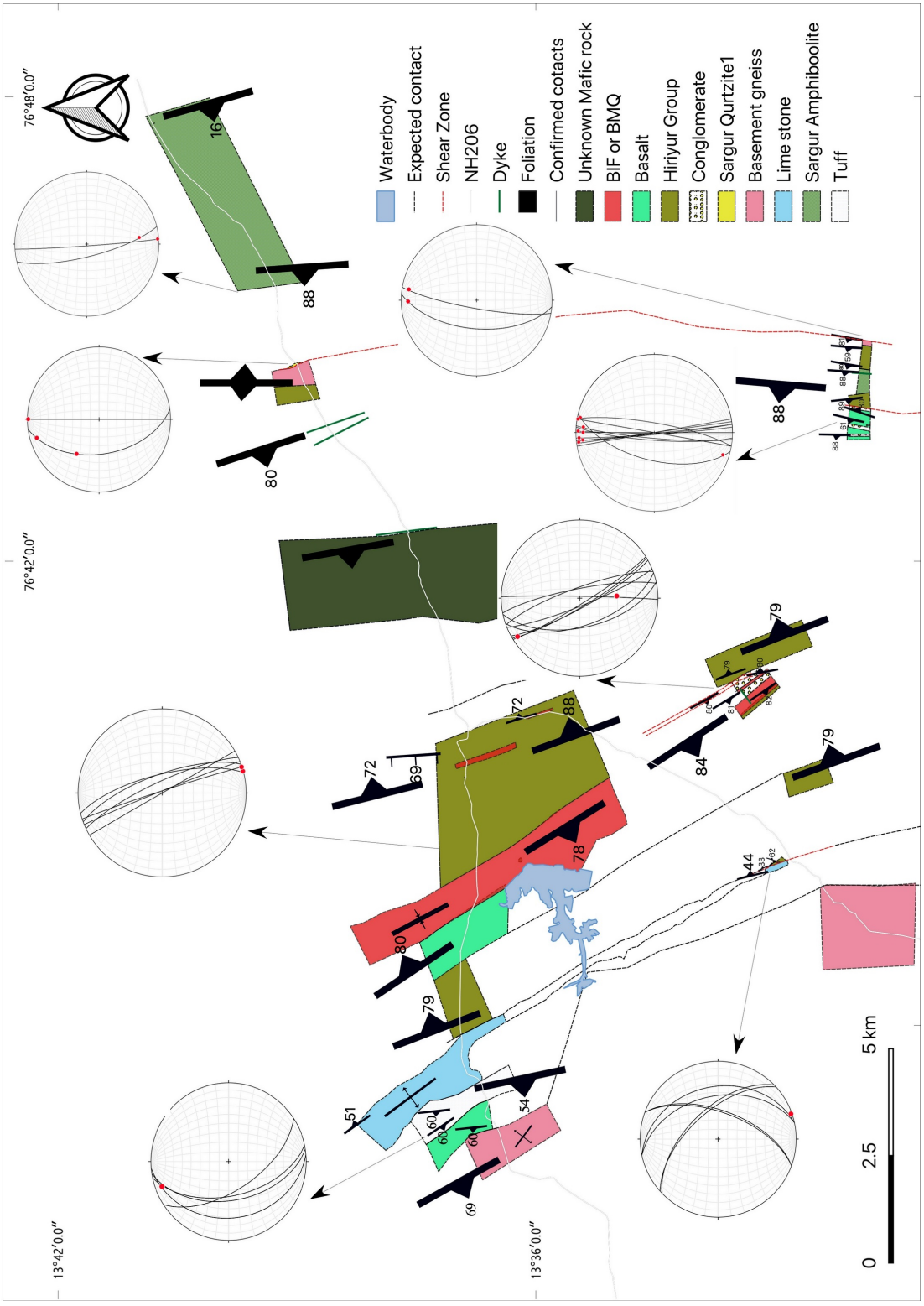

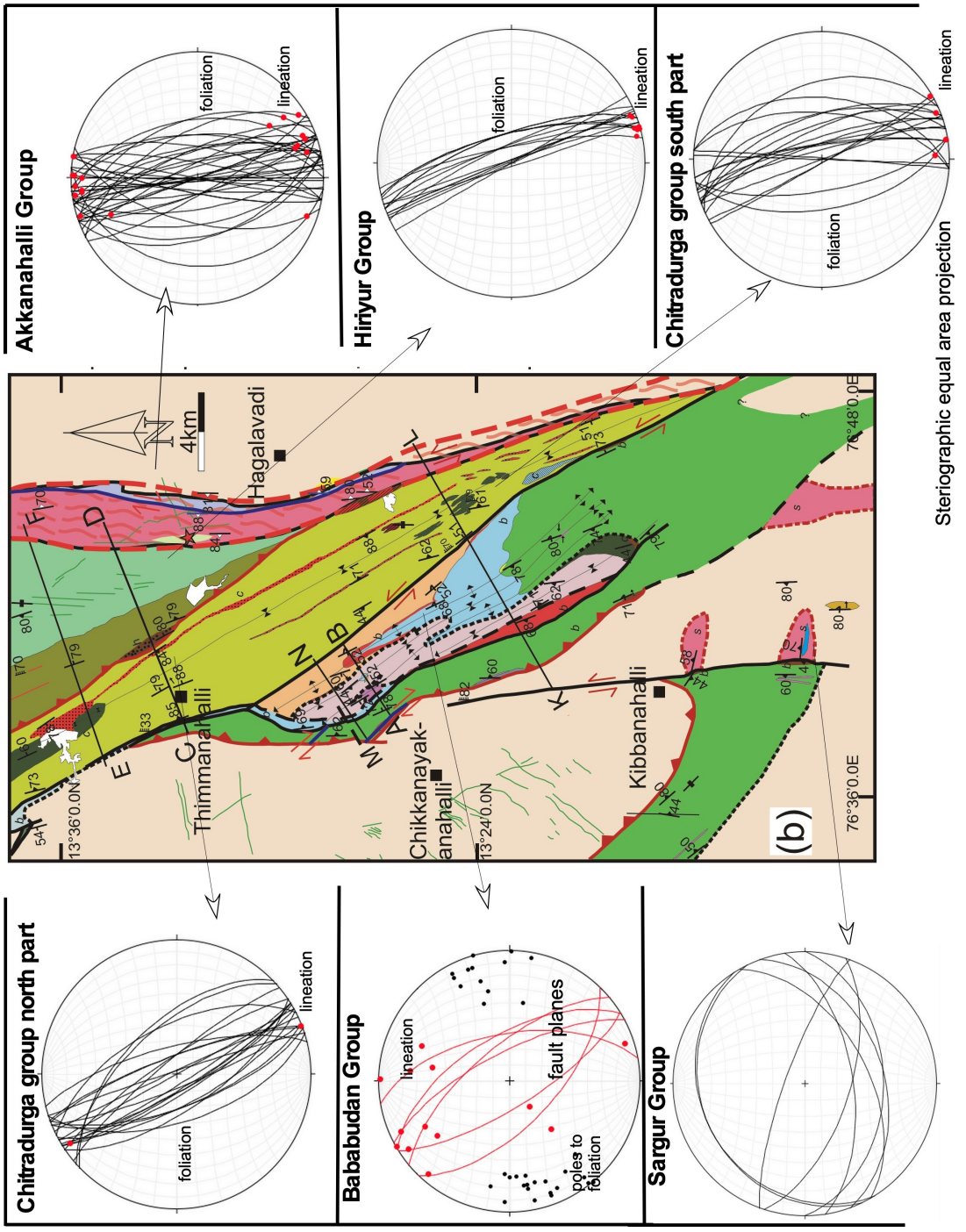

A13. Structural data across CSB, small red circle represents lineation in stereographic equal area projection.

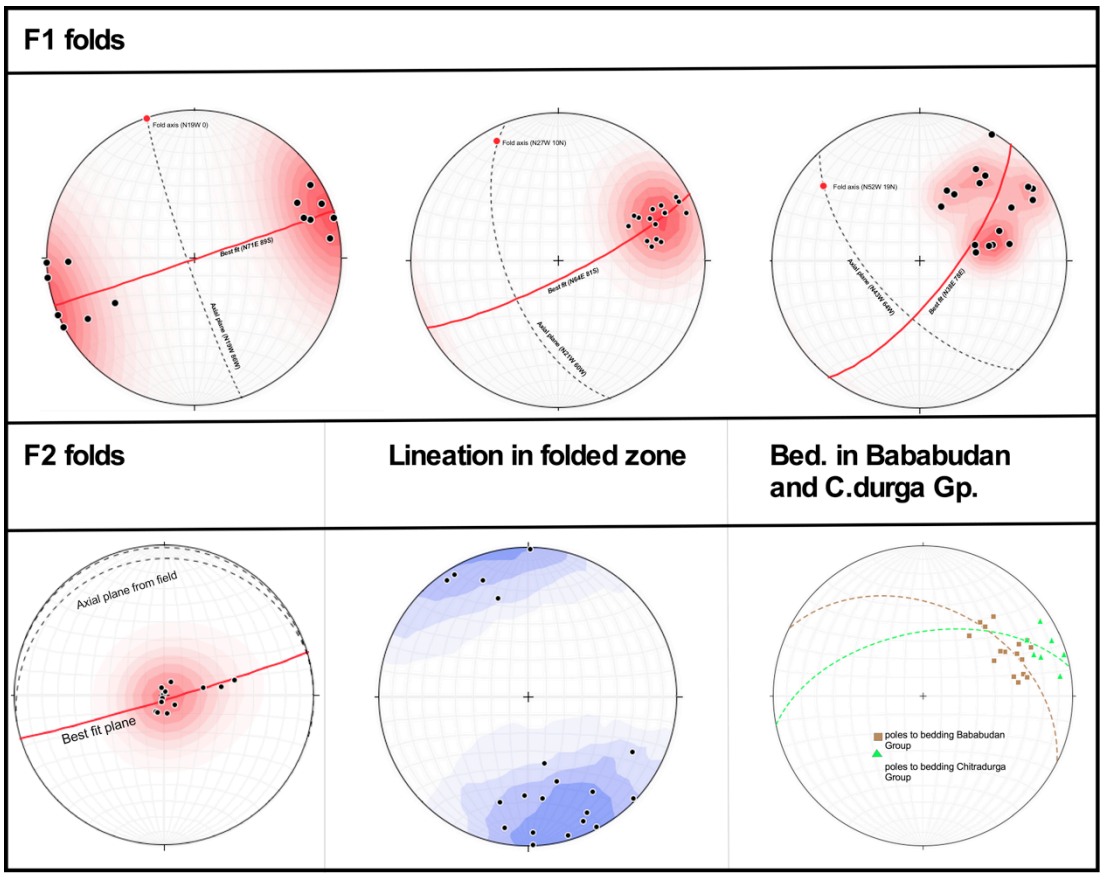

A14. Structural data along folded zone across route map shown in Appendix A1.

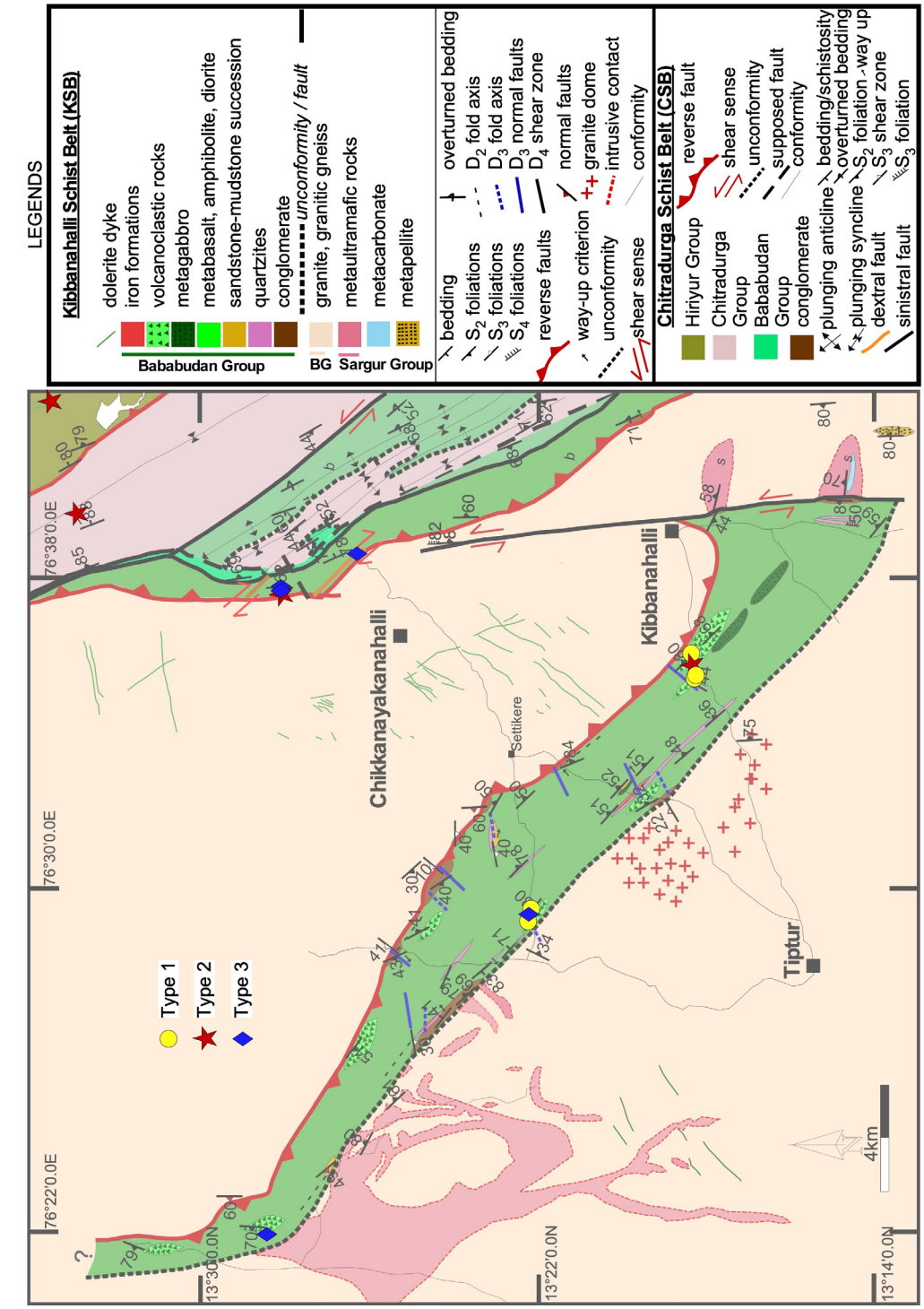

A15. Sample locations for geochemical analysis

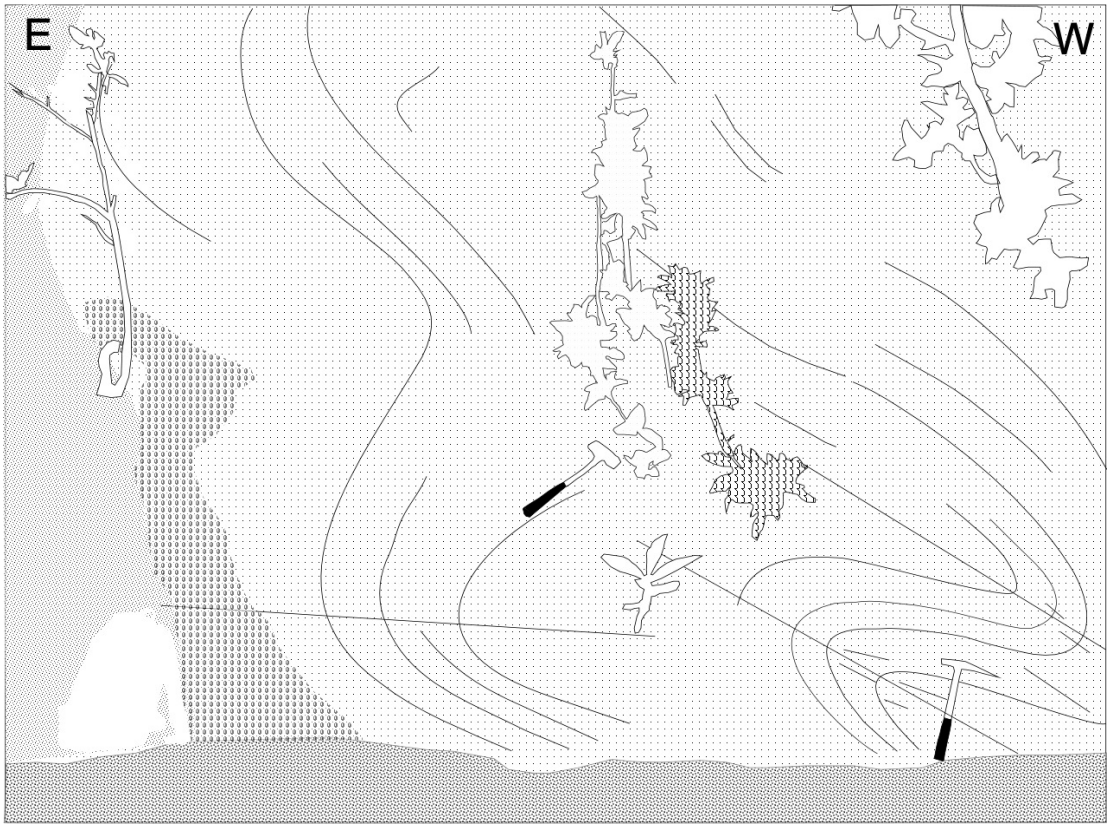

A16. Sketch for two generation folding in CSB

A17. Slump deposits and slump folding in CSB (a, b, c, d) and two generation tectonic folding in CSB (e, f, g, h)

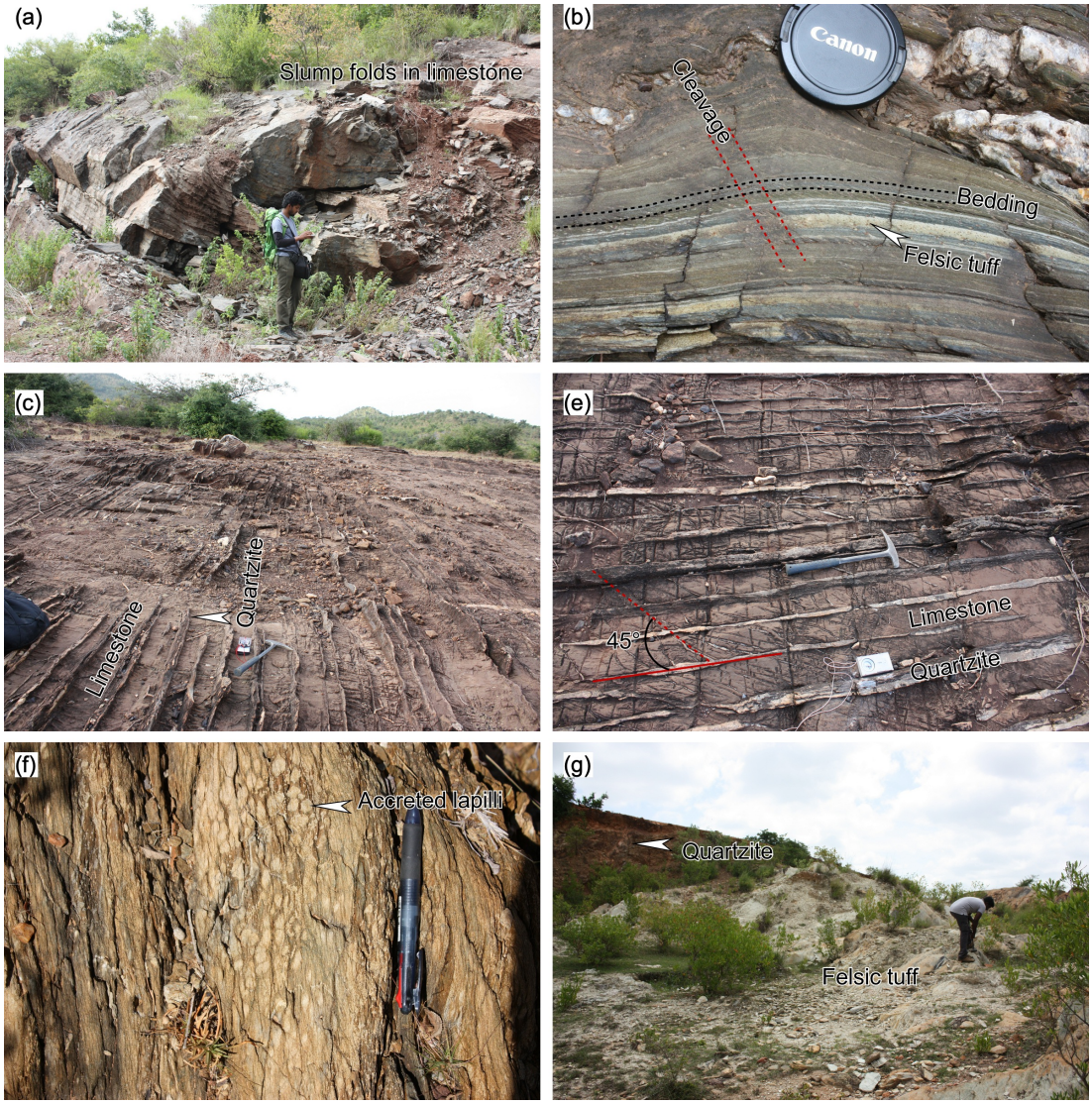

A18. Representative images of major rock types in Bababudan Group of CSB. (a) Slump folding in limestone (b) Tuffaceous sandstone (c) Limestone and quartzite succession

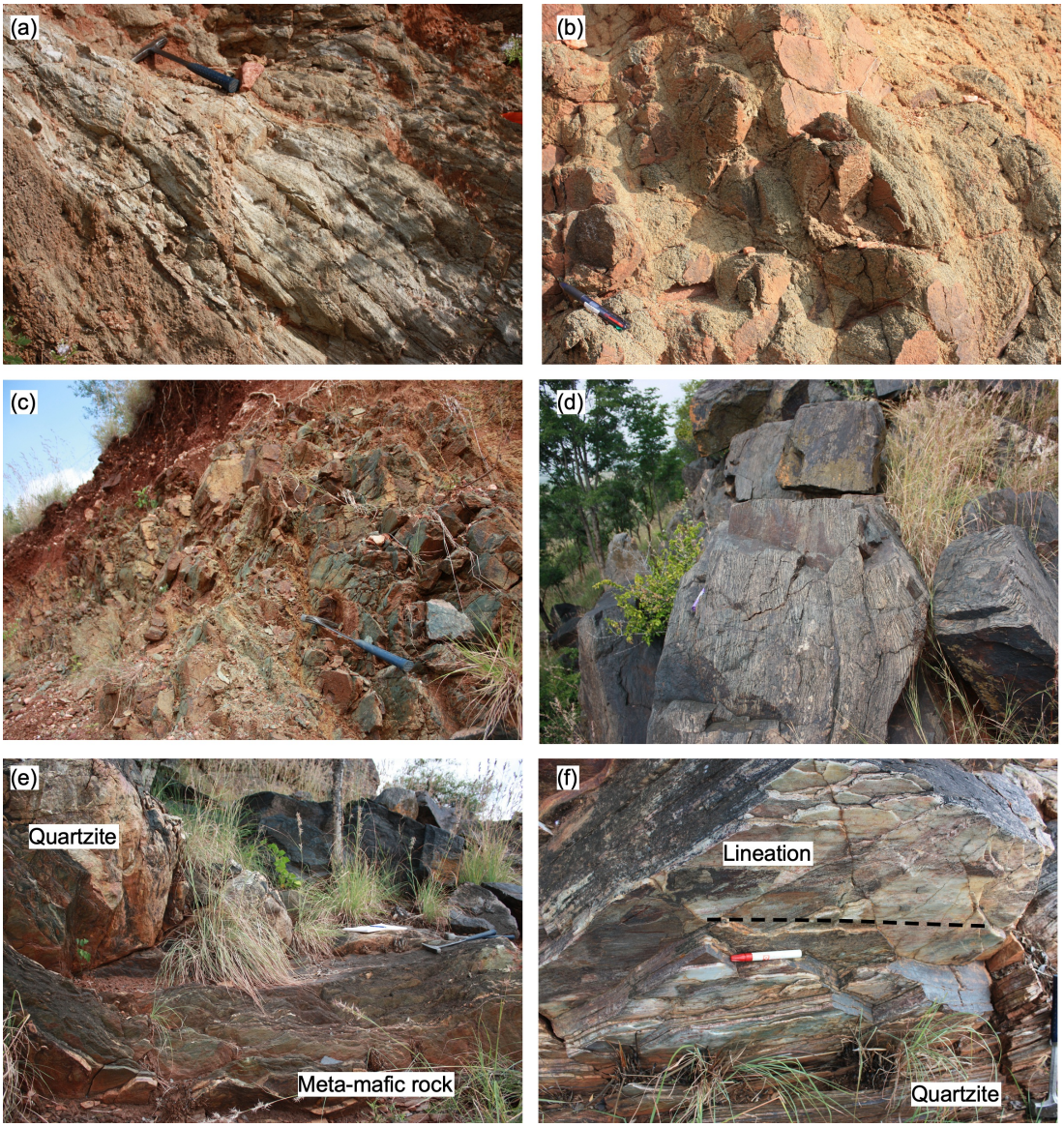

A19. Major lithological units in Chikkanayakanahalli–Kodihalli (see route map in A1) location. (a) Trondhjemite gneiss (b) (c) Metamafic rocks (d) BIF (e) Quartzite metamafic rock contact (f) Strike-parallel lineation in quartzite

A20. Major lithological units in Chitradurga and Hiriyur Group. (a) BIF deposits in Chitradurga Group (b) Boudinage in BIF of Chitradurga Group (c) Dip-parallel lineation in conglomerate between Hiriyur and Chitradurga Group (d, e) BIF, quartzite and basaltic clast in conglomerate (f) Metagreywacke in Hiriyur Group (g) Basaltic flows in Hiriyur Group (h) Dyke boulders in Hiriyur Group.

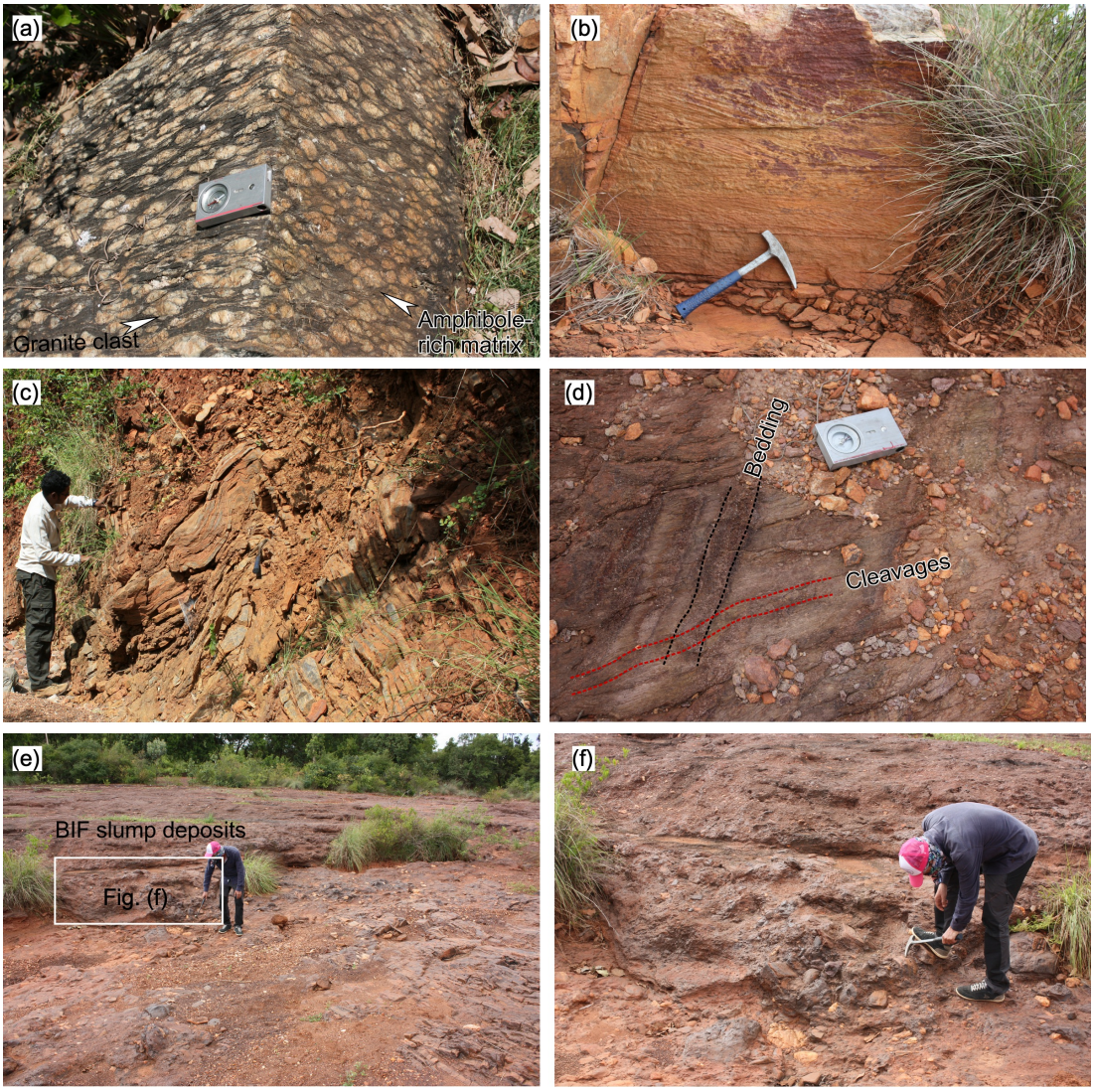

A21. (a) Conglomerate in Bababudan Group with granitic clast in amphibole-rich matrix (b) Cross bedding in quartzite in Bababudan Group (c) Folded quartzite in Bababudan Group (d) Slump deposits in BIF of Bababudan Group (f) Slump deposits in BIF

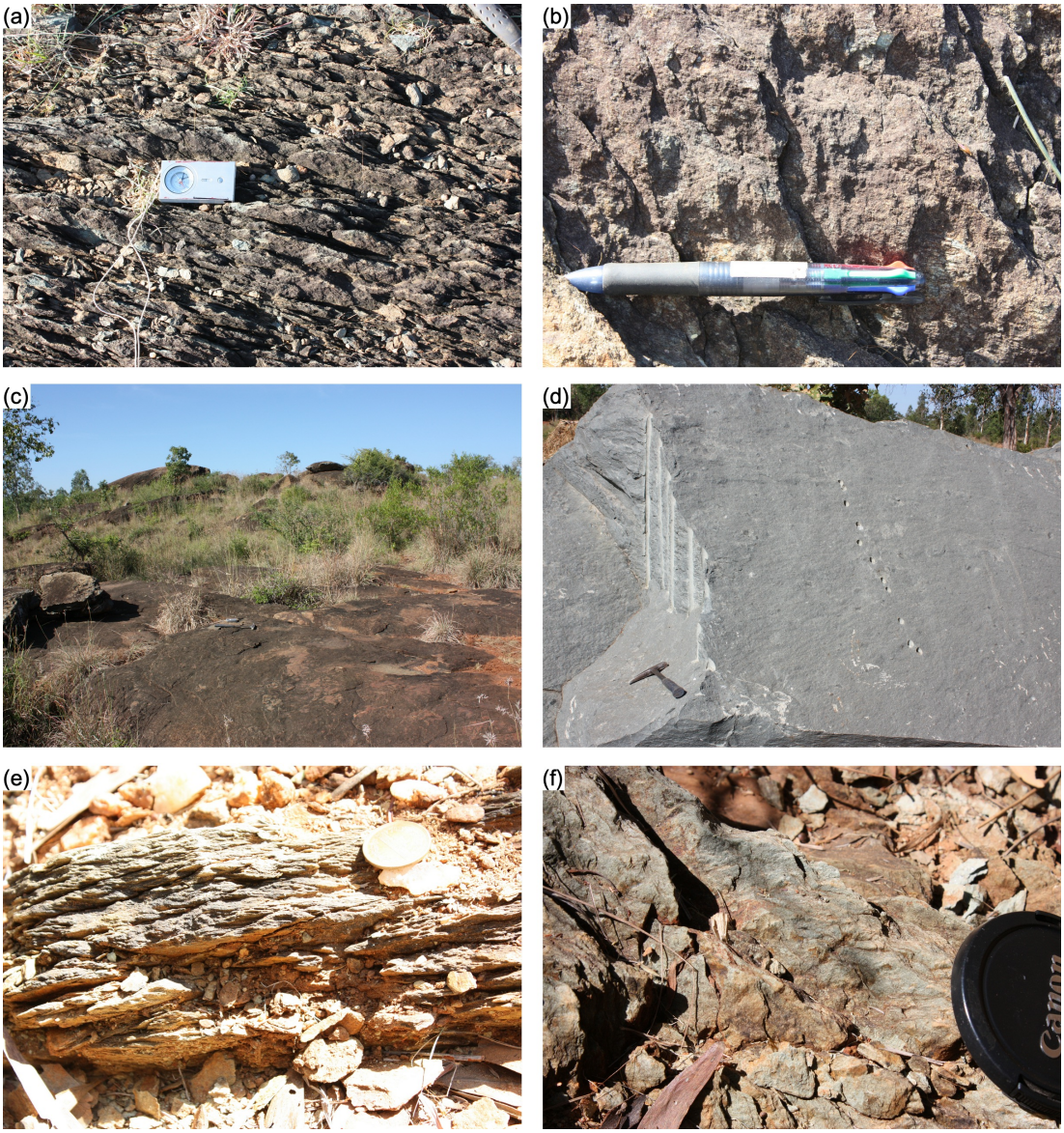

A22. (a) Volcanic rock in KSB (b) Dip-parallel lineation in volcanic rock in Fig (a). (c, d) Volcanic flow in KSB (e) Sheared metasediment and (f) sheared volcanic rock in KSB.

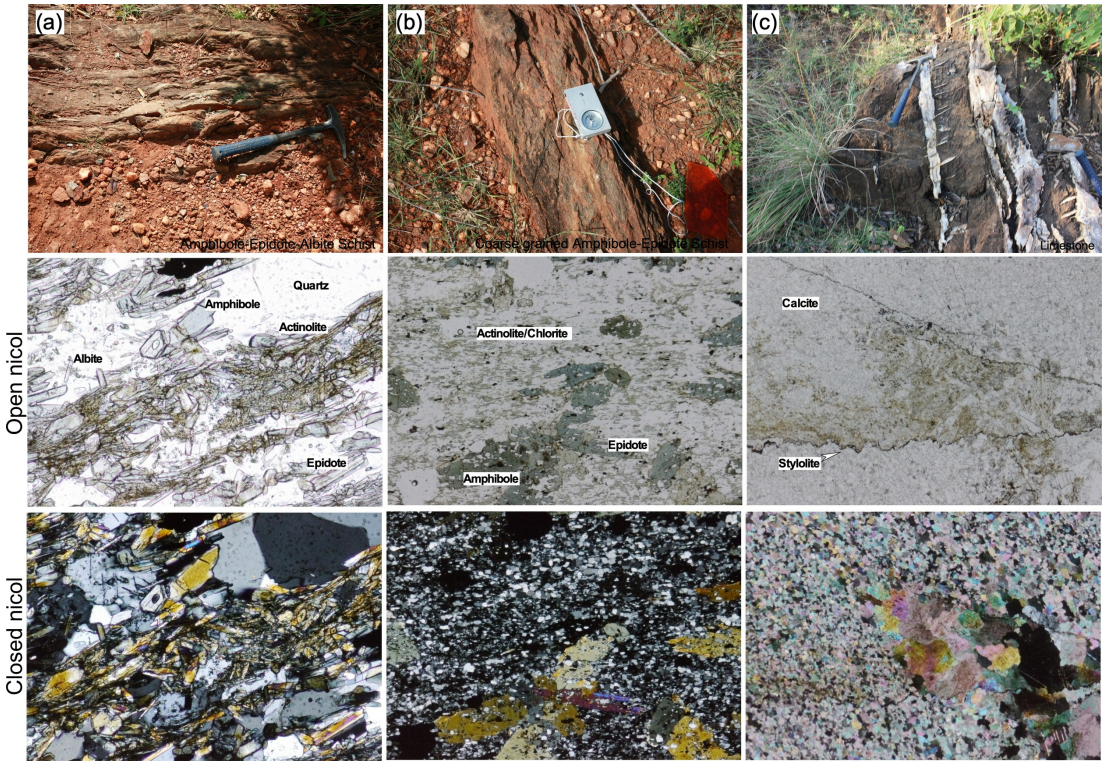

A23. Field and microphotographs of volcaniclastic rocks (a & b) and limestone in Bababudan Group (c).

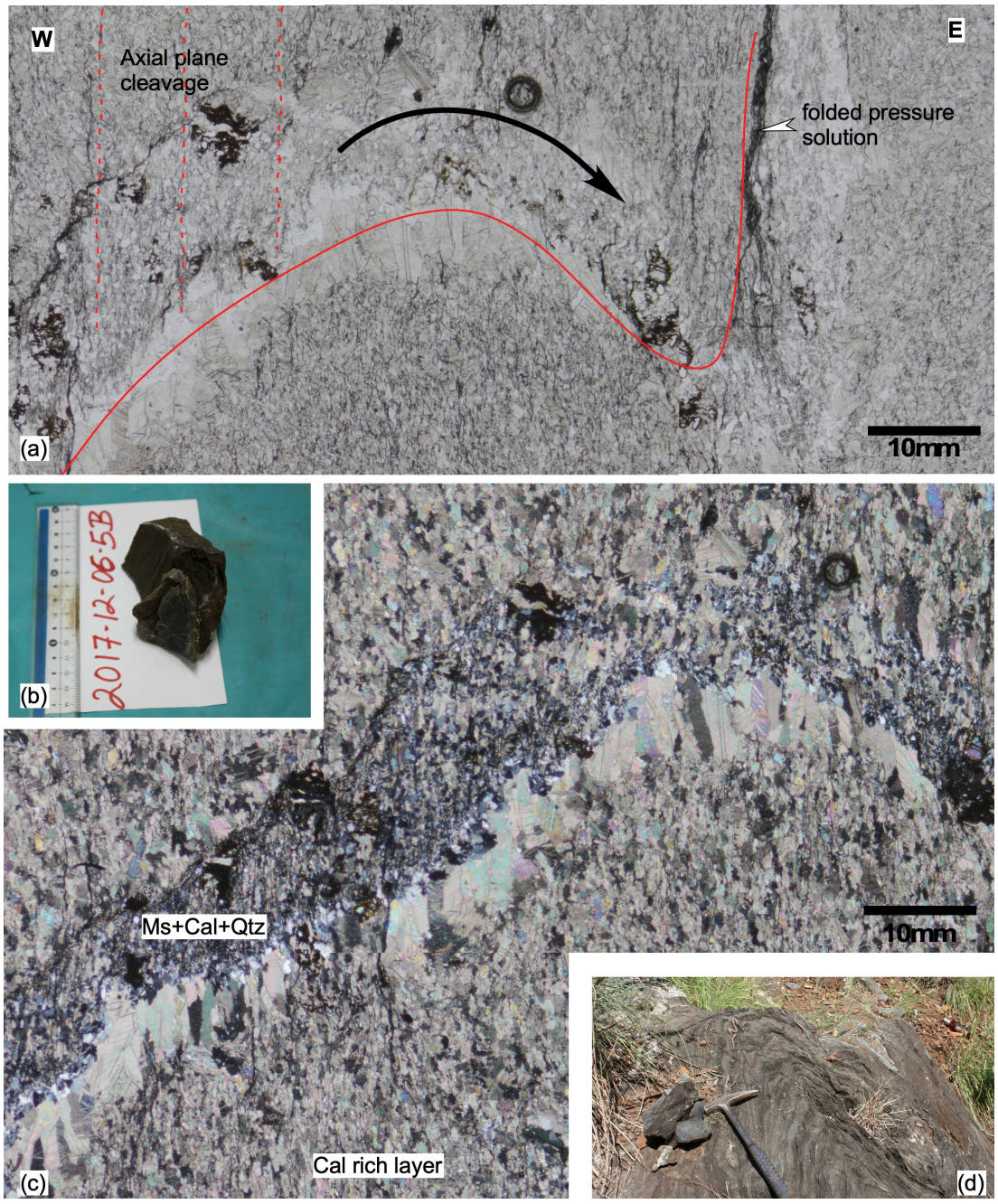

A24. (a) Microphotograph showing folded pressure solution cleavages in limestone, Muscovite and chlorite developed along axial plane cleavages (b) Hand specimen of limestone sample (c) Microphotograph (closed) shows alternating calcite-rich layer and quartz-rich layer in limestone (d) Field occurrence of folded limestones

Field photographs of the samples shown in the route map A9. (a, b, c) Amphibolite (d) Limestone. All samples are from Bababudan Group.

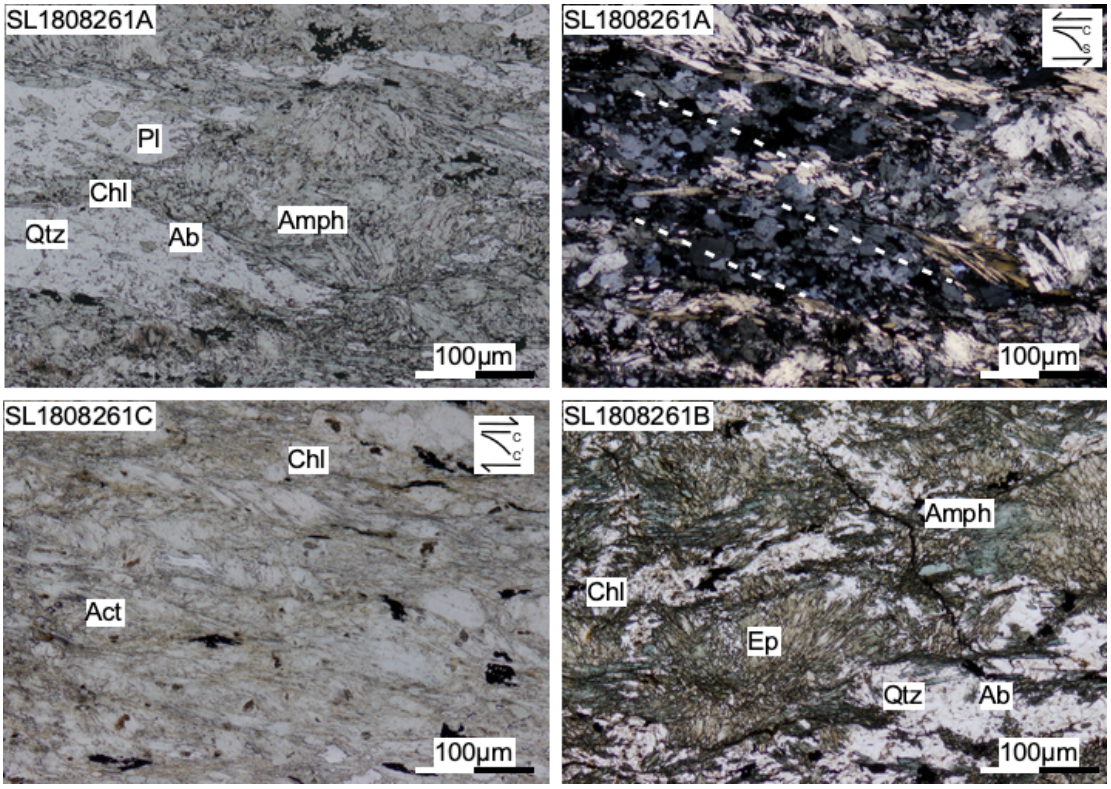

A25. Thin section photographs of the samples from Bababudan Group shown above. Samples numbers of the corresponding thinsection samples are marked in the figure itself.

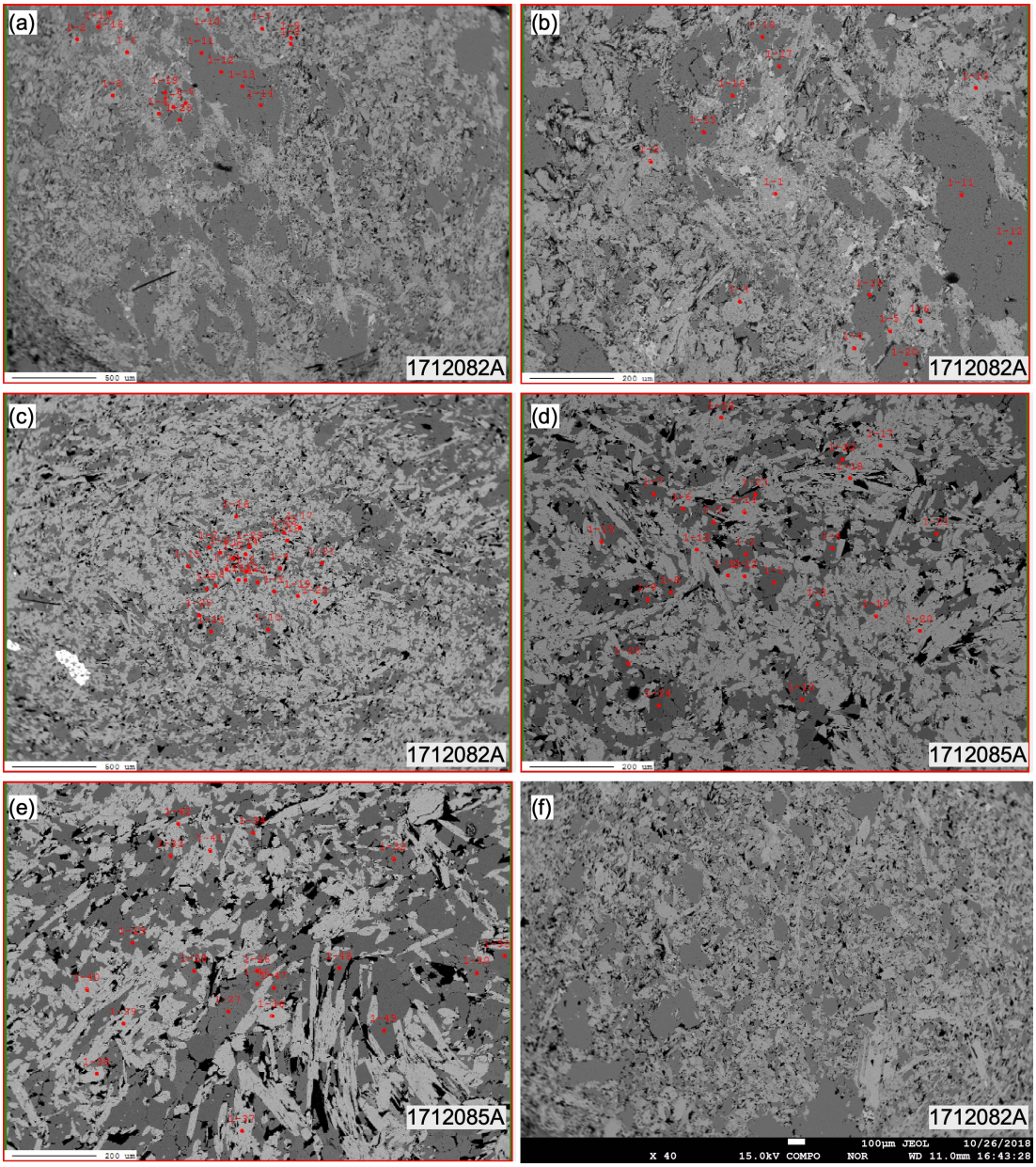

A26. Back-Scattered Images for the amphibolite samples in which EPMA analyses were conducted. Results of the analysis are shown in the Table 4 and Table 5

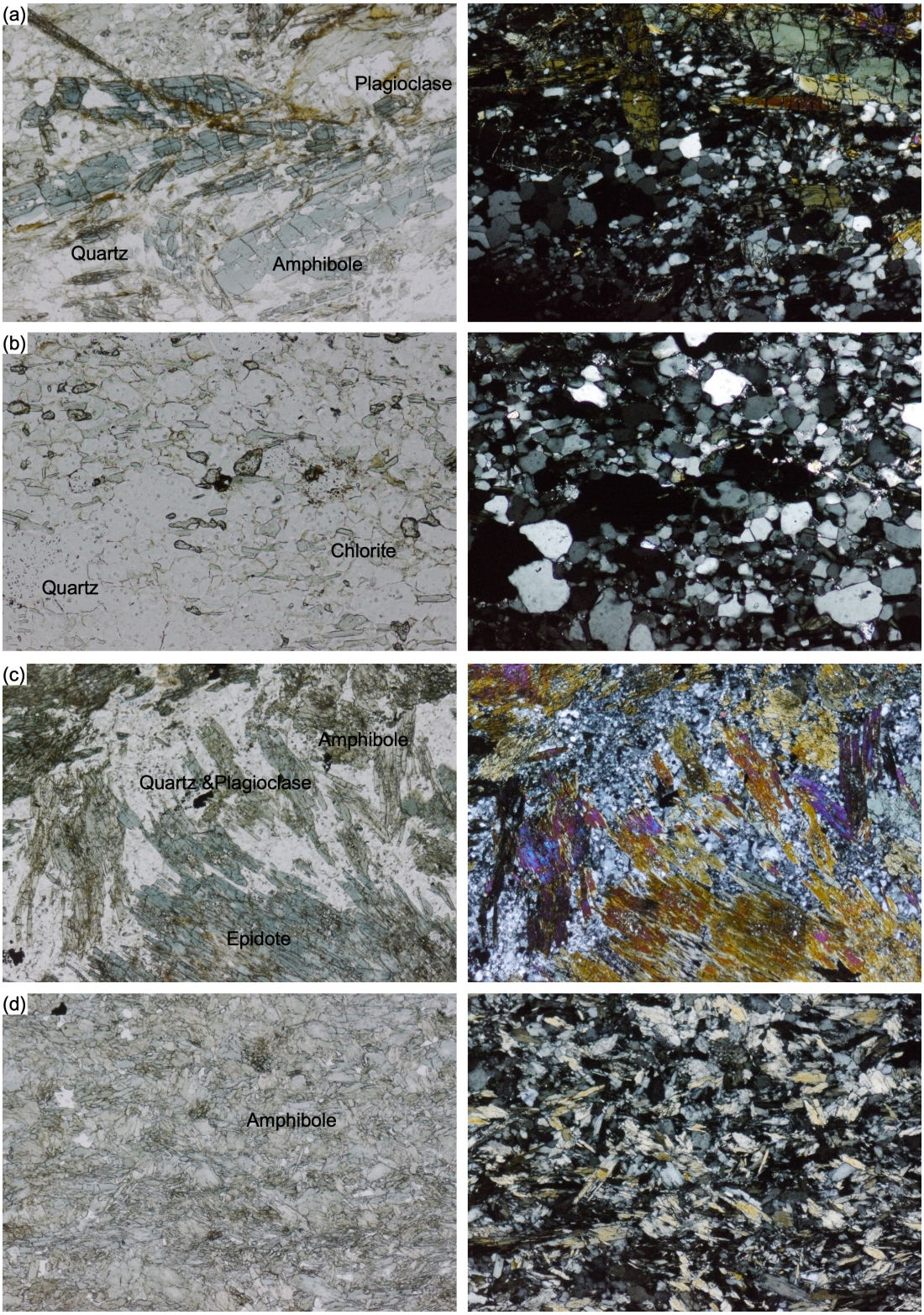

A27. Microphotographs of volcaniclastic (a, b, c) and volcanic (d) rocks in Bababudan Group. All are metamorphosed in low-grade amphibolite facies.

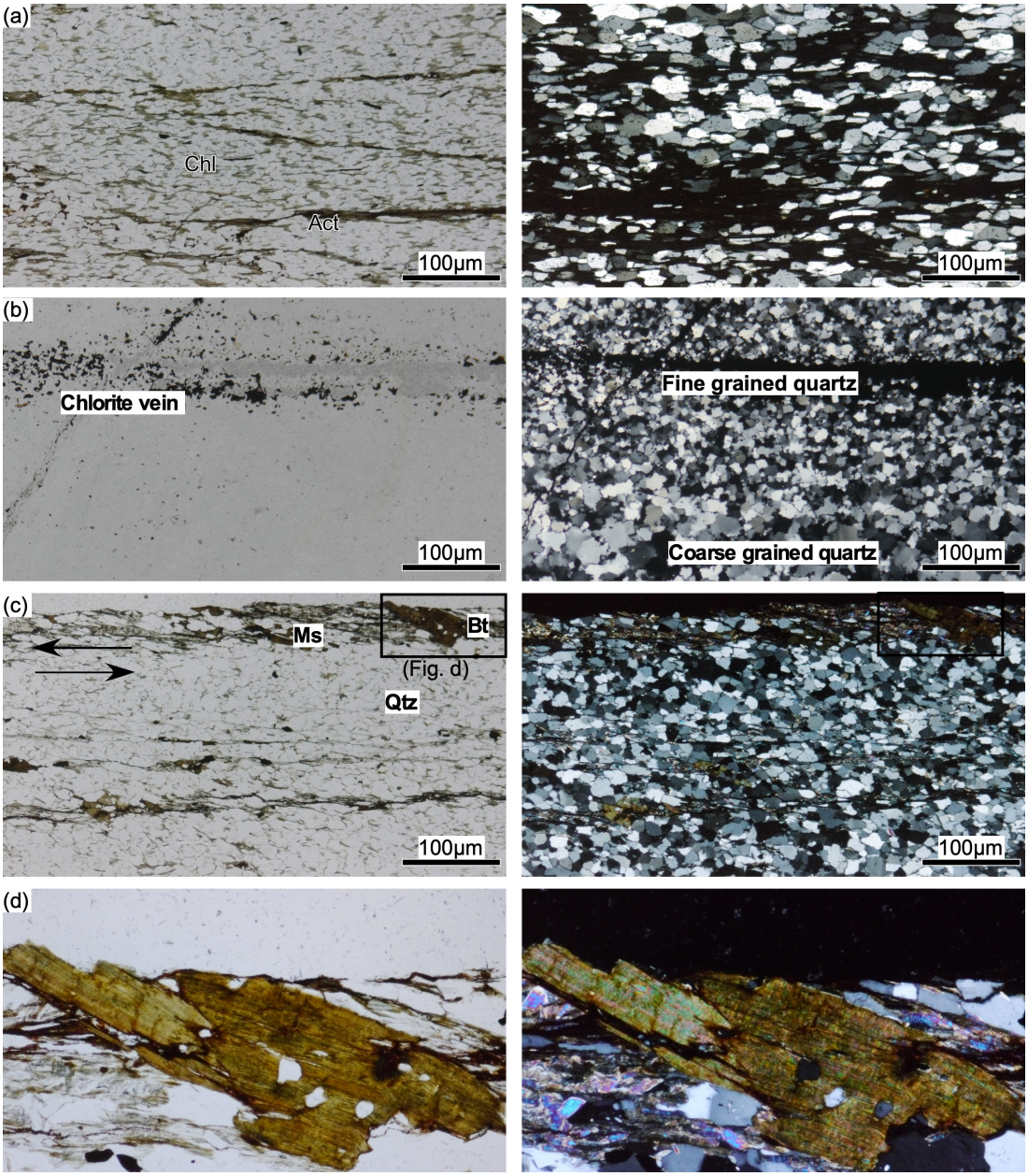

A28. Microphotograph of metasedimentary rocks in Bababudan Group. (a) Quartz-chlorite-actinolite schist (b) Deformed quartzite (c) Sheared metapellite, sinistral sense of movement, muscovite developed along shear plane (d) Enlarged view of detrital biotite defining S foliation in shear plane.

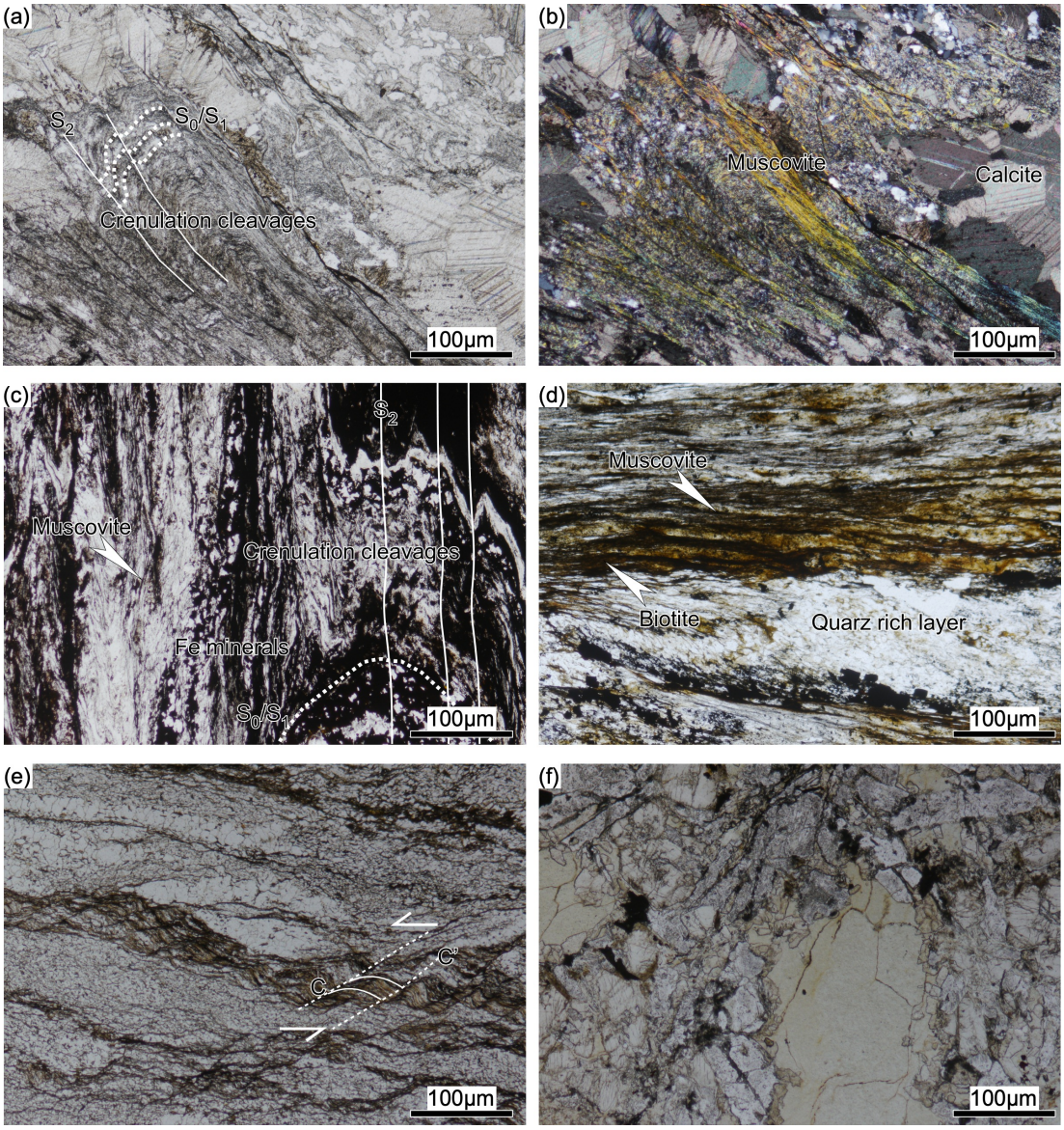

A29. Microphotograph of samples from Chitradurga, Hiriyur and Akkanahalli Zone (a), (b) Axial plane cleavages in limestones. Muscovite developed along these axial plane cleavages. (c) Axial plane cleavages in BIF of Chitradurga Group, muscovite is developed parallel to the axial plane cleavages. (d) Metapellite in Chitradurga Group with alternating quartz rich and biotite-muscovite rich layer. Muscovite is stable along the shear planes. (e) Sinistral shear in quartz-chlorite schist from Akkanahalli Zone. (f) Meta-dolerite in Hiriyur Group.

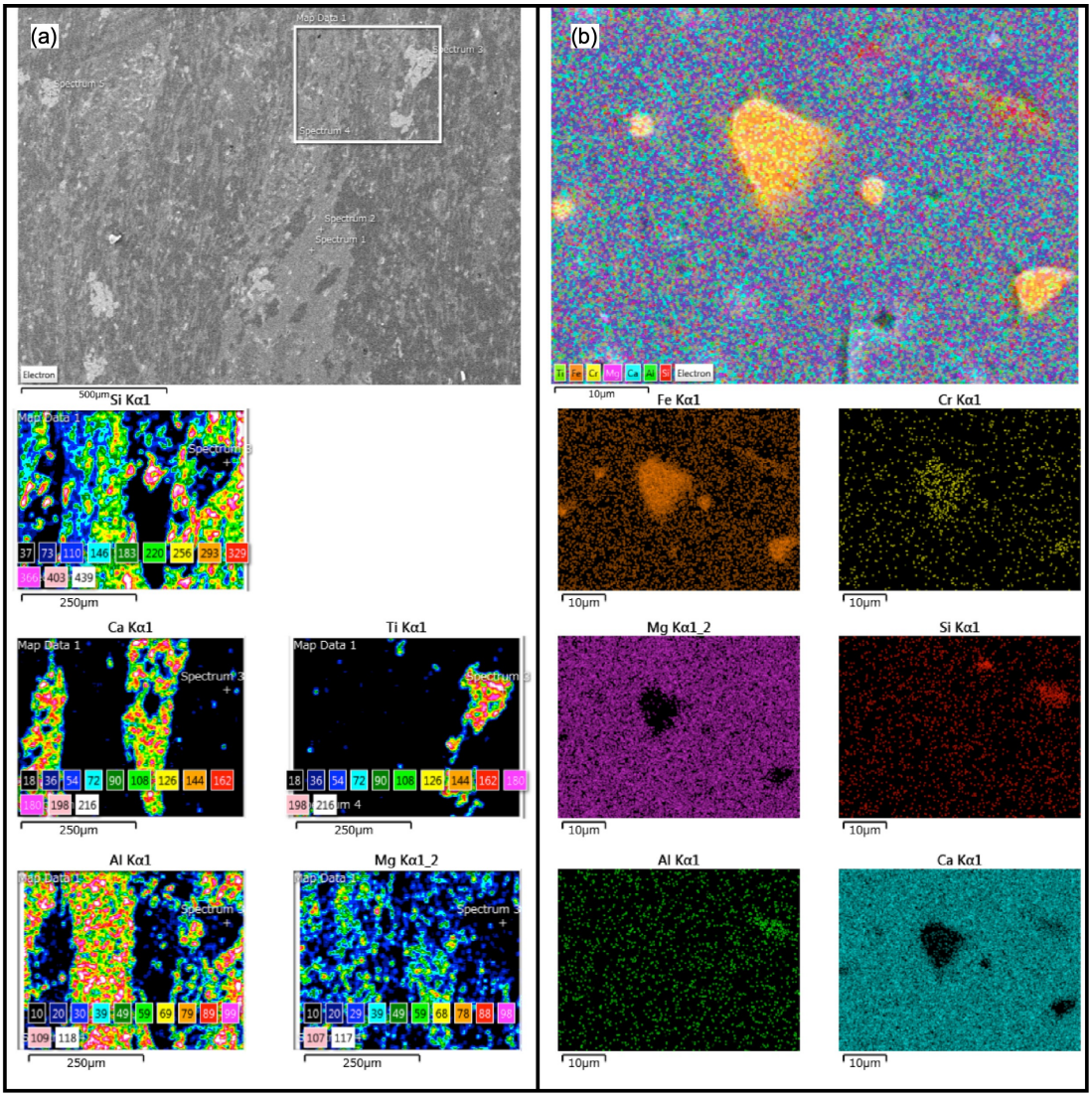

A30. SEM-EDS mapping results in samples from Akkanahalli Zone. (a) Shows inclusions of ilmenite and rutile in dolomite. (b) Detailed map of another inclusion in the same sample.

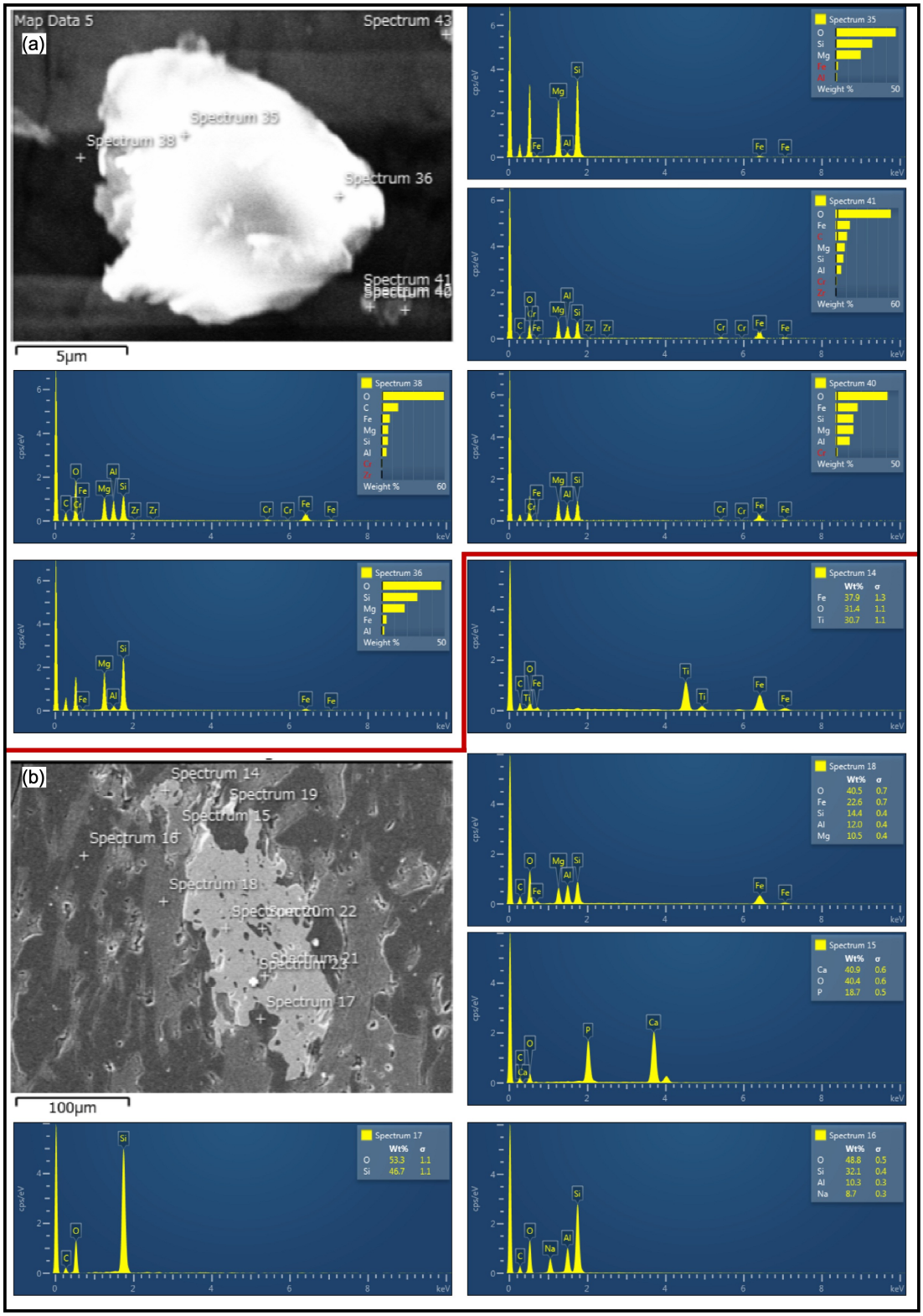

A31. EDS analysis results in samples from Akkanahalli Zone. (a) Olivine inclusion in chlorite (b) Rutile, ilmenite inclusions in metavolcanic rock in Akkanahallli Zone.

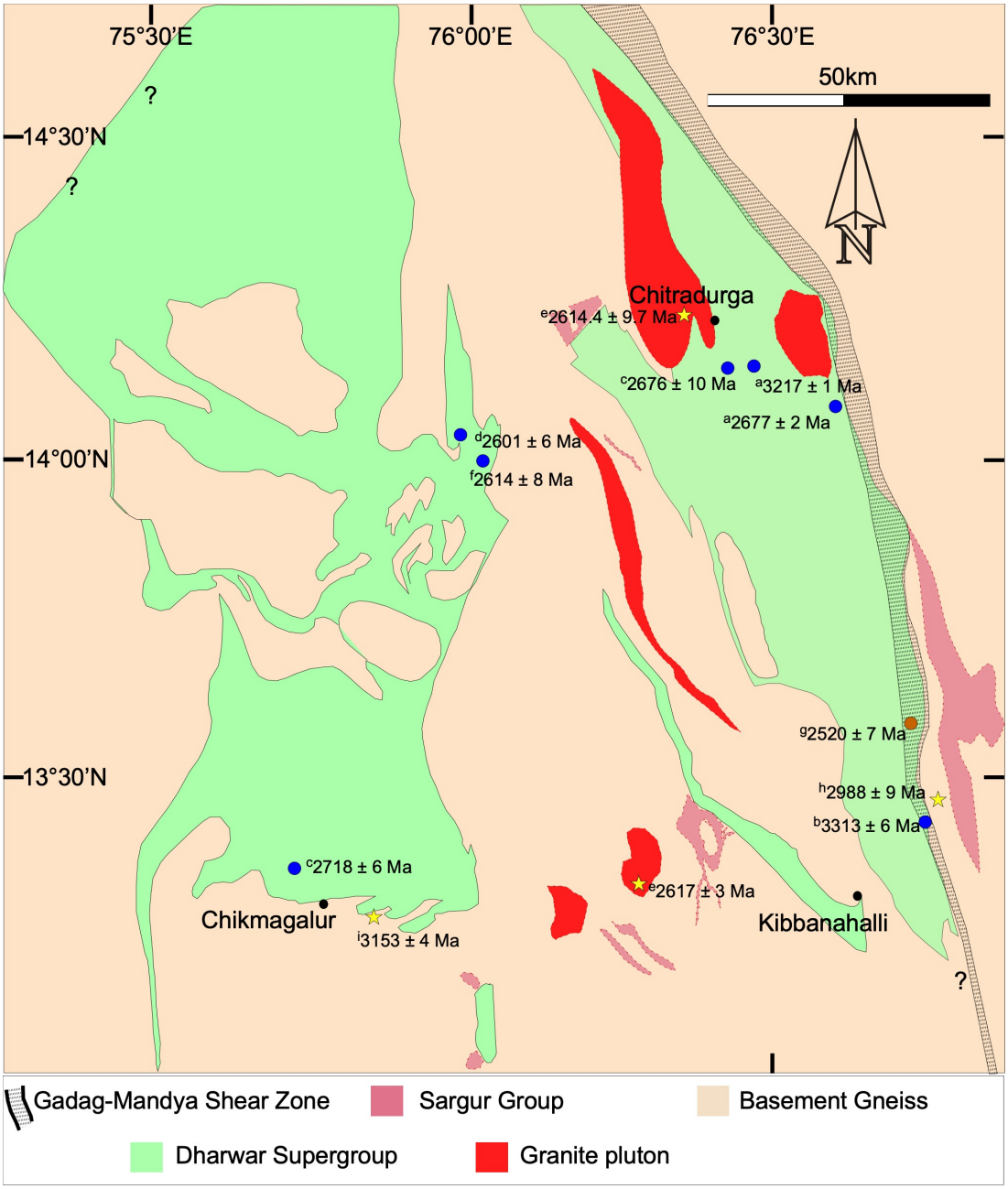

[a]Jayananda et al., 2013
[b] Sreehari and Toyoshima, 2020
[c]Trendall et al., 1997a
[d]Nutman et al., 1996
[e]Jayananda et al., 2006
[f]Trendall et al., 1997b
[g]Sarma et al., 2011
[h]Chardon et al., 2011
[i]Jayananda et al., 2015

● Felsic volcanics(Zircon U-Pb) ☆ Granites and Basement Gneiss(Zircon U-Pb)

● Monazite and Xenotime age

A32. Published volcanic and plutonic ages (Zircon U-Pb) and metamorphic ages in WDC.

PUBICATIONS and AWARDS

1) *Sreehari, L., & Toyoshima, T.* (2020). **Structural architecture and geological relationships in the southern part of Chitradurga Schist Belt, Dharwar craton, South India.** *Journal of Mineralogical and Petrological Sciences*, 191120.

2) Sreehari, L., Toyoshima, T., Satish—Kumar, M., Takahashi, T & Ueda, H. **Structural and geochemical evidence for a failed rift crustal evolution model in Western Dharwar Craton, South India.** (*Submitted in Lithos*)

Best oral presentation award

Maricon 2019 December 16-20 held at Cochin University of Science and Technology

Title: Structural Architecture of southern part of Chitradurga Schist Belt, Western Dharwar Craton.Sterioplots

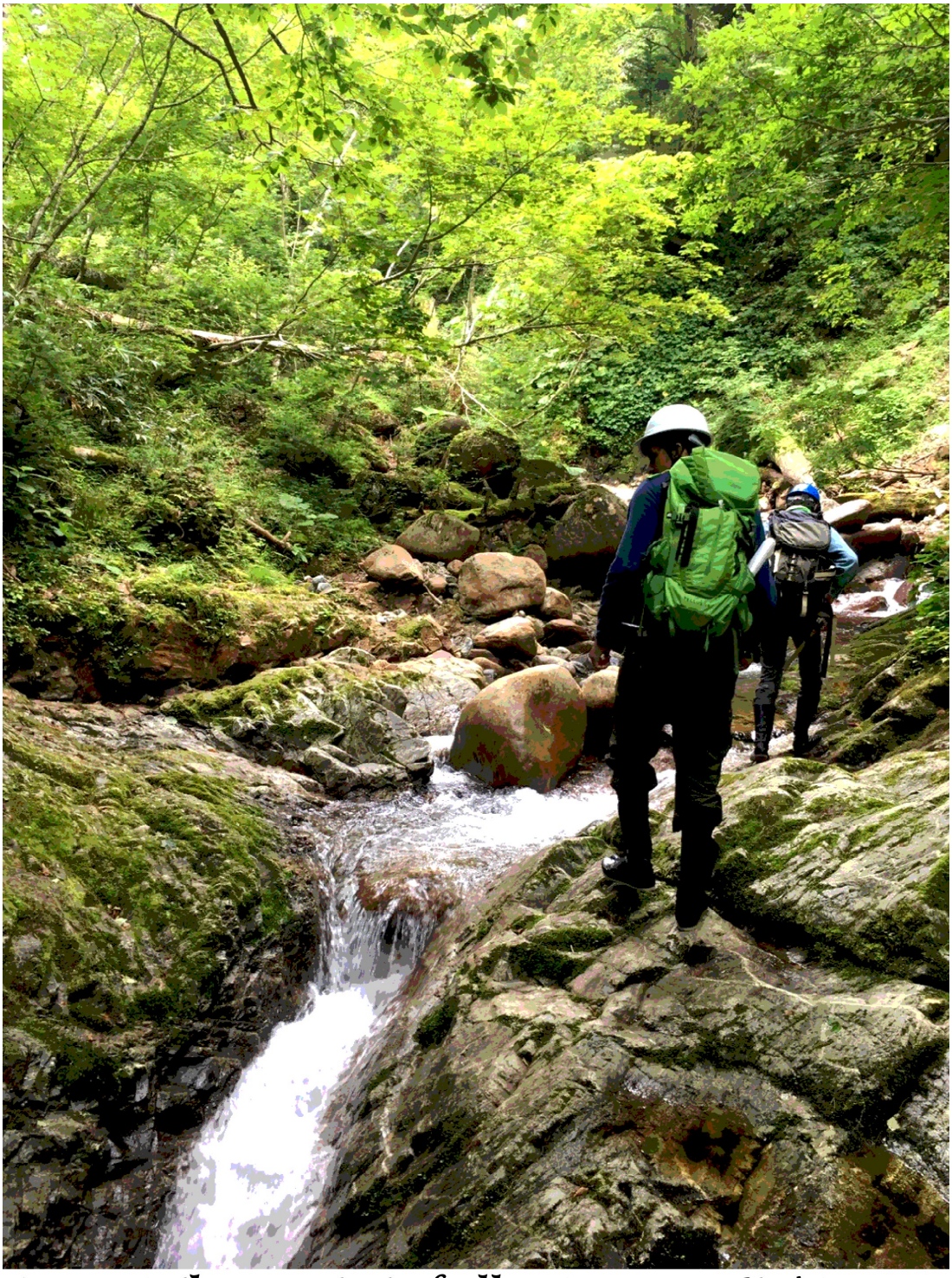

A map is the greatest of all epic poems. Its Lines and colors show the realisation of great dreams

-Gilbert H. Grosvenor